TECHNISCHE UNIVERSITÄT MÜNCHEN

Fakultät für Medizin

"The Role of Calcium and its Transporter P2RX5 in Brown Adipocyte Function"

Ines Ursula Nicola Pramme-Steinwachs

Vollständiger Abdruck der von der Fakultät für Medizin der Technischen Universität München zur Erlangung des akademischen Grades eines Doktors der Naturwissenschaften (Dr. rer. nat.) genehmigten Dissertation.

Vorsitzender:	Prof. Dr. Heiko Lickert
Prüfer der Dissertation:	1. Prof. Dr. Matthias Tschöp
	2. Prof. Dr. Martin Klingenspor

Die Dissertation wurde am 12.09.2018 bei der Technischen Universität München eingereicht und durch die Fakultät für Medizin am 08.10.2019 angenommen.

Eidesstattliche Erklärung

Ich erkläre an Eides statt, dass ich die bei der Fakultät für Medizin zur Promotionsprüfung vorgelegte Arbeit mit dem Titel:

„The Role of Calcium and its Transporter P2RX5 in Brown Adipocyte Function"

am Institut für Diabetes und Adipositas (Helmholtz Zentrum München) unter der Anleitung und Betreuung durch Prof. Dr. Tschöp ohne sonstige Hilfsmittel erstellt und bei der Abfassung nur die gemäß § 6 Abs. 6 und 7 Satz 2 angegebenen Hilfsmittel benutzt habe.

Ich habe keine Organisation eingeschaltet, die gegen Entgelt Betreuerinnen und Betreuer für die Anfertigung von Dissertationen sucht, oder die mir obliegenden Pflichten hinsichtlich der Prüfungsleistungen für mich ganz oder teilweise erledigt.

Ich habe die Dissertation in dieser oder ähnlicher Form in keinem anderen Prüfungsverfahren als Prüfungsleistung vorgelegt.

Die vollständige Dissertation wurde noch nicht veröffentlicht.

Ich habe den angestrebten Doktorgrad noch nicht erworben und bin nicht in einem früheren Promotionsverfahren für den angestrebten Doktorgrad endgültig gescheitert.

Die öffentlich zugängliche Promotionsordnung der TUM ist mir bekannt, insbesondere habe ich die Bedeutung von § 28 (Nichtigkeit der Promotion) und § 29 (Entzug des Doktorgrades) zur Kenntnis genommen. Ich bin mir der Konsequenzen einer falschen Eidesstattlichen Erklärung bewusst.

Mit der Aufnahme meiner personenbezogenen Daten in die Alumni-Datei bei der TUM bin ich einverstanden.

Ort, Datum Ines Pramme-Steinwachs

ACKNOWLEDGEMENTS

After an intense period of learning and researching I would like to thank all the people who supported me and contributed to my work.

In particular, I want to express my sincere appreciation to my mentor Dr. Siegfried Ussar who gave me the opportunity to work in his junior research group and who enabled this scientific work. He promoted my research ideas from the very beginning and trusted in my abilities. Siegfried spared neither cost nor effort to facilitate high level experiments and academic exchange. I am grateful for his outstanding scientific advice and personal support over all these years.

Moreover, I thank my first supervisor Prof. Dr. Matthias Tschöp for the opportunity to conduct my experiments at his well-equipped and modern institute. He always supported scientific and social interaction within and across working groups and thereby created a fruitful and productive environment.

I also want to thank my second supervisor Prof. Dr. Johannes Beckers. He was always at my disposal, asked the right questions and gave helpful support and advises to expedite my scientific progress.

Further appreciation applies to Prof. Dr. Martin Jastroch for his stimulating suggestions and very productive and successful collaboration on our joint publication and beyond.

I owe special thanks to Dr. Francisco Javier Ruiz Ojeda, Dr. Susanne Keipert, Dr. Siegfried Ussar and Thomas Steinwachs for proofreading my doctoral thesis and providing constructive comments.

During the past years, I have received a lot of support from colleagues and friends at the IDO and, particularly, in our research group. I am very grateful for all the inspiring discussions, invaluable comments and all the enjoyable breaks.

Finally, the deepest gratitude goes to my precious family, my beloved husband and to my closest friends, who always supported me and put their faith in my ability to pursue my dreams. Their loving patience and steady support made all of this possible and gave me fresh strength when things got rough. Thank you so much!

TABLE OF CONTENTS

ABBREVIATIONS

2-DG	2-deoxyglucose
A2A	Adenosine receptor 2A
AA	Antimycin A
AdrB1-3	Adrenergic receptor beta 1-3
APS	Ammonium persulfate
ATP	Adenosine-5'-triphosphate
AUC	Area under the curve
BAT	Brown adipose tissue
BCA	Bicinchoninic acid
BG corr.	Background corrected
BMPs	Bone morphogenetic proteins
BMSCs	Bone marrow stromal cells
BSA	Bovine serum albumin
C/ebps	CCAAT/Enhancer Binding Proteins
$CaCl_2$	Calcium chloride
CaSR	Calcium sensing receptor
cDNA	Complementary DNA
Cl	Chloride
CO_2	Carbon dioxide
cre	Cre recombinase
DMEM	Dulbecco's Modified Eagle Medium
DMSO	Dimethyl sulfoxide
DNA	Deoxyribonucleotide acid
DNase	Deoxyribonuclease
DTT	1,4-Dithiothreitol
ECAR	Extracellular acidification rate
ECL	Enhancer chemiluminescence
EDL	Musculus extensor digitorum longus
EDTA	Ethylendiamintetraacetic acid
ELISA	Enzyme-linked immunosorbent assay
ERK	Extracellular signal-regulated kinase
Ex/Em	Excitation/Emission
FBS	Fetal bovine serum
FCCP	Trifluoromethoxy carbonylcyanide phenylhydrazone
fl	Flox (loxP sites)
flp	Flippase recombinase
FRT	Flippase recognition target
GMC	German Mouse Clinic
GTT	Glucose tolerance test
H&E	Haematoxylin Eosin
HCl	Hydrochloride acid
HEPES	4-(2-hydroxyethyl)-1-piperazineethanesulfonic acid
HRP	Horseradish peroxidase
i.p.	Intraperitoneal
IBMX	3-Isobuthyl-1-methylxanthin
Iono	Ionomycin
ISO	Isoproterenol

ITT	Insulin tolerance test
IVC	Individually ventilated cages
KCl	Potassium chloride
KD	Knock down
KH_2PO_4	Potassium dihydrogen phosphate
ko	Knock out
LAP	Liver-enriched activating protein
LIP	Liver-enriched inhibitory protein
Max.	Maximum
MEK (MAPKK)	Mitogen-activated protein kinase kinase
Me-S-ATP	2-Methylthioadenosine-5'-triphosphate tetrasodium salt
$MgCl_2$	Magnesium chloride
MHC	Myosin heavy chain
MOPS	3-(N-morpholino)propanesulfonic acid
Myf5	Myogenic factor 5
Na_2HPO_4	Disodium hydrogen phosphate
NaA	Sodium azide
NaCl	Saline, sodium chloride
NaOH	Sodium hydroxide
NF449	4,4',4'',4'''-[carbonylbis(imino-5,1,3-benzenetriyl-bis(carbonylimino))]tetrakis-1,3-benzenedisulfonic acid
NFAT	Nuclear factor of activated T-cells
NP-40	Nonylphenolethoxylat 40
OCR	Oxygen consumption rate
Oligo	Oligomycin
P2RX1-7	Purinergic ion channel 1-7[1]
P2Y2, 12	Purinergic receptor subtype Y 2, 12

[1] In the literature, P2RXs are accounted to the family of purinergic (P2) receptors as members of ligand-gated ion channels (Webb, Simon et al. 1993; Brake, Wagenbach et al. 1994; Valera, Hussy et al. 1994). In the following, P2RXs are referred to as purinergic ion channels because their structural function and subgroup definition clearly characterize P2RXs as channels but not as receptors.

TABLE OF TABLES

TABLE OF FIGURES

ABSTRACT

Obesity and related disorders, like type 2 diabetes, are major health problems that pose a burden to affected individuals and to society. One potential treatment approach lies in the hyperactivation of the mitochondria-rich brown adipose tissue (BAT). A hyperactivated BAT increases whole body energy expenditure through non-shivering thermogenesis, which improves body composition and health. Cold exposure activates BAT and causes the release of beta-adrenergic agonists from sympathetic nerve vesicles. These agonists increase lipolysis and glucose uptake to deliver electrons for mitochondrial respiration, which generates the energy source ATP. In parallel, they activate uncoupling protein 1 (UCP1), which is a characteristic protein for BAT and uncouples the electron force in the mitochondrial respiratory chain. This results in the production of heat instead of ATP and enables an increased energy turnover in BAT. Besides the beta-adrenergic agonist noradrenaline, ATP has been shown to be co-secreted from sympathetic nerves and to play an important role in regulating BAT activity. Also, calcium regulates mitochondrial enzyme activity and thus is important for BAT activation and thermogenesis. The ATP-dependent calcium channel P2RX5 is specifically expressed in BAT. Studies in beta-less mice have shown that P2RX5 is up-regulated in BAT upon stress stimulation, suggesting P2RX5 as a target for co-activation of BAT.

This study shows that high extracellular calcium during differentiation affects brown adipocyte identity and function *in vitro*. Defects in differentiation occur together with ERK hyperphosphorylation and altered phosphorylation patterns of the C/EBPβ transcription factor isoforms in early adipogenesis. High calcium later in differentiation, impacts brown adipocyte marker gene expression, albeit similar oxidative capacity.

Global P2RX5 knock out mice reveal an improved glucose tolerance and lower basal insulin levels. Moreover, mitochondrial protein content and increased lipolysis in SCF of P2RX5 ko mice suggest induced beiging. Similarly, higher mitochondrial protein content, including UCP1, is observed in BAT of P2RX5 ko mice. *In vitro* data showing improved isoproterenol-stimulated mitochondrial respiration suggest a higher activity of BAT in the absence of P2RX5. An increased expression of the muscle fiber type isoform *Mhc IIa* in TA of P2RX5 ko mice indicates that muscular P2RX5 is of high importance in glucose homeostasis. Secondary effects of P2RX5 loss, like the impact of the skeletal muscle phenotype, are circumvented in BAT-specific P2RX5 ko mice. Here, impaired mitochondrial respiration and reduced glucose transporter mRNAs are observed *in vitro*. However, body composition and glucose homeostasis *in vivo*

remain unaltered. These data suggest that P2RX5 in BAT might be a potential target to hyperactivate BAT. However, P2RX5-specific agonists could result in severe side effects for example due to unintended stimulation of the skeletal muscle.

ZUSAMMENFASSUNG

Adipositas und daraus hervorgehende Krankheitsbilder, wie zum Beispiel Typ 2 Diabetes, stellen ein großes Gesundheitsproblem mit immensen individuellen und gesellschaftlichen Belastungen dar. Eine Behandlungsmöglichkeit besteht in der Hyperaktivierung des braunen Fettgewebes, welches reich an Mitochondrien ist. Ein hyperaktiviertes braunes Fett kann durch sogenannte zitterfreie Thermogenese (Wärmebildung) die gesamtkörperliche Energieumsetzung erhöhen und somit zur Verbesserung von Körperfettkompositionen und Gesundheit beitragen. Kälte setzt beta-adrenerge Agonisten vom sympathetischen Nervensystem frei und aktiviert somit das braune Fett. Die Agonisten induzieren Lipolyse und erhöhen die Glukoseaufnahme, was zur Generierung von Elektronen führt. Diese werden in der mitochondrialen Atmung zur Produktion der Energieressource ATP eingesetzt. Parallel wird das für braunes Fett charakteristische Entkopplungsprotein UCP1 (uncoupling protein 1) aktiviert. UCP1 entkoppelt die mitochondriale Atmungskette und generiert dabei Hitze anstelle von ATP, was einen höheren Energieumsatz innerhalb des braunen Fettgewebes ermöglicht. Neben dem beta-adrenergen Agonisten Noradrenalin ist auch für ATP bekannt, dass es aus Vesikeln des sympathischen Nervensystems sezerniert wird und eine Rolle in der Aktivitätsregulierung des braunen Fettes spielen kann. Auch Calcium zeigt eine regulatorische Rolle bei der Aktivierung mitochondrialer Enzyme. Damit hat es einen Einfluss auf die Aktivierung des braunen Fettes und die Thermogenese. Der ATP-abhängige Calciumkanal P2RX5 ist spezifisch auf braunem Fett exprimiert. Studien in beta-less Mäusen zeigen, dass P2RX5 in braunem Fett hoch reguliert wird, sobald die Mäuse unter einem Stressstimulus stehen. Dies macht P2RX5 zu einem potentiellen Ziel für die Co-Aktivierung des braunen Fettes.

Diese Studie zeigt, dass erhöhtes extrazelluläres Calcium während der Differenzierung die Identität und Funktion von braunen Adipozyten *in vitro* beeinträchtigt. Die Defekte in der Differenzierung treten gemeinsam mit einer Hyperphosphorylierung von ERK sowie veränderten Phosphorylierungsmustern der C/EBPβ Isoformen während der frühen Adipogenese auf. Hohes Calcium in späteren Phasen der Differenzierung beeinflusst die Expression von Genen spezifisch für braune Adipozyten. Dennoch bleibt die Atmungskapazität unverändert.

Globale P2RX5 „knock out“ (ko) Mäuse zeigen verbesserte Glukosetoleranz und niedrigere Insulinlevels im Blut. Zudem treten erhöhte mitochondriale Proteinlevels und Lipolyseraten in subkutanem Fett von P2RX5 ko Mäusen auf, was auf ein induziertes Beiging hindeutet. Weiterhin sind mitochondriale Proteine (inklusive UCP1) auch im braunen Fett von P2RX5 ko

Mäusen erhöht. *In vitro* Daten zeigen, dass in Abwesenheit von P2RX5 die Isoproterenol-stimulierte mitochondriale Atmung erhöht ist. Dies impliziert eine erhöhte Aktivität des braunen Fettes *in vivo*. Eine erhöhte Expression der Muskelfaserisoform *Mhc IIa* suggeriert zudem, dass P2RX5 im Muskel eine wichtige Rolle bei der Glukosehomöostase spielt. Sekundäre Effekte des Verlusts von P2RX5, wie z.B. der Phänotyp des Skelettmuskels im globalen P2RX5 ko, können im Braunfett-spezifischen P2RX5 ko umgangen werden. Hier wiederum wird eine beeinträchtigte mitochondriale Atmung und eine gehemmte Expression von Glukosetranporter-mRNAs *in vitro* festgestellt. *In vivo* jedoch sind Körperfettkomposition und Glukosehomöostase unverändert. Diese Daten zeigen, dass P2RX5 ein mögliches Ziel für die Hyperaktivierung von braunem Fett ist. Dennoch könnte ein spezifischer P2RX5 Agonist zu dramatischen Nebenwirkungen führen, welche durch eine unabsichtliche Stimulation z.B. des Skelettmuskels hervorgerufen werden könnten.

1 INTRODUCTION

1.1 Obesity and related disorders as a major health problem

Obesity is described as an excessive accumulation of adipose tissue, based on a positive energy balance resulting from a mismatch between energy intake and expenditure (Hall, Sacks et al. 2011). While people with a body mass index (BMI) above 25 kg/m^2 are considered overweight, the term obesity applies to people with a BMI above 30 kg/m^2. Obesity is a multifactorial disease to which genetic prevalence and epigenetics as well as environmental factors contribute (Yoshida and Umekawa 1998, Rooney, Mathiason et al. 2011). Besides the increasing appearance of overweight and obesity in low- and middle-income countries, particularly in urban environments (Figure **1**) (WHO 2011, Ng, Fleming et al. 2014), overweight and obesity are mostly associated with sedentary lifestyle and high caloric food intake mainly in western high-income countries (Kushner and Choi 2010).

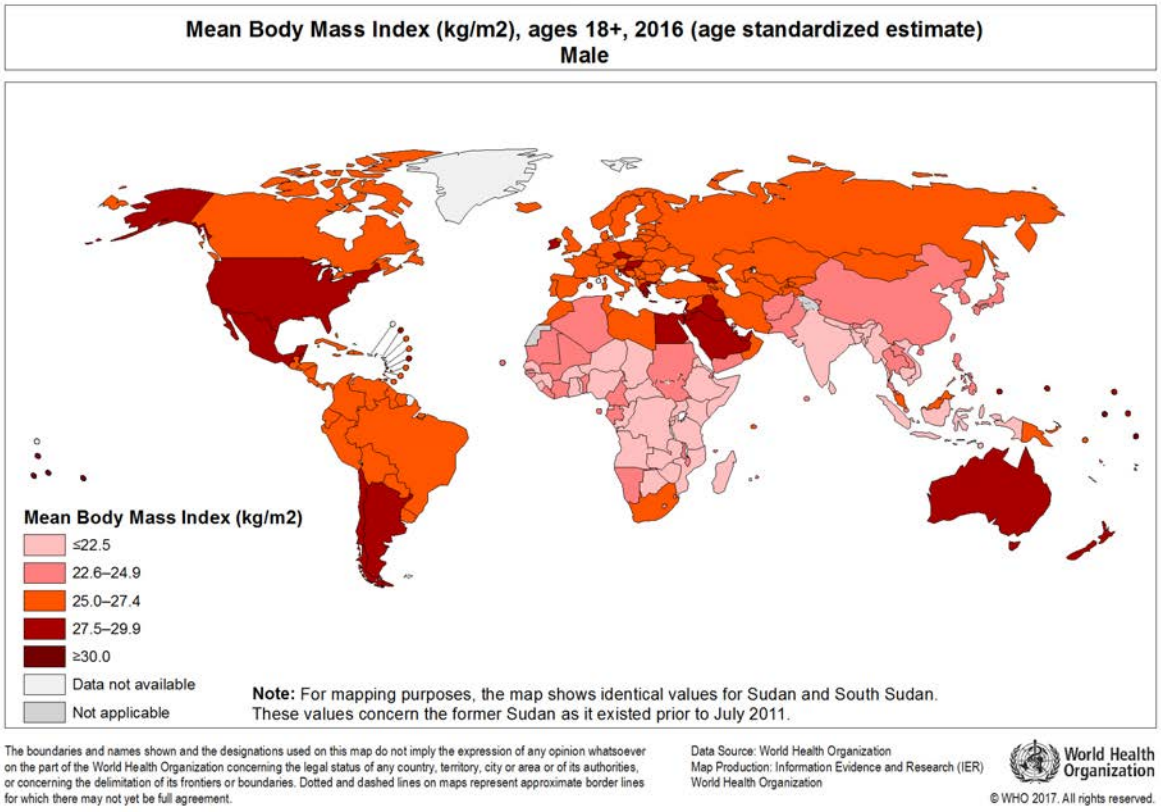

Figure 1 Mean body mass indices of adult males across the world (WHO 2006-2011).

Next to physical disabilities including asthma or sleep apnea, psychological problems are also related to obesity. Furthermore, obesity is associated with metabolic diseases like musculoskeletal disorders, cardiovascular diseases, certain types of cancer and type 2 diabetes. Accordingly, 2.8 million people die of obesity-related diseases per year, turning obesity into a major burden for human health and the healthcare economy (WHO 2017).

1.1.1 Role of adipose tissue in obesity and diabetes

Obesity results from an imbalance between energy intake and energy expenditure. Excess calories are stored as lipids in adipose tissue to serve as an energy source in times of low energy intake. Continuous energy overdose results in accumulating severe amounts of adipose tissue. This results in obesity and potentially in related comorbidities. Distinct types of adipose tissue are observed in human and rodents, which differ dramatically in morphology, function and developmental origin: white adipose tissue (WAT), beige fat and brown adipose tissue (BAT) (Cinti 1999, Cannon and Nedergaard 2004).

1.1.1.1 White adipose tissue and beige fat

WAT is located in the abdomen and under the skin and is distinguished into visceral and subcutaneous adipose tissue. White adipocytes have a unilocular morphology and their primary function is to store triacylglycerols as a source of energy. In addition, WAT serves as a thermal insulation and protects organs from mechanical violation (Frayn, Karpe et al. 2003). WAT secretes smaller bioactive peptides, such as adipokines, and many other metabolites. Thereby it serves as an important endocrine organ (Zhang, Proenca et al. 1994). As a result, WAT influences body energy and glucose homeostasis (Ouchi, Parker et al. 2011). Severe accumulation of triacylglycerols in WAT causes an imbalance in its function, resulting in metabolic syndrome, which is characterized by altered adipokine secretion, lipid spillover into plasma, WAT inflammation and insulin resistance (Schoettl, Fischer et al. 2018).

Previous work has shown, that white adipocytes originate from myogenic factor 5 (Myf5)-negative precursor cells (Seale, Bjork et al. 2008, Walden, Petrovic et al. 2010, Schulz, Huang et al. 2011). More recent data indicate that *myf5*-positive precursor cells also rise within white fat depots, predominantly in visceral adipose tissue depots (Sanchez-Gurmaches and Guertin 2014). Current lineage-tracing experiments suggest the existence of a white preadipocyte subpopulation capable of forming or converting into thermogenic beige adipocytes (i.e. brown-like adipocytes residing within white fat) (Sanchez-Gurmaches and Guertin 2014). The origins of

beige adipocytes however remain under active investigation. Beige adipocytes are characterized by lipid droplet multilocularity and enriched amounts of mitochondria compared to white adipocytes. Upon cold exposure or beta-adrenergic stimulation beige adipocytes appear with higher frequency within the subcutaneous fat (SCF). Upon cold or beta-adrenergic stimulation, beige adipocytes can contribute to negative energy balance due to their thermogenic potential, defined in section 1.1.1.2 (Seale, Conroe et al. 2011).

1.1.1.2 Brown adipose tissue

Different from beige adipocytes, brown adipocytes - just as skeletal muscle cells - originate from distinct, *myf5*-positive precursor cells (Seale, Bjork et al. 2008, Walden, Petrovic et al. 2010, Schulz, Huang et al. 2011). Unlike WAT, the multilocular BAT does not mainly store lipids but rather dissipates energy in the form of heat. This process is mediated by uncoupling protein 1 (UCP1), which is located in the mitochondrial inner membrane. Upon cold exposure or beta-adrenergic stimulation UCP1 is activated and uncouples the electron force of the mitochondrial respiratory chain, resulting in heat instead of ATP production. Thus, the mitochondria-rich BAT plays a significant role in negative energy balance and thermoregulation via non-shivering thermogenesis (Argyropoulos and Harper 2002, Scherer 2006, Fedorenko, Lishko et al. 2012). Hence, BAT is located in the interscapular region of rodents and in periaortic, cervical, interscapular and perirenal regions of infants. Within the last decade, the existence of cold-inducible BAT in the neck and supraclavicular regions of adult humans has also been well established (Skala, Barnard et al. 1970, Nedergaard, Bengtsson et al. 2007, Cypess, Lehman et al. 2009, Saito, Okamatsu-Ogura et al. 2009). The quantity or activation capacity of BAT is negatively correlated with obesity and diabetes in humans (Cypess, Lehman et al. 2009, Saito, Okamatsu-Ogura et al. 2009). Hyperactivating BAT successfully lowers body weight and fat mass, accelerates glucose clearance and improves insulin sensitivity (Orava, Nuutila et al. 2011, Stanford, Middelbeek et al. 2013, Yoneshiro, Aita et al. 2013). These effects are attributed to the metabolic function of BAT.

Negative energy balance and non-shivering thermogenesis

Mice acutely exposed to cold increase non-shivering thermogenesis to maintain their body temperature (Yoneshiro, Aita et al. 2011, Harms and Seale 2013). In humans, cold exposure elevates glucose uptake, measured with radioactively labeled 2-deoxyglucose, which is considered to reflect BAT activity (Nedergaard, Bengtsson et al. 2007, van der Lans, Hoeks et

al. 2013). Cold is sensed by the parasympathetic nerve system. Under the control of the Hypothalamus-pituitary-adrenal (HPA) axis, catecholamines and other signaling molecules are released from sympathetic nerve vesicles within the highly innervated BAT. Noradrenaline binds beta3-adrenergic receptors, which are more frequently expressed on BAT than their beta-adrenergic receptor family members (Collins, Daniel et al. 1994). Beta3-adrenergic stimulation results in increased lipolysis and thermogenic gene expression, increasing *Ucp1* mRNA levels. In parallel, UCP1 is activated by free fatty acids released from lipolysis and uncouples the mitochondrial respiratory chain, resulting in non-shivering thermogenesis. The mitochondrial respiratory chain consists of five oxidative phosphorylation complexes (OXPHOS): complex I (NADH:ubiquinone-oxidoreductase, also: NADH-dehydrogenase), complex II (succinate:ubiquinone-oxidoreductase, also: succinate-dehydrogenase), complex III (ubiquinone-cytochrome c oxidoreductase), complex IV (cytochrome c oxidase) and complex V (ATP synthase) (Figure **2**).

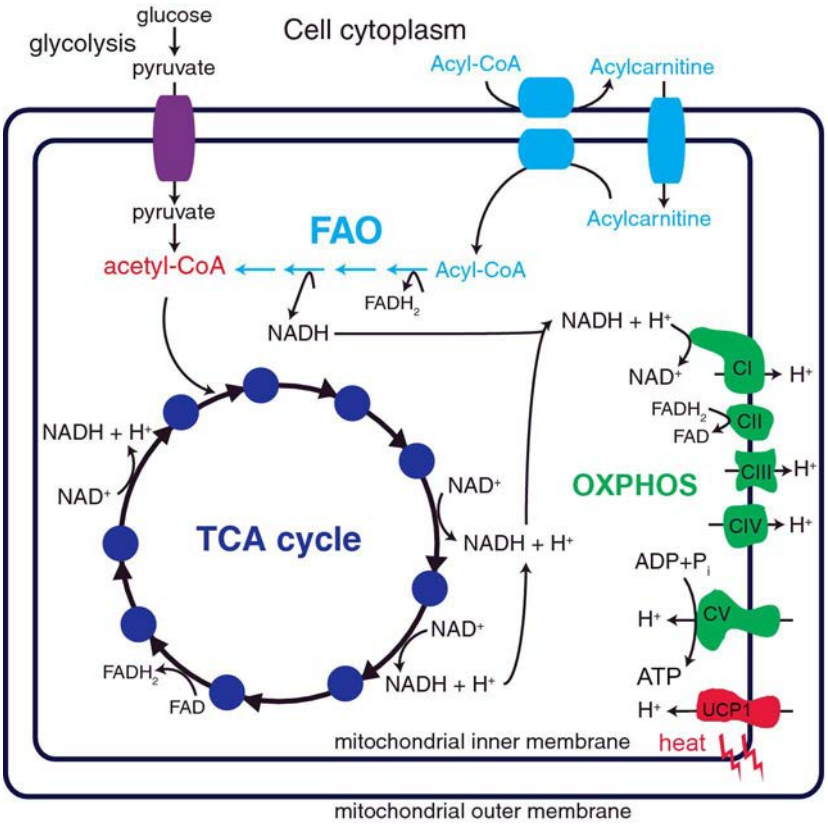

Figure 2 The mitochondrial respiratory chain and the citric acid cycle (also: tricarboxylic acid (TCA) cycle) delivering electron equivalents and protons. *Adapted from the review of Nsiah-Sefaa and McKenzie (2016).*

The citric acid cycle (also: tricarboxylic acid (TCA) cycle) releases electron equivalents and protons in form of $NADH/H^+$ (complex I), $FADH_2$ (complex II) and succinate (complex III). The respective complexes transport the electrons across the mitochondrial inner membrane to complex IV, using iron-sulfur-clusters and ubiquinone. Complex IV oxidizes oxygen (O_2) and uses protons ($2\ H^+$) to generate water (H_2O). In parallel, protons are translocated via ubiquinone from the mitochondrial matrix into the intermembrane space to build a proton gradient. This gradient is necessary for the function of complex V, where ATP is generated by the flux of protons from the intermembrane space back to the mitochondrial matrix through the ATP synthase. In the presence of UCP1, the proton gradient is degraded and heat instead of ATP is produced, leading to non-shivering thermogenesis. This process enables BAT to increase the caloric turnover and thereby to burn excess calories.

Adrenergic signaling in BAT

Adrenergic receptors are broadly expressed on the BAT cell surface, among others, and are part of the G protein-coupled receptor (GPCR) family. Alpha- and beta-adrenergic receptors are bound by catecholamines, resulting in different signaling pathways within the cell. Stimulating alpha1-adrenergic receptors with noradrenaline increases calcium influx from intracellular stores, whereas alpha2-adrenergic receptor activation through adrenaline results in influx inhibition. Upon alpha1-adrenergic receptor stimulation, phospholipase C (PLC) is activated and degrades Phosphatidylinositol-4,5-bisphosphate (PIP2) into diacylglycerol (DAG) and inositol-3-phosphate (IP3). IP3 in turn binds IP3 receptors (IP3R) on endoplasmic/sarcoplasmic reticulum (ER/SR), which are the most important calcium stores in the cell. This enables massive calcium influxes from ER/SR into the cytoplasm. Calcium together with DAG activates protein kinase C (PKC), which is involved in receptor desensitization, lipid homeostasis, mitochondrial function and glucose uptake, among others (Chernogubova, Cannon et al. 2004, Mehta 2014). In parallel, IP3 binding induces calcium efflux from ER into mitochondria via mitochondrial calcium uniporters (MCUs) within mitochondria-associated membrane (MAM) connections. The calcium influx into mitochondria leads to ROS production and modulates the kinetics of glycolysis and TCA cycle enzymes, like pyruvate dehydrogenase (PDH), pyruvate dehydrogenase phosphatase 1 (PDP1) and alpha-ketoglutarate dehydrogenase (α-KGDH) (Denton 2009).

Through binding of catecholamines to beta-adrenergic receptors, the adenylate cyclase (AC) is activated and forms cyclic adenosine monophosphate (cAMP) from ATP. cAMP levels are degraded by phosphodiesterases (PDE) while increased calcium levels support adenylate

cyclase activation and cAMP binding to protein kinases A (PKA). PKAs phosphorylate and activate mitogen-activated protein kinase kinases (MKKs), like protein 38 (p38), and key lipolytic proteins, like adipose triglyceride lipase (ATGL), hormone-sensitive lipases (HSL) and the lipid droplet-associated protein perilipin (PLIN) (Miyoshi, Souza et al. 2006, Krintel, Morgelin et al. 2009, Pagnon, Matzaris et al. 2012). Activated p38 phosphorylates the transcription factor peroxisome proliferator-activated receptor gamma (PPARγ) coactivator 1-alpha (PGC1-α) (Fernandez-Marcos and Auwerx 2011), which is one of the most important regulators in mitochondrial biogenesis. P*gc1-α* expression is induced by the transcription factor PPARγ, which also induces *Ucp1* expression. In parallel, free fatty acids generated through lipolysis activate UCP1, driving non-shivering thermogenesis. PKA is also considered to interact with the insulin signaling pathway by phosphorylating phosphatidylinositol-3-kinase (PI3K). PI3K in turn activates PKC and thereby increases glucose uptake via glucose transporter 4/1 (GLUT4/GLUT1)-dependent mechanisms in BAT. This explains the delta in glucose uptake in BAT upon cold and insulin stimulation (Chernogubova, Cannon et al. 2004, Orava, Nuutila et al. 2011).

Taken together, beta-adrenergic stimulation itself increases glucose uptake and elevates non-shivering thermogenesis. Additionally, experiments with noradrenaline and the beta-adrenergic receptor-specific antagonist propranolol have shown that propranolol reduces noradrenaline-stimulated glucose uptake completely in humans and rodents (Tatsumi, Engles et al. 2004, Jacobsson, Bruzelius et al. 2005). This indicates that glucose uptake is regulated independently of alpha-adrenergic receptors, suggesting beta-adrenergic signaling as the main driver of glucose uptake and non-shivering thermogenesis in BAT. So far, beta-adrenergic receptors on BAT seem to be the main target for hyperactivation to improve energy expenditure.

1.2 Role of calcium in obesity and diabetes[2]

Calcium is the most abundant ion in the body, regulating key cellular functions, including lineage commitment and differentiation. Increased extracellular calcium inhibits adipogenesis in classical white adipocytes (Neal and Clipstone 2002), whereas it promotes differentiation of white adipocytes from bone marrow-derived stem cells (BMSCs) (Hashimoto, Katoh et al. 2012,

[2] The following section is published in Pramme-Steinwachs, I., M. Jastroch and S. Ussar (2017). "Extracellular calcium modulates brown adipocyte differentiation and identity." Sci Rep **7**(1): 8888. Text is in parts adapted and revised.

Mellor, Mohiti-Asli et al. 2015). Calcium signaling is also of critical importance for controlling mitochondrial function of brown adipocytes (Denton 2009, Golic, Velickovic et al. 2014, Hou, Kitaguchi et al. 2017). Nevertheless, surprisingly little is known about its role in brown adipocyte differentiation.

1.2.1 Calcium concentration regulation

Calcium regulates essential body functions, such as calcification of bones, neuronal transmission, muscle contraction, insulin release and many more (Szent-Györgyi 1975, Draznin 1988, Simons 1988, Agata, Park et al. 2013). Thus, its intracellular and extracellular concentrations are highly regulated. The usual calcium concentration in human blood is 2.2 - 2.7 mM in total. 10% of calcium are bound in complexes with citrate, phosphate or bicarbonate, 40% are bound by proteins, namely albumin (80 - 90%) and globulins (10 - 20%), and 50% occur in ionic form as free calcium (approx. 1.1 - 1.4 mM) (Schaafsma 1988, Goldstein 1990). The calcium homeostatic system in the blood is strictly regulated by many factors, including steady pH, magnesium and phosphate levels, albumin configuration, parathyroid hormone (PTH) and calcitonin content as well as vitamin D availability. For instance, a drop in ionic calcium concentration (hypocalcemia) increases PTH serum levels. PTH together with vitamin D releases calcium from extracellular fluid of bones. Vitamin D further enables intestinal absorption and bone and tubular reabsorption of calcium. PTH secretion is also regulated by magnesium and its action on calcium release in bones is counteracted by calcitonin. In addition, phosphate buffers ionic calcium in complexes (Copp, Cameron et al. 1962, Goldstein 1990). Importantly, calcium concentrations are only half as high in interstitial fluids compared to blood (Schaafsma 1988).

In contrast to the high calcium levels in interstitial fluid, the cytosolic calcium concentration within cells is more than 10,000 times lower (50 - 100 nM) regardless of calcium levels in intracellular stores, like the endoplasmic reticulum (ER) and the sarcoplasmic reticulum (SR) (Goldstein 1990). Accordingly, calcium does not easily enter cells and its entry is highly regulated via several different types of voltage-gated calcium channels (VGCCs) and ligand-gated calcium channels, including the purinergic ion channels (P2RXs)[3] and store-operated

[3] In the literature, P2RXs are accounted to the family of purinergic (P2) receptors as members of ligand-gated ion channels (Webb, Simon et al. 1993; Brake, Wagenbach et al. 1994; Valera, Hussy et al. 1994). In the following, P2RXs are referred to as purinergic ion channels because their structural function and subgroup definition clearly characterize P2RXs as channels but not as receptors.

channels (SOCs) (Gever, Cockayne et al. 2006, Catterall 2011, Prakriya and Lewis 2015). Depending on the channels involved in calcium entry, cells are flooded or spiked with calcium influxes, resulting in different intracellular actions (Kar, Nelson et al. 2012). As described earlier, GPCRs increase intracellular calcium levels via IP3-mediated calcium release from the ER/SR, flooding the cytosol and nucleus. An increasing number of studies show that, in addition to ER calcium release, local calcium influxes are very important for specific actions in the cell (Zhang, Yeromin et al. 2006, Kar, Nelson et al. 2012). Indeed, calcium entry via calcium release-activated calcium channels (CRACs) is observed upon stromal interaction molecule 1 (STIM) and calcium-selective channel Orai interaction. STIM senses the decrease of ER calcium levels and binds Orai located in the plasma membrane (PM). This results in direct calcium influx and store-operated calcium entry via ER/PM junction as well as in site-specific activation of calcium-dependent enzymes, like calcineurin (Kar, Nelson et al. 2011, Zhou, Nwokonko et al. 2018). P2RXs activate calcium entry via VGCCs to modulate calcium-mediated secretion (Tomic, Jobin et al. 1996, Hansen, Krabbe et al. 2008).

1.2.2 Calcium-related disorders

To this end, it is not surprising that serum calcium levels are tightly regulated and alterations can have detrimental consequences for human health (Bonny and Bochud 2014, Davies 2015, Marcelo, Means et al. 2016). Deficiency in PTH and vitamin D can cause hypocalcemia, which can cause psychiatric diseases, lens degeneration, dystrophic calcifications in teeth, hair and nails and cardiac and neuronal dysfunction, among others (Goldstein 1990). Hypercalcemia, on the other hand, is a sporadic or familial disorder, resulting in elevated protein-bound calcium (pseudohypercalcemia) or in increased ionized calcium levels in the blood. Hyperparathyroidism, vitamin D/A excess and sarcoidosis, among others, can cause hypercalcemia, which results in soft tissue calcification, renal and gastrointestinal diseases as well as in brain syndrome and cardiovascular abnormalities (Goldstein 1990). In infants, hypercalcemia is one of the most dangerous complications following visceral fat necrosis right after birth (Michael, Hong et al. 1962, Lara, Villa et al. 2017).

Nevertheless, local interstitial calcium concentrations are much less studied, even though changes have dramatic consequences. There is limited knowledge about the role of extracellular calcium fluctuations in obesity. However, vitamin D, which is essential for intestinal absorption and bone reabsorption of calcium, is reduced in obese subjects (Park, Park et al. 2015). *In vitro* studies in BMSCs reveal that elevated extracellular calcium results in increased

adipocyte formation (Hashimoto, Katoh et al. 2012, Hashimoto, Katoh et al. 2015). Thus, serum calcium levels and, consequently, interstitial calcium levels are supposed to influence adipogenesis in bone marrow. Moreover, alterations in cytosolic calcium levels are associated with adipocyte dysfunction, obesity and the metabolic syndrome (Guerrero-Hernandez and Verkhratsky 2014, Arruda and Hotamisligil 2015). Nevertheless, the impact of altered interstitial calcium on (brown) adipose tissue function has not been addressed in detail yet.

1.2.3 Calcium in adipogenesis

Various extrinsic (Ma, Yu et al. 2012, Vosselman, van der Lans et al. 2012, Bahler, Molenaars et al. 2015) and endocrine factors (Watanabe, Yamamoto et al. 2008, Whittle, Carobbio et al. 2012, Gnad, Scheibler et al. 2014), such as ambient temperature, bone morphogenetic proteins (BMPs) among others, modulate brown adipocyte differentiation and activity. Interestingly, relatively little is known about how the local microenvironment, comprising the extracellular matrix, proximity to blood vessels and local concentrations of nutrients, regulates (brown) adipocyte differentiation and function. In white adipocytes, elevated calcium, extracellular or intracellular, reveals contradicting results concerning adipogenesis and white adipocyte function. Elevated intracellular calcium levels during early differentiation inhibit *Pparγ* induction and triglyceride accumulation in both human (Shi, Halvorsen et al. 2000) and murine (Neal and Clipstone 2002) white preadipocytes. These effects are most likely mediated through calcium-dependent activation of calcineurin (Neal and Clipstone 2002) and calcium/calmodulin-dependent kinases (Lin, Ribar et al. 2011) in an ERK-dependent manner, inhibiting expression of early adipogenic transcription factors, like *C/ebpβ* (Neal and Clipstone 2002, Dougherty, Ritt et al. 2009). Adipocyte differentiation is also inhibited upon elevated extracellular calcium concentration, without affecting intracellular calcium levels (Jensen, Farach-Carson et al. 2004). In contrast, elevating intracellular calcium concentration later in adipocyte differentiation promotes lipogenesis and adipocyte marker gene expression (Shi, Halvorsen et al. 2000). These effects of extra- and intracellular calcium on adipogenesis seem specific to “classical” white adipocytes, as treatment of bone marrow stromal cells (BMSCs) with high extracellular and intracellular calcium accelerates proliferation and differentiation into adipocytes (Hashimoto, Katoh et al. 2012). This differential impact of calcium on the differentiation of BMSCs and white preadipocytes suggests that altering the local calcium concentration may have a specific impact on individual preadipocyte populations. However, the impact of varying extracellular calcium concentrations on brown adipocyte differentiation and function has not been studied so far.

1.3 Measures to treat obesity

1.3.1 Natural strategies and complications

Strategies to prevent obesity and promote human health include improving nutritional education, increasing taxes for unhealthy food (high-sugar, energy-dense nutrient-poor products), regulating food marketing and promoting physical activity (PAHO 2014), but turn out more complicated. For instance, lowering caloric intake or increasing exercise in adult humans shows little sustainable success in clinical trials (Johnson and Drenick 1977, Franz, VanWormer et al. 2007) and keeping reduced bodyweight seems difficult. Former-obese subjects feel hungrier despite food intake comparable to never-obese controls, exhibiting also a reduced metabolism and a predisposition for a positive energy balance. This phenomenon is also shown in mice (Leibel, Rosenbaum et al. 1995, Fischer, Irmler et al. 2018).

1.3.2 Surgical and pharmacological reduction of energy uptake

Drugs, such as sibutramine affecting the satiety center in the brain, or orlistat decreasing the intestinal absorption efficacy, successfully reduce body weight (Kushner and Manzano 2002, Early, Apovian et al. 2007). However, continuous application showed also increasing risks for gastrointestinal and cardiovascular diseases (Kolanowski 1999, Siebenhofer, Jeitler et al. 2016). Also, bariatric surgeries show promising impacts on weight loss and metabolic health. However, it is often correlated with postoperative complications, such as infections, bleeding and leak (Daigle, Brethauer et al. 2018). For sustainable success in combatting existing obesity, medical treatments targeted at increasing energy expenditure instead of reducing energy intake are of relevance.

1.3.3 Stimulating energy expenditure

Due to its beneficial function regarding energy balance and glucose homeostasis, BAT is considered a potential target-candidate to treat diabetes and obesity. So far, drugs increasing energy expenditure pharmacologically also reveal side effects on the cardiovascular system, described in detail below (Vosselman, van der Lans et al. 2012, Cypess, Weiner et al. 2015). Therefore, more investigation regarding alternative targets is needed.

1.3.3.1 Adrenergic agonists and their risks

As the beta-adrenergic receptor signaling is responsible for glucose uptake and non-shivering thermogenesis induction in BAT, possible treatment strategies focus on beta-adrenergic receptors. While the natural agonist noradrenaline stimulates also alpha-adrenergic receptors, agonists specific for beta-adrenergic receptors have been designed. Isoproterenol (also: isoprenaline (ISO)) increases lipolysis and mitochondrial uncoupling in *in vitro* studies (Meyers, Skwish et al. 1997). In humans, systemic administration of isoproterenol increases energy expenditure to an extent comparable with cold exposure. However, no changes in glucose uptake in BAT are observed upon isoproterenol stimulation, suggesting a systemic, non-selective action of isoproterenol rather than a BAT-specific activation (Vosselman, van der Lans et al. 2012). Indeed, systemic stimulation of beta-adrenergic receptors boosts heart rate and blood pressure. However, chronic beta-adrenergic receptor stimulation causes severe side effects in the cardiovascular system, like myocardial damages and cardiac hypertrophy (Taylor and Tang 1984, Metrich, Lucas et al. 2008).

Reduced side effects are expected with sympathomimetics, such as ephedrine. However, systemic ephedrine treatment just results in minor effects on energy expenditure compared to mild cold exposure in human BAT (Cypess, Chen et al. 2012, Carey, Formosa et al. 2013). More selective treatments, like the beta3-adrenergic receptor agonists BRL 37344 and CL316,243, seem more promising. A significant increase in BAT glucose uptake is observed but no effects on blood pressure and heart rate are detected upon CL316,243 treatment in humans (Weyer, Tataranni et al. 1998, Chernogubova, Cannon et al. 2004). Different to humans, CL316,243 in rodents also increases thermogenesis and lipolysis in white fat and thus has anti-obesity and anti-diabetic effects (Umekawa, Yoshida et al. 1997). These differences in response are observed also for other beta3-adrenergic receptor agonists. This potentially attributes to different beta3-adrenergic receptor sequences, expression frequencies and receptor efficacies in humans compared to rodents (Larsen, Toubro et al. , Strosberg 1997, Takakura and Yoshida 2001). One promising anti-obesity candidate is the beta3-adrenergic receptor agonist mirabegron (Myrbetriq, Astellas Pharma), an approved drug to treat overactive bladder. It successfully stimulates thermogenesis in human BAT of healthy male subjects in a dose four times higher than originally approved (Cypess, Weiner et al. 2015). However, side effects, such as tachycardia - especially under chronic and higher dose treatment -, need to be considered, and the reproducibility with respect to differences in sex, age and body health are still under

investigation (Cypess, Weiner et al. 2015). Conclusively, beta3-adrenergic signaling is supposed to play the major role in glucose uptake and non-shivering thermogenesis in BAT. However, species-specific side effects and functions are observed. Thus, alternative ways to hyperactivate BAT must to be considered.

1.3.3.2 ATP as a co-activator of BAT

Both cold and beta-adrenergic agonists enhance thermogenesis in BAT, whereas beta-adrenergic agonists alone cannot fully mimic cold-induced BAT activity without dramatic side effects due to low specificity (Cypess, Chen et al. 2012, Vosselman, van der Lans et al. 2012). In addition, beta-adrenergic receptor knock out (beta-less) mice do not show a complete reduction in BAT and BAT activity (Razzoli, Frontini et al. 2016). Upon cold or stress stimulation, the brown fat of beta-less mice regains in parts its original morphology and function. This suggests that beta-adrenergic signaling is supported by an additional signaling pathway. Upon cold or other stress stimulation, ATP is co-secreted from sympathetic nerve vesicles with beta-adrenergic agonists, like noradrenaline. ATP is thought to induce UCP1 expression and lipolysis in brown adipocytes *in vitro* (Schodel, Weise et al. 2004) and to synergistically activate thermogenesis in mice (Razzoli, Frontini et al. 2016). Purinergic receptors (P2s) are broadly expressed on brown adipocytes. They are distinguished into two classes: nucleotide-activated G protein-coupled (P2Y) receptors, comprising P2RY1, 2, 4, 6 and 11-14, as well as purinergic ion channels (P2RXs), comprising P2RX1-7 (Webb, Simon et al. 1993, Brake, Wagenbach et al. 1994, Valera, Hussy et al. 1994). While activating P2Y receptors leads to calcium influx from intracellular calcium stores, like the endoplasmic/sarcoplasmic reticulum (Fischer and Krugel 2007), binding to P2RXs gates extracellular calcium into the cytoplasm, as investigated with several purinergic agonists and antagonists in the presence and absence of extracellular calcium (Pappone and Lee 1996, Wu and Mori 1999, Coddou, Yan et al. 2011). Calcium, as a second messenger, is responsible for many cellular processes, including lipolysis and mitochondrial respiration (Denton 2009, Rapold, Wueest et al. 2013). The purinergic calcium channel P2RX5 shows a high specificity for calcium-inward currents and ATP-binding (Wildman, Brown et al. 2002). Jointly with its specific expression in brown compared to white adipose tissue (Ussar, Lee et al. 2014), P2RX5 is seen as a potential regulatory site in BAT activation and thus as a potential drug target to treat obesity and diabetes.

1.4 The ATP-dependent calcium channel P2RX5 as a potential anti-obesity and anti-diabetic target

1.4.1 Structure and channel function

The P2RXs protein structures are highly conserved. In fact, the protein structure of P2RX2 and P2RX4 are very well established and allow structural and functional comparison with P2RX5 (Nicke, Baumert et al. 1998, Barrera, Ormond et al. 2005, Silberberg and Swartz 2009, Browne, Jiang et al. 2010). P2RX5 homo- or heterotrimerizes with other P2RXs and consists of two transmembrane domains, which form a cation–selective ion channel and an ATP-binding extracellular loop. ATP-binding, in micromolar concentrations, activates the channel by changing its conformation such that mainly calcium is gated through the pore-forming transmembrane domain into the cytoplasm. This activation phase is followed by a desensitizing phase, which is characteristic for the respective channels and very similar across P2RX2 and P2RX5 (Garcia-Guzman, Soto et al. 1996). The very long desensitizing phase of P2RX5 is regulated by modulations at the intracellular C-terminus. The protein length varies from 30 to 215 amino acids (P2RX5: ca. 100 amino acids), with no high similarity between the different channel types. The intracellular N- and C-termini form sites for post-translational modification, like phosphorylation through PKA and PKC; solely for P2RX5 there are two PKC binding sites at the N-terminus and two sites at the extracellular loop (Surprenant, Buell et al. 1995, Garcia-Guzman, Soto et al. 1996). This suggests a modulatory role of PKC in P2RX5 desensitization and a potential interaction between beta3-adrenergic and purinergic signaling. Another regulatory mechanism is the interaction with phospholipids (phosphoinositides - PIP_n) (North 2002, Bernier, Ase et al. 2013). However, pharmacological depletion of PIP_n does not affect the ion traffic through the P2RX5 homotrimer but through the P2RX5/P2RX1 heterotrimer (Ase, Bernier et al. 2010). The N-terminus (25 amino acids) also serves as a site for post-transcriptional modification like splicing, which might also affect desensitization and ATP-binding affinity (Brandle, Spielmanns et al. 1997, Townsend-Nicholson, King et al. 1999). All in all, upon ATP-binding, P2RX5 mediates long-lasting extracellular calcium influxes (long desensitization phase), which are supposed to regulate BAT activity via site-specific signaling.

1.4.2 P2RX5 expression and cellular function

The highly regulated calcium influx via P2RX5 leads to depolarization that activates VGCCs which in turn further increase intracellular calcium levels. Intracellular calcium acts as a second

messenger by interacting with many cellular signaling pathways, mainly by stabilizing or inducing enzyme activity. This includes adenylate and guanylate cyclase, PKCs, several calcium/calmodulin kinases, the calcium/calmodulin-dependent phosphatase calcineurin and many more (Neal and Clipstone 2002, Lin, Ribar et al. 2011, Pfeifer, Kilic et al. 2013). These pathways modulate - among other functions - cell proliferation, differentiation, lipid homeostasis, mitochondrial function and glucose uptake in adipocytes (Neal and Clipstone 2002, Ryten, Dunn et al. 2002, Chernogubova, Cannon et al. 2004, Lin, Ribar et al. 2011, Pfluger, Kabra et al. 2015). These specific actions in intracellular signaling could be regulated additionally by respective enzymes recruited to the N- and C-termini of either P2RX5 or its potential heterotrimerization partners P2RX1, P2RX2 or P2RX4 in BAT (Roger, Pelegrin et al. 2008, Compan, Ulmann et al. 2012).

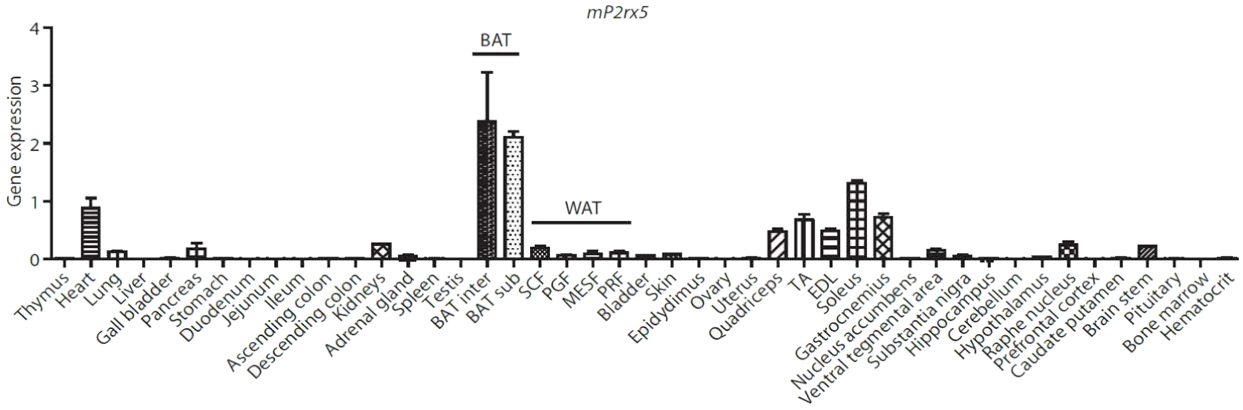

Figure 3 P2rx5 expression in several murine tissues (Ussar, Lee et al. 2014).

P2RX5 is mainly described in functions including ATP-mediated synaptic transmission and intercellular communication between neurons and glial cells (Collo, North et al. 1996, Lalo, Pankratov et al. 2008). Besides its role in regulating skeletal muscle satellite cell differentiation via MAPK signaling, little is known about the function of P2RX5 in differentiating tissues other than skeletal muscle, although it is also expressed in epithelial cells of mucosa, gut, bladder, ureter and skin. Furthermore, it is expressed in heart, pancreas, human duct cells and certain types of cancer cells as well as in spinal cord, adrenal gland, macrophages and tooth pulp (Garcia-Guzman, Soto et al. 1996, Le, Paquet et al. 1997, Groschel-Stewart, Bardini et al. 1999, Meyer, Groschel-Stewart et al. 1999, Ryten, Hoebertz et al. 2001, Inoue, Denda et al. 2005, Layhadi and Fountain 2017, Lee, Jo et al. 2017). In humans, *P2rx5* expression is higher in tissues related to the immune system, like spleen, bone marrow, thymus, lymph node and

leukocytes (Le, Paquet et al. 1997). Importantly, the highest expression of murine *P2rx5* is shown in brown, but not in white adipose tissue (Figure 3) (Ussar, Lee et al. 2014, Torriani, Srinivasa et al. 2016), suggesting an important role in brown fat with respect to its specificity and potential function.

1.4.3 Role of P2RX5 in BAT

So far, little is known about the role and function of P2RX5 in BAT signaling and activity regulation. *P2rx5* is very lowly expressed in brown preadipocytes, but its expression increases with brown preadipocyte differentiation *in vitro* (Ussar, Lee et al. 2014). In mice, *P2rx5* expression is increased in BAT upon exposure to cold. Beta3-adrenergic activation with CL316,243 additionally increases *P2rx5* expression in SCF, which is in line with increased accumulation of brown-like adipocytes (Ussar, Lee et al. 2014). In contrast, *P2rx5* expression decreases with obesity, thermoneutrality and beta-adrenergic deficiency (beta-less mice), in accordance with reduced BAT appearance and activity and *Ucp1* expression (Ussar, Lee et al. 2014, Razzoli, Frontini et al. 2016). However, *P2rx5* expression can partially be rescued in BAT of beta-less mice upon or chronic subordination stress (CSS), one form of chronic psychosocial stress, in accordance with *Ucp1* expression. Thus, P2RX5 is suggested as a marker gene for brown adipocytes in BAT (Ussar, Lee et al. 2014, Torriani, Srinivasa et al. 2016) and SCF (Garcia, Roemmich et al. 2016, Gozal, Gileles-Hillel et al. 2017). Due to its very specific expression on brown and brown-like adipocytes and due to its regulatory function in calcium influx, P2RX5 is also suggested as a candidate for BAT co-activation (Razzoli, Frontini et al. 2016).

1.5 Aim of work

The aim of this work is to find new safe and effective activators of BAT to offer a therapeutic approach for increasing energy expenditure, which results in loosing body fat and restoring metabolic health. The overarching aim of this project is to define the role of the brown adipocyte-specific purinergic calcium channel P2RX5 in the sympathetic nervous control of BAT function. Mice lacking P2RX5, specifically in BAT or in the whole body, are characterized phenotypically and metabolically to unravel the role of P2RX5 in BAT and in the whole organism. As P2RX5 is a calcium channel, the influence of extracellular calcium on brown adipocyte identity and function is investigated. *P2rx5* expression increases with brown adipocyte differentiation. Thus, the influence of varied extracellular calcium concentrations on brown

adipocyte differentiation is studied in detail. Overall, the main aim is to define the role of the brown adipocyte-specific calcium channel P2RX5 as a potential regulator of brown fat activity with respect to its function in calcium influx and calcium signaling.

2 MATERIALS

Table 1: Chemicals and compounds

Compounds	Company	Catalogue number
2-3,3'-5 Triiodothyronine sodium salt (T3)	Calbiochem	64245-250MG
2-Deoxy-D-glucose	Alfa Aesar	207338
2-Methylthioadenosine triphosphate	Tocris Bioscience	1062/10
3-Isobuthyl-1-methylxanthin (IBMX)	Sigma-Aldrich	I5879-1G
Acetic Acid	AppliChem	A0661
Agarose	Sigma-Aldrich	A9539-500G
Ammonium persulfate (APS)	Serva	13375.01
Ammonium sulfate (H8N2SO4)	Acros organics	205872500
Antimycin A	Sigma-Aldrich	A8674-25mg
Beta-mercaptoethanol	Carl Roth	4227.3
Bovine serum albumin (BSA) fraction V	Carl Roth	T844.2
Bovine serum albumin essentially fatty acid free	Sigma	A6003
Calcium chloride ($CaCl_2$)	Carl Roth	CN93.1
Chromotrope II R (Eosin)	Alfa Aesar	A17519.14
Collagenase type IV	Gibco by life technologies	17104019
D(+)-Glucose wasserfrei CELLPURE®	Carl Roth	HN06.4
Dexamethasone	Sigma	D4902
Dimethyl sulfoxide (DMSO)	Carl Roth	A994.3
Dithiothreitol (DTT)	VWR lifesciences	0281-5G
DMEM, low glucose, pyruvate	Gibco by life technologies	31885-023
DMEM, high glucose, no glutamine, no calcium	Gibco by life technologies	21068
DMEM, high glucose, GlutaMAX™, pyruvate	Gibco by life technologies	31966-021
EDTA disodium salt dihydrate	Carl Roth	8043.1
Ethanol (99 %)	Merck Millipore	1.009.832.500
EZ-RUN Recombinant Protein Ladder	Fisher Scientific	10785674
FBS	Gibco by life technologies	10270-106
FCCP	Tocris bioscience	0453
FK506 (calcineurin inhibitor)	Abcam	Ab120223
Fluo-4 AM	Thermo Scientific	#F14201
Formaldehyde solution 37 %	Carl Roth	4979.1
Glucose solution (20 %; for GTT)	b.braun	4164483
GlutaMAX™-1	Gibco by life	35050-038

Compounds	Company	Catalogue number
	technologies	
Glycerol	Sigma Aldrich	15523-1L-R
Glycine	Carl Roth	3908.2
Hematoxylin (Mayer)	Merck	1092490500
Hepes-Na	Merck Millipore	1.152.310.025
Hydrochloric acid (HCl 37 %)	Sigma Aldrich	30721-1L-GL
Immobilon TM Western Chemiluminescent HRP Substrate	Merck Millipore	WBKLS0500
Indomethacin	Santa Cruz Biotechnology	Sc-200503A
Insulin (Actrapid Penfill; for ITT)	Novo Nordisk	00536427
Insulin (cell culture)	Sigma-Aldrich	I9278-5ml
Ionomycin calcium salt	Fisher Scientific	10429883
Iso-Pentane	VWR Chemicals ProLab®	24872.260
Isopropanol	Sigma-Aldrich	33539-2.5L
Isoproterenol hydrochloride	Sigma-Aldrich	16504
iTaq Universal SYBR® Green Supermix	BioRad	172-5124
Ketamine	Pharmanovo GmbH	
Magnesium chloride hexahydrate(MgCl2*6H2O)	Carl Roth	2189.2
Methanol	Merck Millipore	1-06009.2500
MOPS Pufferan R	Roth	6979.4
NF449 (P2RX inhibitor)	Tocris Bioscience	1391
Normocin	InvivoGen	Ant-nr-1
NP-40	abcam	ab142227
Oil Red O powder	Alfa Aesar	A12989
Oligomycin	Sigma	O4876
Paraffin wax (Paraplast)	Leica Surgipath	39601006
Paraformaldehyde	Carl Roth	0335.2
PCR clean H_2O	Millipore	H20MB101
PD 0325901 (MEK inhibitor)	Sigma-Aldrich	PZ0162
Penicillin-Streptomycin (PenStrep)	Thermo Fischer Scientific	15140-122
peqGREEN DNA/RNA Dye	peQlab	37-5000
Phosphatase-inhibitor cocktail II	Sigma-Aldrich	P5726-1ml
Phosphatase-inhibitor cocktail III	Sigma-Aldrich	P0044-5ml
Phosphate buffered saline (PBS)	Gibco by life technologies	14190-094
Pierce R IP lysis buffer	Thermo Scientific	87788
Platinum Green master mix (2x) (PGMM)	LIFE Technologies	13001014
Pluronic F-127	Biotium	59005
PolyFect	Qiagen	301107

Compounds	Company	Catalogue number
Potassium dihydrogen phosphate (KH_2PO_4)	Carl Roth	3904.2
Potassium chloride (KCl)	Carl Roth	6781.1
PPADS tetrasodium salt (P2 receptor inhibitor)	Santa Cruz	sc-202770
Probenecid	Santa Cruz	Sc-202773A
Protease-inhibitor cocktail	Sigma-Aldrich	P8340-5ml
Puromycin hydrochloride	Biomol	Cay13884-500
QIAzol	Qiagen	79306
Quick-Load® 2-Log DNA Ladder (0.1-10 kb)	BioLabs	N0469
Rosiglitazone	Santa Cruz Biotechnology	sc-202795
Rotenone	Sigma Aldrich	R8875-1G
Roti®-Histokitt II	Carl Roth	T160.1
Rotiphorese® Gel 30	Carl Roth	3029.2
Sample buffer (4x)	Life technologies	NP0008
Sodium chloride (NaCl)	Carl Roth	3957.1
Sodium chloride solution (0,9 %; for injection)	Fresenius Kabi Deutschland	808765
Sodium dodecyl sulfate (SDS) Pellets	Carl Roth	CN30.3
Sodium hydroxide (NaOH)	Carl Roth	6771.3
Sodium phosphate (Na_2HPO_4)	Acros organics	204855000
Sodium pyruvate (powder)	Sigma-Aldrich	P2256-5G
Sodium pyruvate (solution)	Gibco by life technologies	11360070
SuperSignal R West FEMTO Max. Sensitivity Substrate	Thermo Fisher Scientific	34095
Temed	AppliChem	A1148,0100
TissueTek O.C.T.™	Sakura	4583
Tri-sodium citrate dihydrate	Carl Roth	4088.3
Trichloroform	Carl Roth	4423.1
TRIS PUFFERAN®	Carl Roth	4855.1
Triton™ X-100	Sigma Aldrich	N150
Tween-20	Santa Cruz Biotechnology	Sc-29113
XF Assay Medium Modified DMEM (for seahorse)	Seahorse Bioscience	102365-100
Xylacin as hydrochloride (20mg/ml)	Proxylaz, bela-pharm	
Xylol	Carl Roth	9713.5

Table 2: Genotyping primer sequences 5'-3'

Target gene	Forward sequence	Reverse sequence	Size (bp)

Target gene	Forward sequence	Reverse sequence	Size (bp)
P2rx5 fl^{-}	TCTGGGATGTGGCAGACTTT	CTACACCAGGGCAGCTATGA	316
P2rx5 fl^{+}	TCTGGGATGTGGCAGACTTT	CTACACCAGGGCAGCTATGA	379
Ucp1cre^{-}	CAAGGGGCTATATAGATCTCCC	GTTCTTCAGCCAATCCAAGGG	554
Ucp1cre^{+}	CAAGGGGCTATATAGATCTCCC	ATCAGAGGTGGCATCCACAGGG	336
P2rx5 wt	ATATTGCTGGCCCTGCTATGT	CGTTCTGCAGTCAGTGTGCTA	660
P2rx5 ko	ATATTGCTGGCCCTGCTATGT	CAACGGGTTCTTCTGTTAGTCC	582

Table 3: qPCR primer sequences 5'-3'

Target gene	Forward sequence	Reverse sequence
Acta2	CTGTCAGGAACCCTGAGACGC	GGATGGGAAAACAGCCCTGG
AdrB1	CCGTCGTCTCCTTCTACGTG	CTCGCAGCTGTCGATCTTCT
AdrB2	TCGTGCACGTTATCAGGGAC	AAGGCAGAGTTGACGTAGCC
AdrB3	CCTTCCGTCGTCTTCTGTGT	GCCATCAAACCTGTTGAGCG
A2a	TCGCCATCCGAATTCCACTC	CACCCAGCAAATCGCAATGA
CaSR	GCTTTTCACCAACGGGTCCT	CCTGCTCCCCCATGTTGTT
Cd137	GCCGAACTGTAACATCTGCA	TTCAATGCACTCACACTCCG
C/ebpα	AGGTGCTGGAGTTGACCAGT	CAGCCTAGAGATCCAGCGAC
C/ebpβ	CCAAGAAGACGGTGGACAA	CAAGTTCCGCAGGGTGCT
C/ebpδ	ATCGACTTCAGCGCCTACA	GCTTTGTGGTTGCTGTTGAA
ColI	GAAGCCGAGGTCCCAGTG	CACCCCTCTCTCCTGGAAG
Fabp3	AGAGTTCGACGAGGTGACAG	TGCACATGGATGAGTTTGCC
Fabp4	GATGCCTTTGTGGGAACCT	CTGTCGTCTGCGGTGATTT
Mhc I	AGTTCCGCAAGGTGCAGCACGAGCT	CCACCTAAAGGGCTGTTGCAAAGGC
Mhc IIa	CGGGTGAAGAGCCGGGAGGTTCACA	GAAGATGGTTGCAAACGTGACACTG
Mhc IIb	ACAGACTAAAGTGAAAGCCTACAA	CACATTTTGTGATTTCTCCTGTCAC
Mhc IIx	CGGGTGAAGAGCCGGGAGGTTCACAC	CTCTCCTGATGTACAAATGATCGGC
MyoD	TACAGTGGCGACTCAGATGC	GTGTCGTAGCCATTCTGCC
Pat2	GTGCCAAGAAGCTGCAGAG	TGTTGCCTTTGACCAGATGA
Pgc1-α	AGCCGTGACCACTGACAACGAG	GCTGCATGGTTCTGAGTGCTAAG
Pparγ	CCCTGGCAAAGCATTTGTAT	GAAACTGGCACCCTTGAAAA
Prdm16	CCGCTGTGATGAGTGTGATG	GGACGATCATGTGTTGCTCC
P2rx1	CCAGTTGGTGGTTCTGGTCT	GCTGATAAGGCCACTTGAGG
P2rx2	TCTGGGTAAAATGGCCCCAA	TGCAATGTTGCCCTTGGAGA
P2rx3	AGTTTGCTGGGCAGGATTTTG	CCAGGCCTTGTCCAGATCAC
P2rx4	TGTGGCTGTGACCAACACTT	TTTTCCTCCTGAGCTGGGAC
P2rx5	TGACTTCCAGGACATAGCCC	AGTGGGAGGCAGCTTTATCA
P2rx6	ACCCAGGTTAAGGAGCTGGA	TGGTGTCACGAGGAAGTTGG
P2rx7	GGATGGACCCACAGAGCAAA	CCAGGCAGAGACTTCACAGG
P2y2	GTGACCACTGGCCATTTAGC	GCAGGTGAGGAAGAGGATGC
P2y12	AGGGGTTCAGCCAAAGTTCC	CAGGGTGTAGGGAATCCGTG

Target gene	Forward sequence	Reverse sequence
Runx2	CTCTGGCCTTCCTCTCTCAG	TGAAATGCTTGGGAACTGCC
Tbp	ACCCTTCACCAATGACTCCTATG	TGACTGCAGCAAATCGCTTGG
Tfam	CAGGAGGCAAAGGATGATTC	CCAAGACTTCATTTCATTGTCG
Ucp1	CTGCCAGGACAGTACCCAAG	TCAGCTGTTCAAAGCACACA

Table 4: Primary and secondary antibodies for western blot analysis

Protein	Company	Catalog number
AKT (1:1000)	Cell Signaling	#4685
β-ACTIN (1:5000)	Santa Cruz	sc-47778
C/EBPβ (1:1000)	Cell Signaling	#3087
GAPDH (6C5)	Calbiochem	CB1001
Mouse-IgG-HRP (1:10000)	Santa cruz	sc-2005
p44/42 MAPK (Erk1/2) (1:1000)	Cell Signaling	#4695
PPARγ (1:2000)	Cell Signaling	#2435
p-AKT (S473) (1:1000)	Cell Signaling	#9271
p-C/EBPβ (Thr235) (1:1000)	Cell Signaling	#3084
p-p44/42 MAPK (Erk1/2) (1:1000)	Cell Signaling	#4377
Rabbit-IgG-HRP (1:10000)	Cell signaling	#7074
Total OXPHOS complex kit (1:2000)	novex	458099
UCP1 (1:25000)	Custom (Jastroch, Hirschberg et al. 2012)	Rabbit anti-hamster UCP1

3 METHODS[4]

3.1 Animal-based experiments and housing conditions

All animal experiments were conducted with a protocol approved by the district government of Upper Bavaria (Bavaria, Germany) for breeding and basic metabolic phenotyping (ROB-55.2Vet-2532.Vet_02-14-33). All applied methods were conducted upon certified trainings and in accordance with the German animal welfare law.

Mice were kept in individually ventilated cages (IVC) or in open cages, depending on the mouse facility, at 22+/-2°C in a 12h/12h day/night cycle and were fed with standard laboratory chow diet (Altromin 1314).

3.1.1 Breeding of global and BAT-specific P2RX5 ko mice

3.1.1.1 P2RX5 ko and BAT-specific P2RX5 ko

The German mouse clinic (GMC) at the Helmholtz Center Munich generated C57BL/6 mice containing a P2RX5 knock out first allele (Figure 4). Breeding was started with four whole body $P2RX5^{-/-}$ knock out (ko) mice by mating those mice with wildtype (wt) mice to generate $P2RX5^{+/-}$ heterozygous (het) mice. To generate cohorts with P2RX5 ko and comparable $P2RX5^{+/+}$ wt mice, P2RX5 het siblings were mated with each other.

Figure 4 P2RX5 knock out first allele, reporter-tagged insertion (lacZ) with conditional potential (FRT sites and loxP sites): $P2rx5^{tm1a(eucomm)hmgu}$

(Source: https://www.mousephenotype.org/data/genes/MGI:2137026, 11.05.2018).

Brown fat-specific P2RX5 ko mice were generated by breeding P2RX5 knock out first allele mice with flippase deletion (flp^{del}) mice to remove the stop cassette between exon 1 and 2 of the P2RX5 ko first allele. The offspring was further labeled as $P2RX5^{fl/fl}$ mice and mated with UCP1-

[4] Methods of the experiments investigating the calcium impact on brown adipocyte differentiation and identity are published in Pramme-Steinwachs, I., M. Jastroch and S. Ussar (2017). "Extracellular calcium modulates brown adipocyte differentiation and identity." Sci Rep **7**(1): 8888. Text is in parts adapted and revised to include additional details.

driven cre recombinase (UCP1cre) mice to delete P2RX5 exon 2 in UCP1 expressing tissues. To generate cohorts, $P2RX5^{fl/fl}$;$UCP1cre^{-}$ (fl) and $P2RX5^{fl/fl}$;$UCP1cre^{+}$ (cre) mice were bred together.

3.1.1.2 Genotyping

The litters were weaned with 3-4 weeks and marked with ear punches. Tissue pieces from the ear were used to detect the genotype. The tissue pieces were boiled at 95°C in 100 µl 50 mM NaOH for 30 min. Adding 10 µl 1 M Tris-Cl pH 8 neutralized the DNA solution. For PCR, 1 µl DNA was added to the PCR mastermix containing 5 µl Platinum Green master mix (PGMM), 4 µl DNase-free water and 0.5 µl 20 µM primers. The PCR ran with the respective primers and protocols (Table 2, Table 5) in a PCR cycler (Mastercycler® pro, Eppendorf). Products containing peqGREEN DNA/RNA Dye were separated on a 2% agarose gel (1x TAE buffer (40 mM Tris, 20 mM Acetic Acid, 10 mM EDTA, pH 8.3)) in an electrophoresis chamber to detect the specific product length referring to the genotype.

Table 5: PCR protocol for the respective genotypings

PCR Settings (P2RX5 fl)	**Temperature (°C)**	**Time**	**# of cycles**
1 Denaturation (melting)	94°C	5’	1
2 Amplification (melting, annealing, polymerizing)	94°C	30’’	39
	58°C	45’’	
	72°C	45’’	
3 Polymerization	72°C	10’	1
4 Cooling	12°C	infinite	1

PCR Settings (UCP1cre)	**Temperature (°C)**	**Time**	**# of cycles**
1 Denaturation (melting)	95°C	5’	1
2 Amplification (melting, annealing, polymerizing)	95°C	45’’	35
	58°C	45’’	
	72°C	45’’	
3 Polymerization	72°C	10’	1
4 Cooling	12°C	infinite	1

PCR Settings (P2RX5 ko)	**Temperature (°C)**	**Time**	**# of cycles**
1 Denaturation (melting)	95°C	5’	1
2 Amplification (melting, annealing, polymerizing)	94°C	30’’	39
	65°C	45’’	
	72°C	45’’	
3 Polymerization	72°C	10’	1
4 Cooling	12°C	infinite	1

3.1.2 Metabolic phenotyping *in vivo*

3.1.2.1 Body composition measurements

Animals were weighted and body composition including lean and fat mass was analyzed with a body composition analyzer for small live animals (EchoMRI^{TM} Analyzer). Therefore, mice were kept in an appropriate, locked tube without anesthesia and the body composition was measured within the machine upon weight entry.

3.1.2.2 Glucose tolerance test

Glucose (2 mg/g body weight, 20% solution, B.Braun) was applied intraperitoneally (i.p.) four hours after food withdrawal. Glucose levels were measured before as well as 15, 30, 60, 90 and 120 min after glucose application with a glucometer (Abbott).

3.1.2.3 Insulin tolerance test

Animals were fasted for four hours before blood glucose was measured with a glucometer (Abbott). Values were taken at point zero (before) as well as 15, 30, 60, 90 and 120 minutes after i.p. injection of 0.75 mU/g insulin (Actrapid, novo nordisk) diluted in 0.9% saline (Fresenius Kabi Deutschland).

3.1.3 Metabolic phenotyping *ex vivo*

3.1.3.1 Organ collection

Mice were anesthetized with 10 µl/g of a solution containing 0.02 mg ketamine (Pharmanovo) and 0.015 mg xylazin (Proxylaz, bela-pharm) diluted in 0.9% saline (Fresenius Kabi Deutschland). As soon as reflex action was absent, blood samples were taken from the heart via cardiocentesis. After cervical dislocation, the respective organs, including adipose tissues, muscles and liver, were dissected and the tissue weights were detected. One tail clip was used for re-genotyping. Samples for protein, RNA and triglyceride isolation were kept directly on dry ice and were frozen at -80°C. Blood was centrifuged 5 minutes at 12.000 g and 4°C to remove blood cells from the serum which was then kept at -80°C. For paraffin embedding, parts of fats and liver were put in 4% paraformaldehyde (PFA) at 4°C over night. Parts of muscles were dehydrated in liquid nitrogen cold iso-Pentane and then kept at -80°C for cryosectioning. For *ex vivo* measurements, such as the lipolysis assay, adipose tissues were dissected and were

directly put on ice in DMEM, low glucose, pyruvate (Gibco). Tissues for cell isolation were kept in the digestion solution on ice.

3.1.3.2 Lipolysis assay

The adipose tissues were transferred on a 10 cm cell culture dish and cut into small pieces with razor blades. One piece was transferred into one well of a 96 well cell culture plate containing 150 µl DMEM, low glucose, pyruvate (31885-023, Gibco) supplemented with 2% fatty acid free BSA. Five replicates per condition were used. Tissue pieces were equilibrated at 37°C and 5% CO_2 for 30 minutes. Medium was changed with 240 µl of DMEM, low glucose (1 g/l glucose), 2% free fatty acid free BSA and it was incubated at 37°C in a 37°C-5%-CO_2 incubator for 3 hours, in the presence of either control (medium), isoproterenol (1 µM), 2-methylthio-ATP (20 µM) or isoproterenol and 2-methyl-ATP. 200 µl were transferred into a 96 well PCR plate and were stored at -80°C or on ice to directly measure the free fatty acid (FFA) content in the free fatty acid assay. Tissue pieces were washed with PBS pH 7.4 (137 mM NaCl, 2.7 mM KCl, 10 mM Na_2HPO_4, 1.8 mM KH_2PO_4) and were kept at -80°C until protein extraction was performed. Therefore, tissue pieces were lysed in 100 µl lysis buffer (25 mM Tris pH 7.4, 150 mM NaCl, 1 % NP-40, 1 mM EDTA, 5 % glycerol, 0.1 % SDS, protease and phosphatase inhibitors (Sigma)) with an ultrasonic homogenizer model 150V/T for 30-60 seconds. Samples were incubated with 0.01% SDS on ice for 10 min and were centrifuged at 4°C and 4700 x g for 20 minutes to remove fat from the protein lysate. Protein content was measured with a BCA assay.

3.1.4 Histology

3.1.4.1 Paraffin embedding and sectioning

Tissues were kept in 4% PFA at 4°C overnight and were transferred to 70% Ethanol (v/v with water) and were stored at 4°C until further use. In each step, tissues were dehydrated in rising Ethanol concentrations (80%, 90% and two times 100%) for 1 hour. This was followed by three times 10 minutes xylol incubation (xylol I, II and III). Each time, the tissues were transferred into paraffin wax I and II (paraplast, Leica Surgipath) at 65°C for one hour and then into paraffin wax III (paraplast, Leica Surgipath) at 65° over night. The next day, tissues were embedded in paraffin wax using a paraffin embedding machine and were stored at room temperature. For sectioning, the paraffin blocks were cooled down at -20°C and were sectioned by using the

microtome. The 2 µm sections are collected with SUPERFROST® PLUS glass slides (Thermo Scientific) and were dried at room temperature.

3.1.4.2 Cryosectioning

Muscle samples were snap frozen in liquid nitrogen-cold iso-Pentane and then stored at -80°C. The muscle samples were kept at -20° for 2 hours before sectioning. The muscles were cut on opposite ends with a sharp scalpel to produce straight ends. One end was glued on top of the metal stamp of the cryosection machine (Cryostat CM 3050 S, Leica) with TissueTek O.C.T.™ to allow cross sectioning of the muscle. 7 µm sections were collected on SUPERFROST® PLUS glass slides (Thermo Scientific) and were used for H&E staining.

3.1.4.3 H&E staining

The paraffin sections were de-waxed in two times 5 min in xylol and were hydrated in ethanol with increasing deionized water dilution for 2 min each step (100%, 96%, 90%, 80%, 70%, 0%). Then, sections were stained in Mayer solution (standard diluted in deionized water 1:5 and filtered) and were washed with tab water two times for 2 min. The sections were dewatered with increasing ethanol concentrations in 3 min steps (96%, 100%), followed by chromotrope II R staining (100 mg chromotrope II R + 100 ml 100% ethanol + 100 µl acetic acid, filtered). Slides were kept in 96% ethanol and then 100% ethanol for 1 min each, followed by two times 5 min in xylol. Slides mounted with Histokit II were dried at room temperature.

For muscle cryosections, sections were first incubated in 4% PFA for 10 min. After 3 washing steps in PBS for 10 min each, sections were washed in deionized water for 3 min. Then the H&E staining was performed as described above.

3.1.4.4 Adipocyte size analysis

H&E stained tissue sections were scanned with an AxioScan Z1 by using a 20x fluorescent (488 nm) objective (ZEISS). The adipocyte size was read out and calculated by the collaboration partner Dr. Annette Feuchtinger (Helmholtz Zentrum München - German Research Center for Environmental Health, AAP Research Unit Analytical Pathology) with the Definiens Developer XD software and a threshold below 15 μm^2. Analysis of the data was done with GraphPad prism by generating histograms with the respective bin width of three data sets per genotype.

3.2 Cell culture experiments

3.2.1 Cell isolation and culture

Cells were kept in Dulbecco's Modified Eagle Medium (DMEM + GlutaMAX + high glucose, Gibco) containing 10% fetal bovine serum (FBS, Gibco), penicillin (10 Units/ml) and streptomycin (100 µg/ml) (Pen Strep, Gibco) at 37°C and 5.6% CO_2, if not indicated differently.

3.2.1.1 Generating cell lines and primary cell culture

Murine brown adipose tissue (BAT) was dissected from the mouse interscapular region, cut into ~1mm pieces and digested at 37°C in pure DMEM containing 1 mg/ml collagenase type IV (Gibco) and 10 mg/ml BSA (Albumin fraction V, Roth) for 45 minutes. The digestion was stopped by washing the cells with PBS (Gibco) containing 10 mg/ml BSA. Mature adipocytes were removed and preadipocytes were cultured in Dulbecco's Modified Eagle Medium (DMEM + GlutaMAX + high glucose, Gibco) containing 10% fetal bovine serum (FBS, Gibco), 0.1 mg/ml normocin (InvivoGen), 10 Units/ml penicillin and 100 µg/ml streptomycin (Pen Strep, Gibco).

Primary brown preadipocytes were grown to 90 % confluence and were then seeded 1:1 on Seahorse XF96 Cell Culture Microplates (Seahorse) for mitochondrial respiration measurements and on 96 well Eppendorf Cell Imaging Plates for calcium imaging.

To generate cell lines, primary brown preadipocytes were treated with an ecotropic SV40 large T retrovirus at day 2 after isolation. P2RX5 scrambled (shSCR) and knock down (shP2RX5 KD5) cells were generated by ecotropic lentiviral transfection of plasmids containing a puromycin resistance site and either a random sequence (shSCR) or the P2RX5 silencing RNA (shRNA) sequence TRCN0000068599 (shP2RX5 KD 5). Adding puromycin to the cell culture medium allowed selection of the cells with successful plasmid integration.

3.2.1.2 Cell differentiation

For all cell culture experiments, normal growth medium containing penicillin (10 Units/ml) and streptomycin (100 µg/ml) (Pen Strep, Gibco) as well as 10% fetal bovine serum (FBS, Gibco) was used. Brown preadipocytes were grown to 100 % confluence (day 0, preadipocytes) and differentiation was induced with 0.5 mM 3-Isobuthyl-1-methylxanthin (IBMX, Sigma), 125 µM Indomethacin (Santa Cruz), 5 µM Dexamethasone (Sigma), 100 nM Insulin (Sigma) and 1 nM

Triiodothyronine (T3, Calbiochem) in the appropriate medium. Medium (supplemented with insulin and T3) was changed every other day until day 6 (primary) or day 8 (cell lines).

For calcium experiments, the medium was supplemented with calcium chloride (high calcium) or magnesium chloride (high magnesium) to reach a final concentration of 10mM. Calcium free experiments were conducted using DMEM, high glucose, no glutamine, no calcium (Gibco 21068), supplemented with 1 mM sodium pyruvate (Gibco), 1X GlutaMAX^{TM}-1 (Gibco) [equimolar with 2 mM L-alanyl-L-glutamine], Pen Strep and 10% FBS. These media were used during induction (day 0-2), differentiation (day 2-8) or induction and differentiation (day 0-8).

3.2.1.3 Inhibitor and compound treatment during differentiation

For inhibitor experiments, the compounds were kept as 1 mM stock solutions in DMSO at -20°C and were supplemented to the medium in the appropriate dilution: 1 µM Ionomycin calcium salt (Fisher Scientific), 1 µM calcineurin inhibitor FK506 (*Tacrolismus*, Abcam), 250 nM MEK inhibitor PD 0325901 (Sigma).

3.2.1.4 Calcium measurement with Fluo-4

BAT wt cells were grown to 100% confluence (day 0 / 0 hours). BAT wt cells and primary brown adipocytes were differentiated according to the protocol above in 96 well glass-bottom plates (Eppendorf) to measure fluorescence with a PHERAstar FS (BMG Biotech), using following setting: bottom optic measurement with the optic module FI 485 520 (Ex/Em), gain of 915 (BAT wt) and 1100 (primary BAT) and 20 flashes per well in an orbital averaging mode circling in 3 mm diameter. All further steps were performed at 37°C with pre-warmed dilutions in control buffer 1x SBS (5 mM KCl, 140 mM NaCl, 8 mM glucose, 10 mM HEPES, 0.8 mM $MgCl_2$, 1.8 mM $CaCl_2$, pH 7,4). For high magnesium (10 mM), high calcium (10 mM) and calcium free (0 mM) experiments, specific 1x SBS buffers containing the appropriate magnesium and calcium concentrations were prepared. Cells were washed in 1x SBS buffer containing 1 mM probenecid (Santa Cruz) and were incubated with 4 µM Fluo-4 AM (Cat. #F14201, Thermo Scientific), 0.02% pluronic F-127 (Biotium) and 1 mM probenecid (Santa Cruz) at room temperature for one hour before they were washed again. After 30 min, basal fluorescence was detected in intervals of several seconds. Compounds were diluted to 10-fold concentration in calcium free 1x SBS and were injected with a speed of 190 µl/s. Compounds: IBMX (0.5 mM), induction mix (*see Cell differentiation*), 2-methylthio-ATP (Tocris) (20 µM), Isoproterenol (1 µM), Ionomycin (10 µM). After orbital mixing (100 rpm), the fluorescence emission at 520 nm was detected. Values were

shown as fold increase in fluorescence intensity (%) upon injection. Cells were washed with PBS and frozen at -80°C for further use.

3.2.1.5 Cellular oxygen consumption and extracellular acidification rates

The oxygen consumption rate (OCR) and the extracellular acidification rate (ECAR) were measured with a XF96 Extracellular Flux analyzer (Seahorse Bioscience, Agilent technologies). Cells were differentiated *in vitro* with calcium control medium (1.8 mM), high calcium medium (10 mM), high magnesium medium (10 mM) or low calcium medium (approx. 0.3 mM) for indicated durations. Cells were equilibrated at 37°C in XF Assay Medium Modified DMEM (Seahorse Bioscience) for one hour under the following conditions: BAT wt cells in the presence of 25 mM glucose, BAT1 cells with 25 mM glucose and 1 mM pyruvate and primary BAT cells in the presence of 2% free fatty acid BSA, 25 mM glucose and 2 mM pyruvate. In case of inhibitor experiments, medium was supplemented additionally with the P2RX5 inhibitors PPADS (10 µM) or NF449 (1 µM). All compounds were diluted as ten-fold concentrations in assay medium and loaded in the equilibrated cartridge ports. Used compounds, as indicated in the figure legends: 1 µM Isoproterenol (Sigma), 20 µM 2-methylthio-ATP (Tocris), 20 µg/ml oligomycin (Sigma), 1 µM FCCP (Tocris), 50 mM sodium pyruvate (Gibco), 2.5 µM rotenone (Sigma), 2.5 µM antimycin A (Sigma) and 100 mM 2-deoxy-D-glucose (Alfa Aesar). Each cycle comprised two minutes of each mixing, waiting and measuring. Non-mitochondrial respiration (OCR) and non-glycolytic acidification (ECAR) were subtracted from other values to determine mitochondrial oxygen uptake.

To normalize OCR and ECAR on the cell amount, cells were washed with PBS and lysed in 100 µl RIPA buffer (50 mM Tris (pH=7,4), 150 mM NaCl, 1 mM EDTA, 1 % Triton X100). DNA content was detected with the Quant-it™ PicoGreen® dsDNA Assay kit (Thermo Fisher Scientific).

3.2.1.6 Lactate Assay

Cells were differentiated in 1.8 mM calcium (control) or for day 2-8 in high calcium (10 mM) medium in a 24-well plate. The cell supernatant was collected at day 8. The supernatant was centrifuged in Spin-X® UF 6 concentrators (Corning®) at 4000 g and 4°C for 30 min to remove proteins larger than 10 kDa, like lactate dehydrogenase. The flow-through was stored at -80°C until further use. Samples were diluted 1:8 and 2 µl were used to measure the lactate content

with the Lactate Colorimetric/Fluorometric Assay Kit (bioVision, K607) according to the manufacturer's manual.

3.2.1.7 Oil Red O stain

Differentiated cells were fixed in 10% formalin (Roth), washed in water and dehydrated in 60% isopropanol. Then, filtered 60% (v/v) oil red o working solution in water (stock: 0.35% (w/v) Oil Red O (Alfa Aesar) in 100 % isopropanol (Sigma)) was added. The cells were then incubated at room temperature for 10 minutes, washed with water and dried. The stain was solved with 100 % isopropanol and the absorption at 500 nm was measured with a PHERAstar FS detection system (BMG Biotech), referring to the relative lipid content of the cells.

3.3 Molecular biological methods

3.3.1 Sample preparation

3.3.1.1 RNA extraction from tissue and cells

RNA was extracted with the RNA extraction kit "RNeasy Mini Kit" (Qiagen) according to the manufacturer's manual.

Cells were lysed in 350 µl RPL buffer containing 40 mM DTT. Tissue was homogenized in 1 ml Qiazol (Qiagen) with a metal bead in a TissueLyzer II (Qiagen) at 30Hz/sec for two times 30 seconds. Fat tissues were centrifuged at 10000 g and 4°C for 5 min in order to remove the fat cake. The addition of 200 µl trichloroform (Roth) and shaking for two times 30 seconds allowed the dissipation of proteins. The samples were centrifuged at 12000 g and 4°C for 15 min. The upper aqueous phase (400-600 µl) was used for further RNA extraction according to the manual. RNA was eluted with 40 µl RNase-free water and kept at -80°C.

For RNA extraction of cells in a 96 well format, the QuickExtract™ RNA Extraction kit (QER090150) was used. Therefore, 50 µl quick RNA extraction lysis buffer were added and shaked at 2000 rpm and 4°C for 5 min. In certain cases, RNA digest was performed by heating samples at 65°C for 2 min and incubating samples at 37°C with 9 µl DNase digest solution (5.5 µl DNase Buffer I + 1.25 µl RiboGuard™ RNase Inhibitor + 2.5 µl RNase-free DNase I) for 15 min. This was followed by adding 2 µl stop solution and heating at 65°C for 10 min. Ex post RNA digest in samples isolated with the RNA extraction kit "RNeasy Mini Kit" was performed with 2 µg RNA as above. 10 µl lysate were used for cDNA synthesis.

3.3.1.2 Protein isolation

Samples were lysed in 25 mM Tris pH 7.4, 150 mM NaCl, 1 % NP-40, 1 mM EDTA, 5 % glycerol, 0.1 % SDS containing protease inhibitor and the phosphatase inhibitors II and III (Sigma). Tissue was cut into small pieces and homogenized with a polytron PT 2500 E. Cells were scratched from the cell culture dish and homogenized with a 1 mm syringe. Cell and tissue fragments were removed by centrifugation at 13.000 g and 4°C for 20 minutes. Samples were stored at -20°C.

3.3.1.3 NP40 extracts from liver

Liver was powdered with pistil and mortar in liquid nitrogen. 50 mg liver powder were solved in 500 µl 5% NP40 (v/v in deionized water) on ice and homogenized with a metal bead in a TissueLyzer II (Qiagen) at 30Hz/sec twice for 1.5 min. After full speed centrifugation at 4°C for 30 seconds, the supernatant was transferred into a fresh cold 2 ml tube and boiled at 90°C for 2 minutes. The cloudy extract was kept at room temperature to cool down. Additional boiling for two minutes dissolved the triglycerides. After another full speed centrifugation at room temperature for two minutes, the supernatant was transferred into a fresh tube and stored at -20°C or directly used for triglyceride assays.

3.3.2 Assays and analysis methods

3.3.2.1 cDNA synthesis and qPCR

cDNA synthesis (0.5-1 µg total RNA, High Capacity cDNA Reverse Transcription Kit, Applied Biosystems, 4368813) was conducted according to the manufacturers' instructions. qPCR was performed in a C1000 Touch Thermal Cycler (Bio Rad), using 300 nM forward and reverse primers and iTaq Universal SYBR Green Supermix (BioRad). The target gene expression was normalized on TATA box binding protein (*Tbp*) expression. The primer sequences are shown in Table 3.

3.3.2.2 SDS-PAGE and Western Blot

15-30 µg cell lysate were loaded on 4-12% precast SDS gels (Invitrogen) running with MOPS running buffer (50 mM MOPS, 50 mM Tris, 0.1 % SDS, 1 mM EDTA). 20-40 µg tissue lysate were loaded on homemade 10 % SDS gels prepared as described in Table 6, running with 1x Running Buffer (25 mM TRIS, 192 mM glycine, 0.1% SDS). Proteins were wet-blotted on 0.45 µm PVDF membranes with Blotting Buffer (25 mM TRIS, 192 mM glycine, 20% methanol).

Membranes were blocked in 5% BSA in TBS with 0.1% Tween 20 (TBS-T) at room temperature for one hour (2 hours for UCP1). Membranes were incubated with primary antibodies (Table 4) at 4°C over night, washed in TBS-T and incubated with the appropriate secondary antibody at room temperature for one hour. Membranes were developed with chemiluminescent HRP substrate (Immobilon Western, Millipore) using films (Hyperfilm ECL, GE Life Sciences; CL-XPosure Film, Thermo Scientific).

Table 6: SDS gel recipe

Compound	Volume 10% SDS gel (ml)	Volume stacking gel (ml)
Rotiophorese 30% acrylamide	13.2	1.5
Water	16.4	6
TrisHCl 1.5 mM pH 8.8	10.4	-
TrisHCl 0.5 M pH 6.8	-	2.6
SDS 10%	0.4	0.1
APS 10%	0.2	0.05
Temed	0.06	0.02

3.3.2.3 Triglyceride assay

To measure triglycerides in NP40 liver extracts the Triglyceride Quantification Colorimetric/Fluorometric Kit (bioVision, K622) was used. In this procedure, triglycerides are converted to free fatty acids and glycerol, which is oxidized. This product reacts with a probe and resulting fluorescence (Ex/Em = 535/587 nm) can be measured. Fluorescence directly refers to glycerol content, the production of which is equimolar with triglycerides. The procedure was conducted in line with the manufactures manual, except that only half the volumes were used. 2.25 µl of liver samples diluted 1:10 were used in the fluorometric assay and were adjusted to a volume of 25 µl. Samples with lipase (total glycerol) and without lipase (free tissue glycerol) were measured.

Blanks and values for free tissue glycerol were subtracted from values for total glycerol. Standard curve revealed sample triglyceride concentrations, which were then corrected by dilution factors and used volumes. Multiplication with the molecular weight (885.4 g/mol) and division with the exact amount of liver used for NP40 extracts revealed triglycerides [g] / liver [g].

3.3.2.4 Free fatty acid assay

Free fatty acids in supernatants of the lipolysis assay and in serum were measured following the Free Fatty Acid Quantification Kit (C/F) (bioVision, K612) manufacturer's manual. Thereby, 20 µl of lipolysis supernatants and 5 µl of serum were used. All the volumes in the kit were reduced to half of the amount. Because of the high amount of lipolysis supernatants, the standard solutions were also diluted in blank medium.

3.3.2.5 Insulin ELISA

Insulin levels in the serum were measured by following the Mouse Ultrasensitive Insulin ELISA (Alpco, 80-INSMSU-E01,E10) manufacturer's instructions. 5 µl serum were used and analysis was performed with GraphPad Prism, resulting in ng/ml insulin levels.

3.4 Data analysis

Data are presented as means ± SEM. All statistical analyses were performed with GraphPad Prism. Parametric and nonparametric tests were performed accordingly, as indicated in the figure legends. Unpaired, two-tailed Student's t-tests as well as one-way and two-way ANOVA for multiple comparisons were used with an α-level of 0.05 to determine p-values (* $p<0.05$, ** $p<0.01$, *** $p<0.001$, **** $p<0.0001$).

4 RESULTS

4.2 Extracellular calcium modulates brown adipocyte differentiation and identity[5]

4.2.1 Extracellular calcium modulates differentiation of brown adipocytes

To study the influence of extracellular calcium on brown adipocyte differentiation, immortalized murine brown preadipocytes were differentiated *in vitro* for eight days using regular cell culture medium with 1.8 mM calcium (control), medium supplemented with 10 mM calcium or 10 mM magnesium, or medium without calcium (low calcium - addition of 10% FBS results in ~0.3 mM calcium). Changing medium conditions depending on a specific time frame (day 0-2, day 0-8 and day 2-8) allowed terminating calcium targets at specific points in time during differentiation. Samples were collected in 8-day time course experiments every other day.

While control cells accumulate lipids continuously throughout the 0-8 day differentiation, elevating calcium up to 10 mM over 8 days abolished lipid accumulation completely, as shown by the lipid droplet stain Oil Red O (Figure **5A-B**). Normalizing calcium levels after 2 days resulted in a delayed lipid accumulation compared to controls. Alternatively, elevating calcium levels after 2 days decreased lipid accumulation just slightly (Figure **5A-B**). The divalent cation-control magnesium as well as calcium free medium resulted in a similar lipid accumulation as observed in the control (Figure **5A-B**). Importantly, these treatments did not impair cell viability, shown by similar basal oxygen consumption and DNA content in cells differentiated under indicated conditions up to day 8 (Figure **5C**).

Gene expression analyses of *Pparγ* and *C/ebpα* (Figure **5D**) showed support for the suppressive effects of calcium on adipogenesis in brown preadipocytes. While elevating calcium to 10 mM throughout differentiation diminished *Pparγ* and *C/ebpα* expression, normalizing calcium after two days recovered their expression (Figure **5D**). No differences in gene expression were observed with high calcium for day 2-8 and high magnesium under all three time conditions.

[5] The following results were published in Pramme-Steinwachs, I., M. Jastroch, S. Ussar (2017). "Extracellular calcium modulates brown adipocyte differentiation and identity." Sci Rep **7**(1): 8888. Text, figures and figure legends are in parts adapted or revised.

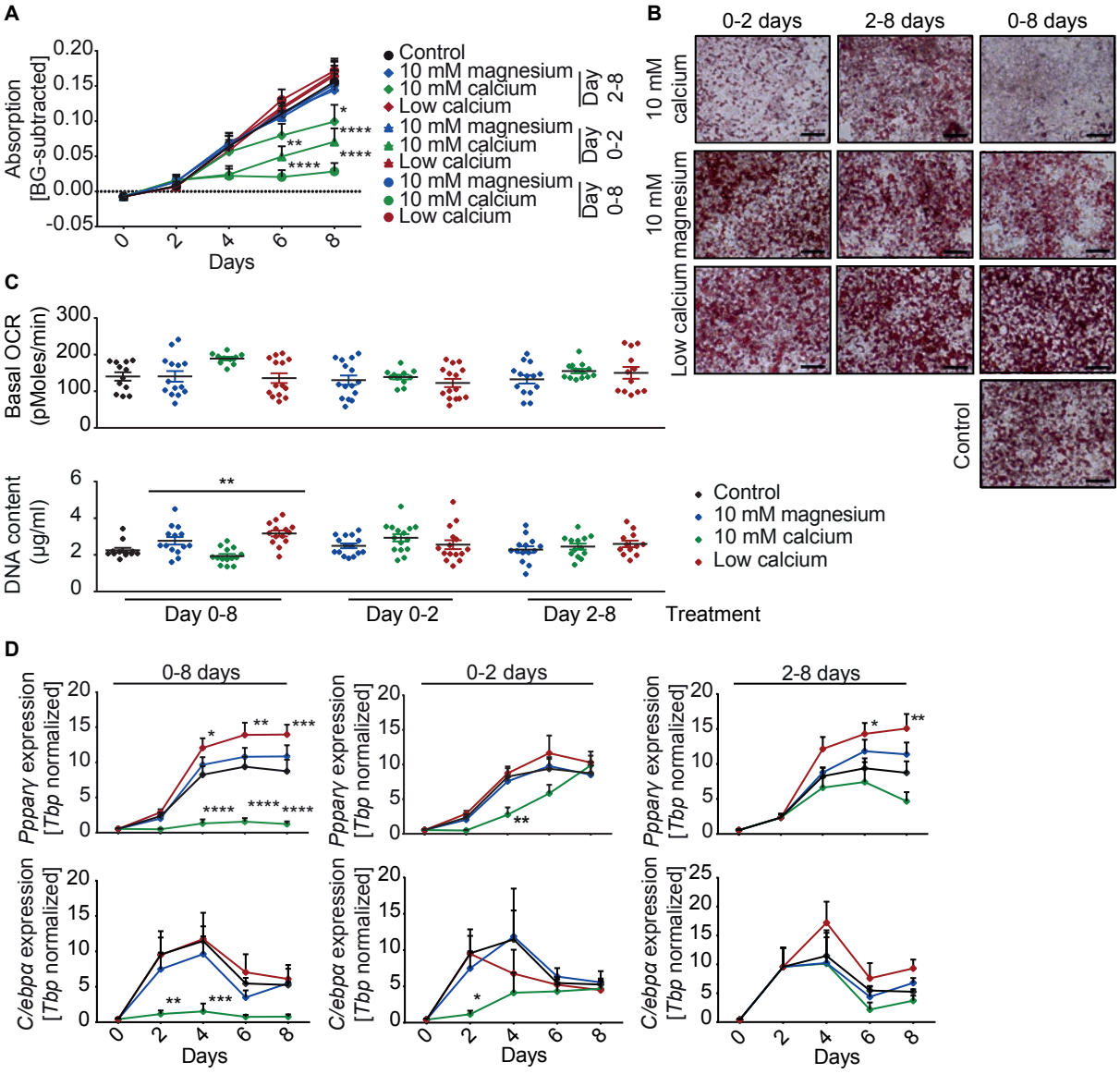

Figure 5 Extracellular calcium reduces differentiation in brown adipocytes. (A) Time course of lipid content of brown adipocytes differentiated *in vitro*. Cells treated with 1.8 mM (control), 10 mM magnesium, 10 mM calcium or calcium free medium for either 8 days (day 0-8), during induction (day 0-2), or after induction (day 2-8). Shown is background (Isopropanol) subtracted lipid content measured by Oil Red O (500 nm) (n=6). **(B)** Representative images of cells stained with Oil Red O at day 8 after control, 10 mM calcium, 10 mM magnesium and low calcium treatment during indicated duration, scale bar = 20 µm. **(C)** Basal oxygen consumption (OCR) and DNA content in cells at day 8 treated with indicated conditions (n=2-3, 3-5 technical replicates each). **(D)** *Pparγ* (n=5) and *C/ebpα* (n=3) expression normalized to *Tbp* during an eight-day time course under above conditions. Ordinary one-way ANOVA with Holm-Sidak's multiple comparison test (**C** top), Kruskal-Wallis one-way ANOVA with Dunn's multiple comparison test (**C** bottom) and two-way ANOVA with Dunnett's posthoc test (**A, D**). Figure adapted from the published manuscript (Pramme-Steinwachs, Jastroch et al. 2017). Original publication attached.

However, lowering calcium throughout differentiation or for days 2-8 promoted *Pparγ* but not *C/ebpα* expression (Figure **5D**). The decrease in *Pparγ* mRNA expression and its rescue upon calcium normalization were also confirmed on protein level (Figure **6A**). Conclusively, elevating calcium for eight days blocked adipogenic differentiation and retained the cells in a preadipogenic state, whereas elevating calcium starting at day 2 did not impact the adipogenic differentiation.

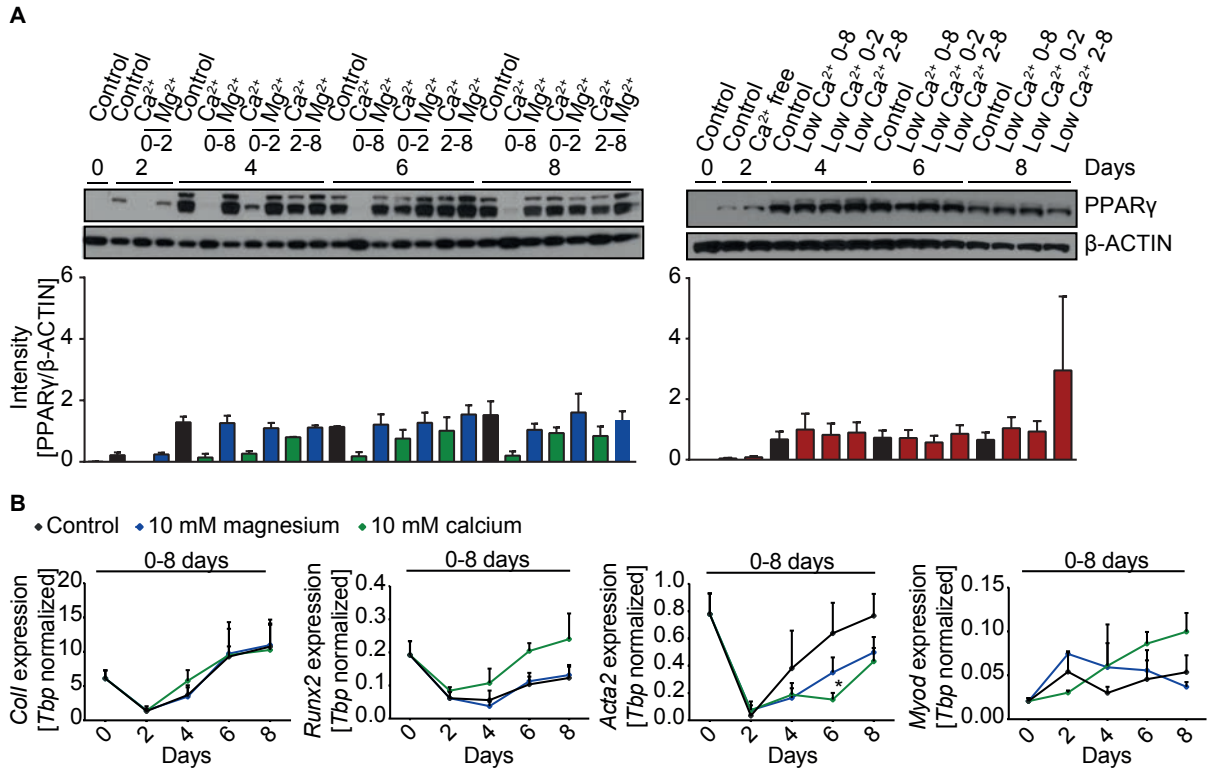

Figure 6 Extracellular calcium modulates differentiation in brown adipocytes. (A) Western Blot for PPARγ and β-ACTIN during the eight-day time course of differentiation with conditions as above during indicated time points. **(B)** Gene expression of the osteogenic marker genes *Coll* and *Runx2* as well as of the muscle marker genes *Acta2* and *Myod* normalized on *Tbp* during eight-day time course differentiation under indicated conditions (n=3). Two-way ANOVA with Dunnett's posthoc test (**A**) or with Tukey's posthoc test (**B**). Figure adapted from the published manuscript (Pramme-Steinwachs, Jastroch et al. 2017). Original publication attached.

Extracellular calcium modulates bone marrow stem cell (BMSC) lineage commitment. In addition, BMSCs and brown adipocytes share common progenitor cells with skeletal muscle. Thus, the expression of osteogenic marker genes, like Collagen I (*Coll*) and Runt-related transcription factor 2 (*Runx2*), as well as myogenic marker genes, like smooth muscle Actin (*Acta2*) and myogenic factor 3 (*Myod*), was examined in cells differentiated in control, high

calcium (10 mM) or high magnesium (10 mM) medium throughout differentiation. The expression of all marker genes was induced during differentiation, without significant differences across treatment groups (Figure **6B**).

Taken together, elevating extracellular calcium throughout differentiation inhibited the induction of adipogenic genes and lipid accumulation, albeit cell viability or marker genes for osteogenesis and myogenesis were not affected. Omitting calcium from the medium increased *Pparγ* expression, whereas elevating the divalent cation control magnesium in the medium did not influence the differentiation capacity. Elevating calcium after the induction did not impair the differentiation, but normalizing calcium levels at day 2 of the differentiation rescued adipogenesis (Pramme-Steinwachs, Jastroch et al. 2017).

4.2.2 Extracellular calcium regulates MAPKs and C/EBPβ activity independently of intracellular calcium

The induction of *Pparγ* and *C/ebpα* during early adipogenesis requires promotor binding of C/EBPβ and C/EBPδ (Tang, Zhang et al. 2004). Altered *C/ebpβ* and *C/ebpδ* expression and protein activation, especially during the early phase of adipogenesis, can inhibit adipocyte differentiation (Karamanlidis, Karamitri et al. 2007, Ussar, Bezy et al. 2012, Lechner, Mitterberger et al. 2013). To study the kinetics of *C/ebpβ* and *C/ebpδ*, time course experiments were performed during the first 48 hours of differentiation under control, high calcium (10 mM) and high magnesium (10 mM).

C/ebpβ and *C/ebpδ* expression peaked after two hours of differentiation regardless of the treatment, while high extracellular calcium seemed to keep *C/ebpδ* mRNA levels elevated also at later points in time (Figure **7A**). The *C/ebpβ* expression was also present on protein levels (Figure **7B**). The transcriptionally active isoform liver-enriched activator protein (LAP) of *C/ebpβ* was hyperphosphorylated at Thr188 in the presence of high extracellular calcium throughout the first 24 hours (Figure **7B-C**). In contrast, the phosphorylation of the other transcriptionally active isoform LAP* at Thr188 as well as the inhibitory isoform liver-enriched inhibitor protein (LIP) at Thr37 were not affected upon high calcium treatment (Figure **7B-C**). Varying LAP/LIP ratios influences the regulation of adipogenic gene expression (Lechner, Mitterberger et al. 2013). Hence, the diminished *C/EBPα* and *Ppary* expression observed in cells treated with high extracellular calcium are most likely due to a shift in the pLAP/pLIP ratio.

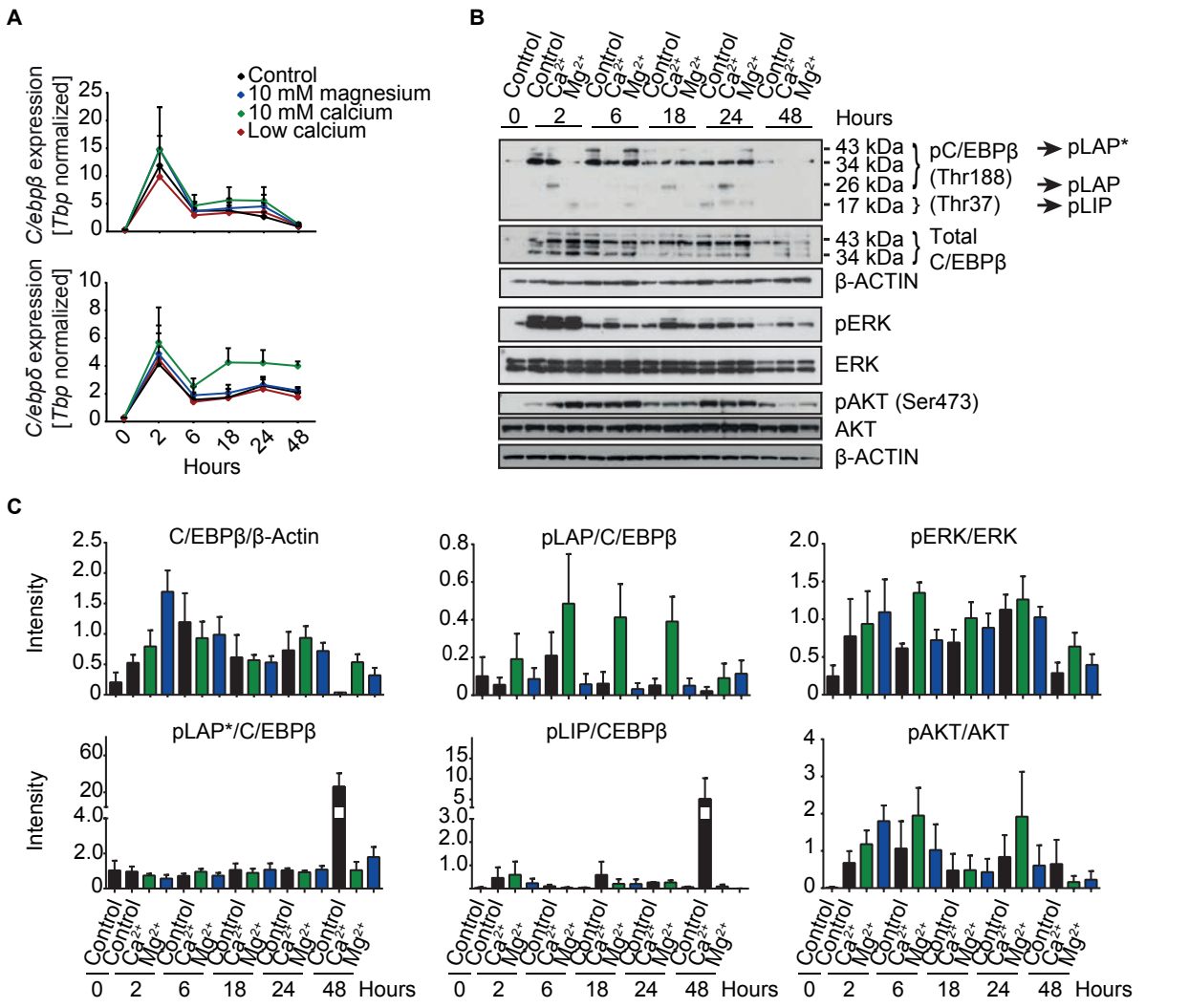

Figure 7 Extracellular calcium regulates MAPKs and C/EBPβ phosphorylation. (A) *C/ebpδ* and *C/ebpβ* expression normalized to *Tbp* during the first 48 hours of differentiation in 1.8 mM calcium (control), 10 mM magnesium, 10 mM calcium and calcium free medium (n=6). **(B)** Western Blot for phospho- (hLAP: Thr235, rLAP: Thr188, rLIP: Thr37)/ total C/EBPβ as well as phospho- / total ERK and phospho- (Ser473)/ total AKT with β-ACTIN as loading control during the first 48 hours of differentiation under the conditions as above. **(C)** Quantification of indicated protein signals in Western Blot normalized in β-ACTIN or total protein during 48 hour time course: total C/EBPβ to β-ACTIN (n = 4); pLAP*, pLAP and pLIP C/EBPβ to total C/EBPβ (n=3-4); pERK to total ERK (n=4); pAKT (S473) total AKT (n=2-3). Ordinary two-Way ANOVA with Dunnett's posthoc test **(A)**. Figure adapted from the published manuscript (Pramme-Steinwachs, Jastroch et al. 2017). Original publication attached.

Phosphorylation of the rat C/EBPβ LAP isoforms at Thr188 and LIP isoform at Thr37 can be mediated by MEK/ERK and results in reduced *C/EBPα* and *Ppary* expression (Park 2004). Indeed, similar phosphorylation patterns upon high extracellular calcium treatment were observed for ERK (Figure **7B-C**), suggesting that LAP phosphorylation was mediated through

pERK. No changes in AKT phosphorylation at Ser472 were observed (Figure **7B-C**). Interestingly, ERK phosphorylation throughout the whole differentiation was higher in the presence of high extracellular calcium compared to controls, while ERK phosphorylation diminished when calcium levels were reduced (Figure **8A**).

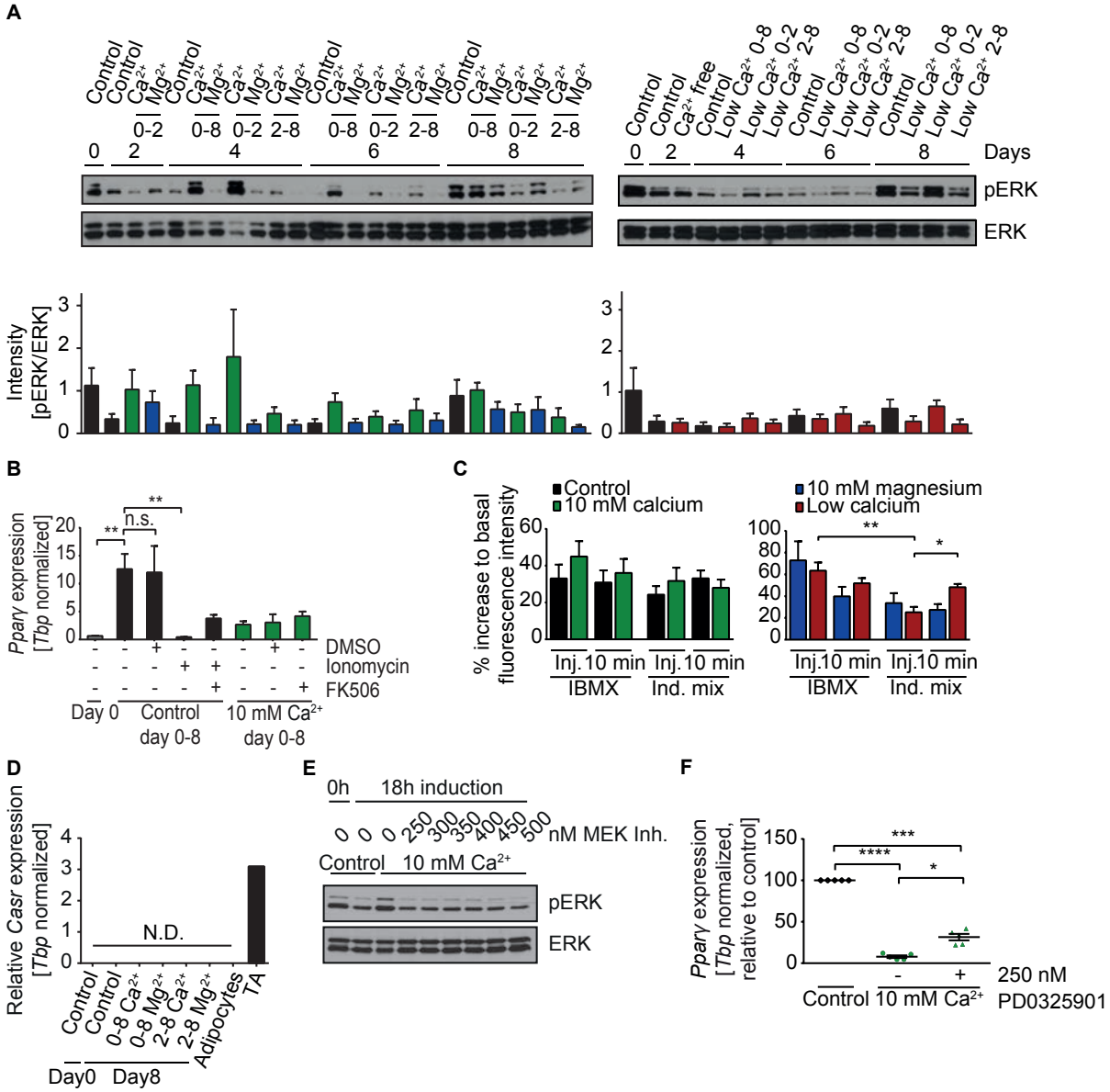

Figure 8 Extracellular calcium regulates MAPKs activity independently of intracellular calcium. (A) Western Blot for phospho- / total ERK and β-ACTIN as loading control and signal quantification during 8 day time course under control (1.8 mM calcium), 10 mM calcium and 10 mM magnesium conditions as well as control and calcium free conditions for the indicated duration: pERK to total ERK (n=4). **(B)** *Pparγ* expression normalized on *Tbp* in preadipocytes (day 0) and in cells (day 8) differentiated with either 1.8 mM calcium (control day 0-8) or 10 mM calcium (10 mM Ca2+ day 0-8) supplemented with DMSO,

ionomycin (2 µM) and / or the calcineurin inhibitor FK506 (1 µM) (n=3). **(C)** Relative increase of intracellular calcium in brown preadipocytes maintained in 1.8 mM calcium (control), 10 mM calcium, 10 mM magnesium or low calcium upon injecting IBMX or induction mix and 10 min later. Data is shown as percentage increase of fluorescence to basal level. Cells loaded with the calcium-binding fluorophore Fluo-4 (4 µM) and fluorescence recorded at Ex/Em = 485/520 in orbital averaging (n=3 with 3-4 replicates each). **(D)** *Casr* expression normalized to *Tbp* in preadipocytes (day 0), and in cells differentiated in vitro with 1.8 mM calcium (control), 10 mM calcium (Ca^{2+}) or 10 mM magnesium (Mg^{2+}) for days 0-8 or 2-8, measured at day 8 (n=3), as well as in primary mature adipocytes and murine musculus tibialis anterior (TA) (pooled samples n=1). **(E)** Western Blot for phospho-/ total ERK in preadipocytes (0h) and induced preadipocytes (18h) with different concentrations of the MEK inhibitor (PD 0325901). **(F)** *Pparγ* expression normalized to *Tbp* in percent of control in adipocytes differentiated with 1.8 mM calcium (control) or 10 mM calcium +/- MEK inhibitor PD 0325901 (250 nM) for days 0-8 (n=5). Repeated measures one-way ANOVA with Tukey's posthoc test **(C, F)** and Kruskal-Wallis one-way ANOVA with Dunn's multiple comparison test **(B).** Figure adapted from the published manuscript (Pramme-Steinwachs, Jastroch et al. 2017). Original publication attached.

This indicates that lower levels of ERK phosphorylation promote adipocyte differentiation. The calcium/calmodulin-dependent serine/threonine protein phosphatase calcineurin is known to regulate ERK and C/EBPβ phosphorylation and thereby adipocyte differentiation in a calcium dependent manner (Neal and Clipstone 2002, Lawrence, McGlynn et al. 2005, Dougherty, Ritt et al. 2009). However, pharmacological inhibition of calcineurin using FK506 throughout differentiation did not rescue adipogenesis upon exposure to high extracellular calcium (Figure **8B**). Calcium influx measurements showed, that 3-isobutyl-1-methylxanthine (IBMX) or the complete induction mix increase intracellular calcium levels, with no difference between control and high calcium treatments (Figure **8C**). Treatments in calcium free buffer also increased intracellular calcium levels, suggesting mobilization of calcium ions from intracellular stores rather than extracellular sources (Figure **8C**). This suggests that ERK hyperphosphorylation and inhibition of adipogenesis are independent of extracellular calcium influx in the experimental set-up.

Calcium sensing receptor (CaSR) mediated ERK phosphorylation is also very unlikely, as *Casr* was neither detected in isolated mature adipocytes nor in preadipocytes differentiated *in vitro* (Figure **8D**). Inhibiting ERK phosphorylation to the level in control cells potentially rescues adipogenic differentiation. Titrating the MEK inhibitor PD0325901 reduced ERK phosphorylation to levels observed in cells cultured in control medium (Figure **8E**). However, reducing ERK phosphorylation that way only partially rescued brown adipogenesis, as shown with *Pparγ* expression (Figure **8F**).

In summary, the suppressive effect of high extracellular calcium on brown adipogenesis is associated with changed pLAP/pLIP ratios and with hyperphosphorylated ERK levels throughout differentiation, independently of extracellular calcium influx. Partial rescue by inhibiting ERK hyperphosphorylation suggests involvement of other calcium-sensing proteins than CaSR, calcineurin or MEK, regulating ERK phosphorylation (Pramme-Steinwachs, Jastroch et al. 2017).

4.2.3 Extracellular calcium modulates brown adipocyte identity and thermogenesis

As shown in figure 5, brown adipogenesis was inhibited in the presence of high extracellular calcium throughout the eight-day time course. Similarly to diminished differentiation, the expression of the brown adipogenic marker genes uncoupling protein 1 (*Ucp1*), PR domain containing 16 (*Prdm16*) and PPARγ coactivator 1-alpha (*Pgc1-α*) was also suppressed upon continued exposure to high extracellular calcium, but recovered upon removal after day 2 (Figure **9A**). In line with *Pparγ* expression in high magnesium or calcium free medium throughout differentiation, *Ucp1*, *Prdm16* and *Pgc1-α* expression tended to increase compared to control (Figure **9A**). Conversely, preadipocytes differentiated under elevated calcium levels (10 mM) during days 2-8 did not impair lipid accumulation or PPARγ and C/EBPα expression (Figure **5**), but inhibited the expression of *Ucp1* and other brown marker genes, like *Pgc1-α* and *Prdm16* (Figure **9A**). Increased *Ucp1* mRNA levels under low calcium conditions and decreased expression under elevated calcium conditions were even more pronounced on protein levels, whereas UCP1 protein levels did not fully recover upon calcium normalization (Figure **9B**).

Among many other functions, PRDM16 and PGC1-α are involved in mitochondrial biogenesis regulation. Therefore, mitochondrial abundance and function were analyzed in brown adipocytes exposed to high extracellular calcium or control medium for days 2-8. The expression of the mitochondrial transcription factor A (*Tfam*) was slightly increased, but differentiation did not show any differences across treatment groups (Figure **10A**). Western Blots for the subunits of the mitochondrial respiratory chain (complex I-V) revealed lower levels of complex V, IV and I in cells treated with elevated calcium for days 2-8 than in control cells, but without statistical significance (Figure **10B**). However, oxygen consumption rate (OCR) recorded by a Seahorse Flux Analyzer in cells at day 8 remained similar across the treatments (Figure **10C**). Basal respiration (basal resp.), ATP production (ATP prod.), proton leak and maximal respiration (max. resp.) were not altered in cells exposed to elevated calcium, even

upon additional substrate supplementation with pyruvate (Figure **10C**). In contrast, extracellular acidification rate (ECAR) detected simultaneously was significantly reduced in cells kept in high calcium levels for days 2-8, compared to cells in control or calcium free medium (Figure **10D**), albeit with similar lactate levels (Figure **10E**).

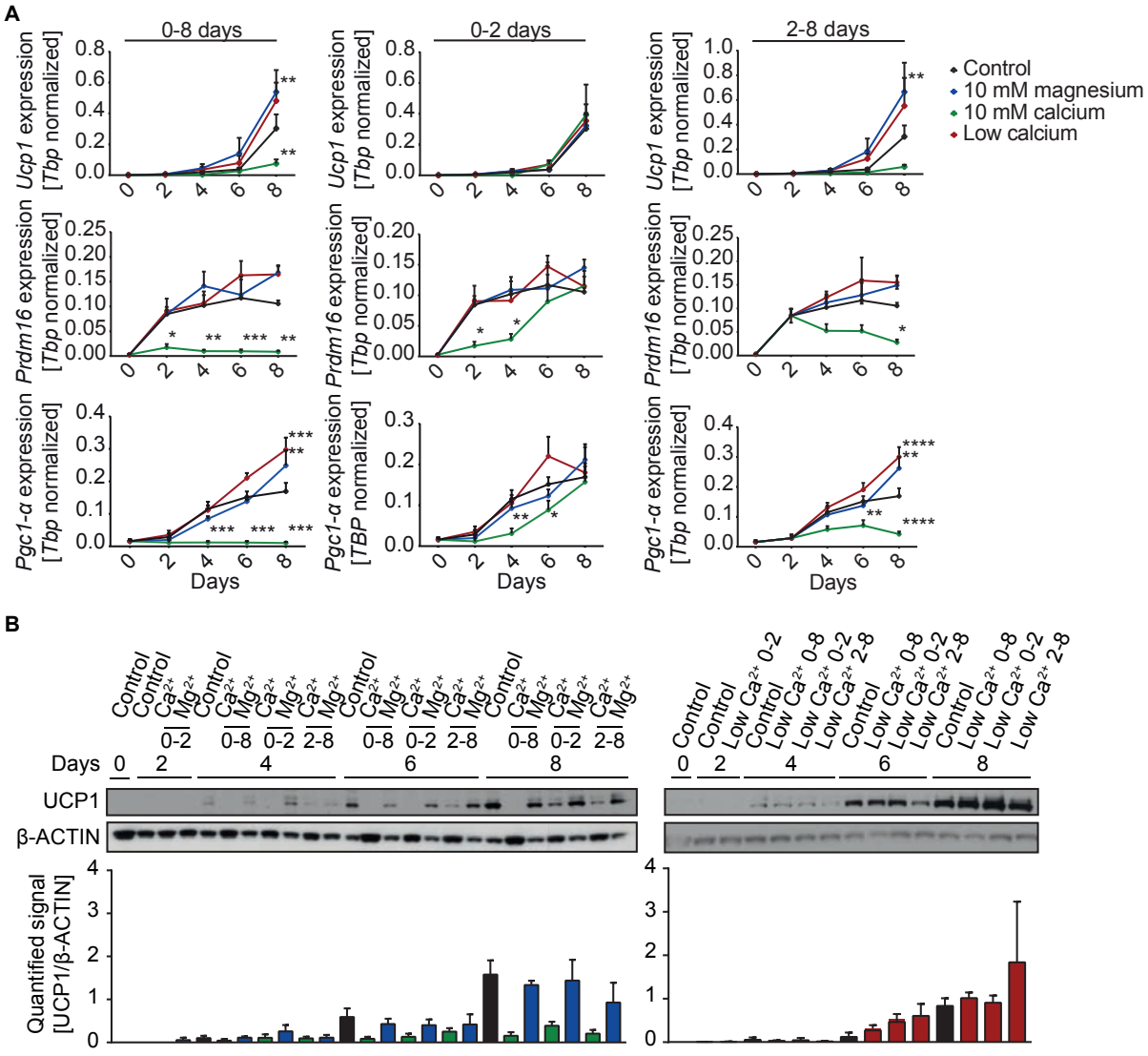

Figure 9 Extracellular calcium modulates brown adipocyte specific gene expression. (A) *Ucp1*, *Prdm16* and *Pgc1-α* expression normalized to *Tbp* in preadipocytes differentiated *in vitro* in an eight-day time course under normal 1.8 mM calcium (control), 10 mM calcium, 10 mM magnesium and calcium free conditions for days 0-8, days 0-2 and days 2-8 (Ucp1, Prdm16 n = 5-7; Pgc1-α n = 4). **(B)** Western Blot for UCP1 and β-ACTIN and signal quantification during the eight-day time course with conditions as above during indicated time points (n=3). **(A)** Ordinary two-way ANOVA with Dunnett's posthoc test. Figure adapted from the published manuscript (Pramme-Steinwachs, Jastroch et al. 2017). Original publication attached.

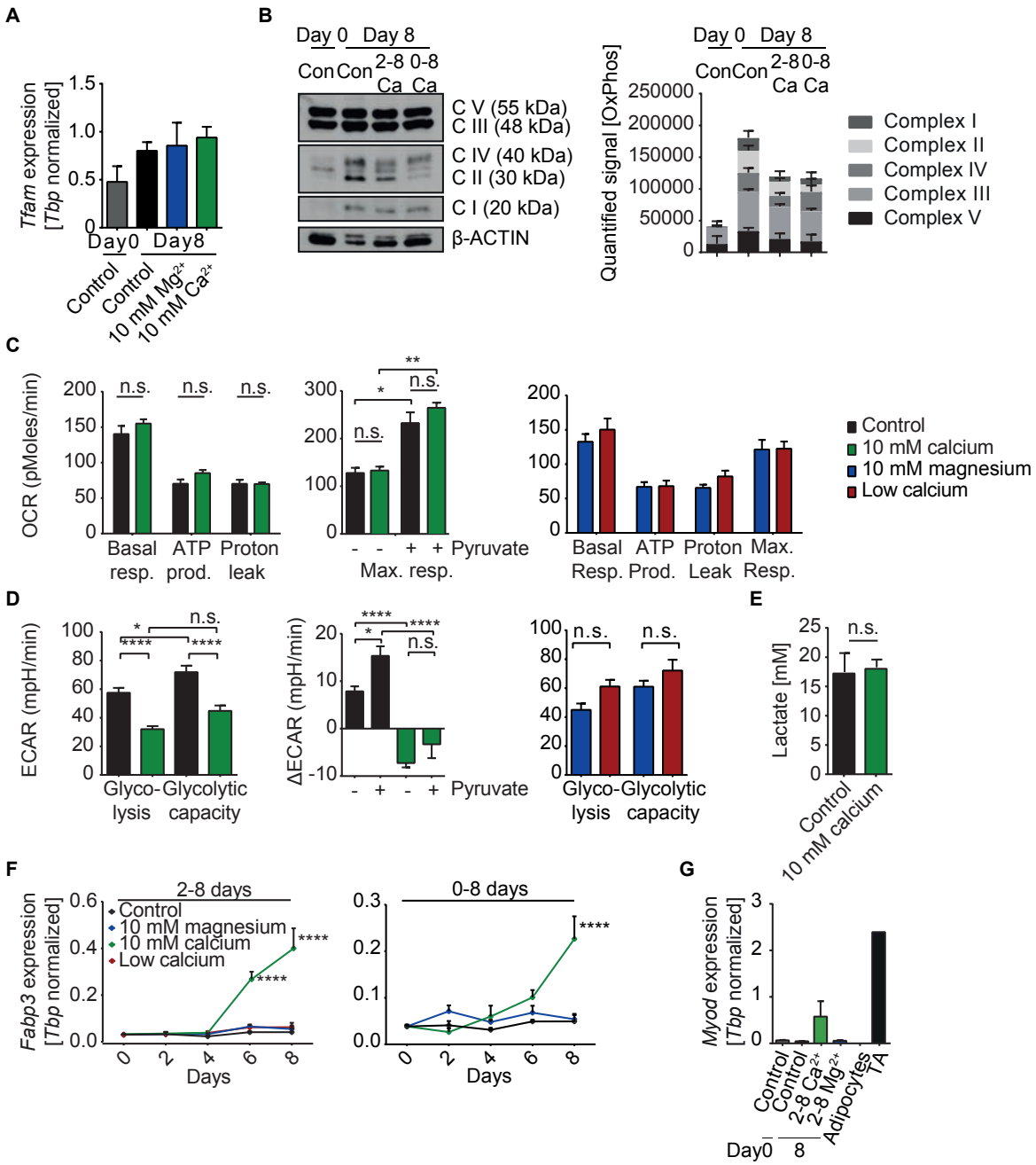

Figure 10 Extracellular calcium modulates brown adipocyte identity. (A) *Tfam* expression normalized on *Tbp* in preadipocytes (day 0) and in preadipocytes differentiated under normal 1.8 mM calcium (control), 10 mM calcium (Ca^{2+}),10 mM magnesium (Mg^{2+}) and calcium free conditions during days 2-8 (n=4). **(B)** OXPHOS western blot of preadipocytes (Con day 0) and adipocytes differentiated in 1.8 mM calcium (Con) or 10 mM calcium for days 2-8 or days 0-8, with β-ACTIN as loading control and signal quantification of mitochondrial complexes I-V protein (n=3; C I n=1). **(C)** Oxygen consumption rate (OCR) and **(D)** extracellular acidification rate (ECAR) measured by the Seahorse extracellular flux analyzer in preadipocytes at day 8 differentiated with 1.8 mM calcium (control), 10 mM magnesium, 10 mM calcium or low calcium for 2-8 days. OCR partitioned into basal respiration, ATP production, proton

leak and maximal respiration, also in the presence of pyruvate (5 mM). ECAR reported as glycolytic rate, glycolytic capacity and difference of glycolytic capacity (ΔECAR) before and after 5 mM pyruvate addition (together with FCCP) (n=3 for pyruvate n=2, 3-5 technical replicates each). **(E)** Lactate concentration of supernatant from cells differentiated under 1.8 mM calcium (control) and 10 mM calcium conditions for days 2-8 at day 8 (n=3). **(F)** *Fabp3* expression normalized to *Tbp* during time course in cells differentiated with 1.8 mM calcium (control), 10 mM calcium or 10 mM magnesium for days 0-8 or 2-8 (n=3). **(G)** *Myod* expression normalized to *Tbp* in preadipocytes (Control d0), in cells differentiated for eight days (day 8) under 1.8 mM calcium (control) or 10 mM calcium/magnesium for days 2-8 (n=3) and in isolated mature brown adipocytes as well as in murine musculus tibialis anterior (TA) (pooled samples n=1). **(A)** Friedmann one-way ANOVA with Dunn's posthoc test, **(C black green)** Kruskal-Wallis one-way ANOVA with Dunn's multiple comparison test. **(C blue/red, D)** ordinary one-way ANOVA with Tukey's posthoc test, **(E)** two-tailed Wilcoxon matched-pairs signed rank test and **(F)** repeated measures two-way ANOVA with Dunnett's posthoc test. Figure adapted from the published manuscript (Pramme-Steinwachs, Jastroch et al. 2017). Original publication attached.

The brown adipocyte-specific fatty acid binding protein 3 (*Fabp3*) correlates with increased long-chain fatty acid uptake and increased β-oxidation in BAT of UCP1 knock out mice (Daikoku, Shinohara et al. 1997, Yamashita, Wang et al. 2008, Vergnes, Chin et al. 2011, Nakamura, Sato et al. 2013). In this cell model, *Fabp3* expression was strongly induced with differentiation in cells exposed to elevated calcium both throughout differentiation and during days 2-8 (Figure **10F**). Similarly, *Myod* expression also tended to be increased upon high calcium treatment during days 2-8 (Figure **10G**).

Thus, the brown preadipocytes differentiated in high extracellular calcium for days 2-8 into adipocytes, shown by similar adipogenic marker gene expression and lipid accumulation, compared to controls. However, brown adipocyte gene expression was highly diminished and mitochondrial biogenesis seemed to be negatively affected under these conditions. Mitochondrial respiration on the other hand was not affected. Instead, *Fabp3* and *Myod* expression was increased in cells kept in high calcium medium for days 2-8 (Pramme-Steinwachs, Jastroch et al. 2017).

4.3 P2RX5 mediates brown fat function and regulates glucose homeostasis

The ATP-dependent calcium channel, P2RX5, is specifically expressed on the surface of BAT. Binding ATP changes the conformation and opens the channel for calcium influxes. It was shown in the previous section that modulating extracellular calcium levels impaired brown adipocyte differentiation completely or in parts and diminished brown adipocyte identity and function. These effects did not correlate with strong calcium increases suggesting either no calcium influx or just a very small calcium influx not detectable with the system used. A small, highly regulated calcium influx could be mediated by ligand-gated ion channels, like the ATP-dependent calcium channel P2RX5. ATP is co-released together with beta-adrenergic agonists from nerve vesicles in the highly innervated BAT. Upon release, ATP can bind to purinergic ion channels, mediate small calcium influxes and thereby regulate BAT identity and function. To investigate the function of P2RX5 in detail, genetically modified mice were generated, lacking either P2RX5 in BAT or in the whole organism. These mice are further referred to as $P2RX5^{fl/fl}$;$UCP1cre^{-}$ (fl) for BAT-specific control and $P2RX5^{fl/fl}$;$UCP1cre^{+}$ (cre) for BAT-specific ko mice as well as $P2RX5^{+/+}$ (wt) for whole body control with $P2RX5^{+/-}$ (het) and $P2RX5^{-/-}$ (ko) for whole body P2RX5 ko. In the following sections, the phenotypical and metabolic characterization of those mice is summarized to further understand the function of P2RX5 in BAT and in the whole organism.

4.3.1 BAT-specific P2RX5 ko impairs brown adipocyte function

To test, whether P2RX5 has an influence on the development of brown adipocytes, a stable knock down of P2RX5 with the respective shRNA (shP2rx5 KD5) was performed in immortalized, brown preadipocytes (BAT1 cells). P2RX5 KD5 BAT1 cells showed an impaired differentiation rate, which was observed by reduced lipid accumulation as well as by *Pparγ, Ucp1* and *Prdm16* expression, compared to control cells (shSCR) (Figure **11A-B**). To investigate the role of P2RX5 in BAT *in vivo*, BAT-specific P2RX5 ko mice were generated, showing a significant decrease in *P2rx5* mRNA levels in BAT but not in SCF or TA (Figure **11C**). BAT-specific P2RX5 ko animals (cre) had similar body weight, lean and fat mass compared to their controls (fl) (Figure **11D**). Conclusively, BAT weight and morphology were similar across genotypes (Figure **11E, G**). Also, PGF and SCF weight and histology did not differ (Figure **11E, G**), which was supported by quantification of the mean adipocyte size in PGF and SCF (Figure **12A**). Similarly, liver weight, histology and triglyceride accumulation were identical between fl

and cre mice (Figure **11E-G**). Differences in serum free fatty acid levels were not detected (Figure **11H**).

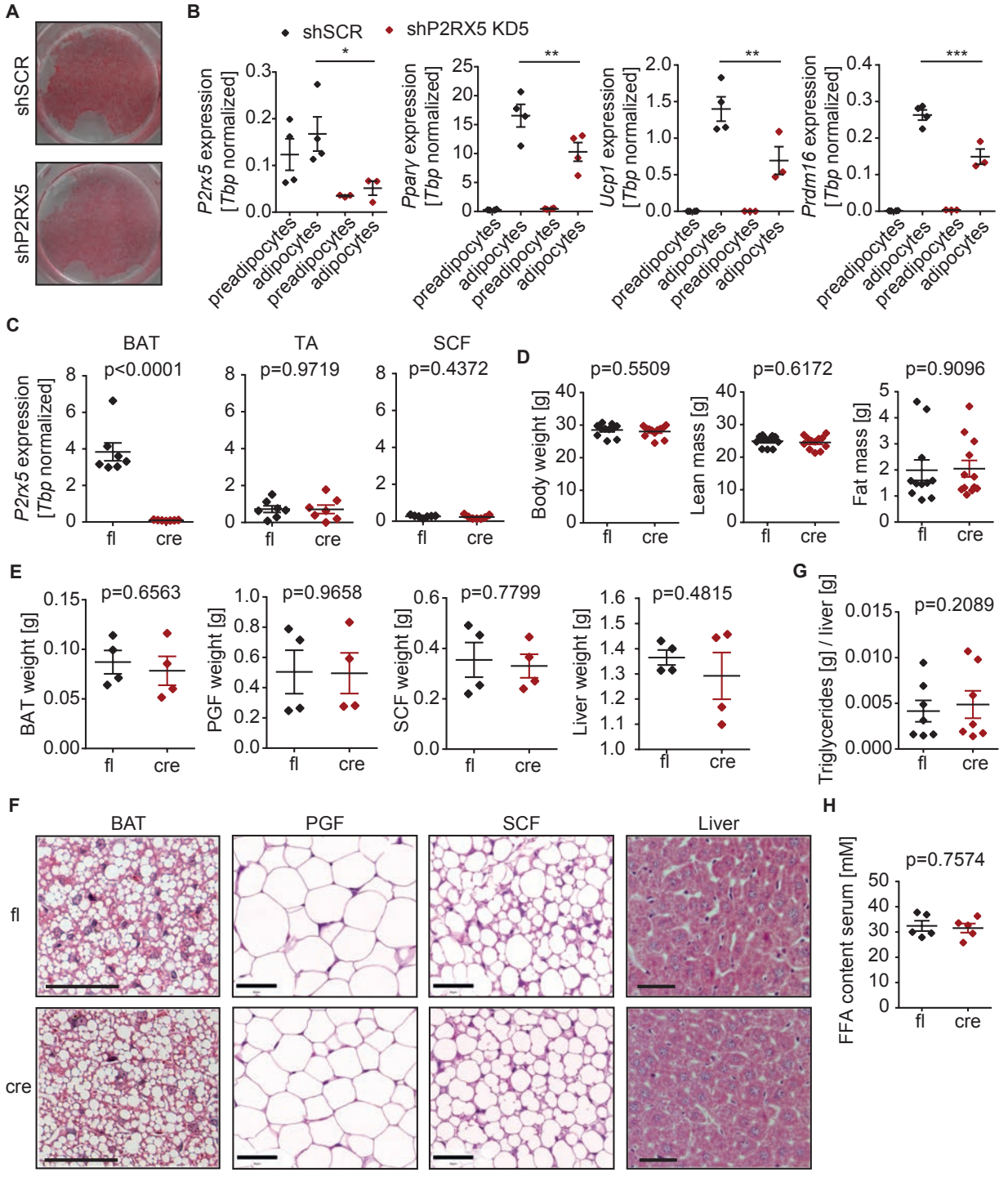

Figure 11 BAT-specific P2RX5 ko does not change body composition. (A) Oil Red O staining of BAT1 P2RX5 knock down (shP2RX5 KD5) and control cells (shSCR) differentiated *in vitro.* **(B)** Gene expression of *P2rx5, Pparγ*, *Ucp1* and *Prdm16* normalized to *Tbp* in preadipocytes and in adipocytes of BAT wt shSCR and BAT wt shP2RX5 differentiated *in vitro*. **(C)** *P2rx5* expression normalized to *Tbp* in BAT, SCF and TA in 3-4-month-old P2RX5$^{fl/fl}$;UCP1cre^{-} (fl) and P2RX5$^{fl/fl}$;UCP1cre^{+} (cre) mice. **(D)** Body weight, lean and fat mass of 3-4-month-old P2RX5 fl and cre mice. Tissue weight **(E)** and H&E stained tissue sections **(F)** of BAT, SCF, PGF and liver of 3-4-month-old fl and cre mice. **(G)** Triglyceride content per gram liver of 3-4-month-old fl and cre mice. **(H)** Free fatty acid content in serum of 3-4-month-old fl and cre mice. Two-Way ANOVA with Sidak's posthoc test **(B)** and unpaired Student's t-test **(C-E, G-H)** with p-values as indicated.

In addition to similar adipocyte size in SCF across genotypes (Figure **12A**), expression for *Ucp1* and *Pat2* did not differ between genotypes either (Figure **12B**). BAT-specific P2RX5 ko exhibited similar glucose tolerances and insulin tolerances (Figure **12C-D**). Moreover, BAT-specific P2RX5 ko did neither affect TA weight nor the gene expression of the slow/oxidative myosin heavy chain type I *(Mhc I)*, fast/oxidative *Mhc IIa,* fast/intermediate *Mhc IIx* or the fast/oxidative *Mhc IIx* (Figure **12E**).

To test the function of P2RX5 in BAT activity regulation, oxygen consumption measurements were conducted in primary brown preadipocytes from female P2RX5$^{fl/fl}$;UCP1cre^{+} (cre) and P2RX5$^{fl/fl}$;UCP1cre^{-} (fl) mice, differentiated *in vitro*. Cells from P2RX5$^{fl/fl}$;UCP1cre^{+} mice, which showed a strongly reduced *P2rx5* expression (Figure **13C**), possessed impaired oxygen consumption upon isoproterenol stimulation (Figure **13A**). Gene expression analysis revealed that *Ucp1* expression was reduced in those cells, even though *Ucp1* expression in male and female BAT of BAT-specific P2RX5 ko and wt mice was expressed evenly (Figure **13B**). The lower *Ucp1* expression could not be attributed to a lower differentiation rate in cells of P2RX5$^{fl/fl}$;UCP1cre^{+} mice compared to cells of P2RX5$^{fl/fl}$;UCP1cre^{-} mice, as the expression of *Pparγ* remained similar (Figure **13C**). Importantly, a reduced expression of *Glut4* and *Glut1* was observed in cells with a reduced *P2rx5* expression (Figure **13C**). In addition, P2RX5 inhibition in BAT wt cells differentiated *in vitro* with the P2RX5 inhibitor PPADS (10 µM) and the P2RX5/P2RX1 inhibitor NF449 (1 µM) one hour before oxygen consumption measurement also resulted in a reduction of mitochondrial respiration (Figure **13D**). These data suggest that reduced P2RX5 decelerated differentiation in immortalized but not in primary brown preadipocytes. However, oxygen consumption was worsened under P2RX5 reduction or inhibition, implying a reduced activation capacity of BAT with abolished P2RX5 presence or function.

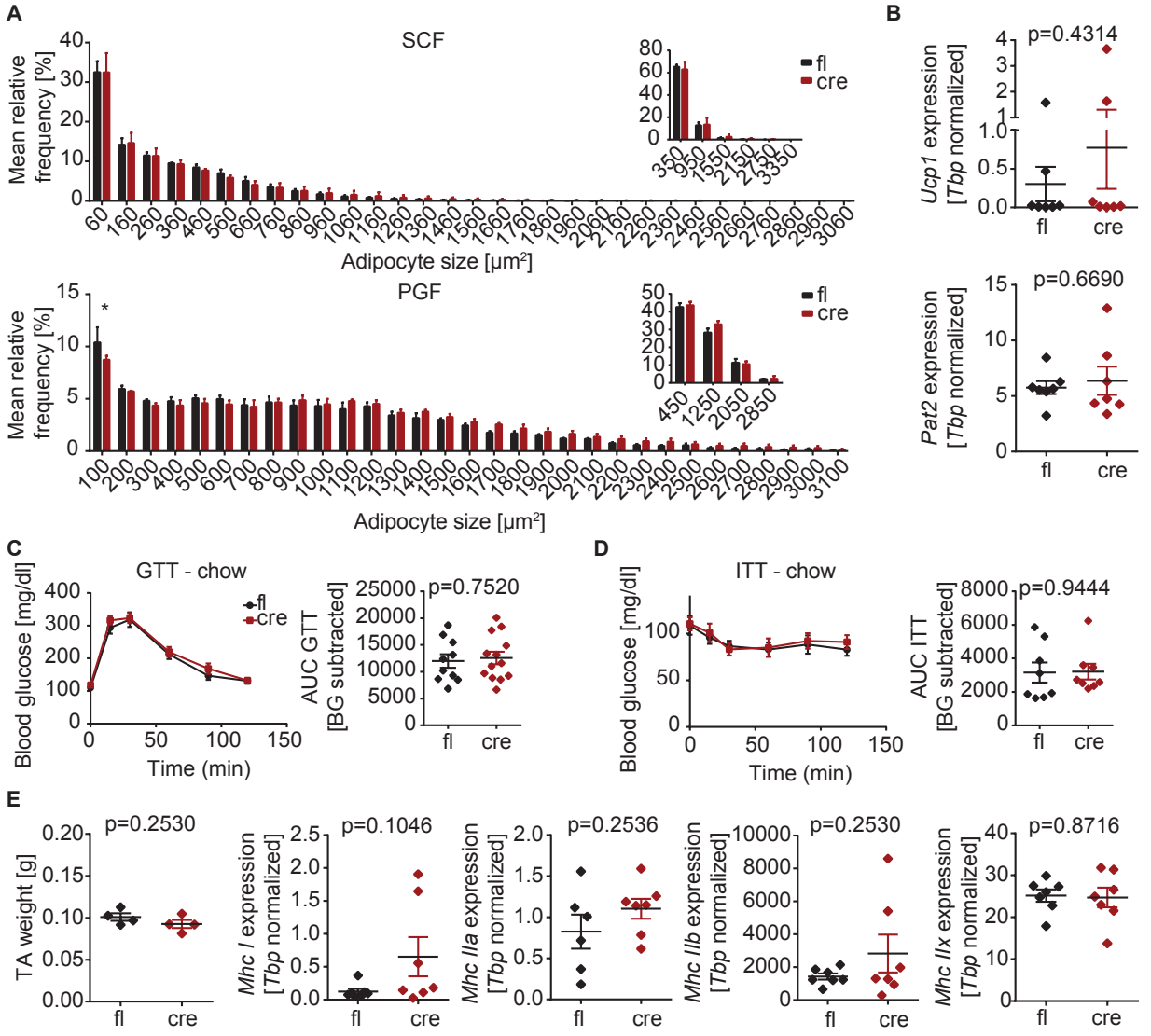

Figure 12 Loss of P2RX5 in BAT does not impair glucose tolerance. (A) Quantified relative frequency of adipocyte size in H&E stained slides of SCF and PGF of 3-4-month-old P2RX5$^{fl/fl}$UCP1cre^{-} (fl) and P2RX5$^{fl/fl}$UCP1cre^{+} (cre) mice (n=3). **(B)** *Pat2* and *Ucp1* expression normalized to *Tbp* in SCF of 3-4-month-old fl and cre mice. **(C)** Glucose tolerance test (GTT) shown as blood glucose levels over time upon glucose injection and AUC of background corrected glucose tolerance curves in 3-4-month-old fl and cre mice (n=10). **(D)** Insulin tolerance test (ITT) shown as blood glucose level over time upon insulin stimulation and AUC of background corrected insulin tolerance curves in 3-4-month-old fl and cre mice (n=8). **(E)** TA weight and myosin heavy chain *(Mhc) I, IIa, IIb, IIx* expression normalized to *Tbp* in TA of fl and cre mice. Two-Way ANOVA with Sidak's posthoc test **(A, E-F),** unpaired Student's t-test **(B, C-D (AUC), E)** with p-values as indicated.

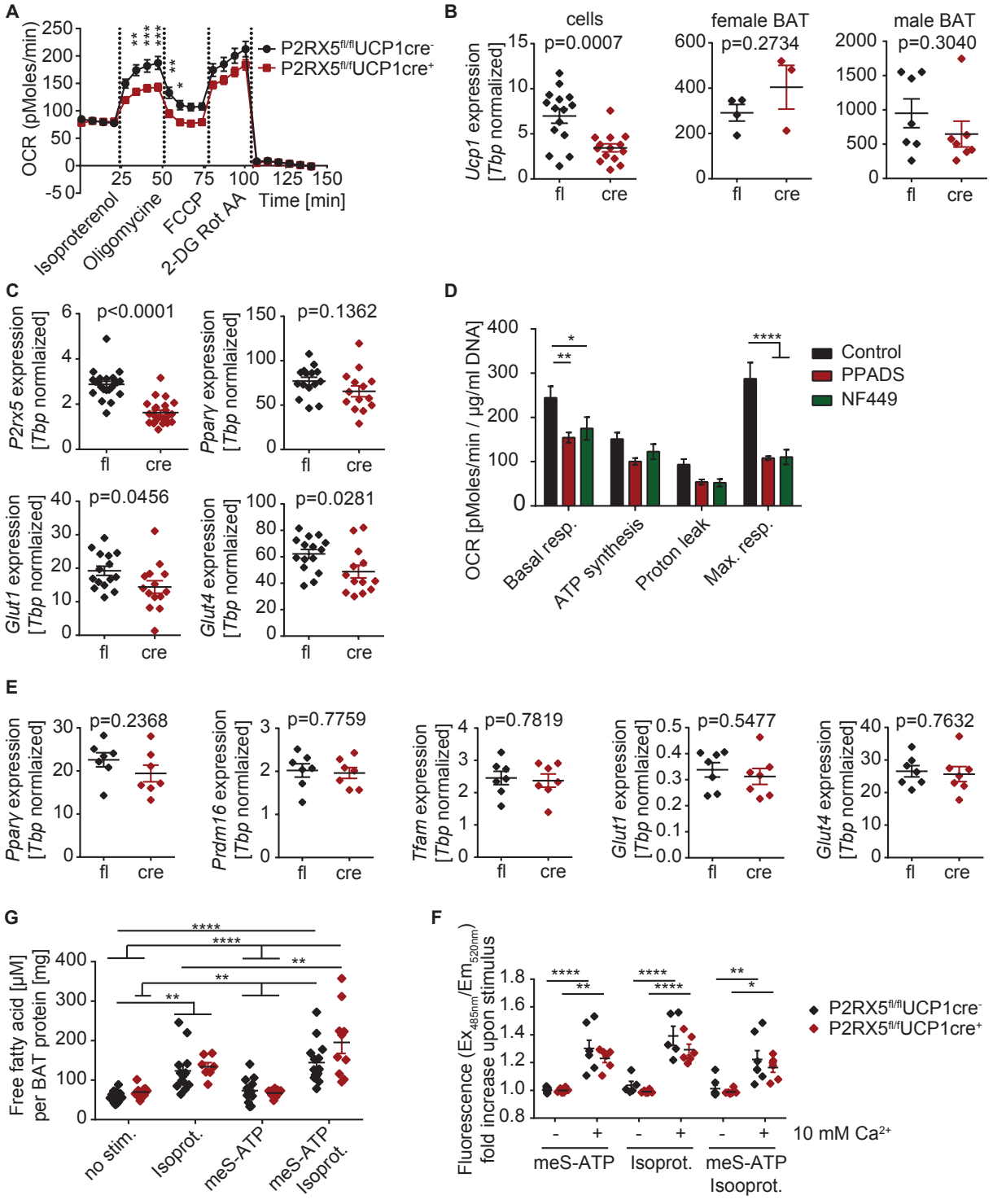

Figure 13 Loss of P2RX5 in BAT impairs mitochondrial respiration in vitro. (A) Oxygen consumption rates (OCR) detected with a 96 well Seahorse Flux Analyzer in brown adipocytes differentiated *in vitro* of female P2RX5$^{fl/fl}$UCP1cre^{-} (fl) and P2RX5$^{fl/fl}$UCP1cre^{+} (cre) mice. Compounds: 1 µM Isoproterenol, Oligomycin (2 mg/ml), FCCP (2 µM), 2-Deoxyglucose containing Rotenone (25 µM) and Antimycin A (25

µM) (n=5). **(B)** *Ucp1* expression normalized to *Tbp* in brown adipocytes differentiated *in vitro* of female fl and cre mice and in BAT of male and female fl and cre mice. **(C)** *P2rx5, Pparγ, Glut4* and *Glut1* expression normalized to *Tbp* in cells differentiated *in vitro* of fl and cre mice. **(D)** Oxygen consumption rates (OCR) per µg/ml DNA detected in brown preadipocytes differentiated *in vitro* (day 8) with a XF96 Extracellular Flux analyzer after one hour incubation with the P2RX5 inhibitors PPADS (10 µM) or NF449 (1 µM) or with medium (control). Shown are bar graphs of background corrected basal respiration, ATP synthesis, proton leakage and maximal respiration (n=3 replicates per condition). **(E)** Gene expression normalized to *Tbp* in BAT of male fl and cre mice. **(F)** Lipolysis assay measured by free fatty acid release from BAT pieces of female fl and cre mice upon no stimulation, isoproterenol, methyl-S-ATP or both isoproterenol and methyl-S-ATP stimulation normalized on BAT protein amount. **(G)** Relative increase of intracellular calcium in brown adipocytes differentiated *in vitro* (day 6) of fl and cre mice, shown as relative increase of fluorescence to basal level. Cells loaded with the calcium binding fluophore Fluo-4 (4 µM) in calcium free or calcium containing buffer (2 mM) and stimulated with either methyl-S-ATP (20 µM) or isoproterenol (1 µM) or both stimuli. Fluorescence recorded at Ex/Em = 485/520 in orbital averaging with a gain of 1100. Two-Way ANOVA with Sidak's posthoc test **(A, D, F-G)** and unpaired Student's t-test **(B-C, E)** with p-values as indicated.

In turn, gene expression analysis in BAT of P2RX5$^{fl/fl}$;UCP1cre^{-} and P2RX5$^{fl/fl}$;UCP1cre^{+} mice showed similar *Pparγ, Glut4, Glut1* and brown marker gene expression, like *Prdm16, Pgc1-α* and *Tfam*, across genotypes (Figure **13E**). Furthermore, BAT pieces stimulated with isoproterenol, 2-methylthio-ATP or both showed a similar lipolysis induction rate across genotypes (Figure **13F**). While 2-methylthio-ATP alone did not induce lipolysis in either control or P2RX5 ko BAT pieces, 2-methythio-ATP together with isoproterenol increased free fatty acid release even more strongly than solely isoproterenol (Figure **13F**). These data suggest, that 2-methylthio-ATP promotes isoproterenol-stimulated lipolysis. However, loss of P2RX5 *in vivo* did not impair BAT function.

To investigate whether calcium influx is influenced by the loss of P2RX5, calcium influx measurements were performed in primary brown preadipocytes differentiated *in vitro*. Upon treatment with isoproterenol, 2-methylthio-ATP or both stimuli, calcium influxes in cells of P2RX5$^{fl/fl}$;UCP1cre^{+} mice tended to be less strong than in cells of P2RX5$^{fl/fl}$;UCP1cre^{-} control mice, albeit without statistical significance. (Figure **13G**). These data also imply that 2-methythio-ATP did not just bind to P2RX5, it further stimulated other surface calcium channels or receptors mediating extracellular calcium influxes.

4.3.2 P2RX5 loss improves glucose tolerance and adipocyte size in white fat

To study the function of P2RX5 in the whole organism male 3-4-month-old and 8-week-old P2RX5 knock out mice were generated and phenotypically characterized. A prominent reduction of *P2rx5* gene expression in BAT was observed in P2RX5 het mice, which was more reduced in P2RX5 ko mice, compared to P2RX5 wt mice (Figure **14A, B**). Also, P2rx5 expression in SCF and TA of 8-week-old P2RX5 ko and P2RX5 het mice tended to be reduced, compared to P2RX5 wt mice (Figure **14B**). According to the literature (Ussar, Lee et al. 2014), P2rx5 was more highly expressed in BAT than in SCF and TA and almost not detectable in PGF (Figure **14B**). The litter size of the whole body P2RX5 breedings showed an expected 1:2:1 (wt:het:ko) genotype distribution for both males and females, even though the average litter size is small (Figure **14C**).

First phenotypical characterizations revealed that P2RX5 wt, het and ko mice at 8 weeks did not differ in body weight, lean and fat mass (Figure **14E**). As the major effect of P2RX5 loss is expected in BAT and the BAT morphology and functionality reduces with age, a second, 3-4-month-old cohort was characterized. Body weight measurements over time (8-14 weeks of age) revealed a slight decrease in weight gain in P2RX5 ko mice, compared to wt and P2RX5 het controls (Figure **14D**). Furthermore, for 3-4-month-old P2RX5 wt, het and ko mice, neither body length nor body weight or lean and fat mass differed between genotypes (Figure **14F-G**). While resting blood glucose levels remained similar across genotypes from week 8 to week 14 (Figure **14H**), 3-4-month-old P2RX5 ko mice showed an improved glucose tolerance, compared to P2RX5 wt and het mice (Figure **14I**). No significant reduction in areas under the curves (AUCs) was observed. However, the reduced blood glucose levels at 15 min clearly showed that loss of P2RX5 positively influences the biological kinetics of glucose clearance (Figure **14I**). In compliance with an improved glucose tolerance, reduced basal serum insulin levels in 3-4-month-old P2RX5 ko mice were obtained (Figure **14J**), indicating an improved insulin sensitivity in P2RX5 ko mice.

Analyses of the tissue weight revealed that BAT as well as SCF and perirenal fat (PRF) tended to a lower weight in both 8-week and 3-4-month-old P2RX5 ko mice, compared to the controls, while the PGF showed a significant reduction in weight in P2RX5 ko mice (Figure **15A-B**). In line with the reduced PGF weight in P2RX5 ko mice, smaller adipocytes were observed in H&E stained histology sections (Figure **15C**).

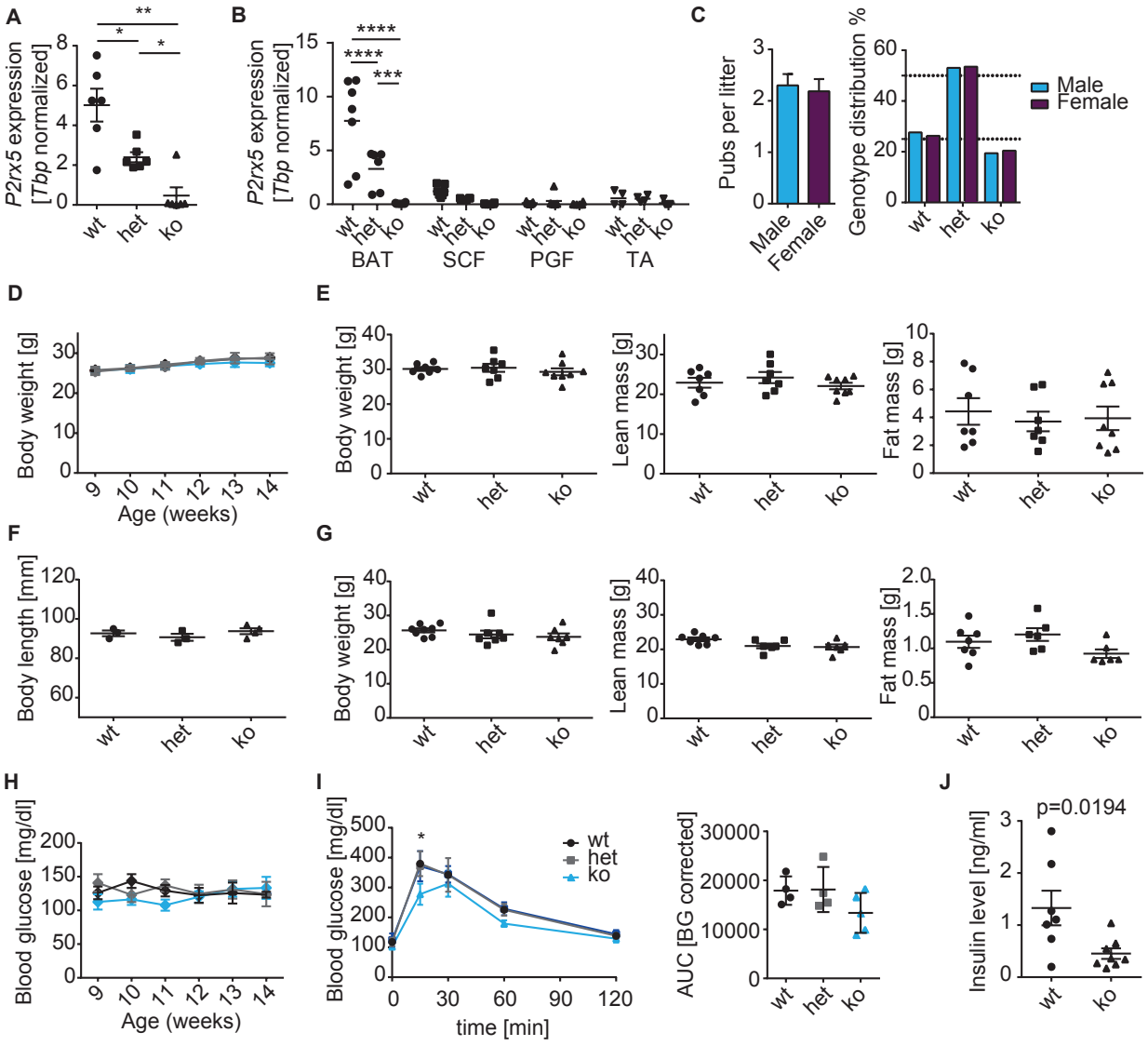

Figure 14 Loss of P2RX5 improves glucose tolerance and lowers basal insulin levels. (A) *P2rx5* expression normalized to *Tbp* in brown adipose tissue (BAT) of male 3-4-month-old P2RX5$^{+/+}$ (wildtype, wt), P2RX5$^{+/-}$ (heterozygous. het) and P2RX5$^{-/-}$ (knock out, ko) mice. **(B)** *P2rx5* expression normalized to *Tbp* in brown adipose tissue (BAT), subcutaneous fat (SCF) and musculus tibialis anterior (TA) of 8-week-old, male P2RX5 wt, het and ko mice. **(C)** Averaged litter size including male/female ratio and genotype distribution (litters n=43). **(D)** Body weight over time in P2RX5 wt, het and ko mice at indicated age in weeks. **(E)** Body weight, lean mass, fat mass and **(F)** body length in 3-4-month-old P2RX5 wt, het and ko mice. **(G)** Body weight, lean and fat mass of 8-week-old P2RX5 wt, het and ko mice. **(H)** Basal blood glucose levels over time in P2RX5 wt, het and ko mice at indicated age in weeks. **(I)** Glucose tolerance test shown as blood glucose levels over time (0-120 min) in 3-4-month-old P2RX5 wt, het and ko mice (n=4) and the background corrected area under the curves (AUCs). **(J)** Basal insulin levels in serum of 3-4-month-old P2RX5 wt and ko mice. One-Way ANOVA with Tukey's posthoc test **(A, E-G, I (AUC)),** two-Way ANOVA with Tukey's posthoc test **(B, H, I)** and unpaired Student's t-test **(J)** with p-values indicated.

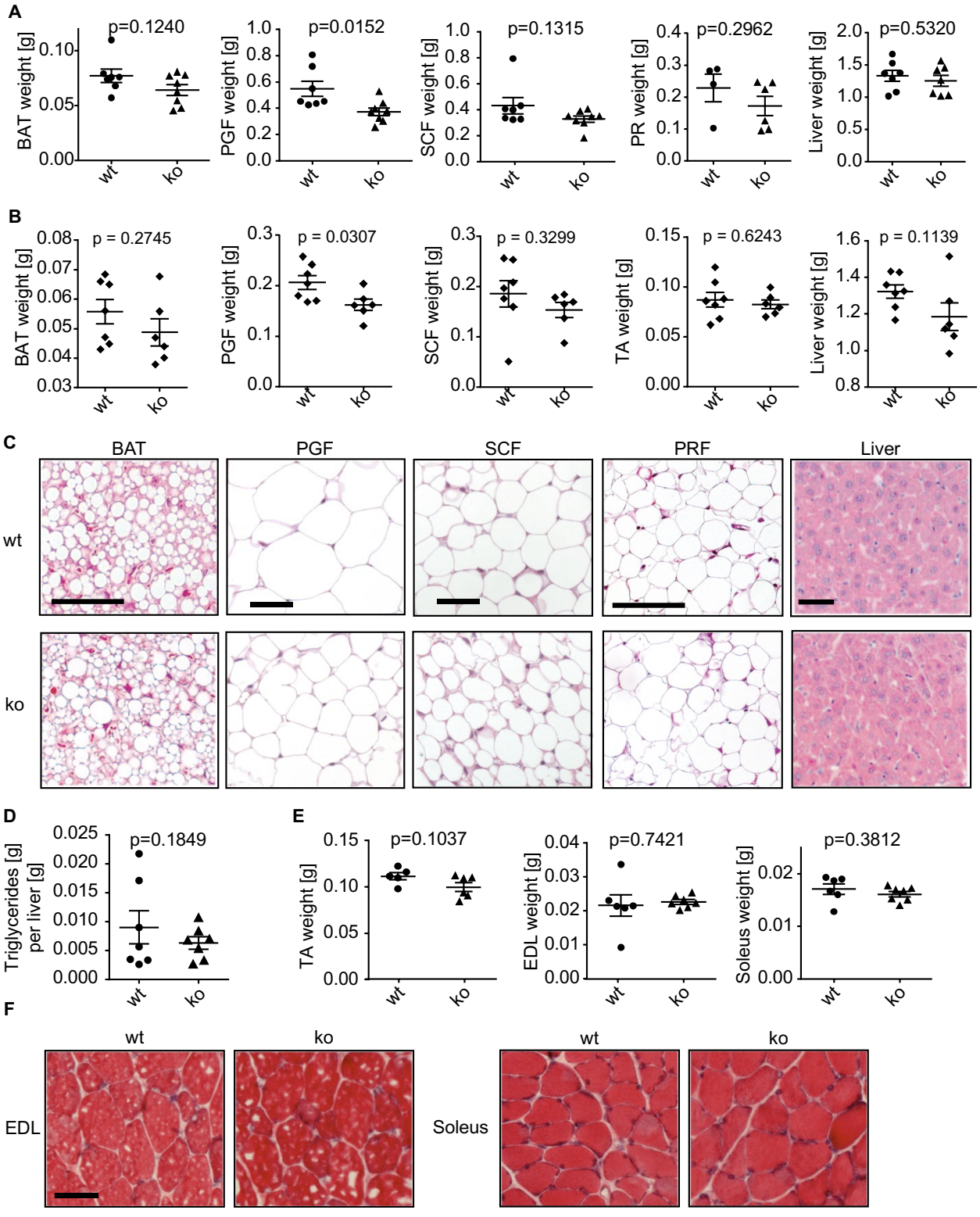

Figure 15 Loss of P2RX5 lowers white fat mass. Tissue weight of BAT, perigonadal fat (PGF), SCF, perirenal fat (PRF) or TA and liver of 3-4-month-old **(A)** and 8-week-old **(B)** P2RX5 wt and ko mice. **(C)** H&E staining of tissue slides of BTA, PGF, SCF, PRF and liver of 3-4-month-old P2RX5 wt and ko mice

(scale bar 100 µm). **(D)** Liver triglyceride levels per gram liver of 3-4-month-old male P2RX5 wt and ko mice. **(E)** Weight of TA, musculus extensor digitorum longus (EDL) and musculus soleus (soleus) of 3-4-month-old P2RX5 wt and ko mice with respective H&E staining in **(F)** for EDL and soleus (scale bar 100 µm). Unpaired Student's t-test **(A, B, D, E)** with p-values indicated.

While histology sections of SCF also showed smaller adipocytes, the histology of brown fat remained similar across genotypes (Figure **15C**). As whole body fat mass was not changed between genotypes, liver histology was analyzed for lipid accumulation. Liver weights and histology as well as triglyceride contents remained similar across genotypes (Figure **15A-D**). P2RX5 is also present in skeletal muscle, but its absence did not change the weight of the mixed musculus tibialis anterior (TA), the oxidative musculus soleus (soleus) and the glycolytic musculus extensor digitorum longus (EDL) (Figure **15E**). In addition, the histology of H&E stained sections of soleus and EDL also remained similar across genotypes (Figure **15F**).

Taken together, P2RX5 ko mice showed improved glucose tolerance and lower basal insulin levels, suggesting improved insulin sensitivity. However, similar body composition of P2RX5 ko mice and their P2RX5 het and wt controls was observed. This suggests an increased glucose uptake by the muscle or brown fat, the mass and morphology of which was not different across genotypes. In addition, reduced adipocyte size and fat pad weight of white fat indicates either decreased lipogenesis or increased lipolysis in white fat.

4.3.3 Absence of P2RX5 results in increased white fat lipolysis and induced beiging

P2RX5 is specifically expressed in brown fat. However, its loss resulted in reduced weight and smaller adipocyte size in white fat, mainly in PGF (Figure **15A-C**). These results were supported by quantifications of all differently sized adipocytes in subcutaneous and perigonadal adipose tissue sections. Adipocytes in SCF sections tended to be smaller in P2RX5 ko mice with 3-4 months and with 8 weeks, compared to the wt controls (Figure **15C**). However, quantifying the differently sized adipocytes in PGF showed a more specific accumulation of smaller adipocytes (50-850 μm^2) in P2RX5 ko mice and a specific accumulation of larger adipocytes (1650-2450 μm^2) in P2RX5 wt mice (Figure **16A**). This was also supported by the data derived from PGF of 8-week-old mice (50-550 μm^2) even though the overall adipocyte size was smaller (Figure **16B**).

To test whether the decreased adipocyte size results from increased lipolysis, Western Blots for specific proteins as well as lipolysis assays in tissue pieces were performed. The phosphorylated enzyme hormone-sensitive lipase (HSL) is responsible for the first step of

lipolysis and degrades triacylglycerides into diacylglycerides and free fatty acids. However, elevated HSL phosphorylation levels were not detected in either SCF or PGF of ad libitum fed P2RX5 ko mice (Figure **16C-D**). The slight decrease in quantified pHSL levels in PGF of P2RX5 ko mice seemed to be related to slightly increased total HSL protein levels (Figure **16D**). As a result, serum free fatty acid levels of 3-4-month-old and 8-week-old mice were also not changed across genotypes (Figure **16E**).

Similarly, *ex vivo* free fatty acid releases from tissue pieces of SCF and PGF were similar across genotypes (Figure **16F**), suggesting that resting lipolysis is not regulated differently in P2RX5 ko mice. However, stimulating lipolysis in fat pieces with isoproterenol *ex vivo* released more free fatty acids in subcutaneous fat pieces of P2RX5 ko mice, compared to controls, while perigonadal fat pieces reacted similarly (Figure **16F**). These data suggest that isoproterenol stimulation is improved in P2RX5 ko mice, probably by secondary effects of P2RX5 loss. Thus, lipolysis in subcutaneous fat might be increased, while the decreased adipocyte size in perigonadal fat could not be referred to elevated lipolysis.

Induced beiging in SCF occurs jointly with decreased adipocyte size and smaller lipid droplets. To test this hypothesis, beige fat specific gene expression and mitochondrial protein accumulation were studied in SCF of P2RX5 wt and ko mice. The beige marker genes *Pat2* and *Cd137* were equally expressed in SCF of P2RX5 ko and wt mice. However, the expression of the mitochondrial uncoupling protein 1 (*Ucp1*) was divergent and in parts tended to be increased in P2RX5 ko animals, compared to controls, in both 8-week and 3-4-month-old mice (Figure **17A, C**). *Ucp1* expression in PRF remained similar across genotypes (Figure **17B**). The mitochondrial, oxidative phosphorylation complexes II-IV (OXPHOS CII-IV) are responsible for the electron transport and proton gradient generation in mitochondria. An increase in those complexes in SCF can refer to an elevated amount of mitochondria and thereby to induced beiging. P2RX5 ko mice show slightly increased protein levels for the OXPHOS complexes, especially complexes II and IV, compared to wt animals (Figure **17D-E**).

Moreover, ERK phosphorylation was strongly reduced in SCF of P2RX5 ko mice, compared to controls (Figure **17F**), which can also indicate macrophage infiltration and inflammation. However, expression of macrophage marker genes, like *F4/80*, *Cd11b*, *Cd86* and *Il1-β*, did not differ between genotypes (Figure **17G**). These data imply increased lipolysis and induced beiging in subcutaneous fat, compared to controls, which could also contribute to improving glucose uptake in P2RX5 ko animals.

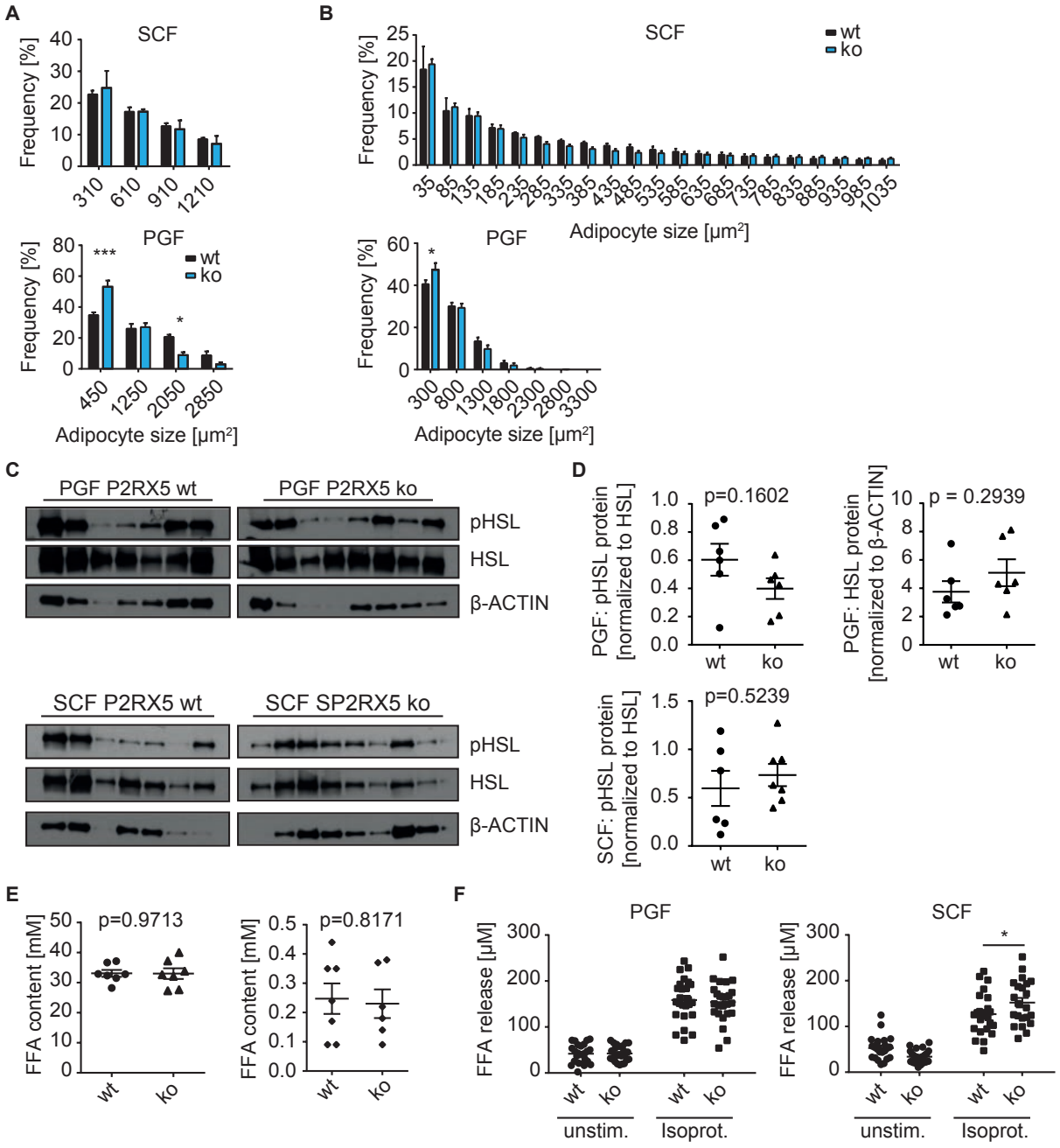

Figure 16 Absence of P2RX5 results in decreased white adipocyte size and increased SCF lipolysis. Histograms of quantified adipocyte size in H&E stained PGF and SCF sections of 3-4-month-old **(A)** and 8-week-old **(B)** P2RX5 wt and ko mice shown as frequency of adipocyte sizes within a defined bin range [%] (**A** – bin = 600 (SCF) and 800 (PGF), **B** – bin = 60 (SCF) and 500 (PGF)) (n=3). **(C)** Detected pHSL and HSL as well as the loading controls β-ACTIN in western blot of protein samples from PGF and SCF of 3-4-month-old P2RX5 wt and ko mice with **(D)** the respective quantification of pHSL or HSL signal normalized to the HSL or β-ACTIN signal. **(E)** Serum free fatty acid levels of male 3-4-month-old (*left*) and 8-week-old (*right*) P2RX5 wt and ko animals. **(F)** Lipolysis assay in PGF and SCF pieces of female P2RX5 wt and ko mice measured as free fatty acid (FFA) release into supernatant upon no

stimulation (unstim.) or Isoproterenol stimulation (Isoprot., 1 µM). Two-Way ANOVA with Sidak's posthoc test **(A-B, F)** and unpaired Student's t-test **(D-E)** with p-values as indicated in the graph.

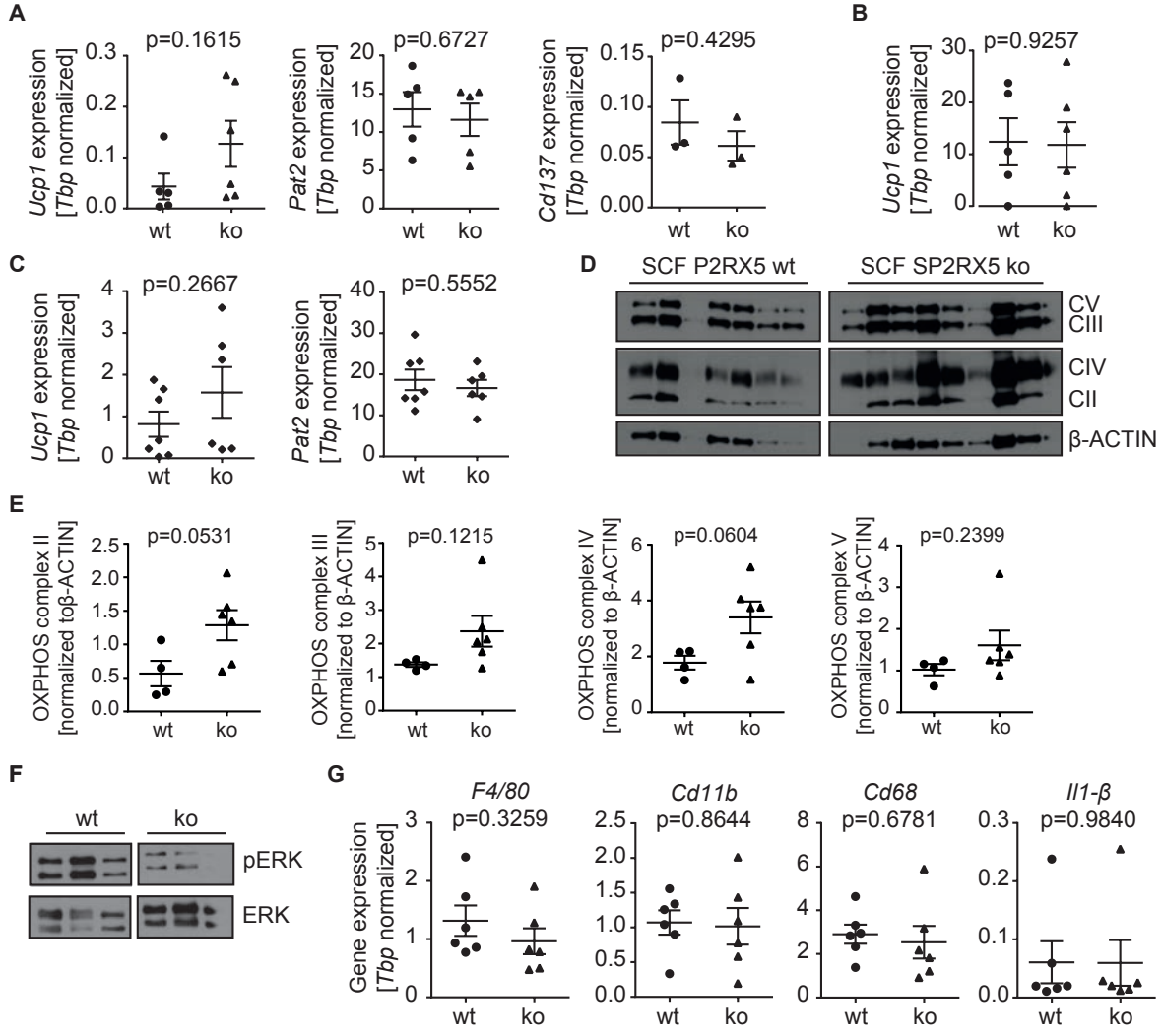

Figure 17 Absence of P2RX5 results in induced beiging in SCF. (A) *Ucp1*, *Pat2* and *Cd137* expression normalized to *Tbp* in SCF and **(B)** *Ucp1* expression normalized to *Tbp* in PRF of 3-4-month-old P2RX5 wt and ko mice. **(C)** *Ucp1* and *Pat2* expression normalized to *Tbp* in SCF of 8-week-old P2RX5 wt and ko mice. **(D)** Western Blot for oxidative phosphorylation (OXPHOS) complexes II-V and β-ACTIN as loading control in SCF protein lysates of 3-4-month-old P2RX5 wt and ko mice and **(E)** the quantified OXPHOS signals normalized to β-ACTIN. **(F)** Western Blot for pERK and ERK in SCF protein lysates of 3-4-month-old P2RX5 wt and ko mice. **(G)** Gene expression of macrophage markers normalized to *Tbp*. Unpaired Student's t-test **(A-C, E-F)** with p-values as indicated in the graph.

4.3.4 P2RX5 knock out improves brown fat identity and activity

Better glucose tolerance combined with reduced resting insulin levels in the serum suggested improved insulin sensitivity in P2RX5 ko mice, which was independent of weight gain. Insulin-dependent glucose uptake is very prominent in muscle and brown fat. As weight and morphology in both organs did not differ between genotypes, their function was studied in more detail. P2RX5 is suggested to mediate co-activation of BAT upon beta-adrenergic signaling stimulation. In fact, whole body P2RX5 absence did not worsen but rather promoted metabolic health of mice, seen by better glucose tolerance, reduced insulin levels and reduced adipocyte size in white fat as well as by indications for beiging in subcutaneous fat (Figure **14-17**).

Oxygen consumption measurements in primary brown adipocytes differentiated *in vitro*, which originated from the stromal vascular fraction (SVF) of female P2RX5 wt and ko BAT, revealed an improved mitochondrial respiration upon isoproterenol stimulation in the absence of P2RX5 (Figure **18A**), resulting in elevated UCP1-dependent respiration in cells from P2RX5 ko mice (Figure **18B**). Stimulating these cells with 2-methylthio-ATP - an agonist showing similar specificity for P2RX5 compared to ATP - did not increase basal mitochondrial respiration. It rather enhanced maximal respiration in cells from P2RX5 ko mice, compared to wt mice, upon treatment with the mitochondrial uncoupler Carbonyl cyanide-4-(trifluoromethoxy)phenylhydrazone (FCCP) (Figure **18A**).

These data indicated an overall improved mitochondrial respiration in cells isolated from BAT of P2RX5 ko mice, suggesting elevated UCP1 protein levels or protein activity. Indeed, UCP1 protein levels in BAT of P2RX5 ko mice were significantly increased, compared to BAT in wt controls, even though *Ucp1* gene expression levels in both female and male BAT were similar across genotypes (Figure **18C-D**). Western Blots for the mitochondrial respiration complexes I-V (OXPHOS, CI-V) showed enhanced levels for all five mitochondrial respiration complexes in P2RX5 ko mice, compared to controls (Figure **18E-F**). This suggests increased mitochondria amounts in BAT of P2RX5 ko mice, which seem responsible for elevated maximal respiration. An increased amount of mitochondria, UCP1 protein levels and elevated mitochondrial uncoupling could explain the improved glucose tolerance observed in P2RX5 ko mice.

However, mRNA levels of *Glut4* and *Glut1* in BAT did not differ between genotypes (Figure **18G**). As *P2rx5* is also expressed in macrophages and anti-inflammatory M2 macrophages can contribute to browning, the expression of macrophage marker genes was analyzed.

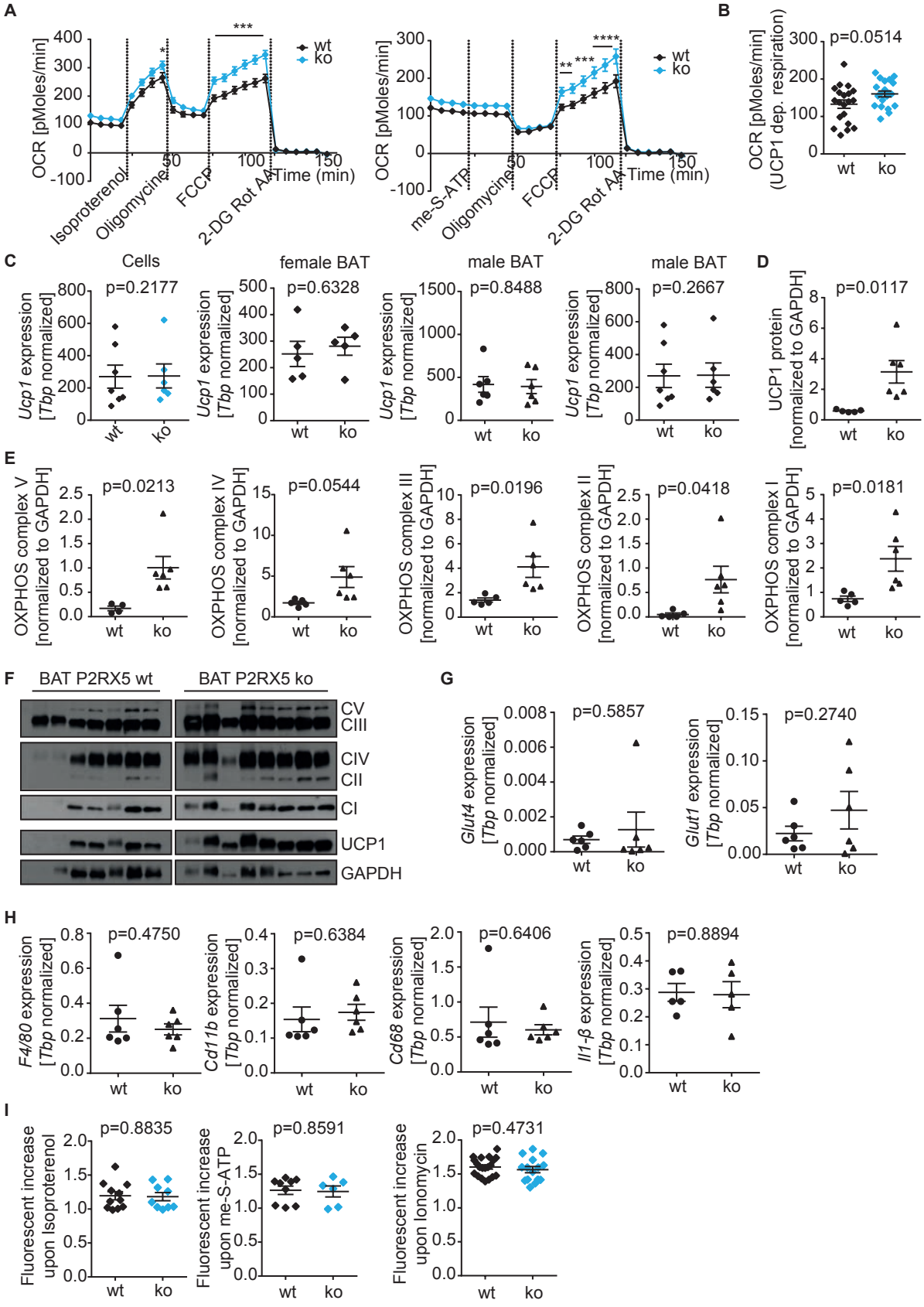
A
OCR [pMoles/min]
wt
ko
Time (min)
Isoproterenol
Oligomycine
FCCP
2-DG Rot AA
me-S-ATP
B
OCR [pMoles/min] (UCP1 dep. respiration)
p=0.0514
C
Cells
female BAT
male BAT
male BAT
Ucp1 expression [Tbp normalized]
p=0.2177
p=0.6328
p=0.8488
p=0.2667
D
UCP1 protein [normalized to GAPDH]
p=0.0117
E
OXPHOS complex V [normalized to GAPDH]
p=0.0213
OXPHOS complex IV [normalized to GAPDH]
p=0.0544
OXPHOS complex III [normalized to GAPDH]
p=0.0196
OXPHOS complex II [normalized to GAPDH]
p=0.0418
OXPHOS complex I [normalized to GAPDH]
p=0.0181
F
BAT P2RX5 wt
BAT P2RX5 ko
CV
CIII
CIV
CII
CI
UCP1
GAPDH
G
Glut4 expression [Tbp normalized]
p=0.5857
Glut1 expression [Tbp normalized]
p=0.2740
H
F4/80 expression [Tbp normalized]
p=0.4750
Cd11b expression [Tbp normalized]
p=0.6384
Cd68 expression [Tbp normalized]
p=0.6406
Il1-β expression [Tbp normalized]
p=0.8894
I
Fluorescent increase upon Isoproterenol
p=0.8835
Fluorescent increase upon me-S-ATP
p=0.8591
Fluorescent increase upon Ionomycin
p=0.4731

Figure 18 P2RX5 knock out promotes mitochondrial gene expression and respiration in BAT. (A) Oxygen consumption rates (OCR) detected in brown preadipocytes of female P2RX5 wt and ko mice differentiated *in vitro* (day 5) with a 96 well Seahorse Flux Analyzer. Compounds: 1 µM Isoproterenol (left), 20 µM 2-methylthio-ATP together with 1 mM $CaCl_2$ (right), Oligomycin (2 mg/ml), FCCP (2 µM), 2-Deoxyglucose containing Rotenone (25 µM) and Antimycin A (25 µM) (n=5) with UCP1-dependent respiration shown separately in **(B). (C)** *Ucp1* expression normalized to *Tbp* in primary brown preadipocytes from female BAT differentiated *in vitro*, female BAT of 14-weeks-old and male BAT of 3-4-months-old (triangle) and 8-week-old (rhombus) P2RX5 wt and ko mice. **(D)** UCP1 protein quantification normalized on GAPDH protein levels in BAT samples in the sample blot in **(F)**. **(E)** Quantified oxidative phosphorylation (OXPHOS) complexes I-V signals normalized to GAPDH signal obtained from western blot in **(F)**. **(F)** Western Blots for UCP1 and OXPHOS complexes I-V with GAPDH as loading controls in protein samples of BAT from 3-4-month-old P2RX5 wt and ko mice. Gene expression of **(G)** glucose transporters and (**H**) macrophage markers normalized to *Tbp* in BAT of 3-4-onths-old P2RX5 ko and wt mice. **(I)** Relative increase of intracellular calcium in brown preadipocytes from P2RX5 wt and ko mice differentiated *in vitro.* Relative increase of fluorescence compared to basal levels. Cells loaded with the calcium binding fluophore Fluo-4 (4 µM) in calcium free or calcium containing buffer (2 mM) and stimulated with 2-methylthio-ATP (me-S-ATP, 20 µM), isoproterenol (1 µM) or finally ionomycin (10 µM). Fluorescence recorded at Ex/Em = 485/520 in orbital averaging with a gain of 1100 (n=5). Two-Way ANOVA with Sidak's posthoc test **(A)** and unpaired Student's t-test with p-values **(B-E, G-I)** indicated in the graph.

The general macrophage marker genes *F4/80* and *Cd11b* as well as the pro-inflammatory M1 macrophage marker gene *Cd68* and the anti-inflammatory M2 macrophage marker gene *Il1-β* were not increased in BAT of P2RX5 ko mice, compared to controls (Figure **18H**). Additionally, calcium influxes upon 2-methylthio-ATP and isoproterenol stimulation were not reduced in the absence of P2RX5 (Figure **18I**), implying that P2RX5 mediated just small calcium influxes instead of massive calcium floods.

Loss of adrenergic receptors in BAT results in a differed regulation of purinergic channels (Razzoli, Frontini et al. 2016). Thus, the expression of purinergic channels and adrenergic receptors, which are both involved directly or indirectly in calcium signaling, were tested in BAT of P2RX5 wt and ko mice. While the expression of *P2rx3* could not be detected, the expression of the purinergic channels *P2rx1-4*, *P2rx6-7*, *P2y2* and *P2y12* as well as of the adrenergic receptors *A2a* and *Adrb1-3* was similar across genotypes in 8-week-old and 3-4-month-old animals (Figure **19A-B**). Also, the expression of Adrb3, which is mainly involved in the isoproterenol stimulation, remained similar in brown preadipocytes differentiated *in vitro,* even though the adrenergic stimulus was absent during differentiation (Figure **19C**). Conclusively, the induction of a compensatory mechanism resulting in enhanced UCP1 levels in the absence of P2RX5 could not be shown by the tested surface proteins.

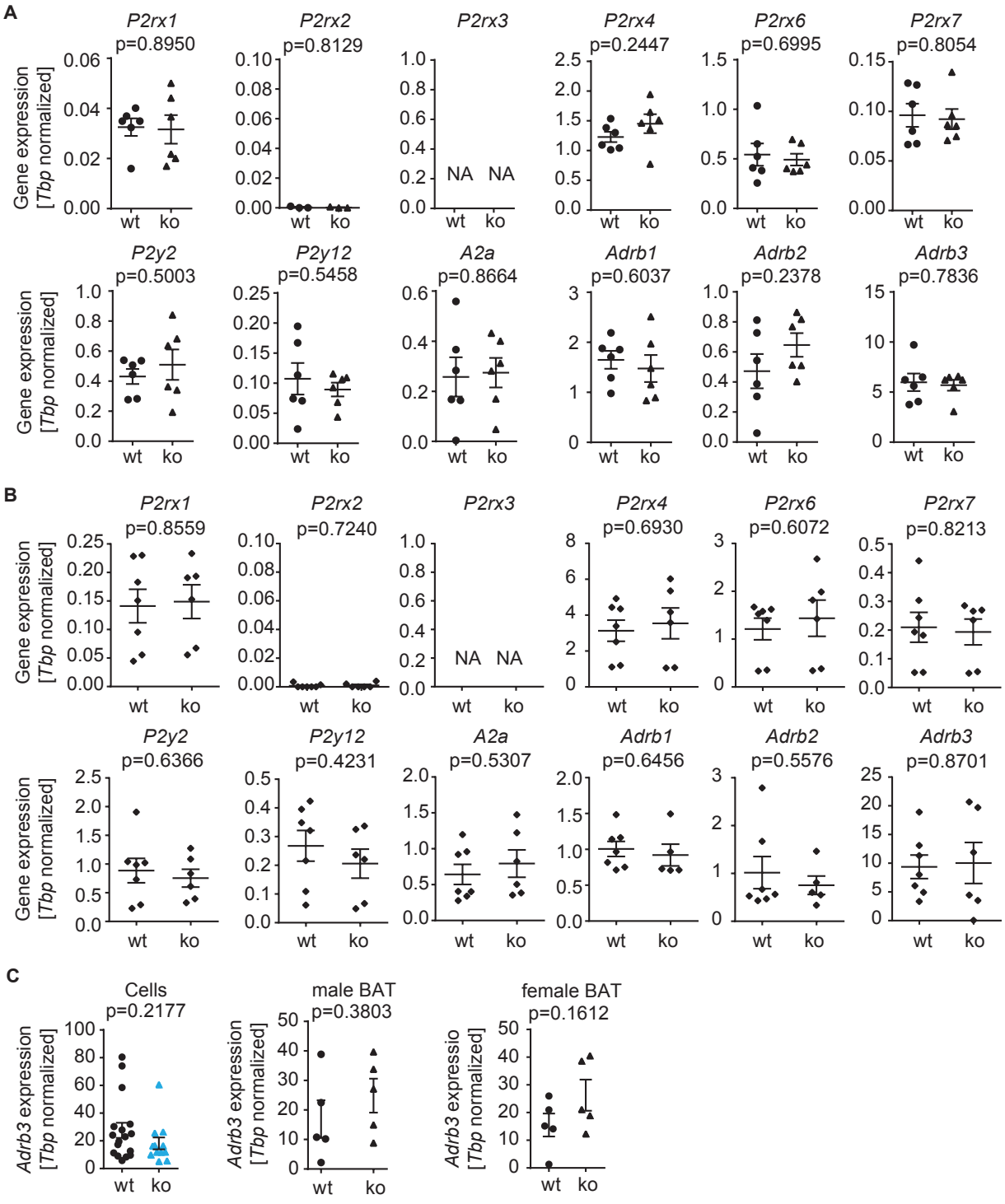

Figure 19 P2RX5 knock out is not compensated by increased expression of the following channels/receptors in BAT. Gene expression normalized to *Tbp* of purinergic and adrenergic channels and receptors being involved in calcium homeostasis (*P2rx1-4*, *P2rx6-7*, *P2y2*, *P2y12*, *A2a*, *Adrb1-3*) in BAT of 3-4-month-old **(A)** and 8-week-old **(B)** P2RX5 wt and ko mice. **(C)** Beta3-adrenergic receptor (*Adrb3*) expression normalized to *Tbp* in brown preadipocytes differentiated *in vitro* (cells), in male BAT of

3-4-month-old and female BAT of 3-4-week-old P2RX5 wt and ko mice. cDNA from RNA samples *ex post* digested with DNase. Unpaired Student's t-tests **(A-C)** with p-values indicated in the graph.

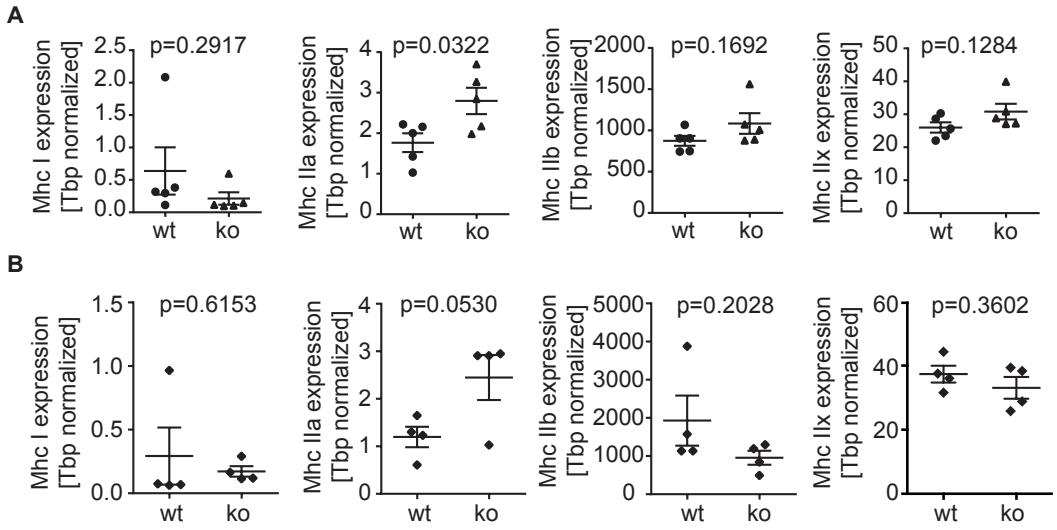

Figure 20 P2RX5 knock out induces muscle fiber type switch in TA. Expression of muscle fiber genes for myosin heavy chain (*Mhc*) *I, IIa, IIb* and *IIx* normalized to *Tbp* in musculus tibialis anterior (TA) of 3-4-month-old **(A)** and 8-wek-old **(B)** P2RX5 wt and ko mice. Unpaired Student's t-tests **(A-B)** with p-values indicated in the graph.

The skeletal muscle also contributes to glucose clearing. Thus, mixed (glycolytic/oxidative, TA), glycolytic (EDL) and oxidative (soleus) skeletal muscles were studied in detail. Weight and histology of those skeletal muscle types did not differ across genotypes (Figure **15E-F**). However, the expression of the slow, oxidative myosin heavy chain I (*Mhc I*), the fast, intermediate *Mhc IIx* and the fast glycolytic *Mhc IIb* remained similar in TA of 8-week and 3-4-month-old P2RX5 ko and wt mice. In contrast, the expression of the fast, oxidative myosin heavy chain IIa (*Mhc IIa*) was increased in TA of both 8-week and 3-4-month-old P2RX5 ko mice compared to P2RX5 wt (Figure **20A-B**). As the fiber type isoform MHC IIA is shown to have the biggest influence on insulin-stimulated glucose uptake, compared to the isoforms MHC IIB and IIX (MacKrell and Cartee 2012), it is hypothesized, that the increases in *Mhc IIa* mRNA levels in TA of P2RX5 ko mice could also mediate a better glucose uptake capacity in skeletal muscle, probably resulting in improved glucose tolerance.

5 DISCUSSION

5.2 Extracellular calcium modulates brown adipocyte differentiation and identity[6]

This work shows that elevated extracellular calcium impairs brown adipocyte differentiation and identity *in vitro*. In line with previous data on white adipocytes (Jensen, Farach-Carson et al. 2004, Lechner, Mitterberger et al. 2013), continuous exposure to high extracellular calcium inhibits lipid accumulation and induction of *Pparγ* and *C/ebpα*, which are key regulators in adipogenesis. Conversely, normalizing calcium levels after induction restores lipid accumulation and adipogenic marker expression. Thus, high extracellular calcium reversibly pauses adipogenesis. Nevertheless, increasing extracellular calcium after induction allows adipogenic marker gene expression but suppresses brown adipogenesis-specific gene expression, without impairing mitochondrial respiration.

5.2.1 Critical role of calcium in lineage commitment and maintenance

Calcium plays an important role in various cellular processes. Adapting extracellular calcium concentration and treatment duration influences cell lineage commitment. Indeed, high extracellular calcium accelerates proliferation and differentiation of bone marrow-derived stem cells (BMSCs) into adipocytes (Hashimoto, Katoh et al. 2012). In contrast to the positive adipogenic effect in BMSCs, white 3T3-L1 preadipocytes show decreased differentiation efficiency into mature adipocytes upon increasing extracellular calcium (Neal and Clipstone 2002). Elevating extracellular calcium concentration induces site-specific osteogenesis and chondrogenesis also in human-derived adipocyte stem cells (Mellor, Mohiti-Asli et al. 2015). However, brown preadipocytes exposed to high extracellular calcium do not exhibit an increased expression of osteoblast markers, like *Runx2* or *Coll*. Moreover, high extracellular calcium reversibly pauses adipogenesis right after lineage commitment, as removal of the calcium block after initiation restores lipid accumulation and adipogenic marker gene expression. Nevertheless, extracellular calcium has a very specific effect on brown adipocytes at later stages of differentiation. Exposure to high extracellular calcium after the induction phase inhibits the expression of brown adipocyte specific genes, such as *Ucp1*, *Prdm16* and *Pgc1-α*,

[6] The following text is adapted and revised from Pramme-Steinwachs, I., M. Jastroch, S. Ussar (2017). "Extracellular calcium modulates brown adipocyte differentiation and identity." Sci Rep **7**(1): 8888.

with little to no impact on the expression of general adipogenic markers and lipid accumulation. Hyperphosphorylation of PPARγ, which results in its inactivation (Adams, Reginato et al. 1997, Shao, Rangwala et al. 1998), could explain the missing expression of genes involved in mitochondrial uncoupling and thermogenesis. Importantly, a calcium free environment during late adipogenesis promotes brown adipocyte differentiation, indicating a direct impact of extracellular calcium on brown adipogenesis.

The reduction of extracellular acidification rates in cells differentiated with high calcium is not directly related to glycolytic rates, since lactate concentrations are similar. Given that mitochondrial respiration does not vary across treatment groups, UCP1 activity is either too low or requires activation (Keipert and Jastroch 2014). Alternatively, UCP1-mediated uncoupling could be replaced by other mechanisms. *Fabp3* expression is higher in UCP1 ko mice, correlating with increased fatty acid oxidation and adaptive thermogenesis in BAT (Yamashita, Wang et al. 2008, Vergnes, Chin et al. 2011). Indeed, increased *Fabp3* expression is observed in cells treated with either high calcium for days 2-8 or high calcium for days 0-8, albeit with a fully suppressed adipogenesis in the latter case. Myogenic lineage commitment could explain both the increasing expression of *Fabp3*, which is also highly expressed in heart muscle, and the reduced expression of *Prdm16*, which drives brown adipogenic lineage from myogenic precursor cells (Seale, Bjork et al. 2008). However, brown preadipocytes treated with high extracellular calcium during differentiation and induction phase do not alter lineage commitment towards myocytes, since *Acta2* and *Myod* expression remain similar across treatments.

5.2.2 ERK phosphorylation is critical throughout differentiation

Elevating extracellular calcium during induction pauses adipocyte differentiation without effecting the initiation. The suppressed differentiation appears to be mediated through inhibited C/EBPβ and C/EBPδ activity, which are key transcription factors for initiating adipocyte differentiation through *Pparγ* and *C/ebpα* induction (Wu, Rosen et al. 1999). Elevated extracellular calcium increases the phosphorylation of the activating C/EBPβ isoform LAP and does not affect the phosphorylation of the inhibitory C/EBPβ isoform LIP, modulating pLAP/pLIP ratios. This is accompanied by hyperphosphorylation of ERK, which is the primary activator of C/EBPβ activity in response to insulin (Prusty, Park et al. 2002, Farmer 2005, Ussar, Bezy et al. 2012). However, prolonged ERK signaling inhibits adipocyte differentiation (Bost, Aouadi et al. 2005). Thus, the continuously hyperactivated ERK may explain both the inhibition and the restoration of adipocyte differentiation. Indeed, reducing ERK activity pharmacologically to a

level observed in control cells partially restores brown adipocyte differentiation, albeit with a much lower differentiation capacity. This indicates the need of a more dynamic regulation of ERK phosphorylation instead of a continuous MEK inhibition throughout the differentiation. Furthermore, it is suggested that other signaling pathways contribute to the regulation of adipogenesis by extracellular calcium. In addition to the inhibitory role of elevated extracellular calcium, removal of calcium from the medium enhances adipocyte differentiation and reduces overall ERK phosphorylation.

The upstream signals mediating increased ERK phosphorylation remain to be determined. In the context of calcium, it is feasible to hypothesize that the calcium sensitive phosphatase calcineurin, which is known to modulate ERK activity (Neal and Clipstone 2002, Dougherty, Ritt et al. 2009), mediates these effects. However, inhibition of calcineurin does not restore brown adipocyte differentiation. In addition, elevated extracellular calcium does not increase intracellular calcium, which is necessary to activate calcineurin. This is also applicable for calcium-calmodulin dependent kinase II (CaMKII) activated through Fas ligand binding, which mediates ERK-dependent lipolysis in 3T3-L1 cells (Rapold, Wueest et al. 2013) or increases AMPK phosphorylation and free fatty acid uptake (Hauser, Saarikettu et al. 2008, Choi, Choi et al. 2013). The data observed show a very general role of extracellular calcium during the early phase of adipocyte differentiation, which is common between white and brown adipocytes. Nevertheless, ERK phosphorylation is crucial throughout the whole differentiation.

5.2.3 Tissue microenvironment is underestimated

Manipulating extracellular calcium as an important constituent of the microenvironment can have profound effects on the kinetics and nature of *de novo* adipogenesis. Omitting calcium in the cell culture medium substantially improves brown adipocyte differentiation and boosts the expression of genes involved in the thermogenic program. Conversely, calcium excess suppresses brown adipogenesis. Calcium levels in the extracellular microenvironment are strictly regulated with respect to PTH, calcitonin and vitamin D (Copp, Cameron et al. 1962, Goldstein 1990). It is hypothesized that altered vitamin D levels observed in obese subjects could perturb local calcium concentrations and contribute to the lower brown fat mass and activity of obese human subjects (Bonny and Bochud 2014, Park, Park et al. 2015). Also, oral application of calcitonin which negatively regulates calcium levels in the blood shows anti-diabetic and anti-obese effects in rats (Feigh, Henriksen et al. 2011). This supports the hypothesis that high calcium levels in the microenvironment may impair BAT function.

The extracellular bone fluid plays a very important role in calcium homeostasis. Altering extracellular calcium concentrations induces adipogenesis in BMSCs (Hashimoto, Katoh et al. 2012, Hashimoto, Katoh et al. 2015), even though adipogenesis in BMSCs is discussed as a default pathway (Pierce, Begun et al. 2018). Accumulating adipocytes within the bone marrow is a natural process and is increased in high fat diet (HFD)-fed animals and under certain diseases (Doucette, Horowitz et al. 2015, Ambrosi and Schulz 2017). The explicit function of bone marrow adipose tissue (BMAT) and its controversial development compared to other adipose tissues are still under investigation. For instance, elevated BMAT mass is observed in patients possessing prolonged hyperglycemia or suffering from anorexia nervosa (Bredella, Fazeli et al. 2009, Baum, Yap et al. 2012). BMAT also changes with age and in case of diabetes and attenuates shared characteristics with brown fat (Krings, Rahman et al. 2012). However, adipogenesis in BMSCs and BAT-derived preadipocytes is conversely influenced by elevated calcium levels. Nevertheless, these data suggest a role of interstitial calcium in adipogenesis of bone marrow, which could also be applicable to adipogenesis in BAT. This hypothesis has hitherto been underestimated and needs further investigation.

Calcium either floods the cells or enters the cell in little spikes via ligand-gated calcium channels, which results in highly specific downstream signaling (Kar, Nelson et al. 2011, Chen, Zeng et al. 2017, Zhou, Nwokonko et al. 2018). Apparently, the smaller the calcium influx the more specific is the reaction following. In fact, calcium cycling, which can barely be detected with fluorescent dyes, modulates adipogenesis and thermogenesis (Ikeda, Kang et al. 2017, Goudarzi, Mohammadalipour et al. 2018). These acute effects are mostly associated with improved BAT function, whereas chronically elevated calcium suppresses BAT adipogenesis and function; a phenomenon potentially related to hypercalcemia.

5.3 Loss of P2RX5 influences brown adipocyte activity and whole body glucose homeostasis

BAT-specific P2RX5 loss does not impact body composition, glucose tolerance or insulin tolerance. Although BAT of $P2RX5^{fl/fl}$;$UCP1cre^{-}$ (fl) and $P2RX5^{fl/fl}$;$UCP1cre^{+}$ (cre) mice demonstrates similar lipolytic rates upon stimulation with isoproterenol or 2-methylthio-ATP, an impaired UCP1-dependent mitochondrial uncoupling is observed in brown preadipocytes of cre mice. In contrast, whole body P2RX5 loss results in an improved glucose tolerance with lower basal insulin levels. However, similar body weight and slightly reduced white fat weight,

attributed to smaller adipocytes in perigonadal fat, are observed in P2RX5 ko, compared to P2RX5 wt. Better insulin sensitivity and improved glucose tolerance are most likely related to induced beiging in SCF and to increased *Mhc IIa* expression in TA of P2RX5 ko animals. In addition, enhanced mitochondrial respiration in brown preadipocytes from P2RX5 ko animals differentiated *in vitro* suggest a better activation capacity of BAT in P2RX5 ko animals, which might contribute to an increased glucose uptake in BAT.

5.3.1 P2RX5 as a co-stimulator of brown adipocyte activity

Sympathetic signaling is important for BAT development and activity regulation. Mice that are kept at thermoneutrality or that lack beta-adrenergic receptor 1-3 (beta-less) present a brown fat with reduced multilocularity and lower or zero *Ucp1* mRNA levels (Geloen, Collet et al. 1992, Razzoli, Frontini et al. 2016). *Ucp1* expression and multilocularity are recovered in parts upon cold exposure and CSS in both thermoneutral and beta-less mice (Razzoli, Frontini et al. 2016). Clearly, beta-adrenergic signaling is important for proper BAT development and activity regulation. However, other stimuli released upon cold or CSS are also involved in BAT activation. ATP is released from sympathetic nerve vesicles upon stress stimulation and is shown to activate BAT function (Burnstock 1987, Burnstock 2014, Razzoli, Frontini et al. 2016). The purinergic calcium channel P2RX5 is highly expressed on BAT and is up-regulated in beta-less mice upon stress stimulation, suggesting a role in stimulating brown fat together with adrenergic receptor activation (Ussar, Lee et al. 2014, Razzoli, Frontini et al. 2016).

Indeed, *in vitro* data of knock down cells show reduced *Ucp1* expression, probably resulting from impaired differentiation as indicated by *Pparγ* and brown adipocyte marker gene expression. However, primary brown preadipocytes derived from BAT of P2RX5$^{fl/fl}$;UCP1cre^{+} mice and differentiated *in vitro* reveal reduced *Ucp1* mRNA levels upon isoproterenol stimulation, with similar *Pparγ* expression across genotypes. Moreover, the reduced *Ucp1* mRNA levels explain the impaired isoproterenol-stimulated mitochondrial respiration in those cells. Accordingly, *in vitro* data with P2RX5 inhibitors support the respiration defect observed in those primary cells, suggesting an influence of P2RX5 on acute *Ucp1* induction and UCP1 activity. Differences in basal respiration upon P2RX5 inhibitor incubation seems to be attributed to the low specificity of PPADS for P2RX5 alone (Jarvis and Khakh 2009). In addition, NF449 is highly specific to P2RX1 and the heterotrimer P2RX5/1 (Jarvis and Khakh 2009), which apparently has different implications on basal respiration than just the inhibition of P2RX5. Importantly, beta-adrenergically mediated lipolysis in BAT is not affected by the absence of

P2RX5. Taken together, P2RX5 does not regulate beta-adrenergically mediated lipolysis, but interferes with acute, beta-adrenergically induced *Ucp1* expression. This impact on beta-adrenergic signaling needs to be investigated further.

Nevertheless, loss of P2RX5 in BAT alone does not influence whole body fat distribution, as shown with similar free fatty acid levels, liver TG contents and PGF, SCF and BAT weights, compared to controls. Importantly, *Ucp1* and other brown adipocyte marker gene expressions in BAT are similar across genotypes. This suggests, that the impact of P2RX5 loss on *Ucp1* expression and on isoproterenol-stimulated mitochondrial respiration *in vitro* might be compensated or overwritten *in vivo*.

Beta-adrenergic stimulation induces cell depolarization, but the precise mechanism is not established (Fink and Williams 1976, Chen, Zeng et al. 2017). P2RX5 potentially mediates extracellular calcium influx, which in turn induces cell depolarization. However, fluo-4 measurements show no significant impact of P2RX5 loss on calcium influx. Because 2-methylthio-ATP is not solely specific for P2RX5 - even though, among other ATP analogues, it has a very high affinity to P2RX5 comparable with ATP - other P2RXs are activated as well (Wildman, Brown et al. 2002, Coddou, Yan et al. 2011). Especially P2RX1, P2RX2 and P2RX4, which are also expressed on murine brown fat, present higher calcium amplitudes than P2RX5. Thus, the impact of P2RX5 loss on acute calcium influx is potentially overwritten (Garcia-Guzman, Soto et al. 1996, North 2002).

PKC binding sites are present on the intracellular domain of P2RX5, indicating a potential role of P2RX5 in PKC-mediated GLUT4 translocation (Deng, Zhu et al. 2018). P2RX5 heterotrimerizes with other P2RXs binding PIP_ns in the plasma membrane. This could also regulate AKT and PKC signaling, resulting in GLUT4 translocation (Marin-Vicente, Gomez-Fernandez et al. 2005, Funaki, DiFransico et al. 2006, Ase, Bernier et al. 2010, Bernier, Ase et al. 2013). In fact, brown preadipocytes differentiated *in vitro* show a decreased *Glut4* expression upon isoproterenol-stimulation in the absence of P2RX5, but no reduction in differentiation capacity. Thus, P2RX5 loss in BAT could result in a diminished glucose uptake via GLUT4. However, its mRNA levels in BAT of $P2RX5^{fl/fl}$;$UCP1cre^{+}$ and $P2RX5^{fl/fl}$;$UCP1cre^{-}$ mice are similar. Importantly, beta-adrenergically mediated glucose uptake does not necessarily need GLUT4 translocation. Instead, it can also depend on *de novo* synthesis of GLUT1 by an mTORC2-dependent pathway (Dallner, Chernogubova et al. 2006, Olsen, Sato et al. 2014). Also here, *Glut1* mRNA levels are reduced *in vitro* in the absence on P2RX5, but are similar across genotypes *in vivo*. Moreover,

no changes in glucose or insulin tolerance are observed in BAT-specific P2RX5 ko mice compared to control mice.

5.3.2 Whole body P2RX5 loss improves metabolic health in mice

Whole body P2RX5 knock out mice, unlike the BAT-specific P2RX5 ko mice, show higher glucose tolerance and lower basal insulin levels, compared to controls, and a similar body weight, albeit with reduced perigonadal fat. These differences in 3-4-month-old animals are already observed in younger mice (8 weeks). Generally, brown fat in 8-week-old mice shows a higher activity capacity and therefore has a stronger influence on whole body energy expenditure and glucose homeostasis than BAT of older mice (McDonald and Horwitz 1999). The slight difference in the glucose tolerance curves observed in P2RX5 wt and ko mice aged 3-4 months is attributed to improved kinetics in glucose uptake. 8-week-old P2RX5 ko mice, which show the same body composition as 3-4-month-old mice, could contribute to an even greater difference in glucose tolerance.

Importantly, lower plasma insulin levels are observed in P2RX5 ko mice. Lower plasma insulin levels could result from reduced insulin secretion from the pancreas, where P2RX5 expression is found as well (Hansen, Krabbe et al. 2008, Ussar, Lee et al. 2014). ATP regulates insulin secretion in pancreatic beta cells, which is mediated by purinergic signaling (Rodrigue-Candela, Martin-Hernandez et al. 1963, Bertrand, Chapal et al. 1986). While P2RXs are supposed to mediate a transient release in the presence of low glucose levels, P2Y receptors play a role in acutely stimulated, strong insulin releases (Petit, Hillaire-Buys et al. 1998, Ohtani, Ohura et al. 2011). Based on expression analysis and agonist experiments, P2RX3 and P2RX4 are described as the important mediators of ATP-dependent insulin release (Jacques-Silva, Correa-Medina et al. 2010, Ohtani, Ohura et al. 2011). Also, P2RX5 is expressed in the pancreas, especially in beta cells, but its response to agonists is generally lower than the response of other P2RXs (North 2002, Wildman, Brown et al. 2002). Thus, its role is very likely underestimated. Either P2RX5 loss hampers insulin secretion, indicating an important role of P2RX5 in pancreatic beta cells, or reduced insulin secretion is a metabolic response to increased insulin sensitivity in other tissues.

P2RXs are shown to modulate ATP-mediated gonadotropin secretion in pituitary gonadotropin cells, affecting the sexual development and reproductive function (Tomic, Jobin et al. 1996).

Even though average litter size is small, sex and genotype distributions are normal, indicating no defect in sexual development and reproduction.

As mentioned above, the whole body P2RX5 knock out mice have less perigonadal fat, compared to controls, which is attributed to a prevalence of smaller adipocytes. Since, *P2rx5* is hardly expressed in PGF, secondary effects of the whole body P2RX5 loss could have an impact on lipid accumulation in PGF. However, neither basal phosphorylation of HSL nor stimulated lipolysis differs between genotypes in perigonadal fat. These results suggest that loss of whole body P2RX5 does not impair PGF lipolysis. Importantly, even though the adipocyte size and the basal HSL phosphorylation in subcutaneous fat do not differ significantly between genotypes, isoproterenol-stimulated lipolysis is higher in P2RX5 ko mice, compared to controls. As serum free fatty acid levels are similar across genotypes, free fatty acids generated in SCF are most likely burned directly in the subcutaneous fat. Indeed, SCF of P2RX5 ko mice tends to have higher *Ucp1* expression and mitochondrial respiration complex levels. The latter are significant for OXPHOS complex II. This suggests increased mitochondria content and mitochondrial respiration, which are responsible for elevated free fatty acid turnover in SCF. These effects are potentially amplified under cold exposure and need to be determined in future investigation.

P2RX5 is expressed specifically in brown and beige adipocytes. Therefore, its expression in SCF is very low but increases with the amount of beige adipocytes in SCF, as seen with cold exposure (Ussar, Lee et al. 2014). In SCF, ATP inhibits insulin-stimulated glucose transport and counteracts insulin signaling (Hashimoto, Robinson et al. 1987). As P2RX5 expression increases with SCF beiging, contributing to a stronger glucose uptake in SCF, it is unlikely that P2RX5 mediates the inhibitory effect of ATP on insulin signaling.

P2RX5 is also expressed in monocytes and macrophages (Layhadi and Fountain 2017) and is supposed to play a role in ATP-mediated inflammasome activation and Interleukin 1-β (IL1-β) production in osteoclasts, without affecting bone development and homeostasis *in vivo* (Kim, Walsh et al. 2017). White adipose tissue dysfunction in obese or pre-obese (HFD fed) animals correlates with increased classically activated pro-inflammatory macrophage (M1) infiltration in adipose tissue. Chronic inflammation through elevated expression of *Il1-β* and tumor necrosis factor-α (*Tnf-α*) results in reduced brown gene expression and reduced insulin sensitivity (Hotamisligil, Shargill et al. 1993, Bhattacharya, Dominguez et al. 2015). In contrast, caloric restriction and cold exposure are shown to induce a polarization towards alternatively activated

anti-inflammatory macrophages (M2) correlating with WAT beiging and BAT thermogenesis (Wu, Molofsky et al. 2011, Hui, Gu et al. 2015, Fischer, Ruiz et al. 2017). Whole body P2RX5 ko mice exhibit increased lipolysis in SCF compared to wt controls, which can recruit macrophages (Kosteli, Sugaru et al. 2010). Elevated M1 macrophage infiltration results in increased TNF-α secretion, which suppresses brown adipocyte gene expression via ERK hyperphosphorylation (Sakamoto, Takahashi et al. 2013). Subsequently, a lower ERK phosphorylation and induced beiging in SCF of P2RX5 ko mice are observed, compared to controls. This may indicate M2 macrophage accumulation in SCF of P2RX5 ko mice. However, macrophage marker gene expression in SCF remains similar across genotypes.

Currently, the hypothesis that M2 macrophages induce noradrenalin-mediated beiging in white fat is under discussion (Fischer, Ruiz et al. 2017). *In vitro* data show that interleukin-4 (IL-4) induced M2-polarized bone marrow-derived macrophages do not secret sufficient amounts of noradrenaline to modulate white adipocyte beiging or thermogenic gene expression in brown adipocytes, which is further related to a lack of tyrosine hydroxylase mRNA in WAT and BAT macrophage populations (Fischer, Ruiz et al. 2017). It is also shown that noradrenalin-mediated beta-adrenergic signaling is not the sole driver of BAT activation and WAT beiging (Razzoli, Frontini et al. 2016). Thus, alternative mechanisms seem to be involved. This potentially includes purinergic signaling. ATP is also secreted by macrophages and induces inflammatory gene expression via autocrine signaling or mediates ATP-dependent signaling in neighboring cells via paracrine signaling. Mostly, P2RX7 is described as the purinergic mediator of pro-inflammatory gene expression in macrophages (Gudipaty, Munetz et al. 2003, Kawamura, Kawamura et al. 2012, Stoffels, Zaal et al. 2015). Heterotrimers of P2RX5 and P2RX2, which both are expressed in macrophages, can simulate the function of P2RX7 (Compan, Ulmann et al. 2012, Layhadi and Fountain 2017). However, the role of P2RX5 is frequently underestimated as its response to agonists is generally lower in comparison to other P2RXs (North 2002). Thus, P2RX5 is barely described to modulate inflammatory gene expression in macrophages (Kim, Walsh et al. 2017). However, also in BAT, loss of P2RX5 has no influence on macrophage marker gene expression. Taken together, SCF beiging and improved BAT thermogenic capacity might not be related to macrophage infiltration in P2RX5 ko or wt mice.

ATP and 2-methylthio-ATP induce thyroid hormone release from thyroid glands, where P2RXs are also expressed (Ekokoski, Webb et al. 2001, Burnstock 2014). Thyroid hormones are important for brown adipocyte differentiation and are also used in *in vitro* differentiation of brown

adipocytes. However, loss of P2RX5 in thyroid glands does not impair brown fat development, as shown by similar morphology and *Ucp1* expression. The BAT development is rather promoted, as protein levels for UCP1 and mitochondrial respiration complexes are increased in P2RX5 ko mice.

As mentioned above, heterotrimers of P2RXs can simulate functions of other P2RX trimers. This compensatory effect of other surface proteins is also seen in beta-adrenergic ko mice (Bachman, Dhillon et al. 2002). In addition, receptors and channels with functions comparable to P2RX5 could also take over its role. The purinergic receptor A2A is shown to mediate beiging and BAT activation (Gnad, Scheibler et al. 2014), and P2Y2 and P2Y12 receptors change their expression pattern in beta-less mice (Razzoli, Frontini et al. 2016). However, the “even browner” BAT phenotype cannot be explained with over-compensation by the respective channels and receptors in the absence of P2RX5, as gene expression remains similar across genotypes.

In fact, the higher mitochondrial protein composition in brown fat and the hyperactive respiration in brown adipocytes of P2RX5 ko mice suggest that P2RX5 loss contributes to improving glucose tolerance. However, P2RX5 is also expressed in skeletal muscle and purinergic channels seem to matter for skeletal muscle development (Ryten, Hoebertz et al. 2001, Ryten, Dunn et al. 2002). Depending on its condition, skeletal muscle takes up and oxidizes either glucose (postprandial, basal conditions), to maintain energy and store energy sources, or free fatty acids (fasting, prolonged exercise), to generate ATP (DeFronzo, Gunnarsson et al. 1985, Blaak 2005, Kiens 2006). In P2RX5 ko mice, free fatty acid levels are similar as in wt mice and lower insulin levels are sufficient to improve glucose tolerance.

In mice, glucose is mainly cleared from the blood by the skeletal muscle due to its high mass share, albeit a higher glucose uptake capacity in BAT (Hofmann, Perez-Tilve et al. 2008, Stanford, Middelbeek et al. 2015) with a 3-fold increase upon insulin or norepinephrine stimulation (Inokuma, Ogura-Okamatsu et al. 2005). Thus, the metabolic phenotype in P2RX5 ko mice could be mediated by an up-regulated insulin sensitivity and glucose uptake in skeletal muscle. P2RX5 reveals binding sites for PKCs and thus could be involved in PKC signaling. PKCs phosphorylate insulin receptor substrate-1 (IRS-1) at Ser307, which inhibits tyrosine phosphorylation, impairing insulin receptor activity and signaling (Schmitz-Peiffer, Browne et al. 1997). Loss of P2RX5 could impair the inhibitory phosphorylation and thereby boost insulin receptor activity, leading to higher insulin sensitivity and increased glucose uptake. In addition, the composition of myosin heavy chain isoforms seems to influence the capacity in insulin-

stimulated glucose uptake, with greater uptake rates for MHC IIA than IIB and IIX (MacKrell and Cartee 2012). In P2RX5 ko mice, *Mhc IIa* mRNA levels in muscle tibialis anterior (TA) are higher than in wt animals. *Glut4* and *Glut1* expression together with IRS-1 phosphorylation as well as glucose uptake studies could yield important insights into the role of P2RX5 for skeletal muscle functionality and thereby for whole body glucose homeostasis.

5.3.3 P2RX5 as a potential drug target to improve metabolic health

P2RX5 seems to promote mitochondrial respiration in brown adipocytes, as mitochondrial respiration is impaired in brown adipocytes treated with P2RX5 inhibitors and in primary brown adipocytes isolated from BAT-specific P2RX5 ko mice, compared to controls. In addition, primary brown adipocytes of P2RX5 ko mice express less *Ucp1*, *Glut4* and *Glut1* mRNA than observed in control cells. This suggests a lower mitochondrial respiration capacity and glucose uptake rate in BAT of BAT-specific P2RX5 ko mice. *In vivo* however*,* brown adipocyte marker gene expression, glucose tolerance and body weight are similar across genotypes. This suggests that the effects observed *in vitro* are compensated or overwritten *in vivo*. Contradictive data are observed in the whole body P2RX5 ko animals. Improved glucose tolerance and insulin sensitivity as well as lower perigonadal fat mass is observed in P2RX5 ko mice compared to wt mice. Moreover, primary brown adipocytes of P2RX5 ko mice show improved mitochondrial respiration. Mitochondrial respiration complexes and UCP1 protein levels are increased in BAT of P2RX5 ko mice, compared to controls. This phenotype might be attributed to secondary effects of P2RX5 ko, for instance via the skeletal muscle, where P2RX5 is also expressed.

This work strongly suggests an important influence of P2RX5 in regulating insulin sensitivity and glucose uptake, mainly in skeletal muscle. Moreover, P2RX5 is expressed in other organs, like the heart muscle, pancreas and macrophages (Ussar, Lee et al. 2014, Kim, Walsh et al. 2017, Layhadi and Fountain 2017), putting the hypothesis of a BAT-specific target under discussion. However, its role in inflammation processes might be of minor relevance, as macrophage marker gene expression was similar in P2RX5 ko and wt mice. The whole body knock out data imply that synthetic stimulation of P2RX5 would result in severe side-effects with respect to insulin resistance. Nevertheless, BAT-specific P2RX5 stimulation could improve metabolic health. Due to a lack of agonists specific exclusively for P2RX5 (North 2002, Wildman, Brown et al. 2002), it is complicated to investigate whether P2RX5 stimulation potentiates beta-adrenergically mediated BAT activation, a necessary precondition to make it a target for hyperactivating BAT. Moreover, like other P2RXs, P2RX5 is supposed to be in charge of basal

functions rather than acute signaling (Petit, Hillaire-Buys et al. 1998). This implies that P2RX5 might mainly be important for maintaining BAT activation capacity.

To discuss whether P2RX5 is a potential drug target to improve metabolic health it is important to know that *P2rx5* expression occurs at every age. It can likewise be detected in UCP1-positive adipose tissue samples of children (Rockstroh, Landgraf et al. 2015) and in brown adipocytes in BAT and SCF of adults (Garcia, Roemmich et al. 2016, Torriani, Srinivasa et al. 2016). Moreover, rodent and human *P2rx5* sequences are highly related. Most importantly, P2RX5 misses the second transmembrane domain. This results in a non-functional calcium channel in most of the humans, predominantly in White American, Middle Eastern and Chinese and with higher frequency in African American populations (Duckwitz, Hausmann et al. 2006). The lack of the second transmembrane domain is based on a single nucleotide polymorphism (SNP) that generates a new splicing site. Due to this species-specific splicing, either exon 10 (P2RX5a) or both exon 10 and exon 3 (P2RX5b) are skipped. This heterogeneous distribution of functional P2RX5 within the human population makes achieving a promising and targeted treatment very complicated. On the other hand, it opens the discussion to assessments of potential correlations between obesity and related diseases and the appearance of non-functional P2RX5 in human populations.

5.4 The effects of high extracellular calcium on brown adipocytes are most likely not mediated by P2RX5

In this study, high extracellular calcium inhibits adipogenesis of brown preadipocytes. Vice versa, omitting extracellular calcium promotes brown adipogenesis. High extracellular magnesium, used as ionic control, does not suppress brown adipocyte differentiation. These findings are in line with previous data showing high extracellular calcium to inhibit adipogenesis in white 3T3-L1 preadipocytes without increasing intracellular calcium levels (Jensen, Farach-Carson et al. 2004). This suggests that extracellular calcium acts on surface proteins to modulate anti-adipogenic signaling. The G protein-coupled calcium sensing receptor (CaSR) activates intracellular signaling cascades - especially ERK - upon calcium binding (Cifuentes, Albala et al. 2005). Published work finds *Casr* expression in adipocytes (Cifuentes, Albala et al. 2005). Here however, it is detected neither in brown adipose tissue nor in the cell model used. Furthermore, minimal calcium influxes or calcium oscillation would barely be measureable in the experimental setup used. Minimal calcium influx in the presence of kinases can support ERK

phosphorylation (Dougherty, Ritt et al. 2009), which could be accomplished by purinergic calcium channels, like P2RX5. However, P2RX5 seems to have a positive effect on the function of brown adipocytes, as suggested by impaired mitochondrial uncoupling if P2RX5 is absent. In addition, P2RX5 function decreases in the presence of calcium concentrations higher than 7 mM, which is even lower than the concentration used here (10 mM calcium chloride) (Jarvis and Khakh 2009). This suggests that the suppressive effect of high extracellular calcium on brown adipocyte differentiation is not mediated via P2RX5.

5.5 SUMMARY & OUTLOOK

Obesity and overweight are a major health burden for the society. Psychological complications and physical limitations as well as physiological and metabolic disorders, like type 2 diabetes, can develop from obesity and result in 2.8 million deaths per year. Over the last decades, different approaches with the purpose of stopping the growth of obesity rates in the world have been investigated. Studies on the genetic prevalence, behavior and environmental influences of obesity as well as research for potential treatments have already shown some success. Nevertheless, further research effort is required.

In particular, the brown adipose tissue has been shown to exhibit a strong impact on energy balance and glucose homeostasis in humans and rodents due to its function in mitochondrial uncoupling and related non-shivering thermogenesis. Thus, BAT-directed treatments, like beta3-adrenergic receptor agonists, have been evaluated. However, treatments so far are associated with sever side-affects and different responses in rodents and humans, resulting from a species-specific expression pattern and function. It is shown that - in addition to beta-adrenergic signaling - purinergic signaling is involved in BAT activity regulation. The expression of the purinergic calcium channel P2RX5 specifically on brown (and not white) adipose tissue and its increase in BAT of beta-less mice upon CSS suggest a role of P2RX5 in co-activating BAT. To study the role of P2RX5 in BAT development and activation and thus the role of extracellular calcium on brown adipocyte differentiation and function, brown preadipocyte cell models and P2RX5 knock out animals were characterized. The results are presented and discussed in this work.

In accordance with the impact on white adipocytes, elevating extracellular calcium during brown preadipocyte differentiation suppressed brown adipogenesis. Normalizing calcium after the induction rescued the differentiation, suggesting that high calcium during induction did not change lineage commitment. High extracellular calcium during later stages of adipogenesis impaired brown adipocyte marker gene expression, but differentiation capacity, lineage commitment and mitochondrial respiration capacity were not affected. Increased expression of the heart-type fatty acid binding protein (*Fabp3*) seemed to matter for alternative uncoupling of these cells. Importantly, ERK phosphorylation played a critical role during differentiation, modulating C/EBPβ phosphorylation and brown adipocyte marker gene expression. All in all, modulating extracellular calcium has an impact on brown adipocyte differentiation. This provides

evidence for a role of hypercalcemia in brown adipogenesis and brown fat function, which has hitherto been underestimated.

In contrast to the negative effects of high extracellular calcium on brown adipocyte differentiation and function, P2RX5 was shown to promote brown adipocyte function *in vitro*. Primary brown preadipocytes revealed impaired *Ucp1* induction and UCP1-mediated mitochondrial respiration. Moreover, these cells expressed lower levels of *Glut4* and *Glut1*, while differentiation capacity was not affected. These data suggest that P2RX5 loss in BAT could impair glucose uptake and BAT thermogenesis, resulting in reduced glucose tolerance and increased body weight. However, BAT-specific P2RX5 ko mice showed similar glucose tolerances with similar serum insulin levels and body compositions, compared to control mice. This suggests that UCP1-induced loss of P2RX5 could be overwritten or compensated *in vivo*.

Converse results were obtained in whole body P2RX5 ko mice, showing improved glucose tolerance, lower serum insulin levels and reduced white fat mass, compared to controls. Lower fat mass was attributed to smaller adipocytes in PGF. The increased lipolysis and induced beiging in SCF of P2RX5 ko mice could contribute to a higher insulin sensitivity. Accordingly, elevated mitochondrial protein levels, including UCP1, and higher mitochondrial oxygen consumption upon adrenergic stimulation in primary brown preadipocytes suggest an improved BAT activation capacity in P2RX5 ko mice. Because these results are in contrast to the results obtained in BAT-specific P2RX5 ko mice, other factors must be involved in regulating BAT function and SCF beiging in whole body P2RX5 ko mice. *P2rx5* is also expressed in macrophages, and BAT thermogenesis and SCF beiging are discussed in the context of macrophage infiltration and pro- and anti-inflammatory macrophage conversion. However, no unusual macrophage infiltration and inflammation were observed in BAT or SCF of P2RX5 ko mice, compared to wt mice. The skeletal muscle has the strongest impact on glucose uptake in the organism and also exhibits *P2rx5* expression. The increased expression of *Mhc IIa* in TA of P2RX5 ko mice suggest an elevated insulin-stimulated glucose uptake in those mice, compared to controls. This could explain the improved insulin sensitivity and increased glucose uptake in skeletal muscle of P2RX5 ko mice compared to controls.

All in all, the involvement of P2RX5 in mediating the influence of elevated extracellular calcium on brown adipocyte differentiation and function cannot be fully rejected, but must be considered very unlikely according to the data collected. Nevertheless, the data observed in brown adipocytes derived from BAT-specific P2RX5 ko mice suggest a positive role of P2RX5 in brown

adipocyte function. P2RX5 in BAT clearly shows the potential as an anti-diabetic and anti-obesity target. However, the effects observed *in vitro* were normalized *in vivo* in BAT-specific P2RX5 ko mice. The whole body P2RX5 ko animals showed a strong phenotype, which might be driven by the skeletal muscle. This suggests severe side effects when using P2RX5 as a drug target. Finally, the signaling role of P2RX5 in the respective organs must be explored further, in order to evaluate P2RX5 as a promising target to treat diabetes and obesity.

6 REFERENCES

Adams, M., M. J. Reginato, D. Shao, M. A. Lazar and V. K. Chatterjee (1997). "Transcriptional activation by peroxisome proliferator-activated receptor gamma is inhibited by phosphorylation at a consensus mitogen-activated protein kinase site." J Biol Chem **272**(8): 5128-5132.

Agata, U., J. H. Park, S. Hattori, Y. Iimura, I. Ezawa, T. Akimoto and N. Omi (2013). "The effect of different amounts of calcium intake on bone metabolism and arterial calcification in ovariectomized rats." J Nutr Sci Vitaminol (Tokyo) **59**(1): 29-36.

Ambrosi, T. H. and T. J. Schulz (2017). "The emerging role of bone marrow adipose tissue in bone health and dysfunction." J Mol Med (Berl) **95**(12): 1291-1301.

Argyropoulos, G. and M. E. Harper (2002). "Uncoupling proteins and thermoregulation." J Appl Physiol (1985) **92**(5): 2187-2198.

Arruda, A. P. and G. S. Hotamisligil (2015). "Calcium Homeostasis and Organelle Function in the Pathogenesis of Obesity and Diabetes." Cell Metab **22**(3): 381-397.

Ase, A. R., L. P. Bernier, D. Blais, Y. Pankratov and P. Seguela (2010). "Modulation of heteromeric P2X1/5 receptors by phosphoinositides in astrocytes depends on the P2X1 subunit." J Neurochem **113**(6): 1676-1684.

Bachman, E. S., H. Dhillon, C. Y. Zhang, S. Cinti, A. C. Bianco, B. K. Kobilka and B. B. Lowell (2002). "betaAR signaling required for diet-induced thermogenesis and obesity resistance." Science **297**(5582): 843-845.

Bahler, L., R. J. Molenaars, H. J. Verberne and F. Holleman (2015). "Role of the autonomic nervous system in activation of human brown adipose tissue: A review of the literature." Diabetes Metab **41**(6): 437-445.

Barrera, N. P., S. J. Ormond, R. M. Henderson, R. D. Murrell-Lagnado and J. M. Edwardson (2005). "Atomic force microscopy imaging demonstrates that P2X2 receptors are trimers but that P2X6 receptor subunits do not oligomerize." J Biol Chem **280**(11): 10759-10765.

Baum, T., S. P. Yap, D. C. Karampinos, L. Nardo, D. Kuo, A. J. Burghardt, U. B. Masharani, A. V. Schwartz, X. Li and T. M. Link (2012). "Does vertebral bone marrow fat content correlate with abdominal adipose tissue, lumbar spine bone mineral density, and blood biomarkers in women with type 2 diabetes mellitus?" J Magn Reson Imaging **35**(1): 117-124.

Bernier, L. P., A. R. Ase and P. Seguela (2013). "Post-translational regulation of P2X receptor channels: modulation by phospholipids." Front Cell Neurosci **7**: 226.

Bertrand, G., J. Chapal and M. M. Loubatieres-Mariani (1986). "Potentiating synergism between adenosine diphosphate or triphosphate and acetylcholine on insulin secretion." Am J Physiol **251**(4 Pt 1): E416-421.

Bhattacharya, I., A. P. Dominguez, K. Dragert, R. Humar, E. Haas and E. J. Battegay (2015). "Hypoxia potentiates tumor necrosis factor-alpha induced expression of inducible nitric oxide synthase and cyclooxygenase-2 in white and brown adipocytes." Biochem Biophys Res Commun **461**(2): 287-292.

Blaak, E. E. (2005). "Metabolic fluxes in skeletal muscle in relation to obesity and insulin resistance." Best Pract Res Clin Endocrinol Metab **19**(3): 391-403.

Bonny, O. and M. Bochud (2014). "Genetics of calcium homeostasis in humans: continuum between monogenic diseases and continuous phenotypes." Nephrol Dial Transplant **29 Suppl 4**: iv55-62.

Bost, F., M. Aouadi, L. Caron and B. Binetruy (2005). "The role of MAPKs in adipocyte differentiation and obesity." Biochimie **87**(1): 51-56.

Brake, A. J., M. J. Wagenbach and D. Julius (1994). "New structural motif for ligand-gated ion channels defined by an ionotropic ATP receptor." Nature **371**(6497): 519-523.

Brandle, U., P. Spielmanns, R. Osteroth, J. Sim, A. Surprenant, G. Buell, J. P. Ruppersberg, P. K. Plinkert, H. P. Zenner and E. Glowatzki (1997). "Desensitization of the P2X(2) receptor controlled by alternative splicing." FEBS Lett **404**(2-3): 294-298.
Bredella, M. A., P. K. Fazeli, K. K. Miller, M. Misra, M. Torriani, B. J. Thomas, R. H. Ghomi, C. J. Rosen and A. Klibanski (2009). "Increased bone marrow fat in anorexia nervosa." J Clin Endocrinol Metab **94**(6): 2129-2136.
Browne, L. E., L. H. Jiang and R. A. North (2010). "New structure enlivens interest in P2X receptors." Trends Pharmacol Sci **31**(5): 229-237.
Burnstock, G. (1987). "A basis for distinguishing two types of purinergic receptor." Cell Membrane Receptors For Drugs and Hormones,A Multidisciplinary Approach.: 107-118.
Burnstock, G. (2014). "Purinergic signalling in endocrine organs." Purinergic Signal **10**(1): 189-231.
Cannon, B. and J. Nedergaard (2004). "Brown adipose tissue: function and physiological significance." Physiol Rev **84**(1): 277-359.
Carey, A. L., M. F. Formosa, B. Van Every, D. Bertovic, N. Eikelis, G. W. Lambert, V. Kalff, S. J. Duffy, M. H. Cherk and B. A. Kingwell (2013). "Ephedrine activates brown adipose tissue in lean but not obese humans." Diabetologia **56**(1): 147-155.
Catterall, W. A. (2011). "Voltage-Gated Calcium Channels." Cold Spring Harb Perspect Biol **3**(8).
Chen, Y., X. Zeng, X. Huang, S. Serag, C. J. Woolf and B. M. Spiegelman (2017). "Crosstalk between KCNK3-Mediated Ion Current and Adrenergic Signaling Regulates Adipose Thermogenesis and Obesity." Cell **171**(4): 836-848.e813.
Chernogubova, E., B. Cannon and T. Bengtsson (2004). "Norepinephrine increases glucose transport in brown adipocytes via beta3-adrenoceptors through a cAMP, PKA, and PI3-kinase-dependent pathway stimulating conventional and novel PKCs." Endocrinology **145**(1): 269-280.
Choi, Y. H., J. H. Choi, J. W. Oh and K. Y. Lee (2013). "Calmodulin-dependent kinase II regulates osteoblast differentiation through regulation of Osterix." Biochem Biophys Res Commun **432**(2): 248-255.
Cifuentes, M., C. Albala and C. Rojas (2005). "Calcium-sensing receptor expression in human adipocytes." Endocrinology **146**(5): 2176-2179.
Cinti, S. (1999). "Adipose tissues and obesity." Ital J Anat Embryol **104**(2): 37-51.
Coddou, C., Z. Yan, T. Obsil, J. P. Huidobro-Toro and S. S. Stojilkovic (2011). "Activation and regulation of purinergic P2X receptor channels." Pharmacol Rev **63**(3): 641-683.
Collins, S., K. W. Daniel, E. M. Rohlfs, V. Ramkumar, I. L. Taylor and T. W. Gettys (1994). "Impaired expression and functional activity of the beta 3- and beta 1-adrenergic receptors in adipose tissue of congenitally obese (C57BL/6J ob/ob) mice." Mol Endocrinol **8**(4): 518-527.
Collo, G., R. A. North, E. Kawashima, E. Merlo-Pich, S. Neidhart, A. Surprenant and G. Buell (1996). "Cloning OF P2X5 and P2X6 receptors and the distribution and properties of an extended family of ATP-gated ion channels." J Neurosci **16**(8): 2495-2507.
Compan, V., L. Ulmann, O. Stelmashenko, J. Chemin, S. Chaumont and F. Rassendren (2012). "P2X2 and P2X5 subunits define a new heteromeric receptor with P2X7-like properties." J Neurosci **32**(12): 4284-4296.
Copp, D. H., E. C. Cameron, B. A. Cheney, A. G. Davidson and K. G. Henze (1962). "Evidence for calcitonin--a new hormone from the parathyroid that lowers blood calcium." Endocrinology **70**: 638-649.
Cypess, A. M., Y. C. Chen, C. Sze, K. Wang, J. English, O. Chan, A. R. Holman, I. Tal, M. R. Palmer, G. M. Kolodny and C. R. Kahn (2012). "Cold but not sympathomimetics activates human brown adipose tissue in vivo." Proc Natl Acad Sci U S A **109**(25): 10001-10005.

Cypess, A. M., S. Lehman, G. Williams, I. Tal, D. Rodman, A. B. Goldfine, F. C. Kuo, E. L. Palmer, Y. H. Tseng, A. Doria, G. M. Kolodny and C. R. Kahn (2009). "Identification and importance of brown adipose tissue in adult humans." N Engl J Med **360**(15): 1509-1517.
Cypess, A. M., L. S. Weiner, C. Roberts-Toler, E. F. Elía, S. H. Kessler, P. A. Kahn, J. English, K. Chatman, S. A. Trauger, A. Doria and G. M. Kolodny (2015). "Activation of Human Brown Adipose Tissue by a β3-Adrenergic Receptor Agonist." Cell Metab **21**(1): 33-38.
Daigle, C. R., S. A. Brethauer, C. Tu, A. T. Petrick, J. M. Morton, P. R. Schauer and A. Aminian (2018). "Which postoperative complications matter most after bariatric surgery? Prioritizing quality improvement efforts to improve national outcomes." Surg Obes Relat Dis **14**(5): 652-657.
Daikoku, T., Y. Shinohara, A. Shima, N. Yamazaki and H. Terada (1997). "Dramatic enhancement of the specific expression of the heart-type fatty acid binding protein in rat brown adipose tissue by cold exposure." FEBS Letters **410**(2-3): 383-386.
Dallner, O. S., E. Chernogubova, K. A. Brolinson and T. Bengtsson (2006). "β3-Adrenergic Receptors Stimulate Glucose Uptake in Brown Adipocytes by Two Mechanisms Independently of Glucose Transporter 4 Translocation." Endocrinology **147**(12): 5730-5739.
Davies, J. H. (2015). "Approach to the Child with Hypercalcaemia." Endocr Dev **28**: 101-118.
DeFronzo, R. A., R. Gunnarsson, O. Bjorkman, M. Olsson and J. Wahren (1985). "Effects of insulin on peripheral and splanchnic glucose metabolism in noninsulin-dependent (type II) diabetes mellitus." J Clin Invest **76**(1): 149-155.
Deng, B., X. Zhu, Y. Zhao, D. Zhang, A. Pannu, L. Chen and W. Niu (2018). "PKC and Rab13 mediate Ca(2+) signal-regulated GLUT4 traffic." Biochem Biophys Res Commun **495**(2): 1956-1963.
Denton, R. M. (2009). "Regulation of mitochondrial dehydrogenases by calcium ions." Biochim Biophys Acta **1787**(11): 1309-1316.
Doucette, C. R., M. C. Horowitz, R. Berry, O. A. MacDougald, R. Anunciado-Koza, R. A. Koza and C. J. Rosen (2015). "A High Fat Diet Increases Bone Marrow Adipose Tissue (MAT) But Does Not Alter Trabecular or Cortical Bone Mass in C57BL/6J Mice." J Cell Physiol **230**(9): 2032-2037.
Dougherty, M. K., D. A. Ritt, M. Zhou, S. I. Specht, D. M. Monson, T. D. Veenstra and D. K. Morrison (2009). "KSR2 is a calcineurin substrate that promotes ERK cascade activation in response to calcium signals." Mol Cell **34**(6): 652-662.
Draznin, B. (1988). "Intracellular calcium, insulin secretion, and action." Am J Med **85**(5a): 44-58.
Duckwitz, W., R. Hausmann, A. Aschrafi and G. Schmalzing (2006). "P2X5 subunit assembly requires scaffolding by the second transmembrane domain and a conserved aspartate." J Biol Chem **281**(51): 39561-39572.
Early, J. L., C. M. Apovian, L. J. Aronne, M. H. Fernstrom, A. Frank, F. L. Greenway, D. Heber, R. F. Kushner, K. M. Cwik, J. K. Walch, A. C. Hewkin and V. Blakesley (2007). "Sibutramine plus meal replacement therapy for body weight loss and maintenance in obese patients." Obesity (Silver Spring) **15**(6): 1464-1472.
Ekokoski, E., T. E. Webb, J. Simon and K. Tornquist (2001). "Mechanisms of P2 receptor-evoked DNA synthesis in thyroid FRTL-5 cells." J Cell Physiol **187**(2): 166-175.
Farmer, S. R. (2005). "Regulation of PPARgamma activity during adipogenesis." Int J Obes (Lond) **29 Suppl 1**: S13-16.
Fedorenko, A., P. V. Lishko and Y. Kirichok (2012). "Mechanism of fatty-acid-dependent UCP1 uncoupling in brown fat mitochondria." Cell **151**(2): 400-413.
Feigh, M., K. Henriksen, K. V. Andreassen, C. Hansen, J. E. Henriksen, H. Beck-Nielsen, C. Christiansen and M. A. Karsdal (2011). "A novel oral form of salmon calcitonin improves glucose homeostasis and reduces body weight in diet-induced obese rats." Diabetes Obes Metab **13**(10): 911-920.

Fernandez-Marcos, P. J. and J. Auwerx (2011). "Regulation of PGC-1α, a nodal regulator of mitochondrial biogenesis." Am J Clin Nutr **93**(4): 884s-890s.
Fink, S. A. and J. A. Williams (1976). "Adrenergic receptors mediating depolarization in brown adipose tissue." Am J Physiol **231**(3): 700-706.
Fischer, I. P., M. Irmler, C. W. Meyer, S. J. Sachs, F. Neff, M. Hrabe de Angelis, J. Beckers, M. H. Tschop, S. M. Hofmann and S. Ussar (2018). "A history of obesity leaves an inflammatory fingerprint in liver and adipose tissue." Int J Obes (Lond) **42**(3): 507-517.
Fischer, K., H. H. Ruiz, K. Jhun, B. Finan, D. J. Oberlin, V. van der Heide, A. V. Kalinovich, N. Petrovic, Y. Wolf, C. Clemmensen, A. C. Shin, S. Divanovic, F. Brombacher, E. Glasmacher, S. Keipert, M. Jastroch, J. Nagler, K. W. Schramm, D. Medrikova, G. Collden, S. C. Woods, S. Herzig, D. Homann, S. Jung, J. Nedergaard, B. Cannon, M. H. Tschop, T. D. Muller and C. Buettner (2017). "Alternatively activated macrophages do not synthesize catecholamines or contribute to adipose tissue adaptive thermogenesis." Nat Med **23**(5): 623-630.
Fischer, W. and U. Krugel (2007). "P2Y receptors: focus on structural, pharmacological and functional aspects in the brain." Curr Med Chem **14**(23): 2429-2455.
Franz, M. J., J. J. VanWormer, A. L. Crain, J. L. Boucher, T. Histon, W. Caplan, J. D. Bowman and N. P. Pronk (2007). "Weight-loss outcomes: a systematic review and meta-analysis of weight-loss clinical trials with a minimum 1-year follow-up." J Am Diet Assoc **107**(10): 1755-1767.
Frayn, K. N., F. Karpe, B. A. Fielding, I. A. Macdonald and S. W. Coppack (2003). "Integrative physiology of human adipose tissue." Int J Obes Relat Metab Disord **27**(8): 875-888.
Funaki, M., L. DiFransico and P. A. Janmey (2006). "PI 4,5-P2 stimulates glucose transport activity of GLUT4 in the plasma membrane of 3T3-L1 adipocytes." Biochim Biophys Acta **1763**(8): 889-899.
Garcia, R. A., J. N. Roemmich and K. J. Claycombe (2016). "Evaluation of markers of beige adipocytes in white adipose tissue of the mouse." Nutr Metab (Lond) **13**: 24.
Garcia-Guzman, M., F. Soto, B. Laube and W. Stuhmer (1996). "Molecular cloning and functional expression of a novel rat heart P2X purinoceptor." FEBS Lett **388**(2-3): 123-127.
Geloen, A., A. J. Collet and L. J. Bukowiecki (1992). "Role of sympathetic innervation in brown adipocyte proliferation." Am J Physiol **263**(6 Pt 2): R1176-1181.
Gever, J. R., D. A. Cockayne, M. P. Dillon, G. Burnstock and A. P. Ford (2006). "Pharmacology of P2X channels." Pflugers Arch **452**(5): 513-537.
Gnad, T., S. Scheibler, I. von Kugelgen, C. Scheele, A. Kilic, A. Glode, L. S. Hoffmann, L. Reverte-Salisa, P. Horn, S. Mutlu, A. El-Tayeb, M. Kranz, W. Deuther-Conrad, P. Brust, M. E. Lidell, M. J. Betz, S. Enerback, J. Schrader, G. G. Yegutkin, C. E. Muller and A. Pfeifer (2014). "Adenosine activates brown adipose tissue and recruits beige adipocytes via A2A receptors." Nature **516**(7531): 395-399.
Goldstein, D. A. (1990). Serum Calcium. Clinical Methods: The History, Physical, and Laboratory Examinations. H. K. Walker, Hall, W.D., Hurst, J.W. Boston, Butterworths.
Golic, I., K. Velickovic, M. Markelic, A. Stancic, A. Jankovic, M. Vucetic, V. Otasevic, B. Buzadzic, B. Korac and A. Korac (2014). "Calcium-induced alteration of mitochondrial morphology and mitochondrial-endoplasmic reticulum contacts in rat brown adipocytes." Eur J Histochem **58**(3): 2377.
Goudarzi, F., A. Mohammadalipour, I. Khodadadi, S. Karimi, R. Mostoli, M. Bahabadi and M. T. Goodarzi (2018). "The Role of Calcium in Differentiation of Human Adipose-Derived Stem Cells to Adipocytes." Mol Biotechnol **60**(4): 279-289.
Gozal, D., A. Gileles-Hillel, R. Cortese, Y. Li, I. Almendros, Z. Qiao, A. A. Khalyfa, J. Andrade and A. Khalyfa (2017). "Visceral White Adipose Tissue after Chronic Intermittent and Sustained Hypoxia in Mice." Am J Respir Cell Mol Biol **56**(4): 477-487.

Groschel-Stewart, U., M. Bardini, T. Robson and G. Burnstock (1999). "Localisation of P2X5 and P2X7 receptors by immunohistochemistry in rat stratified squamous epithelia." Cell Tissue Res **296**(3): 599-605.
Gudipaty, L., J. Munetz, P. A. Verhoef and G. R. Dubyak (2003). "Essential role for Ca2+ in regulation of IL-1beta secretion by P2X7 nucleotide receptor in monocytes, macrophages, and HEK-293 cells." Am J Physiol Cell Physiol **285**(2): C286-299.
Guerrero-Hernandez, A. and A. Verkhratsky (2014). "Calcium signalling in diabetes." Cell Calcium **56**(5): 297-301.
Hall, K. D., G. Sacks, D. Chandramohan, C. C. Chow, Y. C. Wang, S. L. Gortmaker and B. A. Swinburn (2011). "Quantification of the effect of energy imbalance on bodyweight." Lancet **378**(9793).
Hansen, M. R., S. Krabbe and I. Novak (2008). "Purinergic receptors and calcium signalling in human pancreatic duct cell lines." Cell Physiol Biochem **22**(1-4): 157-168.
Harms, M. and P. Seale (2013). "Brown and beige fat: development, function and therapeutic potential." Nat Med **19**(10): 1252-1263.
Hashimoto, N., F. W. Robinson, Y. Shibata, J. E. Flanagan and T. Kono (1987). "Diversity in the effects of extracellular ATP and adenosine on the cellular processing and physiologic actions of insulin in rat adipocytes." J Biol Chem **262**(31): 15026-15032.
Hashimoto, R., Y. Katoh, Y. Miyamoto, S. Itoh, H. Daida, Y. Nakazato and T. Okada (2015). "Increased extracellular and intracellular Ca(2)(+) lead to adipocyte accumulation in bone marrow stromal cells by different mechanisms." Biochem Biophys Res Commun **457**(4): 647-652.
Hashimoto, R., Y. Katoh, K. Nakamura, S. Itoh, T. Iesaki, H. Daida, Y. Nakazato and T. Okada (2012). "Enhanced accumulation of adipocytes in bone marrow stromal cells in the presence of increased extracellular and intracellular [Ca(2)(+)]." Biochem Biophys Res Commun **423**(4): 672-678.
Hauser, J., J. Saarikettu and T. Grundström (2008). "Calcium Regulation of Myogenesis by Differential Calmodulin Inhibition of Basic Helix-Loop-Helix Transcription Factors." Mol Biol Cell **19**(6): 2509-2519.
Hofmann, S. M., D. Perez-Tilve, T. M. Greer, B. A. Coburn, E. Grant, J. E. Basford, M. H. Tschop and D. Y. Hui (2008). "Defective lipid delivery modulates glucose tolerance and metabolic response to diet in apolipoprotein E-deficient mice." Diabetes **57**(1): 5-12.
Hotamisligil, G. S., N. S. Shargill and B. M. Spiegelman (1993). "Adipose expression of tumor necrosis factor-alpha: direct role in obesity-linked insulin resistance." Science **259**(5091): 87-91.
Hou, Y., T. Kitaguchi, R. Kriszt, Y. H. Tseng, M. Raghunath and M. Suzuki (2017). "Ca(2+)-associated triphasic pH changes in mitochondria during brown adipocyte activation." Mol Metab **6**(8): 797-808.
Hui, X., P. Gu, J. Zhang, T. Nie, Y. Pan, D. Wu, T. Feng, C. Zhong, Y. Wang, K. S. Lam and A. Xu (2015). "Adiponectin Enhances Cold-Induced Browning of Subcutaneous Adipose Tissue via Promoting M2 Macrophage Proliferation." Cell Metab **22**(2): 279-290.
Ikeda, K., Q. Kang, T. Yoneshiro, J. P. Camporez, H. Maki, M. Homma, K. Shinoda, Y. Chen, X. Lu, P. Maretich, K. Tajima, K. M. Ajuwon, T. Soga and S. Kajimura (2017). "UCP1-independent signaling involving SERCA2b-mediated calcium cycling regulates beige fat thermogenesis and systemic glucose homeostasis." Nat Med **23**(12): 1454-1465.
Inokuma, K., Y. Ogura-Okamatsu, C. Toda, K. Kimura, H. Yamashita and M. Saito (2005). "Uncoupling protein 1 is necessary for norepinephrine-induced glucose utilization in brown adipose tissue." Diabetes **54**(5): 1385-1391.
Inoue, K., M. Denda, H. Tozaki, K. Fujishita, S. Koizumi and K. Inoue (2005). "Characterization of multiple P2X receptors in cultured normal human epidermal keratinocytes." J Invest Dermatol **124**(4): 756-763.
Jacobsson, H., M. Bruzelius and S. A. Larsson (2005). "Reduction of FDG uptake in brown adipose tissue by propranolol." Eur J Nucl Med Mol Imaging **32**(9): 1130.

Jacques-Silva, M. C., M. Correa-Medina, O. Cabrera, R. Rodriguez-Diaz, N. Makeeva, A. Fachado, J. Diez, D. M. Berman, N. S. Kenyon, C. Ricordi, A. Pileggi, R. D. Molano, P. O. Berggren and A. Caicedo (2010). "ATP-gated P2X(3) receptors constitute a positive autocrine signal for insulin release in the human pancreatic β cell." Proc Natl Acad Sci U S A **107**(14): 6465-6470.
Jarvis, M. F. and B. S. Khakh (2009). "ATP-gated P2X cation-channels." Neuropharmacology **56**(1): 208-215.
Jastroch, M., V. Hirschberg and M. Klingenspor (2012). "Functional characterization of UCP1 in mammalian HEK293 cells excludes mitochondrial uncoupling artefacts and reveals no contribution to basal proton leak." Biochim Biophys Acta **1817**(9): 1660-1670.
Jensen, B., M. C. Farach-Carson, E. Kenaley and K. A. Akanbi (2004). "High extracellular calcium attenuates adipogenesis in 3T3-L1 preadipocytes." Exp Cell Res **301**(2): 280-292.
Johnson, D. and E. J. Drenick (1977). "Therapeutic fasting in morbid obesity." Arch Intern Med **137**(10): 1381-1382.
Kar, P., C. Nelson and A. B. Parekh (2011). "Selective activation of the transcription factor NFAT1 by calcium microdomains near Ca2+ release-activated Ca2+ (CRAC) channels." J Biol Chem **286**(17): 14795-14803.
Kar, P., C. Nelson and A. B. Parekh (2012). "CRAC channels drive digital activation and provide analog control and synergy to Ca(2+)-dependent gene regulation." Curr Biol **22**(3): 242-247.
Karamanlidis, G., A. Karamitri, K. Docherty, D. G. Hazlerigg and M. A. Lomax (2007). "C/EBPbeta reprograms white 3T3-L1 preadipocytes to a Brown adipocyte pattern of gene expression." J Biol Chem **282**(34): 24660-24669.
Kawamura, H., T. Kawamura, Y. Kanda, T. Kobayashi and T. Abo (2012). "Extracellular ATP-stimulated macrophages produce macrophage inflammatory protein-2 which is important for neutrophil migration." Immunology **136**(4): 448-458.
Keipert, S. and M. Jastroch (2014). "Brite/beige fat and UCP1 - is it thermogenesis?" Biochim Biophys Acta **1837**(7): 1075-1082.
Kiens, B. (2006). "Skeletal muscle lipid metabolism in exercise and insulin resistance." Physiol Rev **86**(1): 205-243.
Kim, H., M. C. Walsh, N. Takegahara, S. A. Middleton, H. I. Shin, J. Kim and Y. Choi (2017). "The purinergic receptor P2X5 regulates inflammasome activity and hyper-multinucleation of murine osteoclasts." Sci Rep **7**(1): 196.
Kolanowski, J. (1999). "A risk-benefit assessment of anti-obesity drugs." Drug Saf **20**(2): 119-131.
Kosteli, A., E. Sugaru, G. Haemmerle, J. F. Martin, J. Lei, R. Zechner and A. W. Ferrante, Jr. (2010). "Weight loss and lipolysis promote a dynamic immune response in murine adipose tissue." J Clin Invest **120**(10): 3466-3479.
Krings, A., S. Rahman, S. Huang, Y. Lu, P. J. Czernik and B. Lecka-Czernik (2012). "Bone marrow fat has brown adipose tissue characteristics, which are attenuated with aging and diabetes." Bone **50**(2): 546-552.
Krintel, C., M. Morgelin, D. T. Logan and C. Holm (2009). "Phosphorylation of hormone-sensitive lipase by protein kinase A in vitro promotes an increase in its hydrophobic surface area." Febs j **276**(17): 4752-4762.
Kushner, R. F. and S. W. Choi (2010). "Prevalence of unhealthy lifestyle patterns among overweight and obese adults." Obesity (Silver Spring) **18**(6): 1160-1167.
Kushner, R. F. and H. Manzano (2002). "Obesity pharmacology: past, present, and future." Curr Opin Gastroenterol **18**(2): 213-220.

Lalo, U., Y. Pankratov, S. P. Wichert, M. J. Rossner, R. A. North, F. Kirchhoff and A. Verkhratsky (2008). "P2X1 and P2X5 subunits form the functional P2X receptor in mouse cortical astrocytes." J Neurosci **28**(21): 5473-5480.
Lara, L. G., A. V. Villa, M. M. Rivas, M. S. Capella, F. Prada and M. A. Ensenat (2017). "Subcutaneous Fat Necrosis of the Newborn: Report of Five Cases." Pediatr Neonatol **58**(1): 85-88.
Larsen, T. M., S. Toubro, M. A. van Baak, K. M. Gottesdiener, P. Larson, W. H. M. Saris and A. Astrup "Effect of a 28-d treatment with L-796568, a novel β3-adrenergic receptor agonist, on energy expenditure and body composition in obese men." Am J Clin Nutr **76**(4): 780-788.
Lawrence, M. C., K. McGlynn, B. H. Park and M. H. Cobb (2005). "ERK1/2-dependent activation of transcription factors required for acute and chronic effects of glucose on the insulin gene promoter." J Biol Chem **280**(29): 26751-26759.
Layhadi, J. A. and S. J. Fountain (2017). "P2X4 Receptor-Dependent Ca(2+) Influx in Model Human Monocytes and Macrophages." Int J Mol Sci **18**(11).
Le, K. T., M. Paquet, D. Nouel, K. Babinski and P. Seguela (1997). "Primary structure and expression of a naturally truncated human P2X ATP receptor subunit from brain and immune system." FEBS Lett **418**(1-2): 195-199.
Lechner, S., M. C. Mitterberger, M. Mattesich and W. Zwerschke (2013). "Role of C/EBPbeta-LAP and C/EBPbeta-LIP in early adipogenic differentiation of human white adipose-derived progenitors and at later stages in immature adipocytes." Differentiation **85**(1-2): 20-31.
Lee, B. M., H. Jo, G. Park, Y. H. Kim, C. K. Park, S. J. Jung, G. Chung and S. B. Oh (2017). "Extracellular ATP Induces Calcium Signaling in Odontoblasts." J Dent Res **96**(2): 200-207.
Leibel, R. L., M. Rosenbaum and J. Hirsch (1995). "Changes in energy expenditure resulting from altered body weight." N Engl J Med **332**(10): 621-628.
Lin, F., T. J. Ribar and A. R. Means (2011). "The Ca2+/calmodulin-dependent protein kinase kinase, CaMKK2, inhibits preadipocyte differentiation." Endocrinology **152**(10): 3668-3679.
Ma, S., H. Yu, Z. Zhao, Z. Luo, J. Chen, Y. Ni, R. Jin, L. Ma, P. Wang, Z. Zhu, L. Li, J. Zhong, D. Liu, B. Nilius and Z. Zhu (2012). "Activation of the cold-sensing TRPM8 channel triggers UCP1-dependent thermogenesis and prevents obesity." J Mol Cell Biol **4**(2): 88-96.
MacKrell, J. G. and G. D. Cartee (2012). "A Novel Method to Measure Glucose Uptake and Myosin Heavy Chain Isoform Expression of Single Fibers From Rat Skeletal Muscle." Diabetes **61**(5): 995-1003.
Marcelo, K. L., A. R. Means and B. York (2016). "The Ca(2+)/Calmodulin/CaMKK2 Axis: Nature's Metabolic CaMshaft." Trends Endocrinol Metab **27**(10): 706-718.
Marin-Vicente, C., J. C. Gomez-Fernandez and S. Corbalan-Garcia (2005). "The ATP-dependent membrane localization of protein kinase Calpha is regulated by Ca2+ influx and phosphatidylinositol 4,5-bisphosphate in differentiated PC12 cells." Mol Biol Cell **16**(6): 2848-2861.
McDonald, R. B. and B. A. Horwitz (1999). "Brown adipose tissue thermogenesis during aging and senescence." J Bioenerg Biomembr **31**(5): 507-516.
Mehta, K. D. (2014). "Emerging role of protein kinase C in energy homeostasis: A brief overview." World J Diabetes **5**(3): 385-392.
Mellor, L. F., M. Mohiti-Asli, J. Williams, A. Kannan, M. R. Dent, F. Guilak and E. G. Loboa (2015). "Extracellular Calcium Modulates Chondrogenic and Osteogenic Differentiation of Human Adipose-Derived Stem Cells: A Novel Approach for Osteochondral Tissue Engineering Using a Single Stem Cell Source." Tissue Eng Part A **21**(17-18): 2323-2333.
Metrich, M., A. Lucas, M. Gastineau, J. L. Samuel, C. Heymes, E. Morel and F. Lezoualc'h (2008). "Epac mediates beta-adrenergic receptor-induced cardiomyocyte hypertrophy." Circ Res **102**(8): 959-965.
Meyer, M. P., U. Groschel-Stewart, T. Robson and G. Burnstock (1999). "Expression of two ATP-gated ion channels, P2X5 and P2X6, in developing chick skeletal muscle." Dev Dyn **216**(4-5): 442-449.

Meyers, D. S., S. Skwish, K. E. Dickinson, B. Kienzle and C. M. Arbeeny (1997). "Beta 3-adrenergic receptor-mediated lipolysis and oxygen consumption in brown adipocytes from cynomolgus monkeys." J Clin Endocrinol Metab **82**(2): 395-401.
Michael, A. F., Jr., R. Hong and C. D. West (1962). "Hypercalcemia in infancy associated with subcutaneous fat necrosis and calcification." Am J Dis Child **104**: 235-244.
Miyoshi, H., S. C. Souza, H. H. Zhang, K. J. Strissel, M. A. Christoffolete, J. Kovsan, A. Rudich, F. B. Kraemer, A. C. Bianco, M. S. Obin and A. S. Greenberg (2006). "Perilipin promotes hormone-sensitive lipase-mediated adipocyte lipolysis via phosphorylation-dependent and -independent mechanisms." J Biol Chem **281**(23): 15837-15844.
Nakamura, Y., T. Sato, Y. Shiimura, Y. Miura and M. Kojima (2013). "FABP3 and brown adipocyte-characteristic mitochondrial fatty acid oxidation enzymes are induced in beige cells in a different pathway from UCP1." Biochem Biophys Res Commun **441**(1): 42-46.
Neal, J. W. and N. A. Clipstone (2002). "Calcineurin mediates the calcium-dependent inhibition of adipocyte differentiation in 3T3-L1 cells." J Biol Chem **277**(51): 49776-49781.
Nedergaard, J., T. Bengtsson and B. Cannon (2007). "Unexpected evidence for active brown adipose tissue in adult humans." Am J Physiol Endocrinol Metab **293**(2): E444-452.
Ng, M., T. Fleming, M. Robinson, B. Thomson, N. Graetz, C. Margono, E. C. Mullany, S. Biryukov, C. Abbafati, S. F. Abera, J. P. Abraham, N. M. Abu-Rmeileh, T. Achoki, F. S. AlBuhairan, Z. A. Alemu, R. Alfonso, M. K. Ali, R. Ali, N. A. Guzman, W. Ammar, P. Anwari, A. Banerjee, S. Barquera, S. Basu, D. A. Bennett, Z. Bhutta, J. Blore, N. Cabral, I. C. Nonato, J. C. Chang, R. Chowdhury, K. J. Courville, M. H. Criqui, D. K. Cundiff, K. C. Dabhadkar, L. Dandona, A. Davis, A. Dayama, S. D. Dharmaratne, E. L. Ding, A. M. Durrani, A. Esteghamati, F. Farzadfar, D. F. Fay, V. L. Feigin, A. Flaxman, M. H. Forouzanfar, A. Goto, M. A. Green, R. Gupta, N. Hafezi-Nejad, G. J. Hankey, H. C. Harewood, R. Havmoeller, S. Hay, L. Hernandez, A. Husseini, B. T. Idrisov, N. Ikeda, F. Islami, E. Jahangir, S. K. Jassal, S. H. Jee, M. Jeffreys, J. B. Jonas, E. K. Kabagambe, S. E. Khalifa, A. P. Kengne, Y. S. Khader, Y. H. Khang, D. Kim, R. W. Kimokoti, J. M. Kinge, Y. Kokubo, S. Kosen, G. Kwan, T. Lai, M. Leinsalu, Y. Li, X. Liang, S. Liu, G. Logroscino, P. A. Lotufo, Y. Lu, J. Ma, N. K. Mainoo, G. A. Mensah, T. R. Merriman, A. H. Mokdad, J. Moschandreas, M. Naghavi, A. Naheed, D. Nand, K. M. Narayan, E. L. Nelson, M. L. Neuhouser, M. I. Nisar, T. Ohkubo, S. O. Oti, A. Pedroza, D. Prabhakaran, N. Roy, U. Sampson, H. Seo, S. G. Sepanlou, K. Shibuya, R. Shiri, I. Shiue, G. M. Singh, J. A. Singh, V. Skirbekk, N. J. Stapelberg, L. Sturua, B. L. Sykes, M. Tobias, B. X. Tran, L. Trasande, H. Toyoshima, S. van de Vijver, T. J. Vasankari, J. L. Veerman, G. Velasquez-Melendez, V. V. Vlassov, S. E. Vollset, T. Vos, C. Wang, X. Wang, E. Weiderpass, A. Werdecker, J. L. Wright, Y. C. Yang, H. Yatsuya, J. Yoon, S. J. Yoon, Y. Zhao, M. Zhou, S. Zhu, A. D. Lopez, C. J. Murray and E. Gakidou (2014). "Global, regional, and national prevalence of overweight and obesity in children and adults during 1980-2013: a systematic analysis for the Global Burden of Disease Study 2013." Lancet **384**(9945): 766-781.
Nicke, A., H. G. Baumert, J. Rettinger, A. Eichele, G. Lambrecht, E. Mutschler and G. Schmalzing (1998). "P2X1 and P2X3 receptors form stable trimers: a novel structural motif of ligand-gated ion channels." Embo j **17**(11): 3016-3028.
North, R. A. (2002). "Molecular physiology of P2X receptors." Physiol Rev **82**(4): 1013-1067.
Nsiah-Sefaa, A. and M. McKenzie (2016). "Combined defects in oxidative phosphorylation and fatty acid beta-oxidation in mitochondrial disease." Biosci Rep **36**(2).
Ohtani, M., K. Ohura and T. Oka (2011). "Involvement of P2X receptors in the regulation of insulin secretion, proliferation and survival in mouse pancreatic beta-cells." Cell Physiol Biochem **28**(2): 355-366.
Olsen, J. M., M. Sato, O. S. Dallner, A. L. Sandström, D. F. Pisani, J.-C. Chambard, E.-Z. Amri, D. S. Hutchinson and T. Bengtsson (2014). "Glucose uptake in brown fat cells is dependent on mTOR complex 2–promoted GLUT1 translocation." The Journal of Cell Biology **207**(3): 365-374.

Orava, J., P. Nuutila, M. E. Lidell, V. Oikonen, T. Noponen, T. Viljanen, M. Scheinin, M. Taittonen, T. Niemi, S. Enerback and K. A. Virtanen (2011). "Different metabolic responses of human brown adipose tissue to activation by cold and insulin." Cell Metab **14**(2): 272-279.
Orava, J., P. Nuutila, Martin E. Lidell, V. Oikonen, T. Noponen, T. Viljanen, M. Scheinin, M. Taittonen, T. Niemi, S. Enerbäck and Kirsi A. Virtanen (2011). "Different Metabolic Responses of Human Brown Adipose Tissue to Activation by Cold and Insulin." Cell Metabolism **14**(2): 272-279.
Ouchi, N., J. L. Parker, J. J. Lugus and K. Walsh (2011). "Adipokines in inflammation and metabolic disease." Nat Rev Immunol **11**(2): 85-97.
Pagnon, J., M. Matzaris, R. Stark, R. C. Meex, S. L. Macaulay, W. Brown, P. E. O'Brien, T. Tiganis and M. J. Watt (2012). "Identification and functional characterization of protein kinase A phosphorylation sites in the major lipolytic protein, adipose triglyceride lipase." Endocrinology **153**(9): 4278-4289.
PAHO (2014). Plan of Action for the Prevention of Obesity in Children and Adolescents. 53rd Directing Council, 66th Session of the Regional Committe of WHO for the Americas. Washington D.C., USA, Pan American Health Organization**:** 35.
Pappone, P. A. and S. C. Lee (1996). "Purinergic receptor stimulation increases membrane trafficking in brown adipocytes." J Gen Physiol **108**(5): 393-404.
Park, B.-H. a. Q., Li and Farmer, Stephen R. (2004). "Phosphorylation of C/EBPβ at a Consensus Extracellular Signal-Regulated Kinase/Glycogen Synthase Kinase 3 Site Is Required for the Induction of Adiponectin Gene Expression during the Differentiation of Mouse Fibroblasts into Adipocytes." Molecular and Cellular Biology **24**(19): 8671-8680.
Park, J. M., C. Y. Park and S. N. Han (2015). "High fat diet-Induced obesity alters vitamin D metabolizing enzyme expression in mice." Biofactors **41**(3): 175-182.
Petit, P., D. Hillaire-Buys, M. Manteghetti, S. Debrus, J. Chapal and M. M. Loubatieres-Mariani (1998). "Evidence for two different types of P2 receptors stimulating insulin secretion from pancreatic B cell." Br J Pharmacol **125**(6): 1368-1374.
Pfeifer, A., A. Kilic and L. S. Hoffmann (2013). "Regulation of metabolism by cGMP." Pharmacol Ther **140**(1): 81-91.
Pfluger, P. T., D. G. Kabra, M. Aichler, S. C. Schriever, K. Pfuhlmann, V. C. Garcia, M. Lehti, J. Weber, M. Kutschke, J. Rozman, J. W. Elrod, A. L. Hevener, A. Feuchtinger, M. Hrabe de Angelis, A. Walch, S. M. Rollmann, B. J. Aronow, T. D. Muller, D. Perez-Tilve, M. Jastroch, M. De Luca, J. D. Molkentin and M. H. Tschop (2015). "Calcineurin Links Mitochondrial Elongation with Energy Metabolism." Cell Metab **22**(5): 838-850.
Pierce, J. L., D. L. Begun, J. J. Westendorf and M. E. McGee-Lawrence (2018). "Defining osteoblast and adipocyte lineages in the bone marrow." Bone.
Prakriya, M. and R. S. Lewis (2015). "Store-Operated Calcium Channels." Physiol Rev **95**(4): 1383-1436.
Pramme-Steinwachs, I., M. Jastroch and S. Ussar (2017). "Extracellular calcium modulates brown adipocyte differentiation and identity." Sci Rep **7**(1): 8888.
Prusty, D., B. H. Park, K. E. Davis and S. R. Farmer (2002). "Activation of MEK/ERK signaling promotes adipogenesis by enhancing peroxisome proliferator-activated receptor gamma (PPARgamma) and C/EBPalpha gene expression during the differentiation of 3T3-L1 preadipocytes." J Biol Chem **277**(48): 46226-46232.
Rapold, R. A., S. Wueest, A. Knoepfel, E. J. Schoenle and D. Konrad (2013). "Fas activates lipolysis in a Ca2+-CaMKII-dependent manner in 3T3-L1 adipocytes." J Lipid Res **54**(1): 63-70.
Razzoli, M., A. Frontini, A. Gurney, E. Mondini, C. Cubuk, L. S. Katz, C. Cero, P. J. Bolan, J. Dopazo, A. Vidal-Puig, S. Cinti and A. Bartolomucci (2016). "Stress-induced activation of brown adipose tissue prevents obesity in conditions of low adaptive thermogenesis." Mol Metab **5**(1): 19-33.

Rockstroh, D., K. Landgraf, I. V. Wagner, J. Gesing, R. Tauscher, N. Lakowa, W. Kiess, U. Buhligen, M. Wojan, H. Till, M. Bluher and A. Korner (2015). "Direct evidence of brown adipocytes in different fat depots in children." PLoS One **10**(2): e0117841.
Rodrigue-Candela, J. L., D. Martin-Hernandez and T. Castilla-Cortazar (1963). "Stimulation of insulin secretion in vitro by adenosine triphosphate." Nature **197**: 1304.
Roger, S., P. Pelegrin and A. Surprenant (2008). "Facilitation of P2X7 receptor currents and membrane blebbing via constitutive and dynamic calmodulin binding." J Neurosci **28**(25): 6393-6401.
Rooney, B. L., M. A. Mathiason and C. W. Schauberger (2011). "Predictors of obesity in childhood, adolescence, and adulthood in a birth cohort." Matern Child Health J **15**(8): 1166-1175.
Ryten, M., P. M. Dunn, J. T. Neary and G. Burnstock (2002). "ATP regulates the differentiation of mammalian skeletal muscle by activation of a P2X5 receptor on satellite cells." J Cell Biol **158**(2): 345-355.
Ryten, M., A. Hoebertz and G. Burnstock (2001). "Sequential expression of three receptor subtypes for extracellular ATP in developing rat skeletal muscle." Dev Dyn **221**(3): 331-341.
Saito, M., Y. Okamatsu-Ogura, M. Matsushita, K. Watanabe, T. Yoneshiro, J. Nio-Kobayashi, T. Iwanaga, M. Miyagawa, T. Kameya, K. Nakada, Y. Kawai and M. Tsujisaki (2009). "High incidence of metabolically active brown adipose tissue in healthy adult humans: effects of cold exposure and adiposity." Diabetes **58**(7): 1526-1531.
Sakamoto, T., N. Takahashi, Y. Sawaragi, S. Naknukool, R. Yu, T. Goto and T. Kawada (2013). "Inflammation induced by RAW macrophages suppresses UCP1 mRNA induction via ERK activation in 10T1/2 adipocytes." Am J Physiol Cell Physiol **304**(8): C729-738.
Sanchez-Gurmaches, J. and D. A. Guertin (2014). "Adipocyte lineages: tracing back the origins of fat." Biochim Biophys Acta **1842**(3): 340-351.
Sanchez-Gurmaches, J. and D. A. Guertin (2014). "Adipocytes arise from multiple lineages that are heterogeneously and dynamically distributed." Nat Commun **5**: 4099.
Schaafsma, G. (1988). Calcium in Extracellular Fluid: Homeostasis. Calcium in Human Biology. B. E. C. Nordin. London, Springer London**:** 241-259.
Scherer, P. E. (2006). "Adipose tissue: from lipid storage compartment to endocrine organ." Diabetes **55**(6): 1537-1545.
Schmitz-Peiffer, C., C. L. Browne, N. D. Oakes, A. Watkinson, D. J. Chisholm, E. W. Kraegen and T. J. Biden (1997). "Alterations in the expression and cellular localization of protein kinase C isozymes epsilon and theta are associated with insulin resistance in skeletal muscle of the high-fat-fed rat." Diabetes **46**(2): 169-178.
Schodel, J., I. Weise, R. Klinger and M. Schmidt (2004). "Stimulation of lipogenesis in rat adipocytes by ATP, a ligand for P2-receptors." Biochem Biophys Res Commun **321**(4): 767-773.
Schoettl, T., I. P. Fischer and S. Ussar (2018). "Heterogeneity of adipose tissue in development and metabolic function." J Exp Biol **221**(Pt Suppl 1).
Schulz, T. J., T. L. Huang, T. T. Tran, H. Zhang, K. L. Townsend, J. L. Shadrach, M. Cerletti, L. E. McDougall, N. Giorgadze, T. Tchkonia, D. Schrier, D. Falb, J. L. Kirkland, A. J. Wagers and Y. H. Tseng (2011). "Identification of inducible brown adipocyte progenitors residing in skeletal muscle and white fat." Proc Natl Acad Sci U S A **108**(1): 143-148.
Seale, P., B. Bjork, W. Yang, S. Kajimura, S. Chin, S. Kuang, A. Scime, S. Devarakonda, H. M. Conroe, H. Erdjument-Bromage, P. Tempst, M. A. Rudnicki, D. R. Beier and B. M. Spiegelman (2008). "PRDM16 controls a brown fat/skeletal muscle switch." Nature **454**(7207): 961-967.
Seale, P., H. M. Conroe, J. Estall, S. Kajimura, A. Frontini, J. Ishibashi, P. Cohen, S. Cinti and B. M. Spiegelman (2011). "Prdm16 determines the thermogenic program of subcutaneous white adipose tissue in mice." J Clin Invest **121**(1): 96-105.

Shao, D., S. M. Rangwala, S. T. Bailey, S. L. Krakow, M. J. Reginato and M. A. Lazar (1998). "Interdomain communication regulating ligand binding by PPAR-gamma." Nature **396**(6709): 377-380.
Shi, H., Y. D. Halvorsen, P. N. Ellis, W. O. Wilkison and M. B. Zemel (2000). "Role of intracellular calcium in human adipocyte differentiation." Physiol Genomics **3**(2): 75-82.
Siebenhofer, A., K. Jeitler, K. Horvath, A. Berghold, N. Posch, J. Meschik and T. Semlitsch (2016). "Long-term effects of weight-reducing drugs in people with hypertension." Cochrane Database Syst Rev **3**: Cd007654.
Silberberg, S. D. and K. J. Swartz (2009). "Structural biology: Trimeric ion-channel design." Nature **460**(7255): 580-581.
Simons, T. J. (1988). "Calcium and neuronal function." Neurosurg Rev **11**(2): 119-129.
Skala, J., T. Barnard and O. Lindberg (1970). "Changes in interscapular brown adipose tissue of the rat during perinatal and early postnatal development and after cold acclimation. II. Mitochondrial changes." Comp Biochem Physiol **33**(3): 509-528.
Stanford, K. I., R. J. Middelbeek, K. L. Townsend, D. An, E. B. Nygaard, K. M. Hitchcox, K. R. Markan, K. Nakano, M. F. Hirshman, Y. H. Tseng and L. J. Goodyear (2013). "Brown adipose tissue regulates glucose homeostasis and insulin sensitivity." J Clin Invest **123**(1): 215-223.
Stanford, K. I., R. J. Middelbeek, K. L. Townsend, M. Y. Lee, H. Takahashi, K. So, K. M. Hitchcox, K. R. Markan, K. Hellbach, M. F. Hirshman, Y. H. Tseng and L. J. Goodyear (2015). "A novel role for subcutaneous adipose tissue in exercise-induced improvements in glucose homeostasis." Diabetes **64**(6): 2002-2014.
Stoffels, M., R. Zaal, N. Kok, J. W. M. van der Meer, C. A. Dinarello and A. Simon (2015). "ATP-Induced IL-1β Specific Secretion: True Under Stringent Conditions." Front Immunol **6**.
Strosberg, A. D. (1997). "Structure and function of the beta 3-adrenergic receptor." Annu Rev Pharmacol Toxicol **37**: 421-450.
Surprenant, A., G. Buell and R. A. North (1995). "P2X receptors bring new structure to ligand-gated ion channels." Trends Neurosci **18**(5): 224-229.
Szent-Györgyi, A. G. (1975). "Calcium regulation of muscle contraction." Biophysical Journal **15**(7): 707-723.
Takakura, Y. and T. Yoshida (2001). "[Beta 3-adrenergic receptor agonists--past, present and future]." Nihon Yakurigaku Zasshi **118**(5): 315-320.
Tang, Q. Q., J. W. Zhang and M. Daniel Lane (2004). "Sequential gene promoter interactions of C/EBPbeta, C/EBPalpha, and PPARgamma during adipogenesis." Biochem Biophys Res Commun **319**(1): 235-239.
Tatsumi, M., J. M. Engles, T. Ishimori, O. Nicely, C. Cohade and R. L. Wahl (2004). "Intense (18)F-FDG uptake in brown fat can be reduced pharmacologically." J Nucl Med **45**(7): 1189-1193.
Taylor, P. B. and Q. Tang (1984). "Development of isoproterenol-induced cardiac hypertrophy." Can J Physiol Pharmacol **62**(4): 384-389.
Tomic, M., R. M. Jobin, L. A. Vergara and S. S. Stojilkovic (1996). "Expression of purinergic receptor channels and their role in calcium signaling and hormone release in pituitary gonadotrophs. Integration of P2 channels in plasma membrane- and endoplasmic reticulum-derived calcium oscillations." J Biol Chem **271**(35): 21200-21208.
Torriani, M., S. Srinivasa, K. V. Fitch, T. Thomou, K. Wong, E. Petrow, C. R. Kahn, A. M. Cypess and S. K. Grinspoon (2016). "Dysfunctional Subcutaneous Fat With Reduced Dicer and Brown Adipose Tissue Gene Expression in HIV-Infected Patients." J Clin Endocrinol Metab **101**(3): 1225-1234.
Townsend-Nicholson, A., B. F. King, S. S. Wildman and G. Burnstock (1999). "Molecular cloning, functional characterization and possible cooperativity between the murine P2X4 and P2X4a receptors." Brain Res Mol Brain Res **64**(2): 246-254.

Umekawa, T., T. Yoshida, N. Sakane, M. Saito, K. Kumamoto and M. Kondo (1997). "Anti-obesity and anti-diabetic effects of CL316,243, a highly specific beta 3-adrenoceptor agonist, in Otsuka Long-Evans Tokushima Fatty rats: induction of uncoupling protein and activation of glucose transporter 4 in white fat." Eur J Endocrinol **136**(4): 429-437.
Ussar, S., O. Bezy, M. Bluher and C. R. Kahn (2012). "Glypican-4 enhances insulin signaling via interaction with the insulin receptor and serves as a novel adipokine." Diabetes **61**(9): 2289-2298.
Ussar, S., K. Y. Lee, S. N. Dankel, J. Boucher, M. F. Haering, A. Kleinridders, T. Thomou, R. Xue, Y. Macotela, A. M. Cypess, Y. H. Tseng, G. Mellgren and C. R. Kahn (2014). "ASC-1, PAT2, and P2RX5 are cell surface markers for white, beige, and brown adipocytes." Sci Transl Med **6**(247): 247ra103.
Valera, S., N. Hussy, R. J. Evans, N. Adami, R. A. North, A. Surprenant and G. Buell (1994). "A new class of ligand-gated ion channel defined by P2x receptor for extracellular ATP." Nature **371**(6497): 516-519.
van der Lans, A. A., J. Hoeks, B. Brans, G. H. Vijgen, M. G. Visser, M. J. Vosselman, J. Hansen, J. A. Jorgensen, J. Wu, F. M. Mottaghy, P. Schrauwen and W. D. van Marken Lichtenbelt (2013). "Cold acclimation recruits human brown fat and increases nonshivering thermogenesis." J Clin Invest **123**(8): 3395-3403.
Vergnes, L., R. Chin, S. G. Young and K. Reue (2011). "Heart-type fatty acid-binding protein is essential for efficient brown adipose tissue fatty acid oxidation and cold tolerance." J Biol Chem **286**(1): 380-390.
Vosselman, M. J., A. A. van der Lans, B. Brans, R. Wierts, M. A. van Baak, P. Schrauwen and W. D. van Marken Lichtenbelt (2012). "Systemic beta-adrenergic stimulation of thermogenesis is not accompanied by brown adipose tissue activity in humans." Diabetes **61**(12): 3106-3113.
Walden, T. B., N. Petrovic and J. Nedergaard (2010). "PPARalpha does not suppress muscle-associated gene expression in brown adipocytes but does influence expression of factors that fingerprint the brown adipocyte." Biochem Biophys Res Commun **397**(2): 146-151.
Watanabe, M., T. Yamamoto, C. Mori, N. Okada, N. Yamazaki, K. Kajimoto, M. Kataoka and Y. Shinohara (2008). "Cold-induced changes in gene expression in brown adipose tissue: implications for the activation of thermogenesis." Biol Pharm Bull **31**(5): 775-784.
Webb, T. E., J. Simon, B. J. Krishek, A. N. Bateson, T. G. Smart, B. F. King, G. Burnstock and E. A. Barnard (1993). "Cloning and functional expression of a brain G-protein-coupled ATP receptor." FEBS Lett **324**(2): 219-225.
Weyer, C., P. A. Tataranni, S. Snitker, E. Danforth, Jr. and E. Ravussin (1998). "Increase in insulin action and fat oxidation after treatment with CL 316,243, a highly selective beta3-adrenoceptor agonist in humans." Diabetes **47**(10): 1555-1561.
Whittle, A. J., S. Carobbio, L. Martins, M. Slawik, E. Hondares, M. J. Vazquez, D. Morgan, R. I. Csikasz, R. Gallego, S. Rodriguez-Cuenca, M. Dale, S. Virtue, F. Villarroya, B. Cannon, K. Rahmouni, M. Lopez and A. Vidal-Puig (2012). "BMP8B increases brown adipose tissue thermogenesis through both central and peripheral actions." Cell **149**(4): 871-885.
WHO. (2006-2011, 11.10.2017). "Global Health Observatory Map Gallery ", from http://gamapserver.who.int/mapLibrary/app/searchResults.aspx.
WHO (2011). Global status report on noncommuicable diseases 2010. Geneva, Switzerland, World Health Organization.
WHO. (2017, 06.11.2017). "Facts on Obesity." from http://www.who.int/news-room/facts-in-pictures/detail/6-facts-on-obesity.
Wildman, S. S., S. G. Brown, M. Rahman, C. A. Noel, L. Churchill, G. Burnstock, R. J. Unwin and B. F. King (2002). "Sensitization by Extracellular Ca2+ of Rat P2X5 Receptor and Its Pharmacological Properties Compared with Rat P2X1." Molecular Pharmacology **62**(4): 957-966.

Wu, D., A. B. Molofsky, H. E. Liang, R. R. Ricardo-Gonzalez, H. A. Jouihan, J. K. Bando, A. Chawla and R. M. Locksley (2011). "Eosinophils sustain adipose alternatively activated macrophages associated with glucose homeostasis." Science **332**(6026): 243-247.
Wu, D. and N. Mori (1999). "Extracellular ATP-induced inward current in isolated epithelial cells of the endolymphatic sac." Biochim Biophys Acta **1419**(1): 33-42.
Wu, Z., E. D. Rosen, R. Brun, S. Hauser, G. Adelmant, A. E. Troy, C. McKeon, G. J. Darlington and B. M. Spiegelman (1999). "Cross-regulation of C/EBP alpha and PPAR gamma controls the transcriptional pathway of adipogenesis and insulin sensitivity." Mol Cell **3**(2): 151-158.
Yamashita, H., Z. Wang, Y. Wang, M. Segawa, T. Kusudo and Y. Kontani (2008). "Induction of fatty acid-binding protein 3 in brown adipose tissue correlates with increased demand for adaptive thermogenesis in rodents." Biochem Biophys Res Commun **377**(2): 632-635.
Yoneshiro, T., S. Aita, M. Matsushita, T. Kameya, K. Nakada, Y. Kawai and M. Saito (2011). "Brown adipose tissue, whole-body energy expenditure, and thermogenesis in healthy adult men." Obesity (Silver Spring) **19**(1): 13-16.
Yoneshiro, T., S. Aita, M. Matsushita, T. Kayahara, T. Kameya, Y. Kawai, T. Iwanaga and M. Saito (2013). "Recruited brown adipose tissue as an antiobesity agent in humans." J Clin Invest **123**(8): 3404-3408.
Yoshida, T. and T. Umekawa (1998). "[Beta 3 adrenergic receptor polymorphism and obesity]." Nihon Rinsho **56**(7): 1871-1875.
Zhang, S. L., A. V. Yeromin, X. H. Zhang, Y. Yu, O. Safrina, A. Penna, J. Roos, K. A. Stauderman and M. D. Cahalan (2006). "Genome-wide RNAi screen of Ca(2+) influx identifies genes that regulate Ca(2+) release-activated Ca(2+) channel activity." Proc Natl Acad Sci U S A **103**(24): 9357-9362.
Zhang, Y., R. Proenca, M. Maffei, M. Barone, L. Leopold and J. M. Friedman (1994). "Positional cloning of the mouse obese gene and its human homologue." Nature **372**(6505): 425-432.
Zhou, Y., R. M. Nwokonko, X. Cai, N. A. Loktionova, R. Abdulqadir, P. Xin, B. A. Niemeyer, Y. Wang, M. Trebak and D. L. Gill (2018). "Cross-linking of Orai1 channels by STIM proteins." Proc Natl Acad Sci U S A **115**(15): E3398-e3407.

7 APPENDIX

SCIENTIFIC REPORTS

OPEN

Extracellular calcium modulates brown adipocyte differentiation and identity

Received: 31 March 2017
Accepted: 19 July 2017
Published online: 21 August 2017

Ines Pramme-Steinwachs[1,2], Martin Jastroch[2,3] & Siegfried Ussar[1,2]

Brown adipocytes are important in regulating non-shivering thermogenesis, whole body glucose and lipid homeostasis. Increasing evidence supports an important role of metabolites as well as macro- and micronutrients in brown adipocyte differentiation and function. Calcium is one of the most abundant ions in the body regulating multiple cellular processes. We observed that increasing extracellular calcium concentration during brown adipocyte differentiation blocks lipid accumulation and suppresses induction of major adipogenic transcription factors such as PPARγ and C/EBPα. In contrast, the depletion of calcium in the medium enhances adipogenesis and expression of brown adipocyte selective genes, such as UCP1. Mechanistically, we show that elevated extracellular calcium inhibits C/EBPβ activity through hyperactivation of ERK, a process that is independent of intracellular calcium levels and reversibly halts differentiation. Moreover, increased extracellular calcium solely after the induction phase of differentiation specifically suppresses gene expression of UCP1, PRDM16 and PGC1-α. Notably, depleting extracellular calcium provokes opposite effects. Together, we show that modulating extracellular calcium concentration controls brown adipocyte differentiation and thermogenic gene expression, highlighting the importance of tissue microenvironment on brown adipocyte heterogeneity and function.

Brown adipose tissue (BAT) differs significantly from white adipose tissue (WAT) with respect to function, morphology and developmental origin[1,2]. Although both tissues are important endocrine organs, the primary function of white adipose tissue is to store energy in form of triglycerides, whereas BAT dissipates energy in form of heat through mitochondrial uncoupled respiration using the uncoupling protein 1 (UCP1)[3–5]. BAT is found in the neck and supraclavicular regions of adult humans[6], as well as in the interscapular region of infants and rodents[7]. Multilocular lipid droplets and a high density of mitochondria morphologically distinguish brown from white adipocytes and are therefore major characteristics of brown adipocytes. Previous work by Spiegelman[8] and others[9,10] has shown that brown adipocytes originate from distinct, Myf5- positive, precursor populations. However, more recent data indicate that Myf5- positive precursor cells can also give rise to distinct white adipocytes, preferentially within visceral adipose tissue depots, suggesting a complex developmental program distinguishing brown from white adipocytes[11].

Various extrinsic[12–14] and endocrine factors[15–17], such as ambient temperature, bone morphogenetic proteins (BMPs) etc., modulate brown adipocyte differentiation and activity. Interestingly, relatively little is known how the local microenvironment, comprising the extracellular matrix, proximity to blood vessels and local concentrations of nutrients, regulates brown adipocyte differentiation and function. Among the diversity of macro- and micronutrients, calcium is one of the most abundant and important ions in the body. Calcium regulates essential body functions, such as calcification of bones, neuronal transmission, muscle contraction, insulin release and many more[18–21]. To this end, it is not surprising that serum calcium levels are tightly regulated and alterations can have detrimental consequences for human health[22–24]. Local interstitial calcium concentrations, however, are much less studied and could be more variable. There is limited knowledge on the role of extracellular calcium fluctuations in obesity, but reducing excess calcium in the blood by nutritional supplements like calcitonin improves body weight in obese rats[25]. The impact of this reduction on calcium homeostasis and (brown-) adipose tissue function has not been addressed in detail yet.

[1]JRG Adipocytes & Metabolism, Institute for Diabetes & Obesity, Helmholtz Center Munich, 85748, Garching, Germany. [2]German Center for Diabetes Research (DZD), 85764, Neuherberg, Germany. [3]Institute for Diabetes & Obesity, Helmholtz Center Munich, 85748, Garching, Germany. Correspondence and requests for materials should be addressed to S.U. (email: siegfried.ussar@helmholtz-muenchen.de)

In contrast, several studies investigated the role of elevating calcium – extracellularly, or via liberation of intracellular calcium stores – on adipogenesis and white adipocyte function, with somewhat contradicting results. Work on human[26] and murine[27] white preadipocytes showed that elevation of intracellular calcium levels in early differentiation inhibits the induction of PPARγ and triglyceride accumulation. These effects are most likely mediated through calcium-dependent activation of calcineurin[27] and calcium/calmodulin-dependent kinase kinases[28], inhibiting early adipogenic transcription factors. A similar inhibition of white adipocyte differentiation was observed upon elevation of extracellular calcium concentrations, however, without affecting intracellular calcium levels[29]. In contrast, elevation of intracellular calcium concentrations later during adipogenesis promotes lipogenesis and adipocyte marker expression[26]. These effects of extra- and intracellular calcium on adipogenesis seem to be specific to "classical" white adipocytes, as treatment of bone marrow stromal cells (BMSCs) with high extracellular and intracellular calcium accelerates proliferation and differentiation into adipocytes[30]. This differential impact of calcium on the differentiation of BMSCs and white preadipocytes suggests that alterations in the local calcium concentration may have specific impact on individual preadipocyte populations. Given similarities in the transcriptional network mediating white and brown adipogenesis, varying extracellular calcium concentrations may also affect brown adipocyte differentiation and function.

Therefore, we investigated the impact of elevated extracellular calcium throughout different stages of brown adipocyte differentiation. In line with data from white adipocytes, we observed suppressed differentiation of brown adipocytes that have been continuously exposed to high extracellular calcium. Calcium free medium, on the other hand, enhanced brown adipocyte differentiation. In both cases, normalization of extracellular calcium concentrations after the initial induction phase allowed adipocytes to resume differentiation and to accumulate lipids. These effects are independent of increased intracellular calcium levels and calcineurin activity, but at least partially depend on hyperactivation of ERK and regulation of C/EBPβ activity.

Results

Extracellular calcium modulates differentiation of brown adipocytes. To study the impact of extracellular calcium on brown adipocyte differentiation, immortalized murine brown preadipocytes were differentiated for eight days in regular cell culture medium containing 1.8 mM calcium, medium supplemented with 10 mM calcium, or 10 mM magnesium, or medium without calcium (referred to as low calcium due to ~0.3 mM calcium supplemented to all media by the use of 10% FBS). Magnesium was used to control for osmotic and charge effects. Samples were collected every other day during the eight-day time course of differentiation. Treatment of cells with 10 mM calcium throughout differentiation (day 0–8) diminished lipid accumulation as measured by Oil Red O staining (Fig. 1A). In contrast, restricting calcium exposure to days 2–8, following the initial induction phase (days 0–2), only slightly reduced lipid accumulation, with significant differences detected only at day 8 of differentiation. Limiting exposure to high calcium to the initial two days of adipocyte differentiation prevented lipid accumulation during the first four days. Following normalization of extracellular calcium concentrations at day two, brown adipocytes were able to accumulate lipids, albeit the amount remained significantly reduced compared to control cells (Fig. 1A). Exposure to 10 mM magnesium, or the use of calcium free medium did not impair lipid accumulation in brown adipocytes (Figs 1A, S1A). Importantly, none of the treatments impaired cell viability (Figure S1B).

Gene expression analysis of PPARγ (Fig. 1B) and C/EBPα (Figure S1C) confirmed the suppressive effect of extracellular calcium on brown adipocyte differentiation. High extracellular calcium throughout differentiation suppressed PPARγ and C/EBPα mRNA levels, whereas exposure from days 2–8 did not significantly alter expression of these differentiation markers. Exposure to high calcium (10 mM) during the induction phase suppressed PPARγ and C/EBPα expression until day four but normalizing calcium levels restored expression at later time points (Fig. 1B, S1C). Interestingly, differentiation in calcium free medium for either eight days or from days 2–8 significantly increased expression of PPARγ, whereas exposure to high magnesium had no effect compared to cells differentiated in control medium. The decrease in PPARy mRNA expression and its rescue upon calcium normalization were confirmed at the protein level (Fig. 1C, S1D).

Extracellular calcium is known to regulate osteogenic versus adipogenic lineage commitment in BMSCs[31] and brown adipocytes share common progenitor cells with skeletal muscle. Thus, we investigated the expression of osteogenic markers Collagen I (ColI) and Runt-related transcription factor 2 (Runx2), as well as the myogenic markers α-smooth muscle actin (ACTA2) and myogenic factor 3 (Myf-3, MyoD) in cells differentiated under control conditions, or continuously exposed to either high calcium or high magnesium. Neither osteogenic nor myogenic markers were significantly increased in calcium treated compared to control or magnesium treated cells at any time point during differentiation (Fig. 1D).

Extracellular calcium regulates C/EBPβ and ERK activity independently of intracellular calcium. The induction of PPARγ expression during early adipogenesis requires promoter binding of C/EBPβ and δ[32]. Alterations of C/EBPβ and δ expression and/or activation have been shown to inhibit adipocyte differentiation in multiple studies[33–35]. Thus, we studied the kinetics of C/EBPβ and δ expression during the first 48 hours of differentiation (Fig. 2A). C/EBPβ and δ expression peaked two hours following the induction of differentiation. However, we did not observe any differences between the treatment groups, except C/EBPδ expression trending to higher levels at later time points in cells treated with high extracellular calcium (Fig. 2A). In contrast, the liver-enriched activator protein (LAP) isoform of C/EBPβ, was hyperphosphorylated throughout the first 24 hours, while the other transcriptionally active C/EBPβ isoform (LAP*) was comparable to controls (Fig. 2B, S2A). Phosphorylation of the inhibitory liver-enriched inhibitor protein (LIP) C/EBPβ isoform was not significantly changed upon calcium treatment. The LAP/LIP ratio is important to regulate adipogenic gene expression[34], suggesting that the inability to induce PPARy expression upon exposure to high extracellular calcium is most likely due to a shifted pLAP/pLIP ratio.

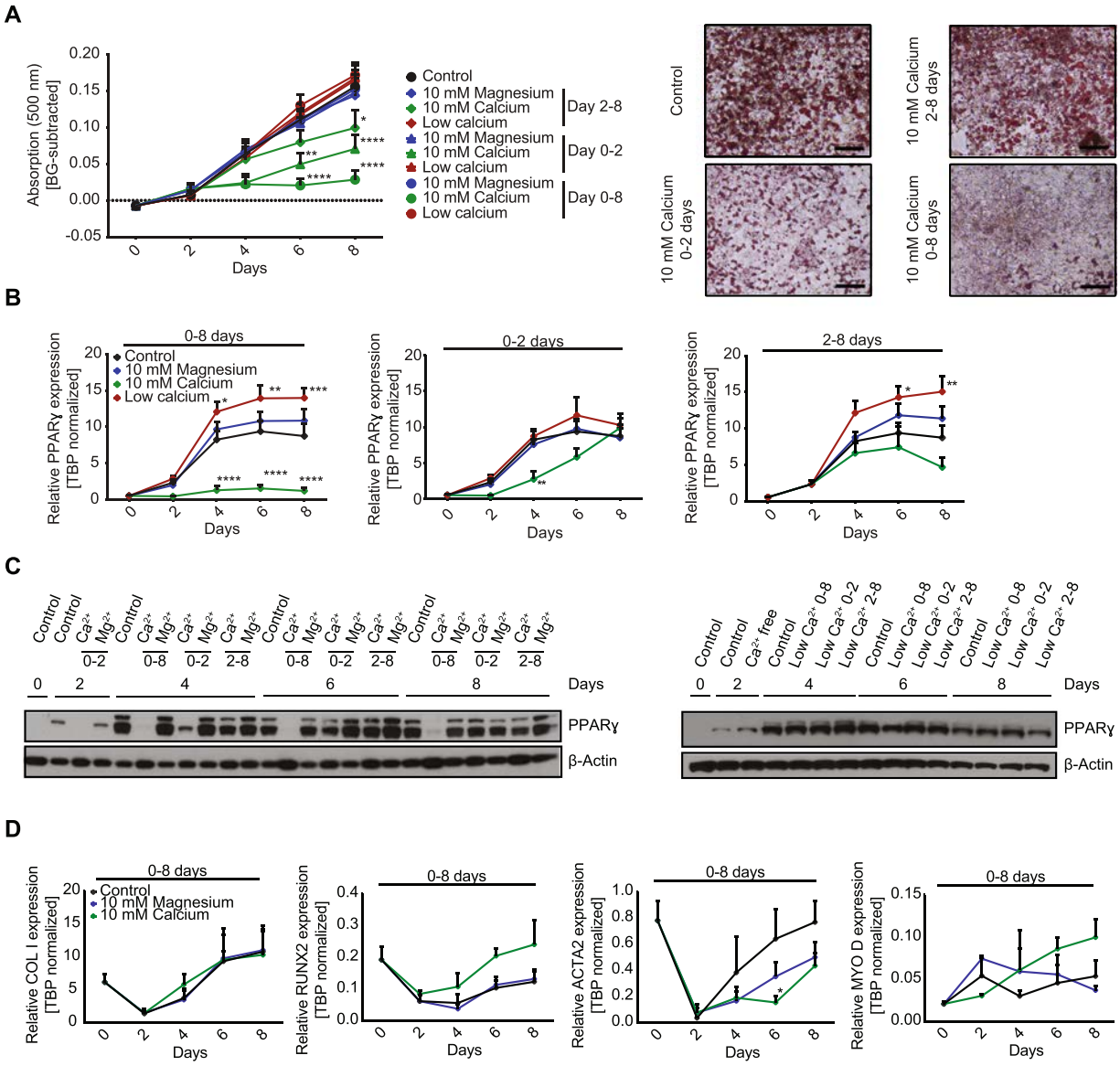

Figure 1. Extracellular calcium modulates differentiation of brown adipocytes. (**A**) Time course of lipid content of *in vitro* differentiated brown adipocytes. Cells were treated with 1.8 mM (control), 10 mM magnesium, 10 mM calcium or calcium free medium for either 8 days (day 0–8), only during induction (day 0–2), or after induction (day 2–8). Shown are background subtracted lipid contents, measured by Oil Red O (500 nm) (n = 6) and representative images of stained cells at day 8 after control or 10 mM calcium treatment. (size bar = 20 µm). (**B**) PPARγ expression normalized on TBP during an eight-day time course under the conditions as above (n = 5). (**C**) Western Blot for PPARγ and β-Actin during the eight- day time course of differentiation with normal 1.8 mM calcium (control), 10 mM calcium (Ca^{2+}), 10 mM magnesium (Mg^{2+}) and calcium free medium during indicated time points. (**D**) Gene expression of osteogenic markers ColI and Runx2 as well as muscle markers ACTA2 and MyoD normalized on TBP during the eight- day time course of differentiation under indicated conditions (n = 3). For (**A**,**B** and **D**) data are shown as mean ± SEM. Two-way ANOVA with Dunnett's posthoc test (**A**,**B**) and Tukey's posthoc test (**D**); *$p < 0.05$, **$p < 0.01$, ***$p < 0.001$, ****$p < 0.0001$. Full Western Blot images are provided in the Supplemental Information.

Phosphorylation of C/EBPβ is primarily mediated through ERK. We observed hyperactivation of ERK upon high extracellular calcium treatment from 6–48 hours, with strongest effects after six hours (Fig. 2B, S2B) and throughout the eight-day time course of differentiation (Fig. 2C, S2C). Interestingly, reducing extracellular calcium decreased ERK phosphorylation throughout the eight-day time course of differentiation, indicating that lower levels of ERK phosphorylation associate with elevated adipocyte differentiation in this experimental setup. In contrast, phosphorylation of Akt, was not significantly altered upon high calcium exposure (Fig. 2B). Regulation of ERK signaling through extracellular calcium via the calcium sensing receptor (CaSR) is very unlikely as its expression is not detectable in our cells, regardless of treatment (Figure S2D). Thus, we hypothesized that raising extracellular calcium could activate the calcium/calmodulin-dependent serine/threonine protein

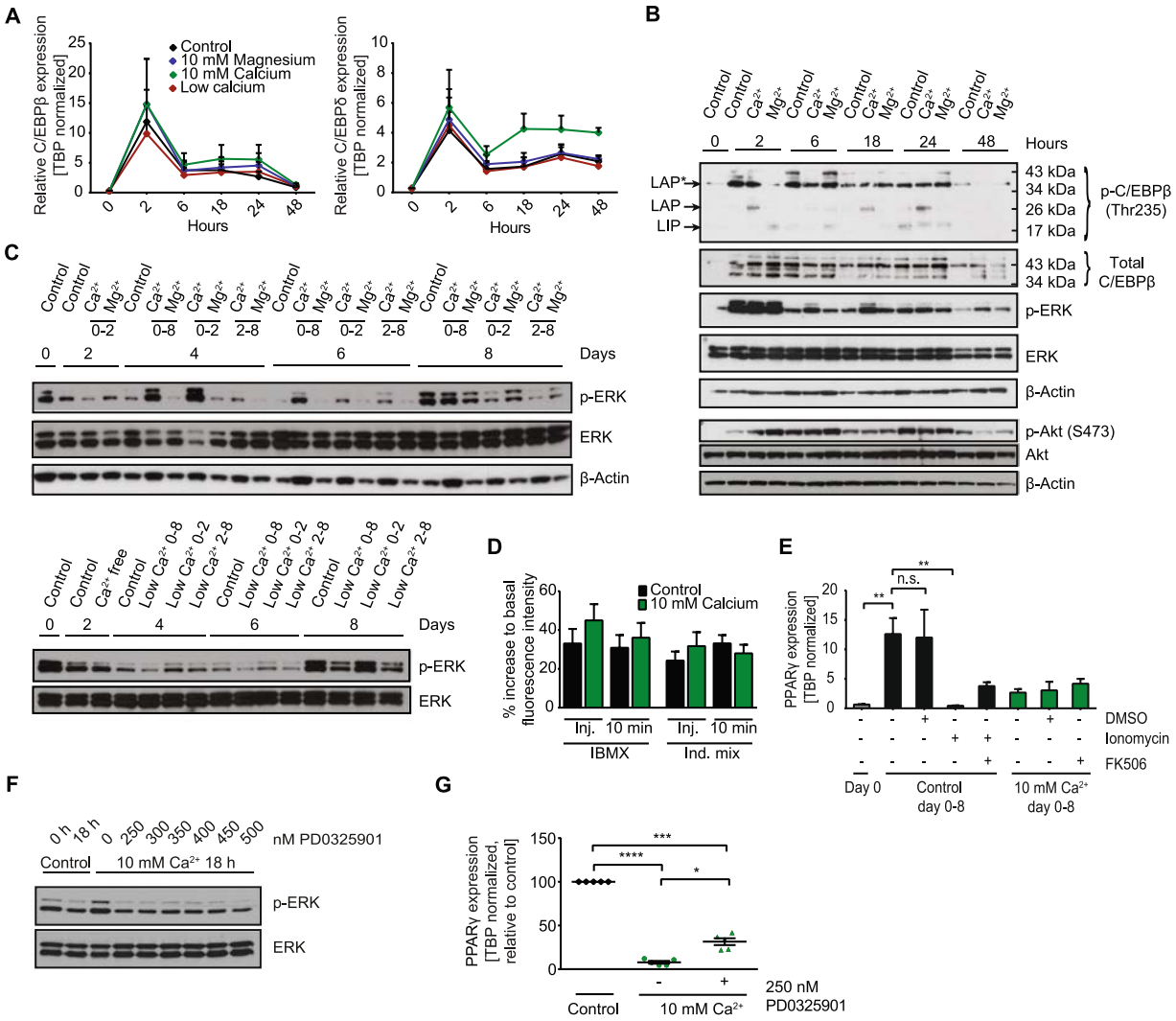

Figure 2. Extracellular calcium regulates MAPKs and C/EBPβ activity independently of intracellular calcium. (**A**) C/EBPδ and C/EBPβ expression normalized to TBP during the first 48 hours of differentiation in 1.8 mM calcium (control), 10 mM magnesium, 10 mM calcium and calcium free medium (n = 6). (**B**) Western Blot for phospho- (Thr235)/total C/EBPβ as well as phospho-/total ERK and phospho- (Ser473)/total AKT during the first 48 hours of differentiation under 1.8 mM calcium (control), 10 mM magnesium (Mg^{2+}) and 10 mM calcium (Ca^{2+}) conditions with β-Actin as loading control. (**C**) Western Blot for phospho- and total ERK and β-Actin as loading control of the 8 day time course under control (1.8 mM calcium), 10 mM calcium and 10 mM magnesium conditions as well as control and calcium free conditions for the indicated duration. (**D**) Relative increase of intracellular calcium in brown preadipocytes maintained in 1.8 mM calcium (control) or 10 mM calcium directly upon and 10 min after injection of IBMX or induction mix shown as percent increase of fluorescence to basal level. Cells were loaded with the calcium binding fluorophore Fluo-4 (4 μM) and fluorescence was recorded at Ex/Em = 485/520 in orbital averaging (n = 3 with 3–4 replicates each). (**E**) PPARγ expression normalized on TBP in preadipocytes (day 0) and differentiated cells at day 8 treated day 0–8 with 1.8 mM calcium (Control day 0–8) or 10 mM calcium (10 mM Ca^{2+} day 0–8) supplemented with DMSO, ionomycin (2 μM) and/or the calcineurin inhibitor FK506 (1 μM) (n = 3). (**F**) Western Blot for phospho-/total ERK in preadipocytes (0 h) and induced preadipocytes (18 h) with different concentrations of the MEK inhibitor PD0325901. (**G**) PPARγ expression as percent of control in differentiated adipocytes treated with 1.8 mM calcium (control) or 10 mM calcium +/− the MEK inhibitor PD0325901 (250 nM) for 0–8 days (n = 5). For (**A**,**D**,**E** and **G**) data are shown as mean ± SEM, *p < 0.05, **p < 0.01, ***p < 0.001, ****p < 0.0001; (**A**) Ordinary two-way ANOVA with Dunnett's posthoc test, (**D**,**G**) Repeated measures one-way ANOVA with Tukey's posthoc test and Kruskal-Wallis one-way ANOVA with Dunn's multiple comparison test (**E**). Full Western Blot images are provided in the Supplemental Information.

phosphatase calcineurin, which in turn regulates ERK and C/EBPβ phosphorylation and thereby adipocyte differentiation[27,36,37]. Cytoplasmic calcium concentrations increased upon the addition of 3-isobutyl-1-methylxanthine (IBMX) or the complete induction mix (Fig. 2D). However, we did not observe differences in cytoplasmic calcium concentrations between control and high extracellular calcium levels nor did the pharmacological inhibition of

calcineurin using FK506 rescue adipogenesis (Fig. 2D and 2E). Experiments using calcium free buffer showed that increases in cytosolic calcium result from intracellular calcium store mobilization, being independent of extracellular calcium concentrations (Figure S2E). These data suggest that hyperphosphorylation of ERK and the inhibition of adipogenesis are independent of calcium influx from the extracellular space in our experimental setup.

Based on these results, we investigated if titrating ERK phosphorylation to the levels observed in cells cultured in control medium could rescue brown adipocyte differentiation. We found that 250 nM of the MEK inhibitor PD0325901 reduced ERK phosphorylation to that of cells induced with control medium for 18 hours (Fig. 2F). However, reducing ERK phosphorylation in that way did only partially rescue adipogenesis as indicated by PPARy expression (Fig. 2G).

Extracellular calcium modulates brown adipocyte identity. As shown for white adipocytes, brown adipocyte differentiation is inhibited by prolonged elevation of extracellular calcium concentrations. Thus, similarly to general markers of adipogenesis, induction of uncoupling protein 1 (UCP1), PR domain containing 16 (PRDM 16) and PPARγ coactivator 1-alpha (PGC1-α) was inhibited during differentiation upon continued exposure to high extracellular calcium, but this recovered upon removal after day 2 (Fig. 3A, S3A). Reducing calcium in the medium or adding magnesium during differentiation showed trends to elevated expression of UCP1, PRDM16 and PGC1-α, in line with PPARγ expression (Fig. 3A, S3A). Conversely, elevation of extracellular calcium following adipogenic induction did not impair lipid accumulation or adipogenic marker expression, but completely inhibited gene expression of UCP1 and other brown adipocyte marker genes such as PGC1-α and PRDM16 (Fig. 3B). Importantly, the increased UCP1 mRNA levels under low calcium conditions and decreased expression under high calcium were even more pronounced on protein level, whereas full recovery of UCP1 after normalization of calcium levels was not observed at the protein level (Fig. 3C, S3C). Among many other functions, PRDM16 and PGC1-α regulate mitochondrial biogenesis. To this end, we analyzed mitochondrial abundance and function in brown adipocytes exposed to high extracellular calcium from days 2–8 and to controls. Mitochondrial transcription factor A (TFAM) was slightly increased, suggesting some increase in mitochondrial content during differentiation, but without any differences between the treatment groups (Figure S3B). Western Blots for subunits of all five complexes of the mitochondrial respiratory chain (complex I–V) revealed a slight reduction in the expression of some subunits of high calcium treated groups compared to controls at day 8 of differentiation (Fig. 3D, S3D). However, we could not observe significant differences in mitochondrial respiration as assessed by plate-based respirometry using a Seahorse extracellular flux analyzer (Fig. 3E and S3E). ATP synthesis, proton leak and maximal respiration, also upon additional substrate supply by pyruvate addition, were not altered in calcium exposed cells (Fig. 3E and S3E). However, cells differentiated in medium containing high extracellular calcium from days 2–8 exhibited lower extracellular acidification rates, albeit equal supernatant lactate concentrations among groups (Fig. 3E). FABP3 expression correlates with increased long-chain fatty acid uptake and β-oxidation in BAT of UCP1 knockout mice[38–41]. In our cell model, FABP3 expression was strongly induced during differentiation in cells exposed to high extracellular calcium from days 2–8 and when cells were continuously exposed to calcium (Fig. 3F and S3F). Similar to cells continuously exposed to calcium, we also observed a trend to increased MyoD at expression at day 8 in cells treated form 2–8 with 10 mM calcium (Figure 1D,S3G).

Discussion

Calcium plays an important role in multiple cellular processes. Here we show that modulation of extracellular calcium concentration and duration of exposure regulates brown adipocyte differentiation and key components of the brown adipocyte cell lineage. In line with previous data on white adipocytes[29, 34], we confirm that continuous exposure to high extracellular calcium inhibits lipid accumulation and the induction of PPARγ and C/EBPα, both being drivers of adipogenic fate. However, exposure to high calcium during the induction phase does not alter lineage commitment in favor towards osteoblasts or myocytes. Conversely, high extracellular calcium reversibly pauses adipogenesis right after lineage commitment, as removal of the calcium block after initiation restores lipid accumulation and adipogenic marker expression. Pausing adipocyte differentiation appears to be mediated through inhibition of C/EBPβ and δ activity, which are key transcription factors initiating adipocyte differentiation through the induction of PPARγ and C/EBPα[42]. We show that elevated extracellular calcium alters the ratio of phosphorylation of the activating C/EBPβ isoforms LAP and LAP* and the inhibitory LIP. C/EBPβ activity is primarily activated by ERK in response to insulin[35, 43, 44]. However, prolonged ERK signaling can also inhibit adipocyte differentiation[45]. Thus, the continuous hyperactivation of ERK, observed in response to elevated extracellular calcium, may explain both the inhibition and the restoration of adipocyte differentiation. Indeed, pharmacologically reducing ERK activity to control cell levels partially restored brown adipocyte differentiation, albeit the differentiation capacity was much lower than in control cells. The diminished ability of this approach to restore adipocyte differentiation could be in part explained by the fact that pharmacological MEK inhibition reduces overall phospho-ERK levels and does not account for spatial and temporal differences in phospho-ERK within different signaling complexes. At this stage, we cannot exclude that other signaling pathways also contribute to the regulation of adipogenesis by extracellular calcium. However, in addition to the inhibitory role of elevated extracellular calcium, we find that reducing calcium in the medium (i) enhances adipocyte differentiation and (ii) reduces ERK phosphorylation during the time course of differentiation.

The upstream signals mediating increased ERK phosphorylation remain to be determined. In the context of calcium, it is feasible to speculate that the calcium sensitive phosphatase calcineurin, which is known to modulate ERK activity[27, 36], mediates these effects. However, we do not detect a rise in intracellular calcium concentrations in response to elevated extracellular calcium that would be necessary to activate calcineurin. Moreover, inhibition of calcineurin does not restore brown adipocyte differentiation. These findings are in line with previous data from Jensen and colleagues showing that high extracellular calcium inhibits adipogenesis in 3T3-L1 cells without

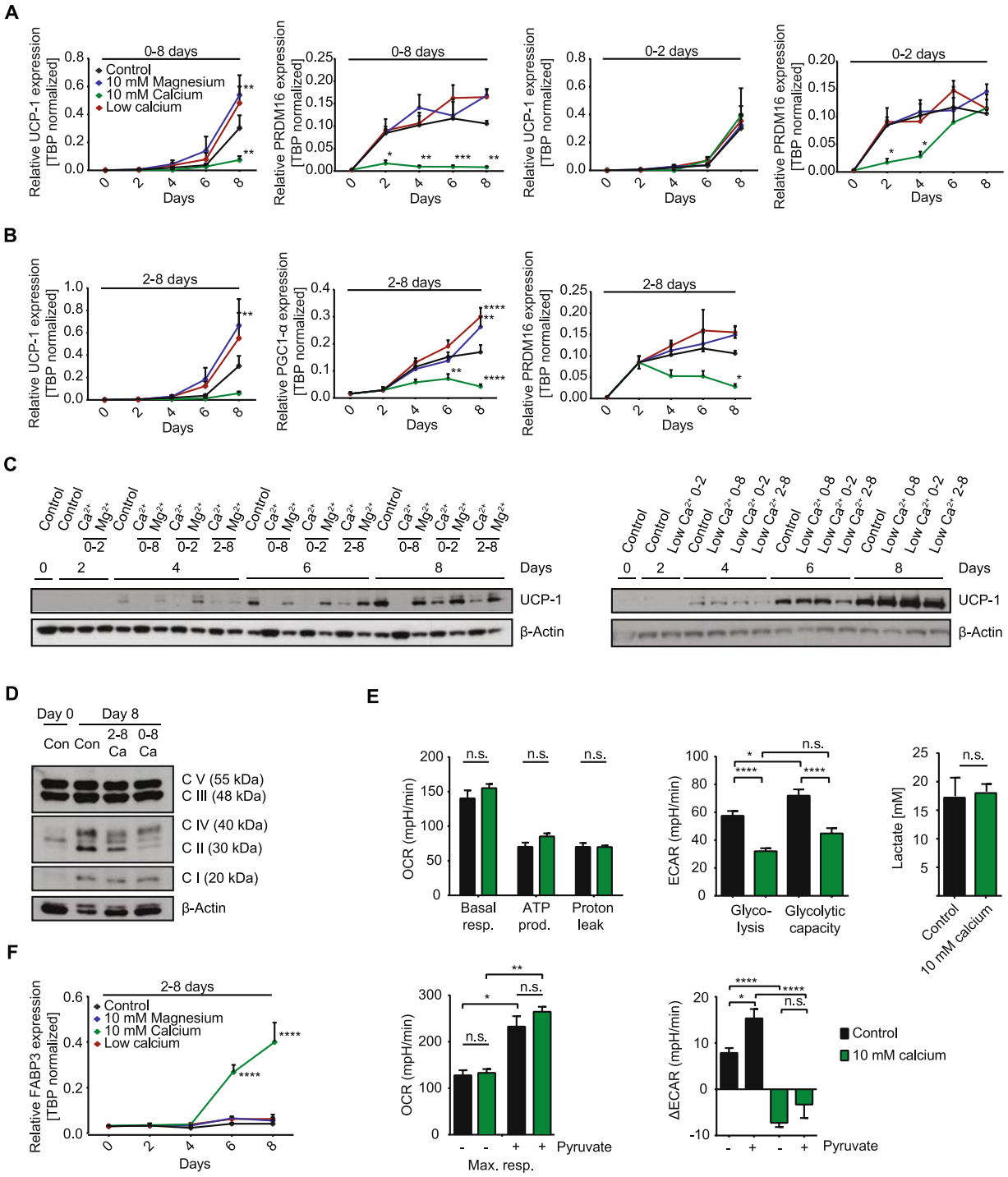

Figure 3. Extracellular calcium modulates brown adipocyte identity and thermogenic markers. (**A**) UCP1 and PRDM16 expression normalized to TBP of *in vitro* differentiated preadipocytes in an eight- day time course under normal 1.8 mM calcium (control), 10 mM calcium,10 mM magnesium and calcium free conditions for days 0–8 and days 0–2 (UCP1, PRDM16 n = 5). (**B**) UCP1, PGC1-α and PRDM16 expression normalized on TBP in these different treatment groups during days 2–8 (UCP1, PRDM16 n = 7, PGC1-α n = 4). (**C**) Western Blot for UCP1 and β-Actin during the eight - day time course of differentiation with normal 1.8 mM calcium (control), 10 mM calcium (Ca^{2+}), 10 mM magnesium (Mg^{2+}) or calcium free medium during indicated time points. (**D**) OxPhos Western Blot of preadipocytes (Con day 0) and differentiated adipocytes in 1.8 mM calcium (Con) or 10 mM calcium for days 2–8 or days 0–8 with β-Actin as loading control. (**E**) Oxygen consumption rate (OCR) and extracellular acidification rate (ECAR) in differentiated adipocytes at day 8 measured by the Seahorse extracellular flux analyzer. Cells were treated with 1.8 mM calcium (control) or 10 mM calcium for 2–8 days during differentiation. OCR was partitioned into basal respiration, ATP production, proton leak and maximal respiration, also in the presence of pyruvate (5 mM), while ECAR reported glycolytic rate, glycolytic capacity and the difference of glycolytic capacity (ΔECAR) before and after 5 mM pyruvate addition

(together with FCCP) (n = 3 for pyruvate n = 2, 3–5 technical replicates each). Lactate concentration of the cell supernatant of 8 day differentiated adipocytes treated with 1.8 mM calcium (control) and 10 mM calcium (2–8 days) (n = 3). (**F**) FABP3 expression normalized to TBP during the time course of differentiation with 1.8 mM calcium (control), 10 mM calcium or 10 mM magnesium for 2–8 days (n = 3). Data are shown as mean ± SEM, *p < 0.05, **p < 0.01, ***p < 0.001, ****p < 0.0001; Ordinary (**A**,**B**) and repeated measures (**F**) two-way ANOVA with Dunnett's posthoc test. Two-tailed wilcoxon matched-pairs signed rank test (**E**:lactate). (**E**:OCR) Kruskal-Wallis one-way ANOVA with Dunn's multiple comparison test. (**E**:ECAR) Ordinary one-way ANOVA with Tukey's posthoc test. Full Western Blot images are provided in the Supplemental Information.

increasing intracellular levels[29], suggesting that extracellular calcium acts outside the cell to modulate the activity of transmembrane proteins. The G-protein coupled calcium sensing receptor (CaSR) for example was shown to be expressed in adipocytes and to activate intracellular signaling cascades especially ERK upon calcium binding[46]. However, we did not detect expression of CaSR in neither isolated brown adipocytes nor in our cell model. Further, we did not observe an increase in intracellular calcium associated with CaSR activation. Thus, while an involvement of this receptor seems to be very unlikely, it is presumable that calcium promotes receptor binding to ligands, such as integrins or cadherins, which in turn would alter intracellular signaling. Overall our data suggest a very general role of extracellular calcium during the early phase of adipocyte differentiation, which appears to be conserved between white and brown adipocytes. In future studies, it may also be addressed why bone marrow derived adipocytes seem to respond differently.

Nevertheless, we find that extracellular calcium has a very specific effect on brown adipocytes at later differentiation stages. Exposure to high extracellular calcium after the induction phase inhibits the expression of brown adipocyte specific genes such as UCP1, PRDM16 and PGC1-α with little to no impact on the expression of general adipogenic markers and lipid accumulation. As we did not observe differences in mitochondrial respiration between the treatment groups, UCP1 activity is either too low or requires activation as suggested previously[47] in our cellular model. Alternatively, FABP3 was shown to accelerate β-oxidation and free fatty acid uptake independent of UCP1 and to mediate uncoupled respiration[38,41]. Thus, it is tempting to speculate that the observed increase in expression of FABP3 in cells treated for eight days or from days 2–8 with 10 mM calcium, could provide an alternative explanation for the lack of differences in mitochondrial respiration, albeit changes in UCP1 expression. The induction of FABP3, which is predominantly expressed in cardiomyocytes and myocytes[39], could also suggest a role of calcium in determining lineage commitment between muscle and brown adipocytes. However, we did not observe substantial expression of muscle specific genes, albeit prolonged exposure could be required to fully dissect this phenomenon.

In conclusion, we provide evidence that manipulation of extracellular calcium as an important constituent of the microenvironment can have profound effects on the kinetics and nature of *de novo* adipogenesis. To date, different biotechnological platforms aim to establish protocols to culture and expand patient-derived human brown adipose tissue *ex vivo* for allograft transplantation. To this end, our data show that omitting calcium in the cell culture medium may substantially improve brown adipocyte differentiation and expression of the thermogenic program. Conversely, our study did not address whether alterations in local calcium concentrations modulate the function of brown adipose tissue *in vivo*, especially in humans. However, it is tempting to speculate that altered local calcium concentrations could contribute to the lower brown fat mass and activity of obese human subjects[22].

Methods

Cell isolation and culture. Murine brown preadipocytes were isolated according to[48] from adult eight week old C57Bl/6 mice. In detail, murine brown adipose tissue (BAT) was dissected from the mouse interscapular region, cut into ~1mm pieces and digested for 30–45 minutes at 37 °C in DMEM containing 1 mg/ml collagenase type IV (Gibco) and 10 mg/ml BSA (Albumin fraction V, Roth). Digestion was stopped by washing the cells with PBS (Gibco) containing 10 mg/ml BSA. Mature adipocytes were removed and preadipocytes cultured in Dulbecco's Modified Eagle Medium (DMEM + GlutaMAX + high glucose, Gibco). Cells were immortalized using an ecotropic SV40 large T retrovirus. Animal experiments were conducted in accordance with the German animal welfare law. The sacrifice of the mouse was performed with permission and in accordance with all relevant guidelines and regulations from the Sachgebiet 54-Tierschutz of the district government of Upper Bavaria (Bavaria, Germany).

For all cell culture experiments normal growth medium containing penicillin (100 Units/ml) and streptomycin (100 µg/ml) (Pen Strep, Gibco) as well as 10% fetal bovine serum (FBS, Gibco) were used, supplemented with calcium chloride (high calcium) or magnesium chloride (high magnesium) to reach a final concentration of 10 mM respectively. Low calcium experiments were conducted using DMEM, high glucose, no glutamine, no calcium (Gibco 21068) supplemented with 1 mM sodium pyruvate (Gibco), 1x GlutaMAX™-1 (Gibco) [equimolar with 2 mM L-alanyl-L-glutamine], Pen Strep and 10% FBS (containing 3.5 mM calcium). Immortalized brown preadipocytes were grown up to 100% confluency (day 0) and differentiation was induced with 0.5 mM 3-Isobuthyl-1-methylxanthin (IBMX, Sigma), 125 µM Indomethacin (Santa Cruz), 5 µM Dexamethasone (Sigma), 100 nM Insulin (Sigma) and 1 nM Triiodothyronine (T3, Calbiochem) in the appropriate medium. Medium (supplemented with insulin and T3) was changed every other day until day 8.

For inhibitor experiments the compounds were kept as 1 mM (FK506, Ionommycin) and 10 mM (PD325901) stock solutions in DMSO at −20 °C and supplemented to the medium in the appropriate dilution: 2 µM Ionomycin calcium salt (Fisher Scientific), 1 µM calcineurin inhibitor FK506 (*Tacrolismus* - Abcam), 250 nM MEK inhibitor PD0325901 (Sigma).

Oil Red O stain. Differentiated cells were fixed in 10% formalin (Roth), washed in water and dehydrated in 60% isopropanol. Then, filtered 60% (v/v) Oil Red O working solution in water (stock: 0.35% (w/v) Oil Red O (Alfa Aesar) in 100% isopropanol (Sigma)) was added, incubated for 10 minutes at room temperature, washed with water and dried. The stain was solved with 100% isopropanol and the absorption at 500 nm was measured with a PHERAstar FS detection system (BMG Biotech) referring the relative lipid content of the cells.

qPCR. RNA extraction (RNeasy Mini Kit, Qiagen) and cDNA synthesis (0.5–1 µg total RNA, High Capacity cDNA Reverse Transcription Kit, Applied Biosystems) were conducted according to the manufacturers' instructions. qPCR was performed in a C1000 Touch Thermal Cycler (Bio Rad), using 300 nM forward and reverse primers and iTaq Universal SYBR Green supermix (BioRad). Target gene expression was normalized on the expression of the housekeeping gene TATA box binding protein (TBP)[49]. The primer sequences are shown in Supplemental Table 1. Calculations for relative expression (RE) of genes of interest (GOI) were performed as follows: $2^{CT(TBP)-CT(GOI)}$.

Western Blot. Cells were lysed in 25 mM Tris pH 7.4, 150 mM NaCl, 1% NP-40, 1 mM EDTA, 5% glycerol, 0.1% SDS containing protease inhibitor and phosphatase inhibitors (Sigma). 15–20 µg of protein (15–30 µg for UCP1 detection) were loaded on 4–12% precast SDS gels (Invitrogen) or on 10% acrylamide-SDS-gels and blotted on 0.45 µm PVDF membranes, which were blocked in 5% BSA in TBS with 0.1% Tween 20 (TBS-T) one hour at room temperature (2 hours for UCP1). Membranes were incubated with primary antibodies (list in Supplemental Table 2) over night at 4 °C, washed in TBS-T and incubated with the appropriate HRP coupled secondary antibodies one hour at room temperature. Membranes were developed with chemiluminescent HRP substrate (Immobilon Western, Millipore) using films (Hyperfilm ECL, GE Life Sciences; CL-XPosure Film, Thermo Scientific). Quantification of Western Blots was performed using ImageJ software.

Calcium measurement with Fluo-4. Cells were grown to 100% confluency (day 0) in 96 well glass-bottom plates (Eppendorf) to measure fluorescence with a PHERAstar FS (BMG Biotech) using bottom optic of the optic module FI 485 520 (Ex/Em), adjusting gain to 915 with 20 flashes per well in an orbital averaging mode circling in 3 mm diameter. All further steps were performed at 37 °C with pre-warmed dilutions in the control buffer, 1x SBS (5 mM KCl, 140 mM NaCl, 8 mM glucose, 10 mM HEPES, 0.8 mM $MgCl_2$, 1.8 mM $CaCl_2$, pH 7,4). For high magnesium (10 mM), high calcium (10 mM) and calcium free (0 mM) experiments specific 1x SBS buffers containing the appropriate magnesium and calcium concentrations were prepared. Cells were washed in SBS buffer containing 1 mM probenecid (Santa Cruz) and incubated with 4 µM Fluo-4 AM (Cat. #F14201, Thermo Scientific), 0.02% Pluronic® F-127 (Biotium) and 1 mM probenecid (Santa Cruz) for one hour at 37°C and washed again. After 30 min, basal fluorescence was detected in intervals of several seconds. IBMX or whole induction mix diluted in calcium free 1x SBS (final concentrations under *Cell isolation and culture*) were injected with a speed of 190 µl/s. After orbital mixing (100 rpm) the fluorescence emission at 520 nm was detected. Values are shown as fold increase in fluorescence intensity (%) upon injection.

Cellular oxygen consumption and extracellular acidification rates. Cells were seeded in Seahorse 96-well plates and differentiated for eight days with 1.8 mM calcium (control), high magnesium (10 mM), high calcium (10 mM) or calcium free conditions for 2–8 days. The oxygen consumption rate (OCR) and the extracellular acidification rate (ECAR) were measured with a XF96 Extracellular Flux analyzer (Seahorse Bioscience, Agilent technologies). Cells were equilibrated at 37 °C in XF Assay Medium Modified DMEM (Seahorse Bioscience) supplemented with 25 mM glucose one hour prior measurement. All compounds were diluted as ten-fold concentrations in assay medium and loaded in the equilibrated cartridge ports as follows: A) 20 µg/ml oligomycin (Merck), B) 10 µM FCCP (R&D systems) +/− 50 mM sodium pyruvate (Gibco), C) 25 µM rotenone and antimycin A (Sigma), D) 1 M 2-deoxy-D-glucose (Alfa Aesar). Each cycle comprised two minutes each of mixing, waiting and measuring. Non-mitochondrial respiration (OCR) and non-glycolytic acidification (ECAR) were subtracted from other values to determine mitochondrial oxygen uptake. For the analysis, the mean values of either the last two cycles prior injection (basal respiration, acidification/glycolysis) or the first two after injection (sum of ATP production and proton leak or maximal respiration (OCR) and maximal acidification/glycolytic capacity (ECAR)) were averaged and calculated.

Lactate Assay. Cells were differentiated in 1.8 mM calcium (control) or for day 2–8 in high calcium (10 mM) medium. The cell supernatant at day 8 was diluted and lactate was measured with the Lactate Colorimetric/Fluorometric Assay Kit (Biovision).

Statistical analysis. Data are presented as means ± SEM. All statistical analyses were performed with GraphPad Prism. Samples were tested for normal distribution with either D'Agostino-Pearson omnibus normality test, Shapiro-Wilk normality test or Kolmogorov-Smirnov test with Dallal-Wikinson Lillie for P value. Parametric or nonparametric tests were performed accordingly as indicated in the figure legends. Two-tailed Student's t test, one-way and two-way ANOVA for multiple comparisons were used with α-level at 0.05 to determine P values.

Data availability. The datasets generated during and/or analyzed during the current study are available from the corresponding author on reasonable request.

References

1. Cannon, B. & Nedergaard, J. Brown adipose tissue: function and physiological significance. *Physiological reviews* **84**, 277–359, doi:10.1152/physrev.00015.2003 (2004).
2. Cinti, S. Adipose tissues and obesity. Italian journal of anatomy and embryology = Archivio italiano di anatomia ed embriologia **104**, 37–51 (1999).
3. Scherer, P. E. Adipose tissue: from lipid storage compartment to endocrine organ. *Diabetes* **55**, 1537–1545, doi:10.2337/db06-0263 (2006).
4. Fedorenko, A., Lishko, P. V. & Kirichok, Y. Mechanism of fatty-acid-dependent UCP1 uncoupling in brown fat mitochondria. *Cell* **151**, 400–413, doi:10.1016/j.cell.2012.09.010 (2012).
5. Argyropoulos, G. & Harper, M. E. Uncoupling proteins and thermoregulation. *J Appl Physiol (1985)* **92**, 2187–2198, doi:10.1152/japplphysiol.00994.2001 (2002).
6. Nedergaard, J., Bengtsson, T. & Cannon, B. Unexpected evidence for active brown adipose tissue in adult humans. *Am J Physiol Endocrinol Metab* **293**, E444–452, doi:10.1152/ajpendo.00691.2006 (2007).
7. Skala, J., Barnard, T. & Lindberg, O. Changes in interscapular brown adipose tissue of the rat during perinatal and early postnatal development and after cold acclimation. II. Mitochondrial changes. *Comparative biochemistry and physiology* **33**, 509–528 (1970).
8. Seale, P. *et al*. PRDM16 controls a brown fat/skeletal muscle switch. *Nature* **454**, 961–967, doi:10.1038/nature07182 (2008).
9. Schulz, T. J. *et al*. Identification of inducible brown adipocyte progenitors residing in skeletal muscle and white fat. *Proceedings of the National Academy of Sciences of the United States of America* **108**, 143–148, doi:10.1073/pnas.1010929108 (2011).
10. Walden, T. B., Petrovic, N. & Nedergaard, J. PPARalpha does not suppress muscle-associated gene expression in brown adipocytes but does influence expression of factors that fingerprint the brown adipocyte. *Biochem Biophys Res Commun* **397**, 146–151, doi:10.1016/j.bbrc.2010.05.053 (2010).
11. Sanchez-Gurmaches, J. & Guertin, D. A. Adipocytes arise from multiple lineages that are heterogeneously and dynamically distributed. *Nature communications* **5**, 4099, doi:10.1038/ncomms5099 (2014).
12. Vosselman, M. J. *et al*. Systemic beta-adrenergic stimulation of thermogenesis is not accompanied by brown adipose tissue activity in humans. *Diabetes* **61**, 3106–3113, doi:10.2337/db12-0288 (2012).
13. Ma, S. *et al*. Activation of the cold-sensing TRPM8 channel triggers UCP1-dependent thermogenesis and prevents obesity. *Journal of molecular cell biology* **4**, 88–96, doi:10.1093/jmcb/mjs001 (2012).
14. Bahler, L., Molenaars, R. J., Verberne, H. J. & Holleman, F. Role of the autonomic nervous system in activation of human brown adipose tissue: A review of the literature. *Diabetes & metabolism* **41**, 437–445, doi:10.1016/j.diabet.2015.08.005 (2015).
15. Gnad, T. *et al*. Adenosine activates brown adipose tissue and recruits beige adipocytes via A2A receptors. *Nature* **516**, 395–399, doi:10.1038/nature13816 (2014).
16. Watanabe, M. *et al*. Cold-induced changes in gene expression in brown adipose tissue: implications for the activation of thermogenesis. *Biological & pharmaceutical bulletin* **31**, 775–784 (2008).
17. Whittle, A. J. *et al*. BMP8B increases brown adipose tissue thermogenesis through both central and peripheral actions. *Cell* **149**, 871–885, doi:10.1016/j.cell.2012.02.066 (2012).
18. Agata, U. *et al*. The effect of different amounts of calcium intake on bone metabolism and arterial calcification in ovariectomized rats. *Journal of nutritional science and vitaminology* **59**, 29–36 (2013).
19. Simons, T. J. Calcium and neuronal function. *Neurosurgical review* **11**, 119–129 (1988).
20. Szent-Györgyi, A. G. Calcium regulation of muscle contraction. *Biophysical Journal* **15**, 707–723 (1975).
21. Draznin, B. Intracellular calcium, insulin secretion, and action. *The American journal of medicine* **85**, 44–58 (1988).
22. Bonny, O. & Bochud, M. Genetics of calcium homeostasis in humans: continuum between monogenic diseases and continuous phenotypes. *Nephrology, dialysis, transplantation: official publication of the European Dialysis and Transplant Association - European Renal Association* **29**(Suppl 4), iv55–62, doi:10.1093/ndt/gfu195 (2014).
23. Davies, J. H. Approach to the Child with Hypercalcaemia. *Endocrine development* **28**, 101–118, doi:10.1159/000380998 (2015).
24. Marcelo, K. L., Means, A. R. & York, B. The Ca(2+)/Calmodulin/CaMKK2 Axis: Nature's Metabolic CaMshaft. *Trends in endocrinology and metabolism: TEM* **27**, 706–718, doi:10.1016/j.tem.2016.06.001 (2016).
25. Feigh, M. *et al*. A novel oral form of salmon calcitonin improves glucose homeostasis and reduces body weight in diet-induced obese rats. *Diabetes, obesity & metabolism* **13**, 911–920, doi:10.1111/j.1463-1326.2011.01425.x (2011).
26. Shi, H., Halvorsen, Y. D., Ellis, P. N., Wilkison, W. O. & Zemel, M. B. Role of intracellular calcium in human adipocyte differentiation. *Physiological genomics* **3**, 75–82 (2000).
27. Neal, J. W. & Clipstone, N. A. Calcineurin mediates the calcium-dependent inhibition of adipocyte differentiation in 3T3-L1 cells. *The Journal of biological chemistry* **277**, 49776–49781, doi:10.1074/jbc.M207913200 (2002).
28. Lin, F., Ribar, T. J. & Means, A. R. The Ca2+/calmodulin-dependent protein kinase kinase, CaMKK2, inhibits preadipocyte differentiation. *Endocrinology* **152**, 3668–3679, doi:10.1210/en.2011-1107 (2011).
29. Jensen, B., Farach-Carson, M. C., Kenaley, E. & Akanbi, K. A. High extracellular calcium attenuates adipogenesis in 3T3-L1 preadipocytes. *Experimental cell research* **301**, 280–292, doi:10.1016/j.yexcr.2004.08.030 (2004).
30. Hashimoto, R. *et al*. Enhanced accumulation of adipocytes in bone marrow stromal cells in the presence of increased extracellular and intracellular [Ca(2)(+)]. *Biochem Biophys Res Commun* **423**, 672–678, doi:10.1016/j.bbrc.2012.06.010 (2012).
31. Mellor, L. F. *et al*. Extracellular Calcium Modulates Chondrogenic and Osteogenic Differentiation of Human Adipose-Derived Stem Cells: A Novel Approach for Osteochondral Tissue Engineering Using a Single Stem Cell Source. *Tissue engineering. Part A* **21**, 2323–2333, doi:10.1089/ten.TEA.2014.0572 (2015).
32. Tang, Q. Q., Zhang, J. W. & Daniel Lane, M. Sequential gene promoter interactions of C/EBPbeta, C/EBPalpha, and PPARgamma during adipogenesis. *Biochem Biophys Res Commun* **319**, 235–239, doi:10.1016/j.bbrc.2004.04.176 (2004).
33. Karamanlidis, G., Karamitri, A., Docherty, K., Hazlerigg, D. G. & Lomax, M. A. C/EBPbeta reprograms white 3T3-L1 preadipocytes to a Brown adipocyte pattern of gene expression. *The Journal of biological chemistry* **282**, 24660–24669, doi:10.1074/jbc.M703101200 (2007).
34. Lechner, S., Mitterberger, M. C., Mattesich, M. & Zwerschke, W. Role of C/EBPbeta-LAP and C/EBPbeta-LIP in early adipogenic differentiation of human white adipose-derived progenitors and at later stages in immature adipocytes. *Differentiation; research in biological diversity* **85**, 20–31, doi:10.1016/j.diff.2012.11.001 (2013).
35. Ussar, S., Bezy, O., Bluher, M. & Kahn, C. R. Glypican-4 enhances insulin signaling via interaction with the insulin receptor and serves as a novel adipokine. *Diabetes* **61**, 2289–2298, doi:10.2337/db11-1395 (2012).
36. Dougherty, M. K. *et al*. KSR2 is a calcineurin substrate that promotes ERK cascade activation in response to calcium signals. *Mol Cell* **34**, 652–662, doi:10.1016/j.molcel.2009.06.001 (2009).
37. Lawrence, M. C., McGlynn, K., Park, B. H. & Cobb, M. H. ERK1/2-dependent activation of transcription factors required for acute and chronic effects of glucose on the insulin gene promoter. *The Journal of biological chemistry* **280**, 26751–26759, doi:10.1074/jbc.M503158200 (2005).
38. Yamashita, H. *et al*. Induction of fatty acid-binding protein 3 in brown adipose tissue correlates with increased demand for adaptive thermogenesis in rodents. *Biochem Biophys Res Commun* **377**, 632–635, doi:10.1016/j.bbrc.2008.10.041 (2008).
39. Vergnes, L., Chin, R., Young, S. G. & Reue, K. Heart-type fatty acid-binding protein is essential for efficient brown adipose tissue fatty acid oxidation and cold tolerance. *The Journal of biological chemistry* **286**, 380–390, doi:10.1074/jbc.M110.184754 (2011).

40. Daikoku, T., Shinohara, Y., Shima, A., Yamazaki, N. & Terada, H. Dramatic enhancement of the specific expression of the heart-type fatty acid binding protein in rat brown adipose tissue by cold exposure. *FEBS Letters* **410**, 383–386, doi:10.1016/s0014-5793(97)00619-4 (1997).
41. Nakamura, Y., Sato, T., Shiimura, Y., Miura, Y. & Kojima, M. FABP3 and brown adipocyte-characteristic mitochondrial fatty acid oxidation enzymes are induced in beige cells in a different pathway from UCP1. *Biochem Biophys Res Commun* **441**, 42–46, doi:10.1016/j.bbrc.2013.10.014 (2013).
42. Wu, Z. *et al*. Cross-regulation of C/EBP alpha and PPAR gamma controls the transcriptional pathway of adipogenesis and insulin sensitivity. *Mol Cell* **3**, 151–158 (1999).
43. Prusty, D., Park, B. H., Davis, K. E. & Farmer, S. R. Activation of MEK/ERK signaling promotes adipogenesis by enhancing peroxisome proliferator-activated receptor gamma (PPARgamma) and C/EBPalpha gene expression during the differentiation of 3T3-L1 preadipocytes. *The Journal of biological chemistry* **277**, 46226–46232, doi:10.1074/jbc.M207776200 (2002).
44. Farmer, S. R. Regulation of PPARgamma activity during adipogenesis. *Int J Obes (Lond)* **29**(Suppl 1), S13–16, doi:10.1038/sj.ijo.0802907 (2005).
45. Bost, F., Aouadi, M., Caron, L. & Binetruy, B. The role of MAPKs in adipocyte differentiation and obesity. *Biochimie* **87**, 51–56, doi:10.1016/j.biochi.2004.10.018 (2005).
46. Cifuentes, M., Albala, C. & Rojas, C. Calcium-sensing receptor expression in human adipocytes. *Endocrinology* **146**, 2176–2179, doi:10.1210/en.2004-1281 (2005).
47. Keipert, S. & Jastroch, M. Brite/beige fat and UCP1 - is it thermogenesis? *Biochim Biophys Acta* **1837**, 1075–1082, doi:10.1016/j.bbabio.2014.02.008 (2014).
48. Boucher, J., Tseng, Y. H. & Kahn, C. R. Insulin and insulin-like growth factor-1 receptors act as ligand-specific amplitude modulators of a common pathway regulating gene transcription. *J Biol Chem* **285**, 17235–17245, doi:10.1074/jbc.M110.118620 (2010).
49. Ussar, S. *et al*. ASC-1, PAT2, and P2RX5 are cell surface markers for white, beige, and brown adipocytes. *Science translational medicine* **6**, 247ra103, doi:10.1126/scitranslmed.3008490 (2014).

Acknowledgements

We thank Andreas Israel, Miriam Ecker and Lisa Suwandhi for excellent technical assistance. The project was supported by a grant of the Else Kröner Fresenius Stiftung and iMed the personalized medicine initiative of the Helmholtz association.

Author Contributions

I.P. performed the experiments. I.P. and S.U. designed and analyzed data, and wrote the manuscript. M.J. analyzed data and contributed to writing the manuscript.

Additional Information

Supplementary information accompanies this paper at doi:10.1038/s41598-017-09025-3

Competing Interests: The authors declare that they have no competing interests.

Publisher's note: Springer Nature remains neutral with regard to jurisdictional claims in published maps and institutional affiliations.

Supplemental information to:

Extracellular calcium modulates brown adipocyte differentiation and identity

Ines Pramme-Steinwachs[1,2], Martin Jastroch[2,3], Siegfried Ussar[1,2]

[1]JRG Adipocytes & Metabolism, Institute for Diabetes & Obesity, Helmholtz Center Munich, 85748 Garching, Germany, [2]German Center for Diabetes Research (DZD), 85764 Neuherberg, Germany, [3]Institute for Diabetes & Obesity, Helmholtz Center Munich, 85748 Garching, Germany

Supplemental Figure 1

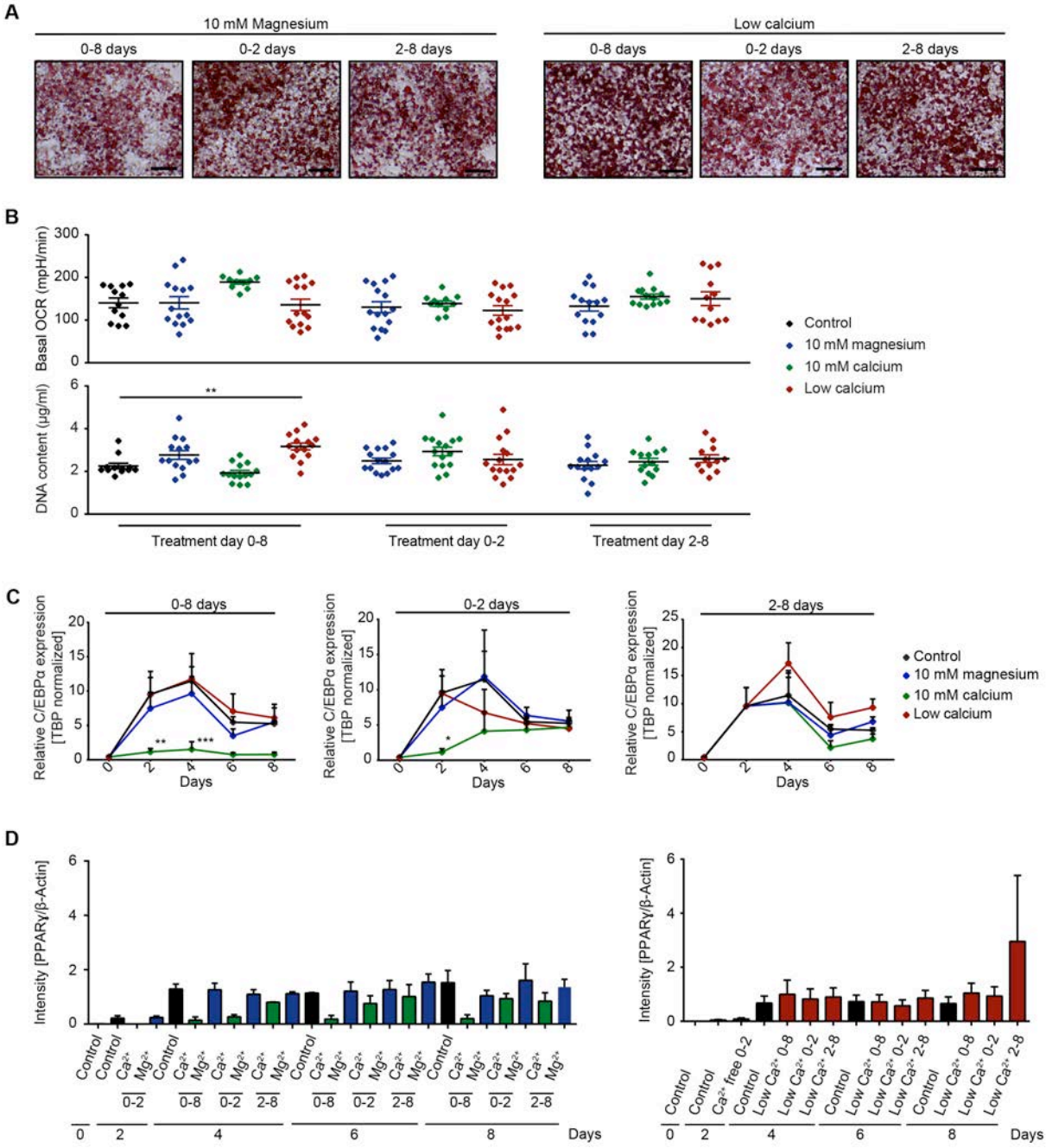

Supplemental Figure 1: (A) Representative pictures of Oil Red O stained adipocytes at day 8 of differentiation under 10 mM magnesium or low calcium conditions for the indicated duration, size bar = 20 µm. **(B)** Basal oxygen consumption (OCR) and DNA content in cells at day 8 treated under indicated conditions (n=2-3, 3-5 technical replicates each). **(C)** C/EBPα expression normalized on TBP of *in vitro* differentiated preadipocytes during an eight day time course under normal 1.8 mM calcium (control), 10 mM calcium (Ca^{2+}), 10 mM magnesium

(Mg^{2+}) and low calcium conditions during days 2-8 (n=3). **(D)** Quantification of PPARγ protein content normalized to β-actin (n=3). Data are shown as mean ± SEM, * $p<0.05$, ** $p<0.01$, *** $p<0.001$, **** $p<0.0001$; Ordinary One-way with Holm-Sidak's multiple comparison test (B top), Kruskal-Wallis one-way ANOVA with Dunn's multiple comparison test (B bottom) and two-Way ANOVA with Dunnett's posthoc test (C).

Supplemental Figure 2

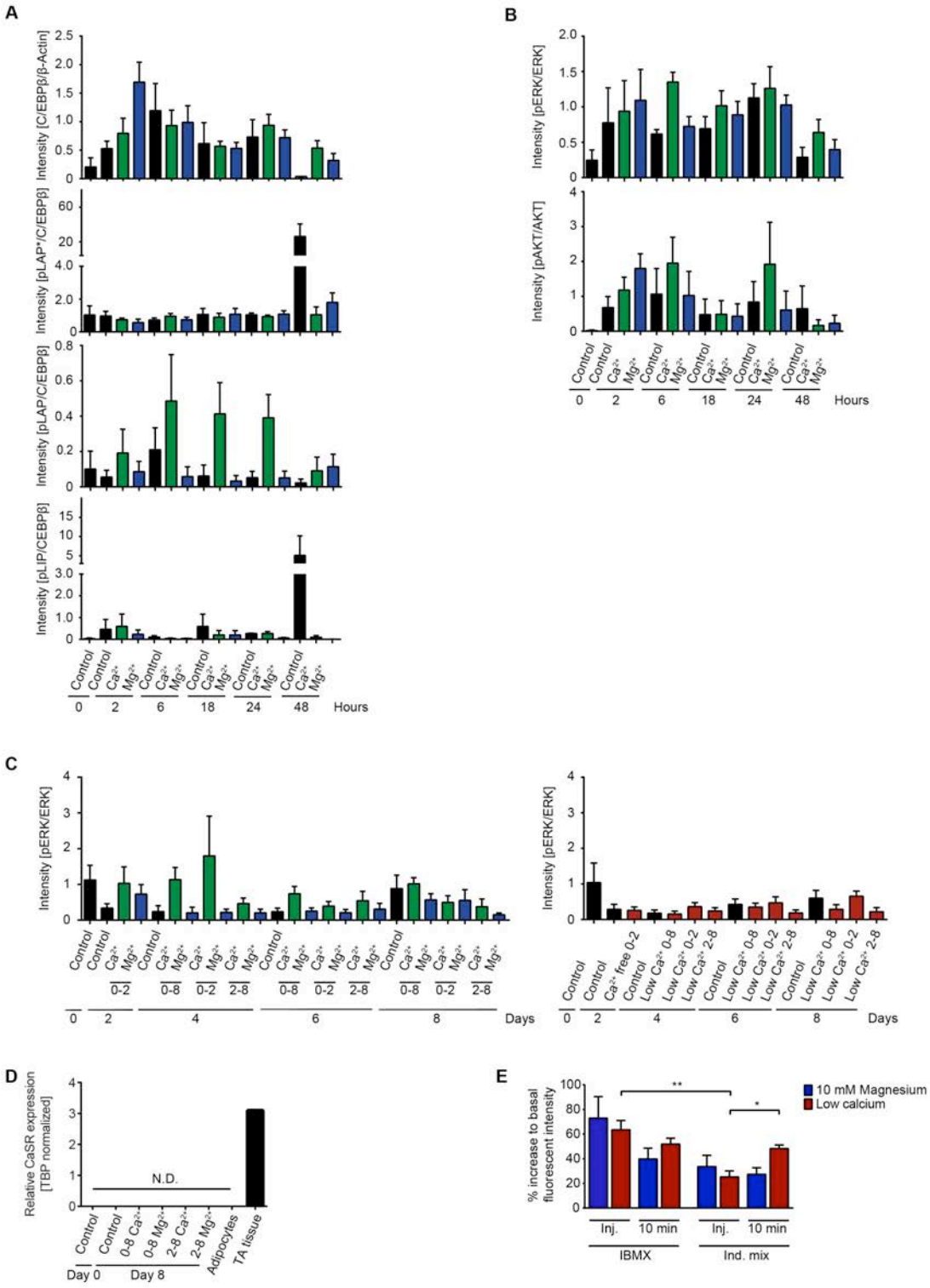

Supplemental Figure 2: Quantification of indicated protein signals in western blot normalized on β-actin or total protein during 48 hour time course: (A) Total C/EBPβ to β-Actin (n=4), pLAP*, pLAP and pLIP C/EBPβ to total C/EBPβ (n=3-4); (B) pERK to toal ERK (n=4), pAKT (S473) to total AKT (n=2-3). (C) Quantification of pERK signal normalized to total ERK signal during 8 day time course (n=4). (D) CaSR expression normalized to TBP in preadipocytes (day 0) and in vitro differentiated cells at day 8 under 1.8 mM calcium (control), 10 mM calcium (Ca2+) or 10 mM magnesium (Mg2+) for day 0-8 or 2-8 (n=3) as well as in primary mature adipocytes and murine muscle (tibia anterior –TA) (pooled samples n=1). (E) Relative increase of intracellular calcium in brown preadipocytes kept in 10 mM magnesium or calcium free medium directly upon and 10 min after injection of IBMX or induction mix shown as percent increase to basal level. Cells were loaded with the calcium binding fluorophore Fluo-4 (4 μM) and change in fluorescence was recorded at Ex/Em = 485/520 in orbital averaging (n=3 with 3-4 replicates each). Data are shown as mean ± SEM, * $p<0.05$, ** $p<0.01$, *** $p<0.001$, **** $p<0.0001$; (E) Repeated measures one-way ANOVA with Tukey's posthoc test.

Supplemental Figure 3

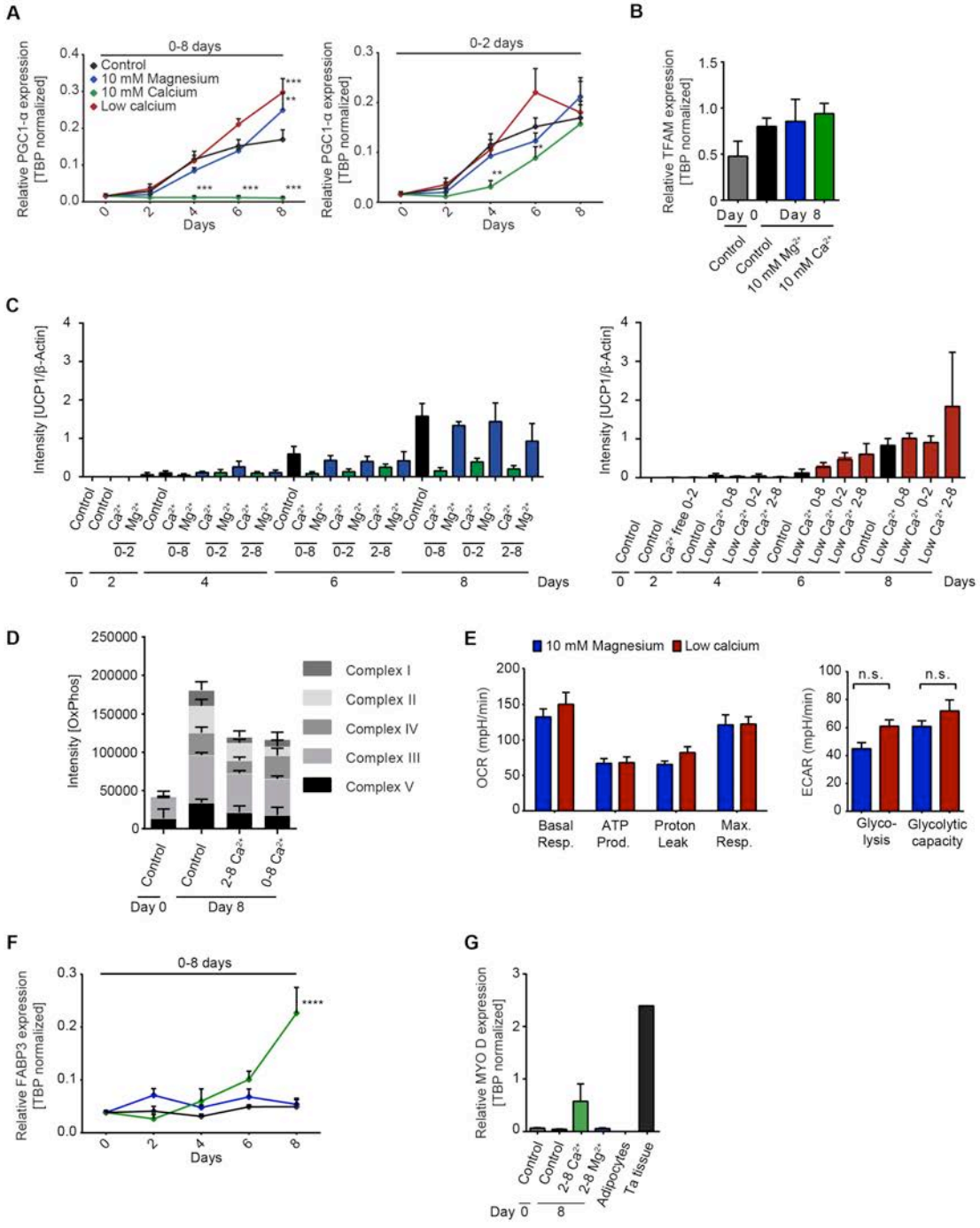

Supplemental Figure 3: (A) PGC1-α expression normalized to TBP during the eight day time course with the various treatment groups for day 0-8 and day 0-2 (n=4). **(B)** TFAM expression normalized on TBP in preadipocytes (day 0) and in vitro differentiated preadipocytes under normal 1.8 mM calcium (control), 10 mM calcium (Ca^{2+}),10 mM magnesium (Mg^{2+}) and calcium free conditions during day 2-8 (n=4). **(C)** Quantification of UCP1 protein content normalized to β-actin (n=3). **(D)** Quantification of mitochondrial complexes I-V protein content (n=3; complex, I n=1). **(E)** Oxygen consumption rate (OCR) and extracellular acidification rate (ECAR) measured by the Seahorse extracellular flux analyzer in differentiated adipocytes at day 8 and shown as values with subtracted non-mitochondrial respiration (OCR) and non-glycolytic acidification (ECAR). Cells were treated with 10 mM magnesium or calcium free medium for 2-8 days. During measurement basal respiration, ATP production, proton leak and maximal respiration in dependence of pyruvate addition (5 mM) as well as glycolytic rate and glycolytic capacity were detected (n=3 and n=2 for pyruvate, 6-7 technical replicates each). **(F)** FABP3 expression normalized with TBP during the time course of differentiation with 1.8 mM calcium (control), 10 mM calcium or 10 mM magnesium for 0-8 days (n=3). **(G)** MyoD expression normalized to TBP in preadipocytes (Control d0), in *in vitro* differentiated cells (day 8) under 1.8 mM calcium (control) or 10 mM calcium/magnesium for day 2-8 (n=3) and in isolated mature brown adipocytes as well as in murine muscle (tibia anterior –TA) (pooled samples n=1). Data are shown as mean ± SEM, * $p<0.05$, ** $p<0.01$, *** $p<0.001$, **** $p<0.0001$; (A, F) Two-Way ANOVA with Dunnett's posthoc test. Ordinary one-way ANOVA with Tukey's posthoc test (E) and Friedman one-way ANOVA with Dunn's multiple comparison test (B).

Supplemental Table 1: qPCR primer sequences 5'-3'.

Target gene	Forward sequence	Reverse sequence
CaSR	**GCTTTTCACCAACGGGTCCT**	**CCTGCTCCCCCATGTTGTT**
C/EBPα	AGGTGCTGGAGTTGACCAGT	CAGCCTAGAGATCCAGCGAC
C/EBPβ	CCAAGAAGACGGTGGACAA	CAAGTTCCGCAGGGTGCT
C/EBPδ	ATCGACTTCAGCGCCTACA	GCTTTGTGGTTGCTGTTGAA
Col I	GAAGCCGAGGTCCCAGTG	CACCCCTCTCTCCTGGAAG
FABP3	AGAGTTCGACGAGGTGACAG	TGCACATGGATGAGTTTGCC
MYO D	TACAGTGGCGACTCAGATGC	GTGTCGTAGCCATTCTGCC
PGC1-α	AGCCGTGACCACTGACAACGAG	GCTGCATGGTTCTGAGTGCTAAG
PPARγ	CCCTGGCAAAGCATTTGTAT	GAAACTGGCACCCTTGAAAA
PRDM16	CCGCTGTGATGAGTGTGATG	GGACGATCATGTGTTGCTCC
RUNX2	CTCTGGCCTTCCTCTCTCAG	TGAAATGCTTGGGAACTGCC
ACTA2	CTGTCAGGAACCCTGAGACGC	GGATGGGAAAACAGCCCTGG
TBP	ACCCTTCACCAATGACTCCTATG	TGACTGCAGCAAATCGCTTGG
TFAM	CAGGAGGCAAAGGATGATTC	CCAAGACTTCATTTCATTGTCG
UCP-1	CTGCCAGGACAGTACCCAAG	TCAGCTGTTCAAAGCACACA

Supplemental Table 2: Primary antibodies for western blot analysis.

Protein	**Company**	**Catalog number**
Akt	Cell Signaling	#4685
Anti-mouse IgG, HRP coupled	Santa Cruz	sc-2005
Anti-rabbit IgG, HRP coupled	Cell Signaling	#7074
β-Actin, HRP coupled	Santa Cruz	sc-47778
C/EBPβ	Cell Signaling	#3087
p44/42 MAPK (Erk1/2)	Cell Signaling	#4695
PPARγ	Cell Signaling	#2435
p-Akt (S473)	Cell Signaling	#9271
p-C/EBPβ (Thr235)	Cell Signaling	#3084
p-p44/42 MAPK (Erk1/2)	Cell Signaling	#4377
OxPhos Complex Kit	Novex	458099
UCP-1 antibody	custom*	Rabbit anti-hamster UCP1

* A detailed characterization of the antibody can be found in: Functional characterization of UCP1 in mammalian HEK293 cells excludes mitochondrial uncoupling artefacts and reveals no contribution to basal proton leak., Jastroch M, Hirschberg V, Klingenspor M., Biochim Biophys Acta. 2012 Sep;1817(9):1660-70

Uncropped western blots:

Supplement Info Figure 1C

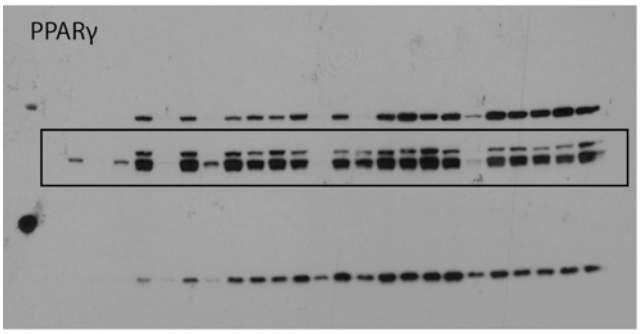

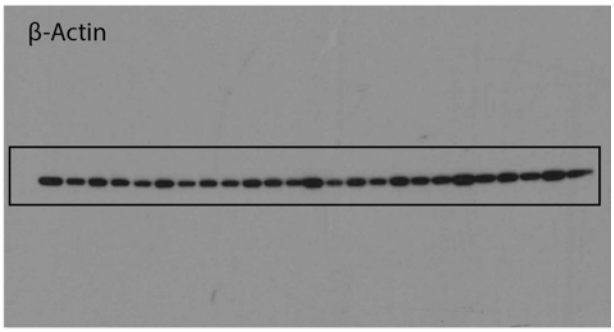

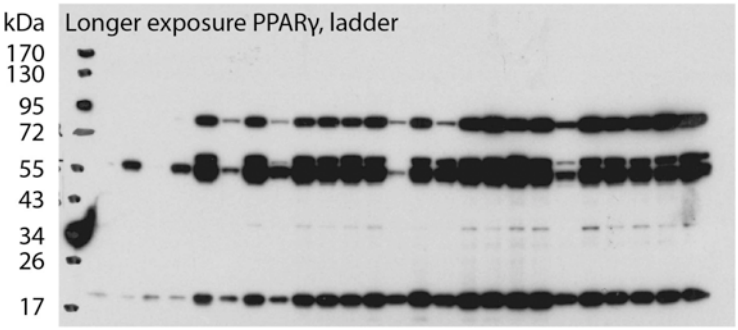

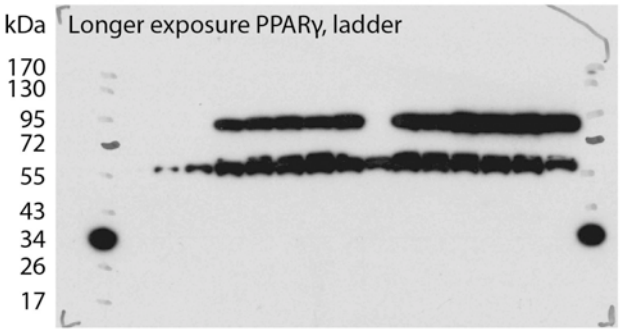

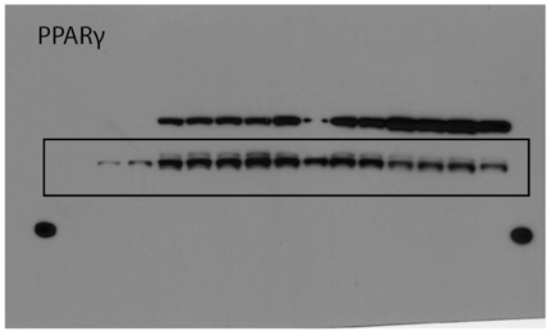

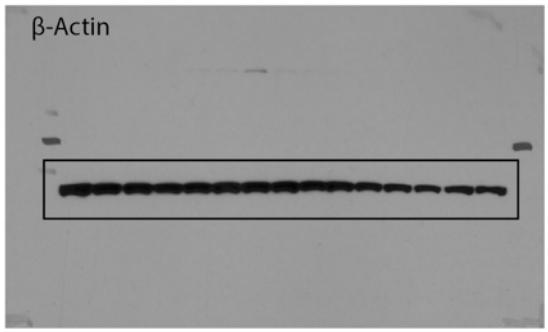

Supplement Info Figure 2B

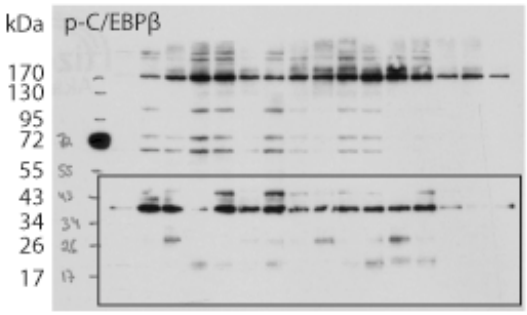

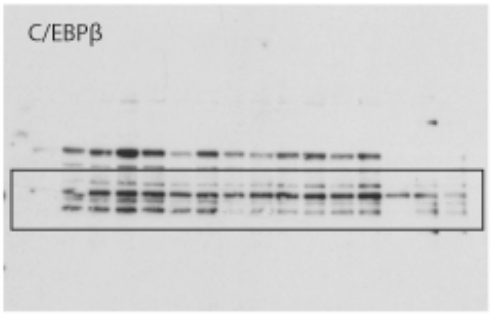

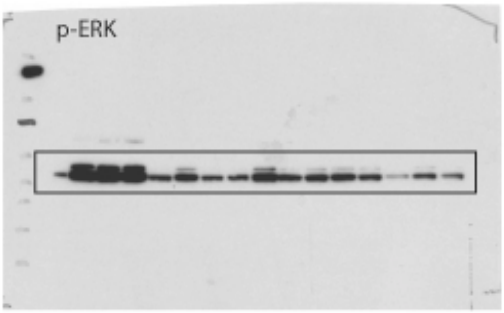

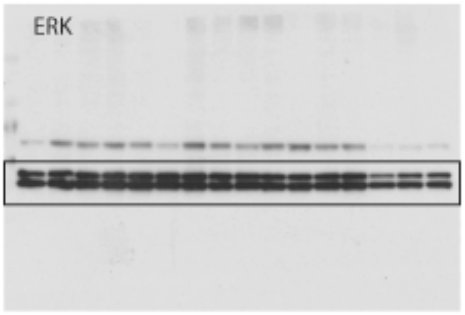

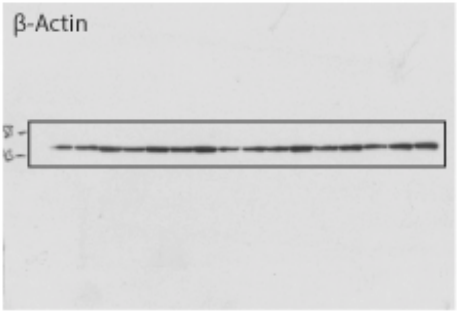

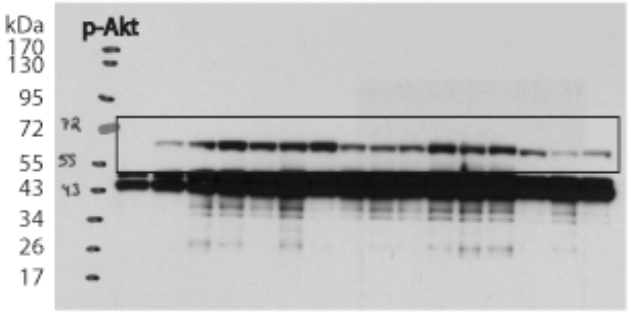

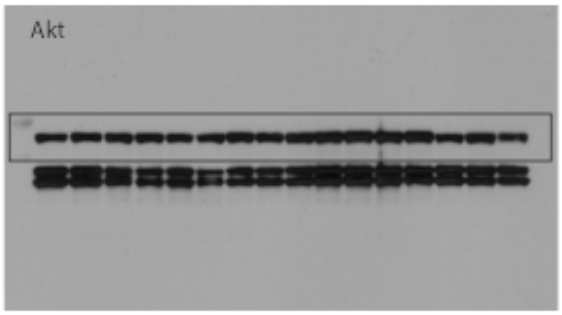

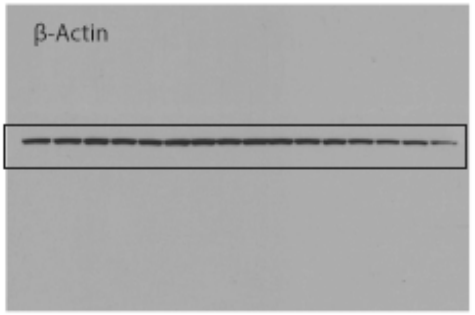

Supplement Info Figure 2C

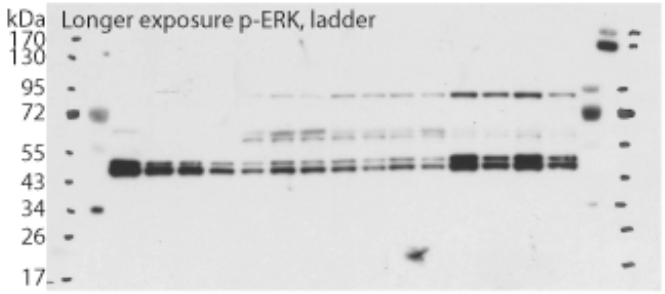

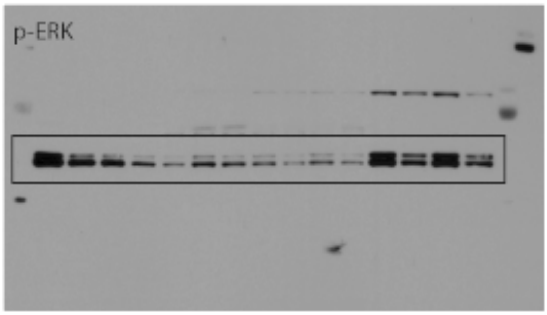

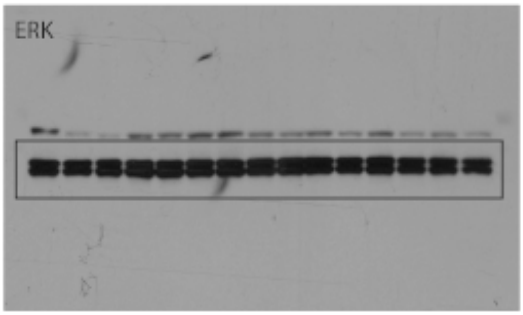

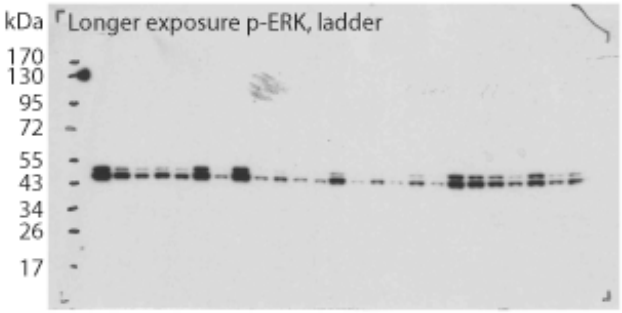

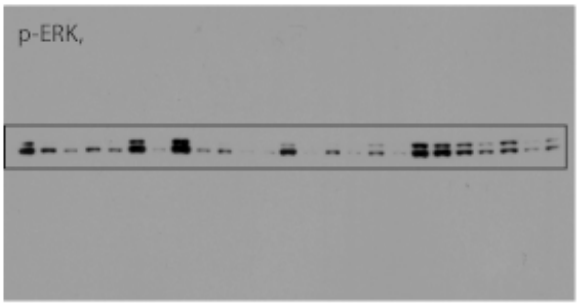

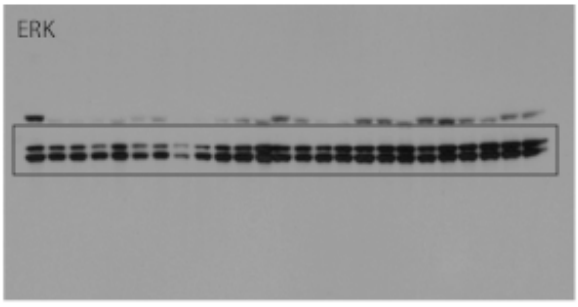

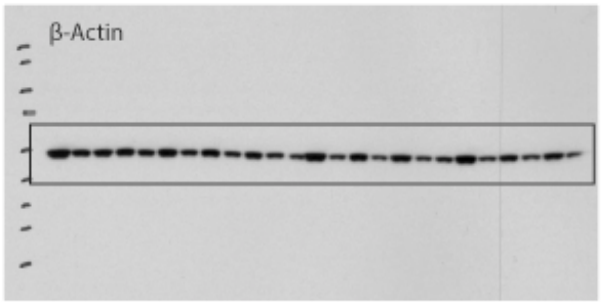

Supplement Info Figure 2F

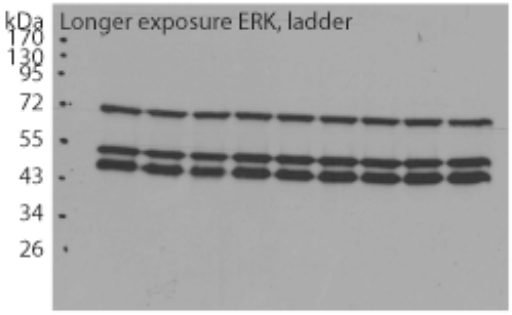

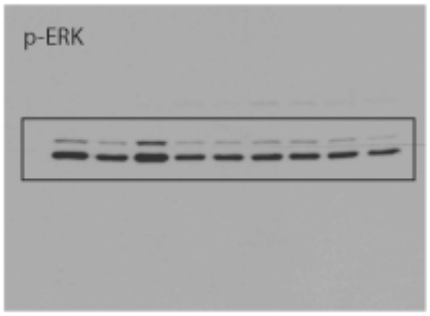

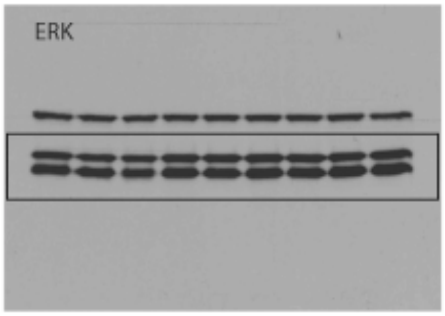

Supplement Info Figure 3C

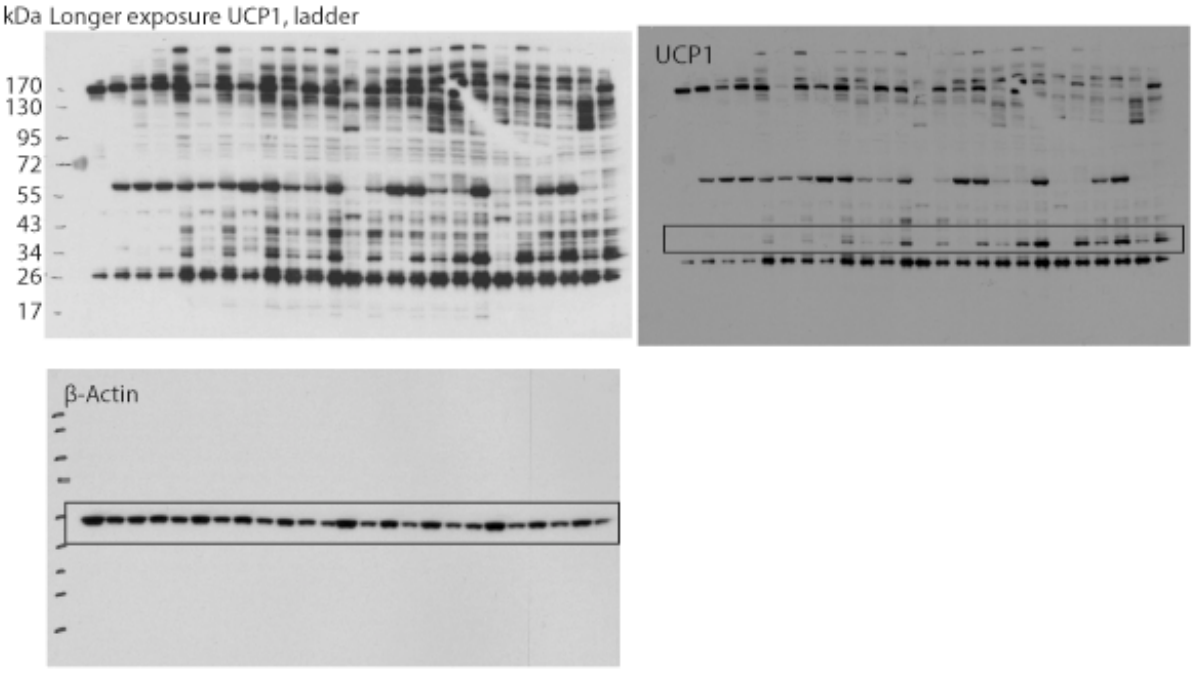

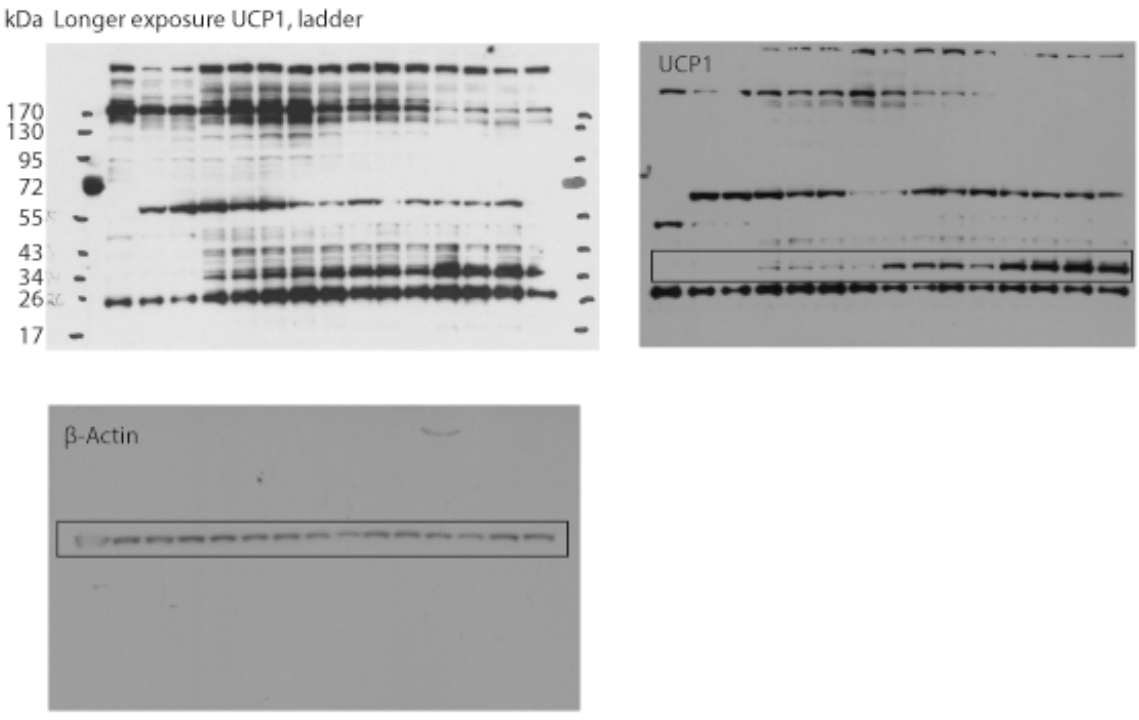

Supplement Info Figure 3D

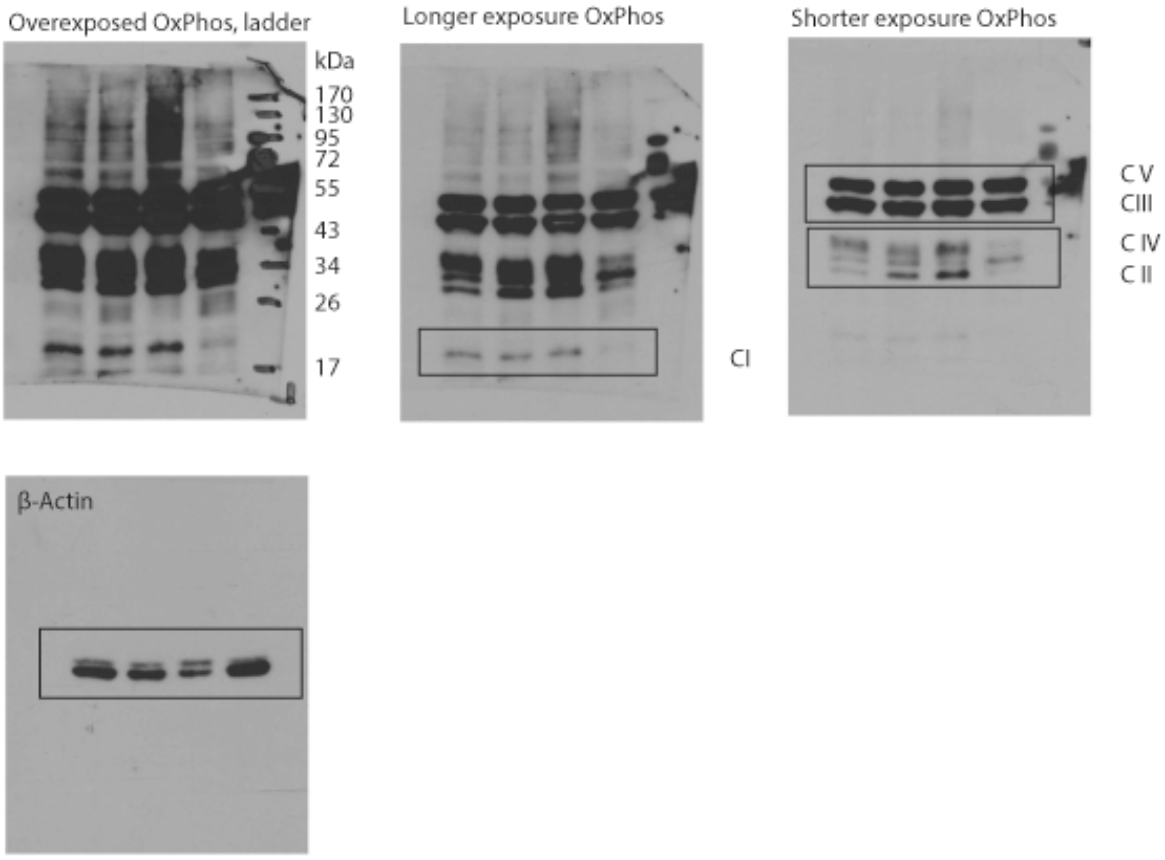

Supplement Info Supplemental Figure 1D left

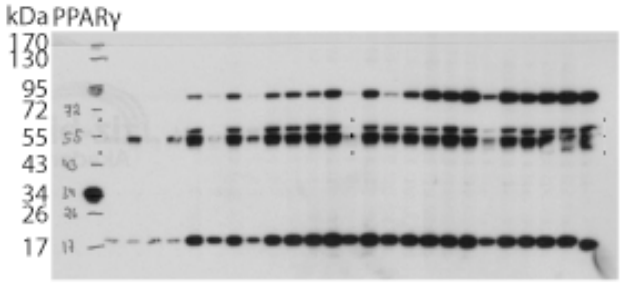

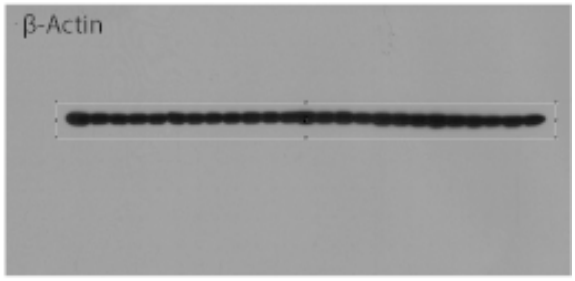

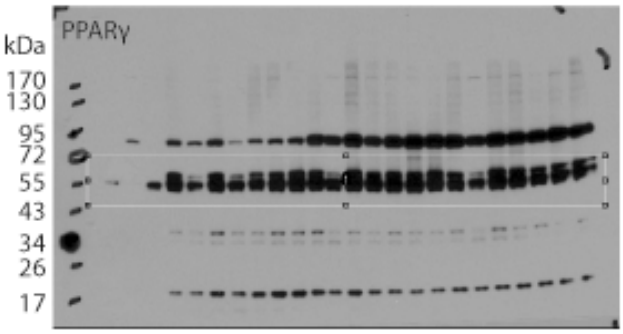

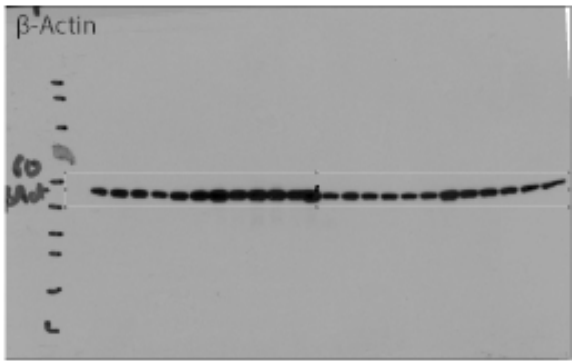

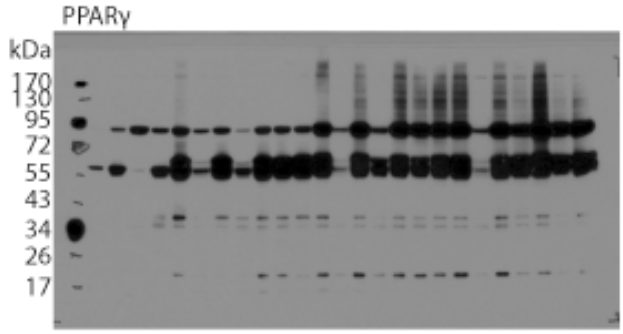

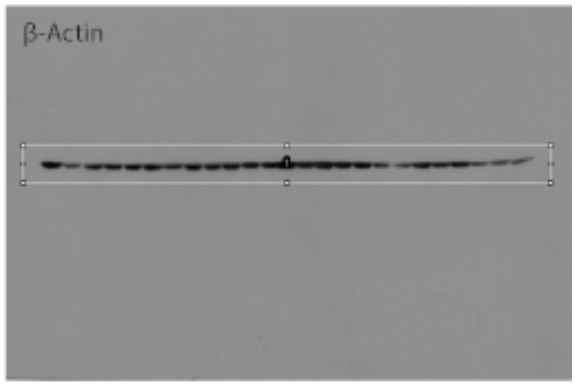

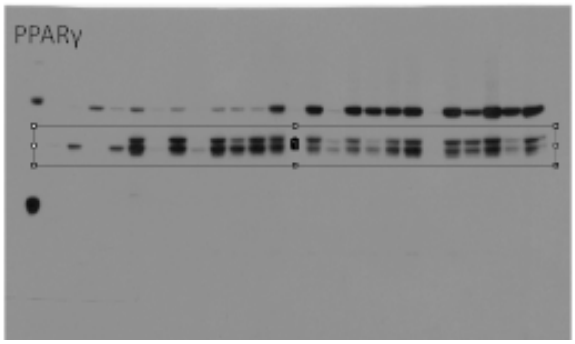

Supplement Info Supplemental Figure 1D right

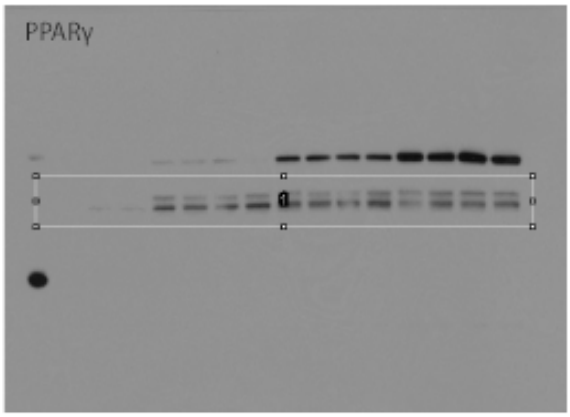

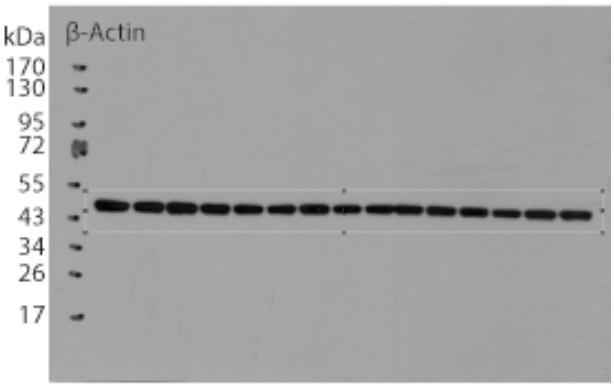

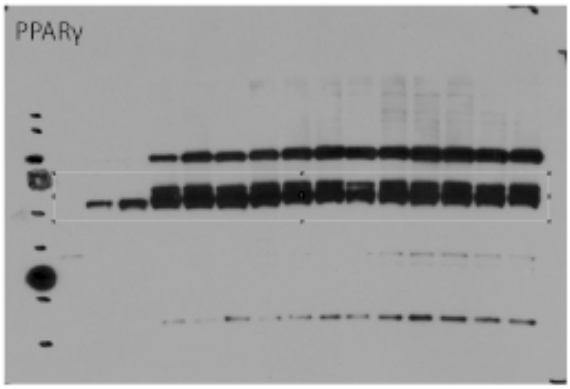

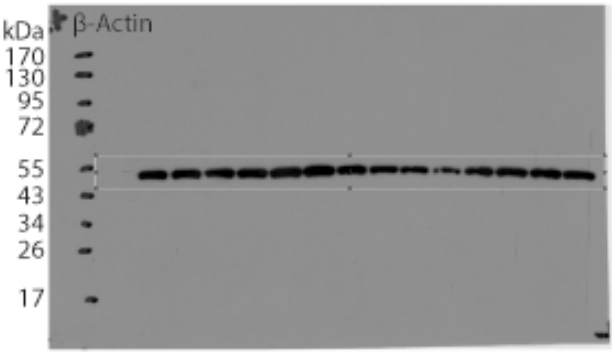

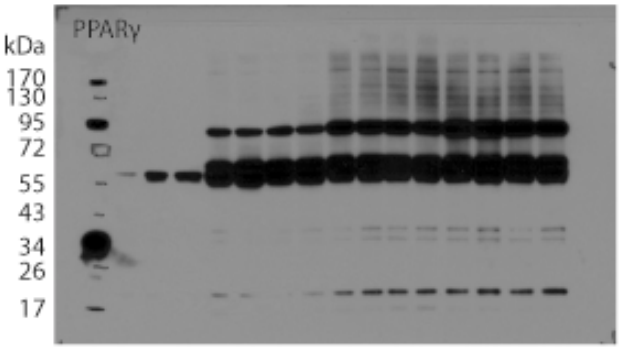

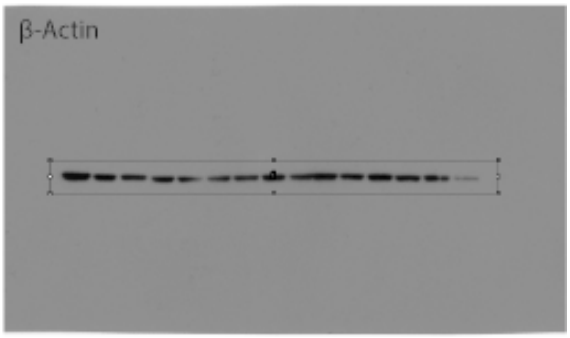

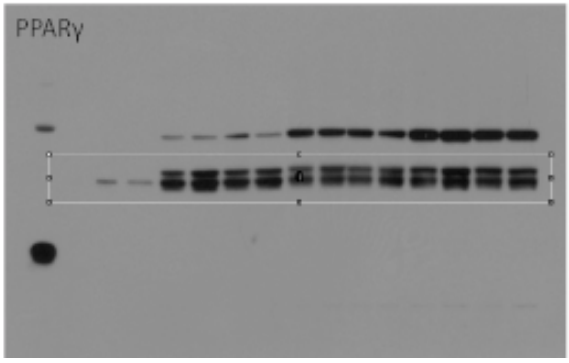

Supplement Info Supplemental Figure 2A

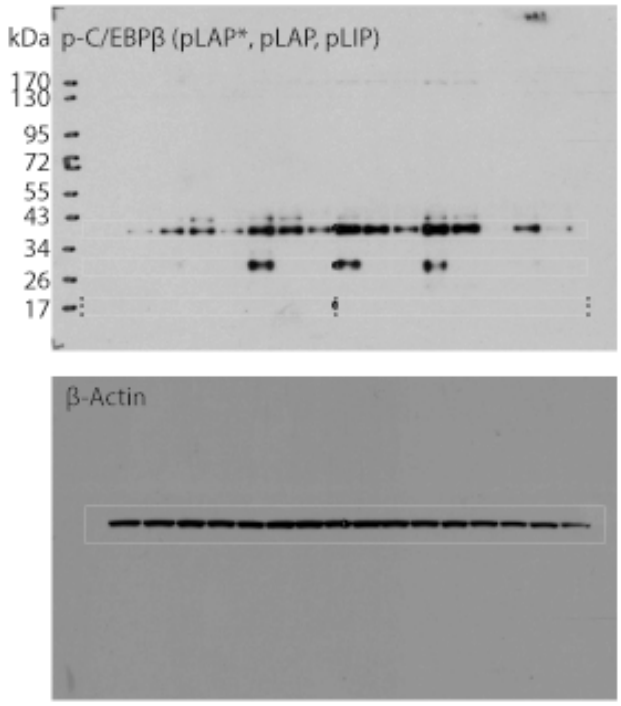

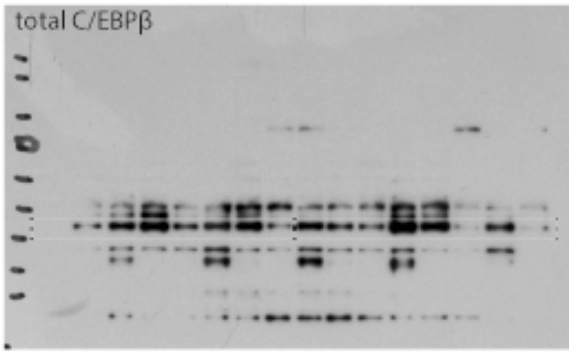

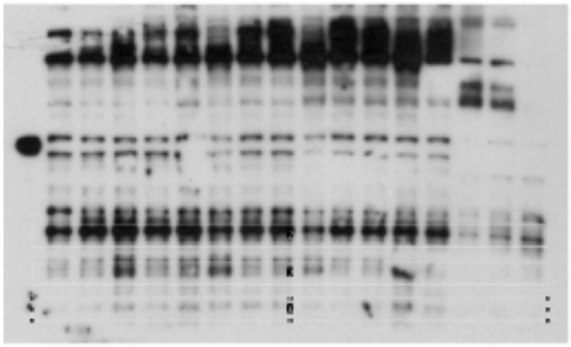

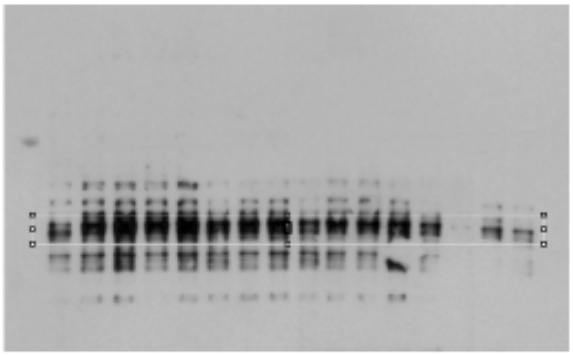

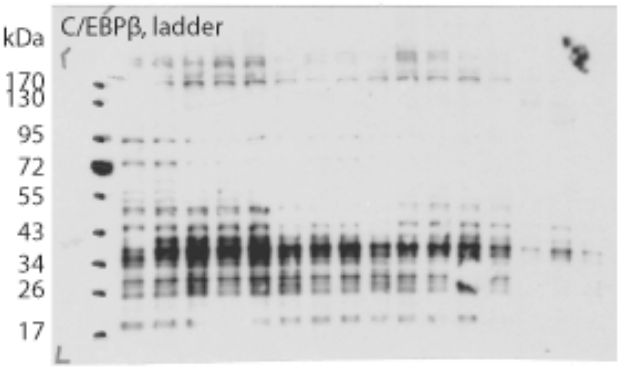

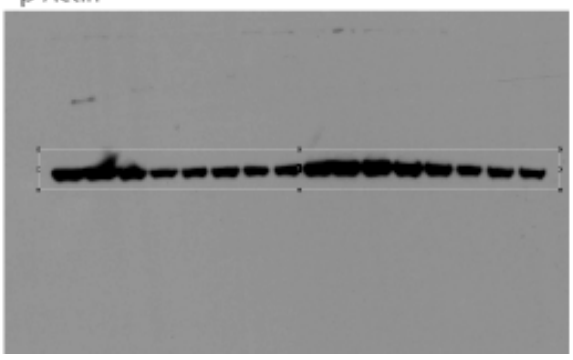

Supplement Info Supplemental Figure 2A

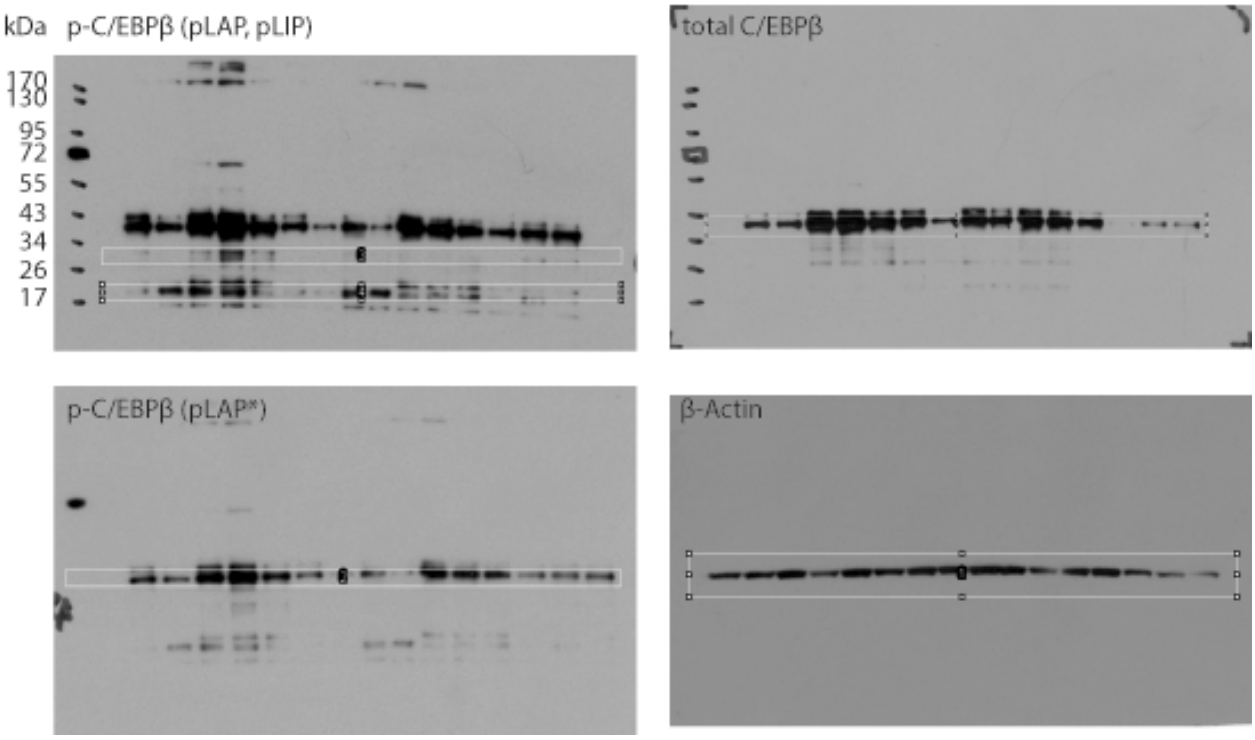

Supplement Info Supplemental Figure 2B

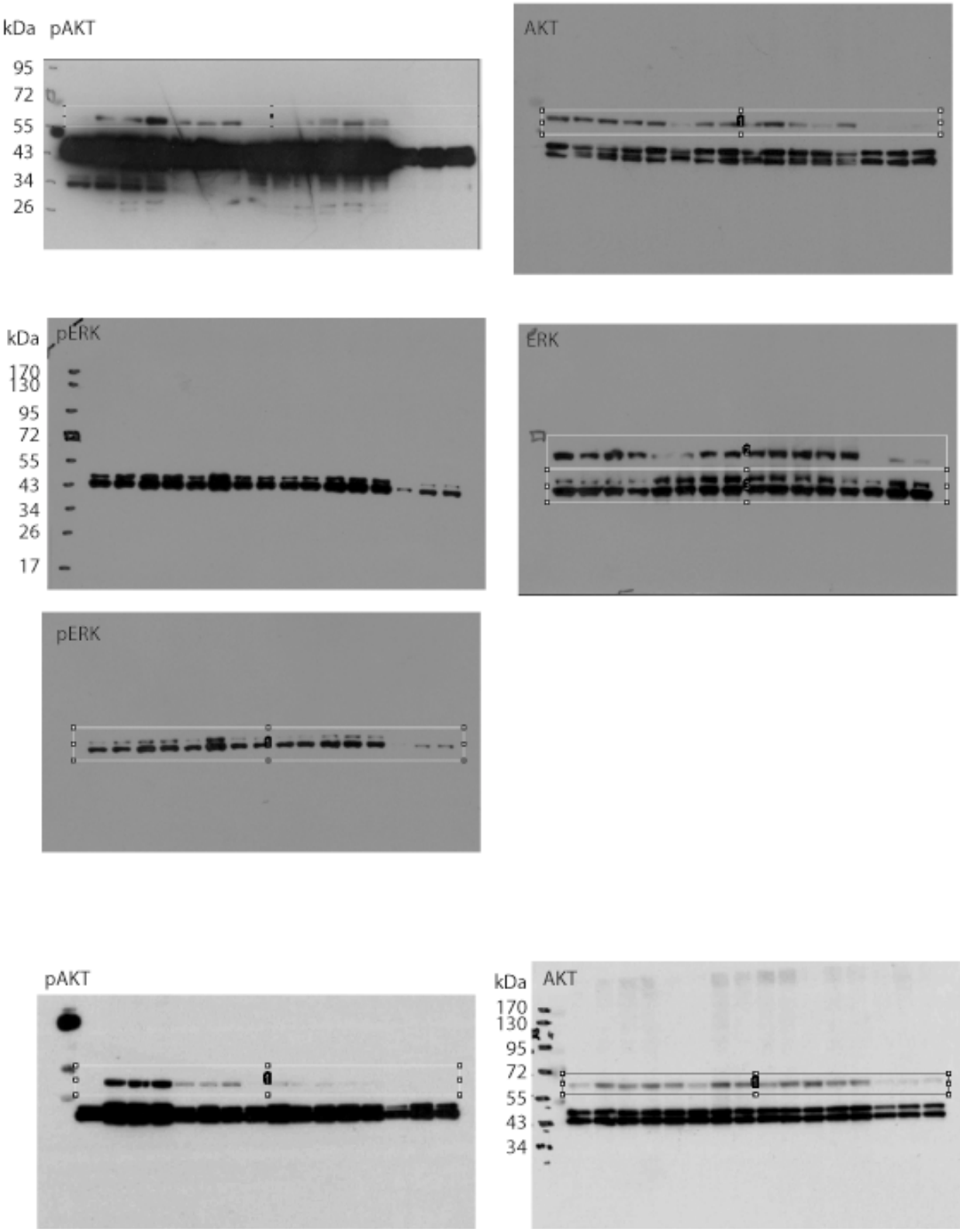

Supplement Info Supplemental Figure 2B

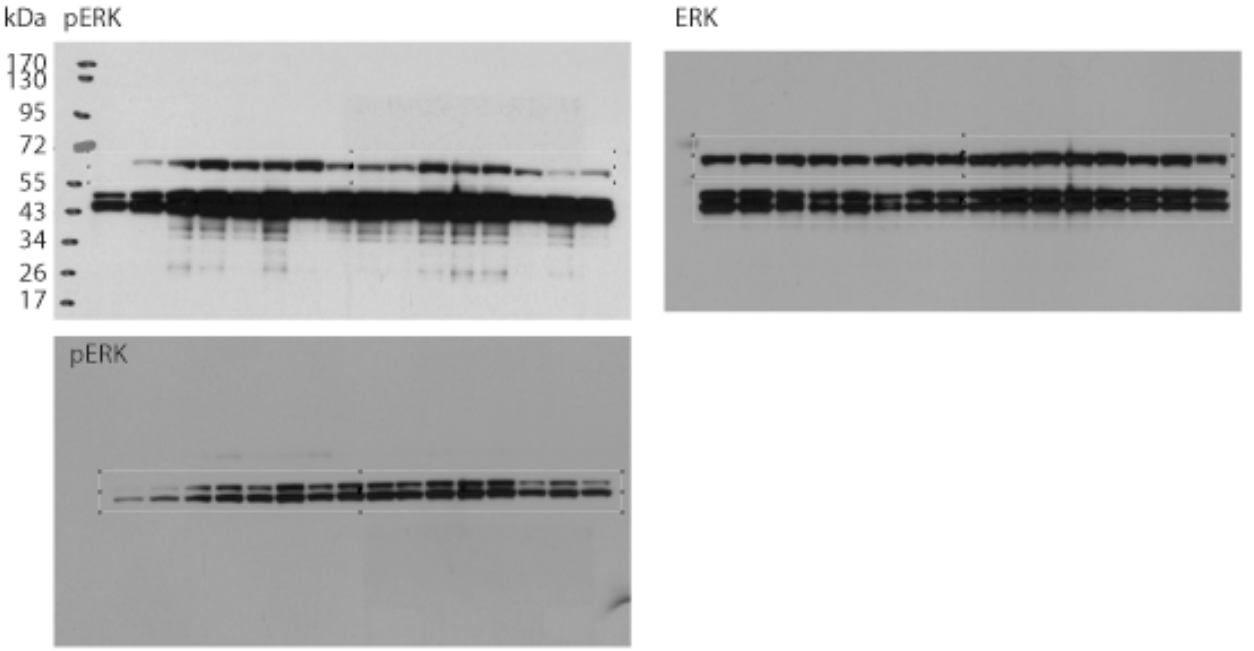

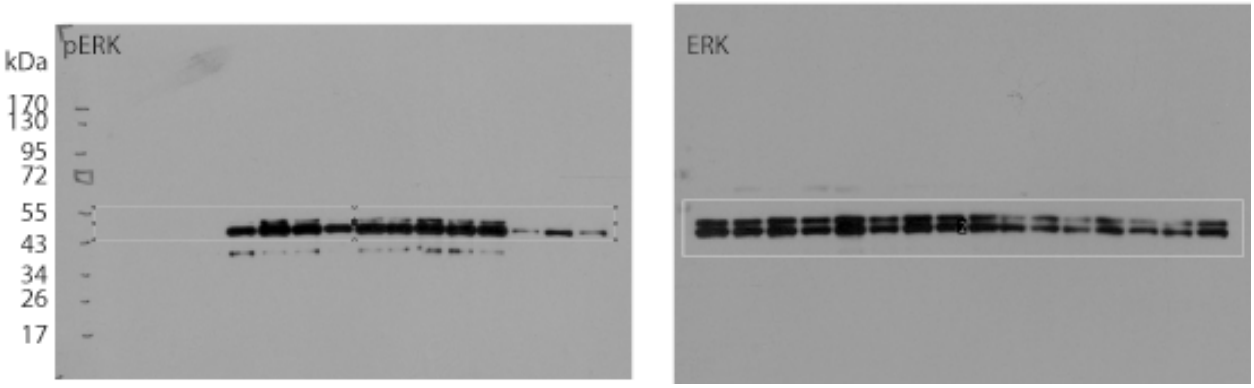

Supplement Info Supplemental Figure 2C left

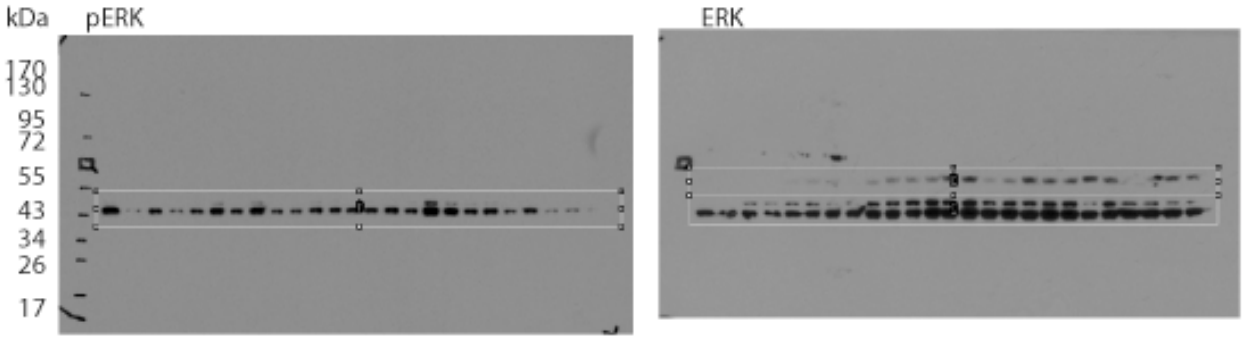

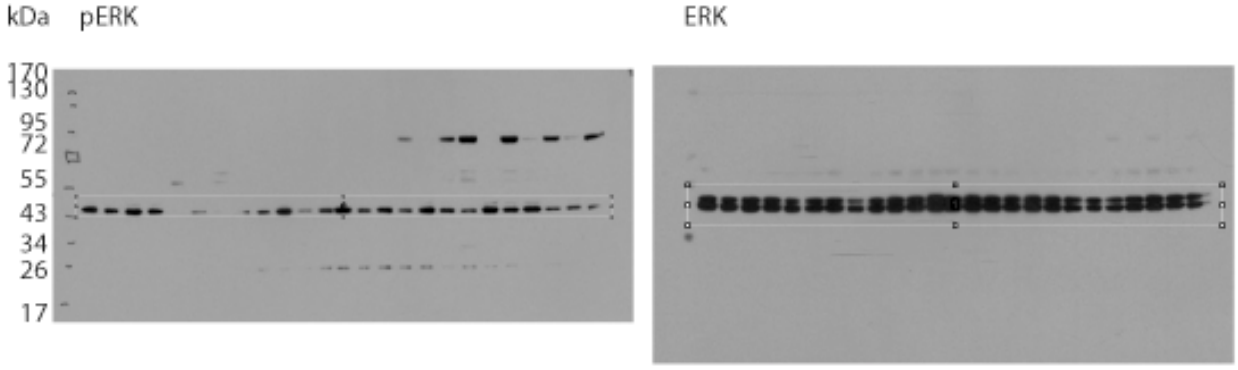

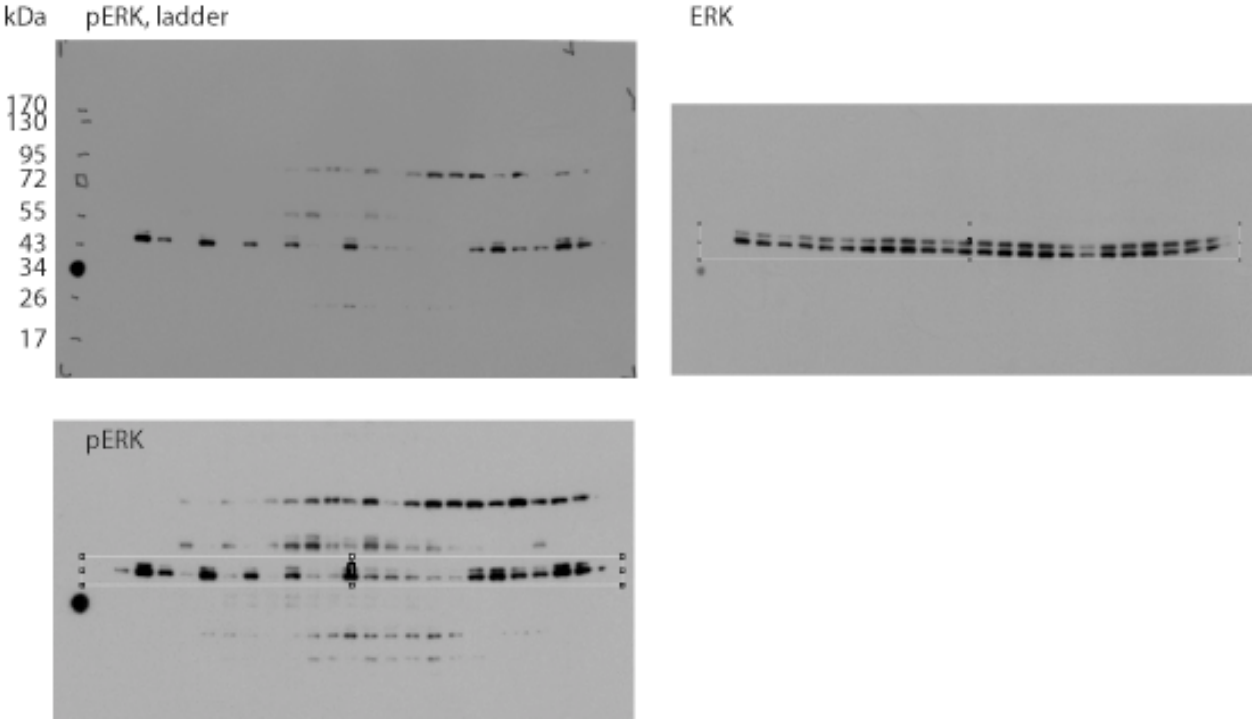

Supplement Info Supplemental Figure 2C right

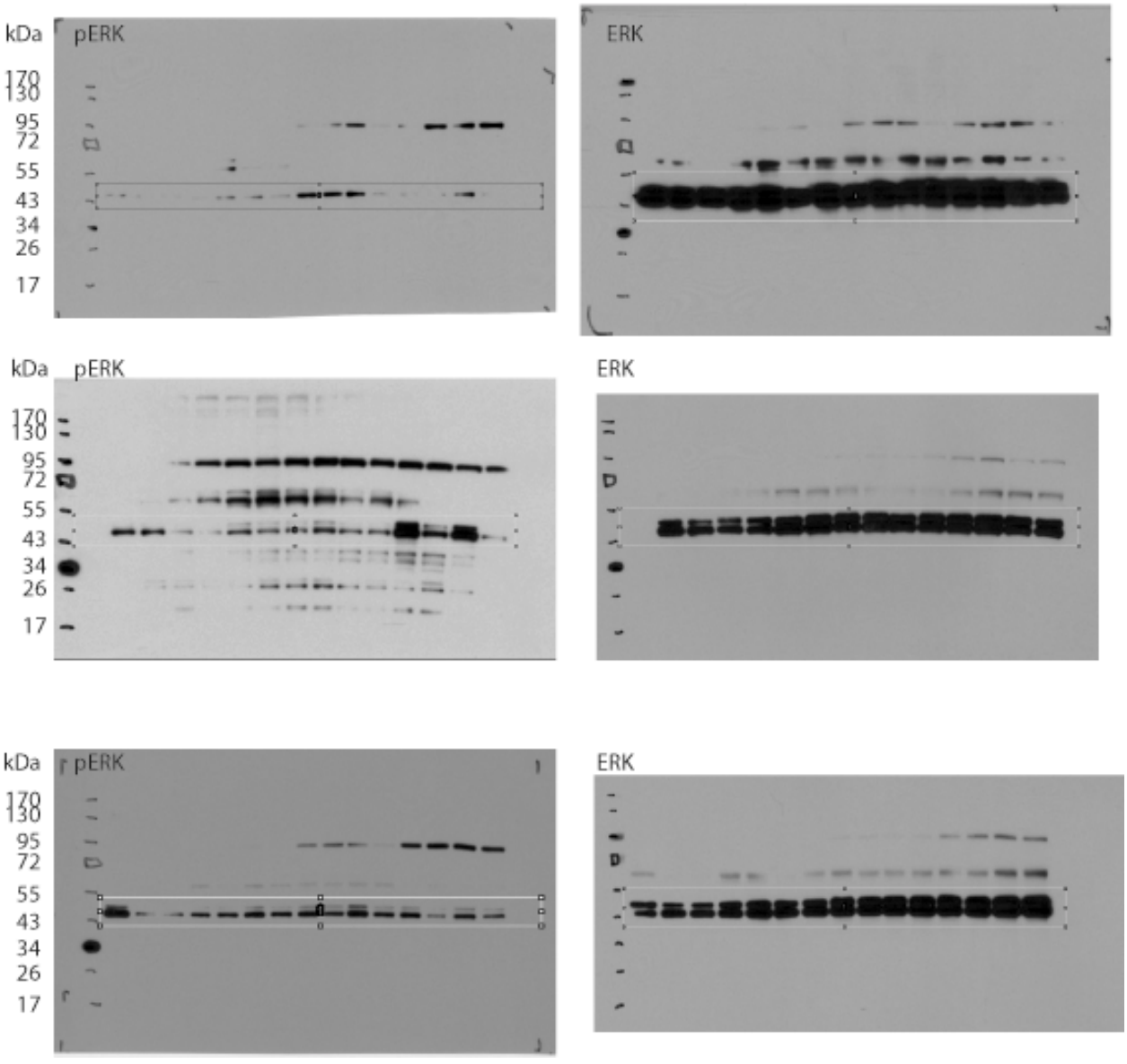

Supplement Info Supplemental Figure 3C left

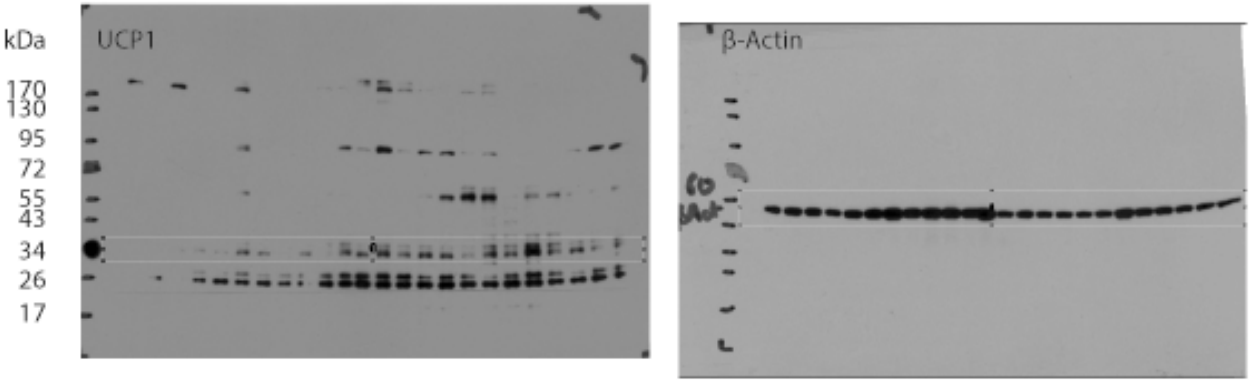

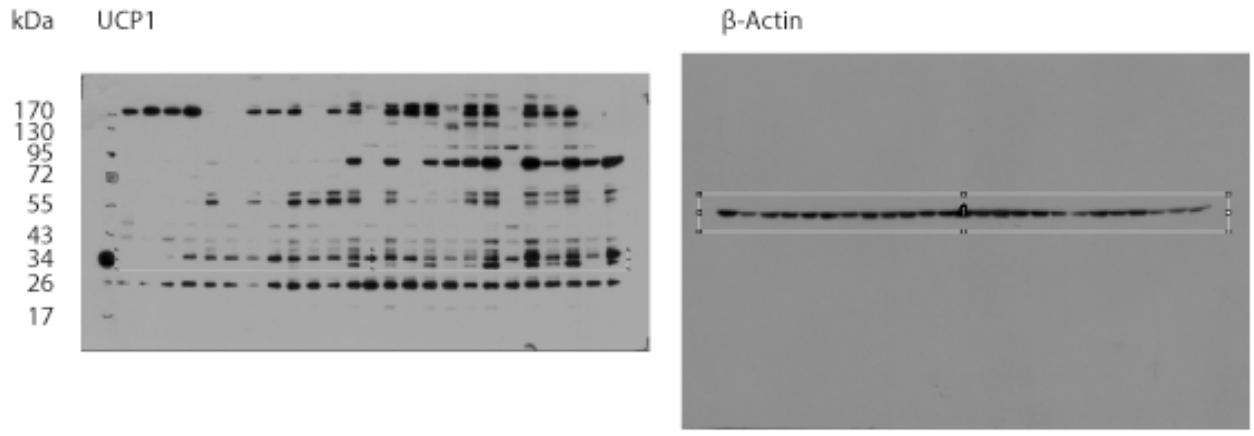

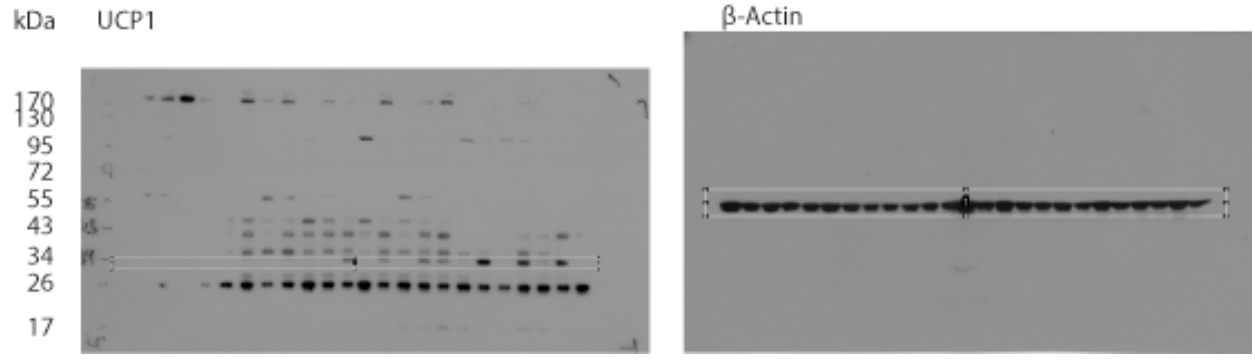

Supplement Info Supplemental Figure 3C right

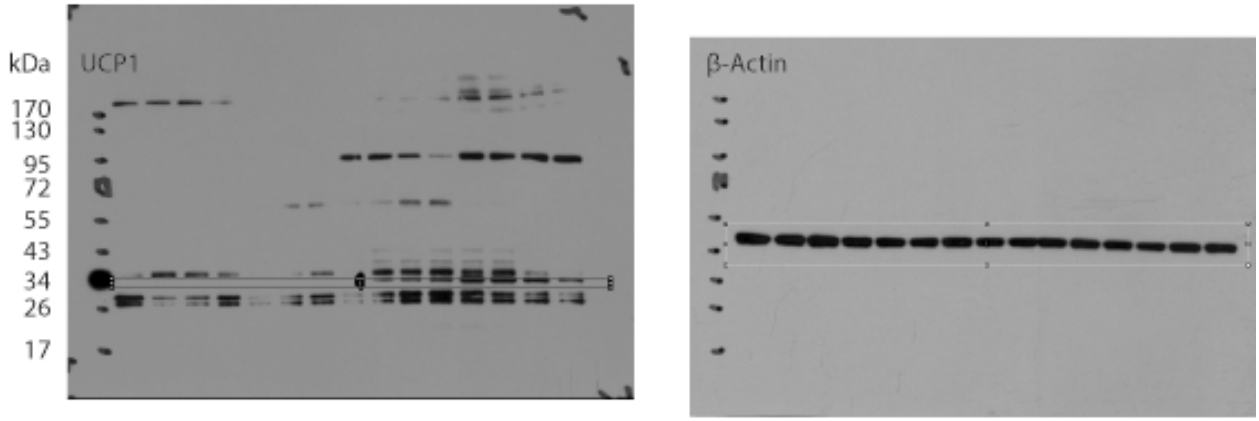

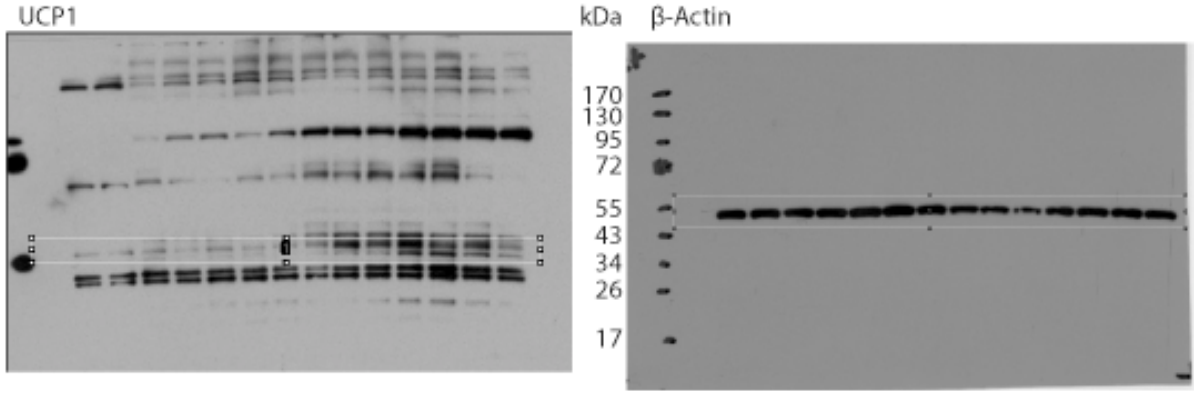

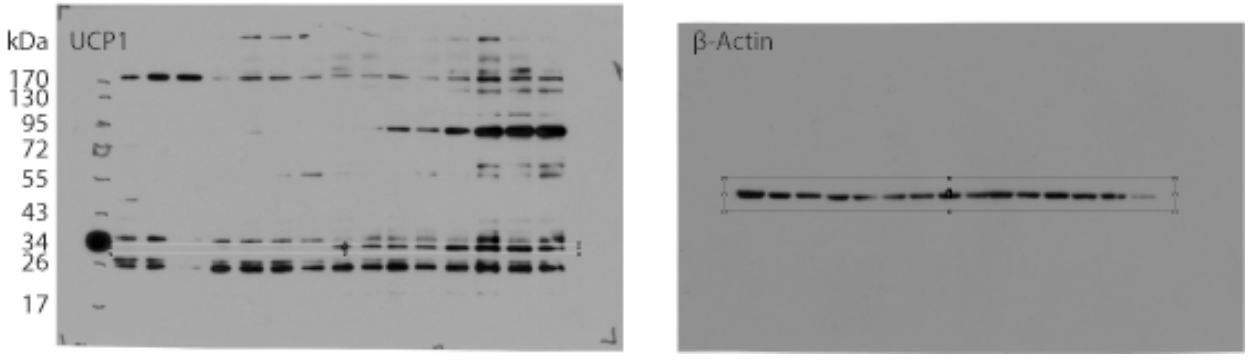

Supplement Info Supplemental Figure 3D